NASA TECHNICAL TRANSLATION

NASA TT F-594

TECH LIBRARY KAFB, NM
0068949

NASA TT F-594

COSMIC RAYS AND THEIR INTERACTIONS

by V. S. Murzin and L. I. Sarycheva

Atom Press, Moscow, 1968

NATIONAL AERONAUTICS AND SPACE ADMINISTRATION • WASHINGTON, D. C. • JUNE 1970

TECH LIBRARY KAFB, NM
0068949

COSMIC RAYS AND THEIR INTERACTIONS

By V. S. Murzin and L. I. Sarycheva

Translation of "Kosmicheskiye luchi i ikh vzaimodeystviye"
Atom Press, Moscow, 1968

NATIONAL AERONAUTICS AND SPACE ADMINISTRATION

For sale by the Clearinghouse for Federal Scientific and Technical Information
Springfield, Virginia 22151 – CFSTI price $3.00

EDITOR'S NOTE

With the exception of certain trigonometric and hyperbolic functions, Soviet mathematical symbols are the same as those encountered in the American literature. For the reader's convenience a list of such exceptions and their American equivalents is given below.

Soviet Usage	American equivalent
Arch	$\cosh^{-1}$
Arcth	$\coth^{-1}$ (ctnh^{-1})
Arsh	$\sinh^{-1}$
Arth	$\tanh^{-1}$
arccos	$\cos^{-1}$ (arc cos)
arcctg	$\cot^{-1}$ (arc cot)
arcsin	$\sin^{-1}$ (arc sin)
arctg	$\tan^{-1}$ (arc tan)
ch	cosh
cosec	csc
ctg	cot (ctn)
cth	coth (ctnh)
rot	curl
sch	sech
sh	sinh
tg	tan
th	tanh

MONOGRAPH

COSMIC RAYS AND THEIR INTERACTIONS

V. S. Murzin and L. I. Sarycheva

Moscow, Atomizdat, 1968

This monograph systematizes the experimental material on the nuclear interactions between particles of the cosmic radiation. An analysis is made of the characteristics of the elementary nuclear interaction process in the energy interval from 10 to 10^5 GeV and of the methodology of experiments on cosmic rays. Considerable attention is given to an examination of the reliability of experimental results. The cross section of the interaction of nuclear-active particles and the multiplicity, nature, and energetic and angular characteristics of secondary particles are considered.

The data adduced have been obtained either by direct registration of the nuclear interactions of particles or by the study of the secondary phenomena created by particles of super-high energy in the atmosphere. A comparison is made between the characteristics obtained experimentally and theoretical models.

The book is intended for specialists working in the fields of high energy physics and cosmic rays, as well as for students and graduate students of the corresponding specialties.

The monograph has 82 illustrations, 79 tables, and a bibliography of 503 citations.

PREFACE

The physics of cosmic rays includes a very wide range of disciplines--from astrophysics to nuclear physics. Because of this it treats of a wider range of distance and time than any other science. Here one may encounter units of distance from the parsec to the fermi, of time from billions of years to 10^{-24} s, and of energy from 0 to 10^{20} eV. The multifarious phenomena occurring in cosmic rays have more than once led physicists to completely unexpected discoveries. To the physics of cosmic rays we are indebted for the discovery of most of the "elementary" particles, electromagnetic cascade showers, multiple meson production, and much else.

The creation of accelerators has permitted the study of these problems in the laboratory. However, the attainment of the region of high energies ($E_0 > > 100$ GeV) is still many years in the future of accelerator technology.

Since the majority of processes occurring in nature depend essentially on energy, investigations at cosmic energies constitute an inevitable stage in our approach to the understanding of natural laws. These investigations permit penetration of the region of minimal times and distances. Here one can expect the appearance of new properties of matter, which may be expressed as changes in the characteristics of the elementary interaction process. Hence at this stage of investigation the determination of the specific properties of the elementary act and their dependence on the energy of the colliding particles is of supreme importance.

Investigations in the field of cosmic rays have already provided information about many features of the interaction. Much of this was obtained even when energies of 1 GeV were considered cosmic.

The most important of these features are: 1) the large cross section of the nuclear interaction, which remains practically unchanged with energy; 2) the small magnitude of the coefficient of inelasticity ($K \sim 0.3$ to 0.5); 3) the increase of multiplicity of secondary particles with energy; 4) the "conservation" of the nucleon after interaction; 5) the constancy of the transverse pulse and its independence on energy. In addition to these qualitative results, extremely precise quantitative data can be obtained in cosmic rays. The understanding of these facts has led in recent times to the broadening of the scope of cosmic ray experiments with the introduction of the most modern techniques. Laboratories for the investigation of nuclear interactions have been carried beyond the limits of the atmosphere in multi-ton satellites (the first of these was "Proton-1", launched in 1965). In the investigative program of such laboratories we find:

1. The study of the dependence of the inelastic cross section of the nuclear interaction on energy in the interval from 10 to 10^4 GeV. For a nucleon-nucleon collision the cross section can be measured with a precision of 0.5% at 100 GeV and 3.6% at 10^3 GeV.

2. The study of the dependence of the cross section of the interaction of protons and α-particles on the dimensions of the target nucleus (precision of measurement 0.1--3% for collisions of α-particles with carbon nuclei).

3. Determination of the dependence of the multiplicity of secondary particles and their fluctuations on energy (precision of measurement of average multiplicity in p-p collisions of the order of 6.5% at 3×10^3 GeV).

4. Measurement of the coefficient of inelasticity and its distribution in a nucleon-nucleus collision.

5. Search for quarks.

These items do not exhaust the possibilities of this method [397].

Mountain stations at elevations of 3--5 km have been highly developed, with the construction of apparatus with Wilson chambers up to 2 m^2 in size, [51, 502] working in a magnetic field, together with ionization calorimeters with a surface area of tens of square meters. The utilization of supermagnets with fields of hundreds of thousands of gauss appears to be imminent.

Until recently research on such a scale was carried out mainly in the Soviet Union. Today the importance of this approach is recognized also in other countries. In the United States there is a proposal to construct an apparatus the scale of which exceeds anything that now exists. According to the authors, this apparatus will make it possible to investigate the effective cross section of the interaction of nucleons and pions with protons in the interval of energies from 100 to 10^3 GeV with a precision of 1 to 10%, the elastic scattering in this energy interval, and the general properties of nuclear interactions. It is also proposed to study ρ- and f-mesons in new heavy resonances. If particles like quarks are found, their properties will be studied.

The projected apparatus includes: 1) A gaseous (xenon) scintillation counter for the separation of primary protons and pions, with the use of the logarithmic ionization increase. 2) Magnets and spark chambers for measuring pulses of charged primary and secondary particles with a precision of 1--2%. 3) A hydrogen target 10 m^3 in volume (2 x 5 x 1 m) containing 700 kg of hydrogen. 4) An ionization calorimeter which will serve for the isolation of electrons, muons, protons, neutrons, and pions and permit the measurement of the energy of primary neutrons and secondary photons. The calorimeter contains 24 rows of ionization chambers (through each 3t-unit) and has an area of about 30 m^2. The height of the apparatus reaches 22.5 m. It is expected that it will register about

10^5 high-energy interactions per year ($E_0 > 100$ GeV). This number is comparable with that obtained in bubble chambers at an accelerator. Undoubtedly the already traditional methods using emulsion chambers and piles will continue to be used.

Thus, in a very few years we may expect a significantly wider range of experiments and, what is particularly important, an increase in their accuracy. Hence this is a good time to sum up what has already been accomplished.

The reviews of the nuclear interactions of cosmic particles that have come off the presses in last decade have been written by theoretical physicists, [19, 200, 290, 379]. In these reviews it is inevitable that the analysis of experimental results from the point of view of agreement with various theoretical models and schemes should dominate.

We have tried to approach the problem of nuclear interaction at superhigh energies from the position of the experimental physicist. Principal attention in the analysis has been given to an examination of the degree of validity of the available experimental facts.

The book we have written is the first attempt at a critical analysis of cosmic experiments and, as a first attempt, undoubtedly has its weak points.

In spite of the fact that we have tried to evaluate the available results objectively, in the treatment of a number of problems we have sometimes expressed ideas that differ from those generally accepted. However, this pertains first of all to those problems for which any other point of view would have the same degree of validity.

The book consits of three parts and 13 chapters. In the first part (Ch. I--III) we discuss some analytical methods and the features of experimental arrangements used in cosmic ray research. In the second part (Ch. V--XI) we examine the information on the basic characteristics of the elementary act of the nuclear interaction of cosmic particles. Where possible a comparison is made with the results obtained in accelerators. The third part (Ch. XII, XIII) sets forth the question of the primary cosmic radiation and its passage through the atmosphere. The phenomena accompanying this process are considered.

We have tried to adhere to the generally accepted notation for the various physical quantities; frequently, therefore, the same symbol stands for different characteristics (e.g., γ is the exponent of the energy spectrum and the Lorentz factor in relativistic transformations; σ is the effective cross section and the halfwidth of the angular distribution). The symbols are explained as they appear in the text.

The authors sincerely thank G. T. Zatsepin for reading the manuscript and making a number of valuable comments.

TABLE OF CONTENTS

Editor's Note iii
Monograph v
Preface vii

PART I

CHAPTER 1. Features of Cosmic Ray Experiments 1
1. The Effect of the Energy Spectrum of the Primary Cosmic Radiation on Measurement Results 1
2. General Approach to the Calculation of the Errors of the Method of Energy Measurement 2
3. Average Measured Characteristics of the Elementary Act . . . 4
4. The Case When the Dispersion d^2 Depends on Energy 8
5. Distortion of the Distributions 9

CHAPTER 2. Kinematic Methods for the Measurement of Particle Energy 11
1. Coordinate Systems 11
2. Estimate of the Energy of Collision From the Angular Distribution of the Created Particles [13-16] 17
3. Calibration of the Castagnoli Method 21
4. Further Development of Kinematic Methods for Energy Determination 27
5. Measurement of the Primary Energy From the Total Energy of the Charged and Neutral Particles 33
6. Measurement of the Energy of Primary Nuclear Fragments . . . 34

CHAPTER 3. The Ionization Calorimeter Method 40
1. Idea of the Method 40
2. Fundamental Processes in the Absorber of an Ionization Calorimeter 41
3. Constructional Features of a Calorimeter 46
4. Accuracy of the Energy Determination 48
5. The Hazards of Event Selection 54
6. Comparison of Different Methods of Energy Determination . . . 56

PART II

Introduction 58

CHAPTER 4. The Interaction Cross Section 61
1. The Study of Interaction Cross Sections at High Energies . . . 61
2. Experimental Methods for the Study of Cross Sections 64
3. Results of Experiments on Cross Sections 70
4. Cross Section of the Interaction of Mesons with Nuclei 78
5. Interaction Paths of Primary Nuclei 80

CHAPTER 5. Multiplicity and Nature of Secondary Particles 84
1. Introduction 84
2. Strongly Ionizing Particles 86
3. Multiplicity of Relativistic Particles n_s 89
4. Secondary Particles Produced in the Collision of Nuclei and Their Multiplicity 97
5. Multiplicity of Secondary Particles in the Collision of Pions with Nuclei 101
6. Distribution of the Multiplicity 105
7. Nature of the Secondary Particles 110

CHAPTER 6. Energy Spectra of Secondary Particles 116
1. Methods of Measuring the Energy of Secondary Charged Particles 116
2. Determination of Photon Energy 119
3. Energy Spectra of Secondary Particles in the Laboratory Coordinate System 125
4. Experiments in Cosmic Rays 132
5. Energy Spectra of π^0-Mesons 136
6. Energy and Momentum Spectra of Secondary Particles in the C System 143

CHAPTER 7. Transverse Momentum 155
1. Introduction 155
2. Distribution of Transverse Momenta 156
3. Dependence of the Average Magnitudes of Transverse Momentum on the Energy and Nature of the Colliding Particles 167

CHAPTER 8. Coefficients of Elasticity 172
1. Definitions 172
2. Measurement of Inelasticity 175
3. Average Values of the Inelasticity 182
4. Partial Coefficients of Inelasticity 190
5. The Relation Between the Coefficients α_0 and $\alpha_\pm$ 193
6. Conclusion 195

CHAPTER 9. Angular Distribution of Secondary Particles 196
1. Introduction 196
2. Some Features of the X-Representation 197
3. Experimental Data on the Angular Distribution of Secondary Particles 201
4. Angular Distribution of Charged Particles in the Laboratory System of Coordinates 206
5. Angular Distribution of Charged Particles in the Symmetric System (S System) 207
6. System of the Center of Mass of the Colliding Particles . . . 218
7. Mass of the Target Particle 231

CHAPTER 10. Four Dimensional Transferred Momentum 234
1. Definition of Four-Dimentional Transferred Momentum . . . 234
2. Analysis of Δ^2 Distributions 238

CHAPTER 11. A Summary 242

PART III.

CHAPTER 12. Energy Spectrum and Composition of the Primary Cosmic Radiation 247
1. Direct Measurements 247
2. Chemical Composition of the Primary Cosmic Radiation . . . 253
3. Measurements of the Intensity of the Cosmic Radiation at the Bottom of the Atmosphere 258
4. Ratio of Neutral and Charged Particles Producing Showers . . 273
5. The Muon Component of Cosmic Rays 277

CHAPTER 13. The Nuclear Cascade Process in the Atmosphere . . 285
1. Introduction 285
2. The Equations of the Nuclear Cascade Process 286
3. The Role of Pions in the Atmosphere 293
4. Calculation of the Change of Slope of the Primary Spectrum. . 297
5. Conclusion 298

Appendix 299

References 302

PART I

CHAPTER 1

FEATURES OF COSMIC RAY EXPERIMENTS

1. The Effect of the Energy Spectrum of the Primary Cosmic Radiation on Measurement Results

The main feature of cosmic ray experiments is the sharp drop in the spectrum of the primary cosmic particles. /7*

The energy spectrum of cosmic particles can be represented in the form of a power law $dN/dE_0 \sim E_0^{-\gamma}$, with the exponent γ of the order 2.7 to 3.0 and very weakly dependent on energy up to 10^5--10^6 GeV.

This characteristic of the primary spectrum, under the condition of independence (or of weak dependence) of the characteristics of the elementary act on energy, causes the energy spectra of the secondary components also to have the form of power functions, although the magnitude of the exponent γ can be different. This feature of the energy spectrum of the cosmic radiation creates a number of unique effects in the measurement of the characteristics of the elementary interaction process.

The effect of the sharply dropping spectrum on the measured characteristics was considered in [1-8]. If the average energy of the particles is measured correctly, their true energy for a monoenergetic beam can be measured with any degree or accuracy.

For this type of spectrum even the average energy of the particles, as well as the average parameters of the interaction, cannot be determined without the introduction of corrections that depend on the degree γ and the mean square error of the measurement of the energy of the individual particles.

---

*Numbers in the margin indicate pagination in the foreign text.

Certain special cases of the calculation of these corrections are considered in the references cited above. Usually, specific methods of energy measurement, for example the Castagnoli method is photoemulsions or in a Wilson chamber, [3, 4] as well as the methods used in the investigation of wide atmospheric showers, [2] have been considered.

Nikishov and Rozental [1] have studied the distribution of possible values of energy as a function of the total number of particles formed in the interaction and have shown that the mean value of the energy is overestimated several times over /8
if the Castagnoli method is used to measure the energy. The problem was analyzed on the basis of the predictions of the Landau theory on the distribution of the multiplicity of the created particles n_s and the dependence of the dispersion of the angular distribution σ^2 on energy.

The effect of the spectrum on the determination of the energy was also considered by Takibaev, [3] who calculated the mean square error of the Castagnoli method from the formula $d = \pm\sigma/\sqrt{n_s}$. The mean values of σ and n_s were taken from experiments. It was found that the average value of the energy was overestimated by a factor of 2, which agrees with the conclusions of similar work by Montanet et al., [4].

Approximately the same overestimation of measured energy occurs in determining it from the number of particles in wide atmospheric showers. This result was obtained by Zatsepin and Dedenko [2].

In a number of other papers the Castagnoli method has been criticized without the mention of quantitative results [9].

In Section 2 it will be shown that, as a result of the effect of the specific form of the spectrum of the cosmic radiation, there can be a deviation of not only the average value of the measured energy, but also of many other characteristics of the interaction of particles [5, 5a]. In this, the method of choosing the events under study plays the principal role (registration threshold; see Section 2).

2. General Approach to the Calculation of the Errors of the Method of Energy Measurement

2.1. Sources of Deviations in the Measured Characteristics

Deviation of the average characteristics of the elementary acts occurs because of the simultaneous effect of the energy spectrum, inaccurate determination of the energy in individual cases, and the threshold for the selection of the /9
investigated phenomena [5, 5a].

Let us say that in each case $E = \Delta E_0$ (E is the measured energy, E_0 is the true energy, and Δ runs from 0 to ∞). The distribution of the quantity ∞, i.e., the distribution of the probability of this or that energy deviation is $W(\Delta)\, d \ln \Delta$.

The threshold effects are determined by the specific conditions of the experiment. If the selection of events is made according to some parameter that depends on energy E_0, i.e., $P(E_0) > \varepsilon_0$, then $P(E/\Delta) > \varepsilon_0$, and for the threshold value ε_0 the variable Δ has the value $\Delta_0 = \varphi(\varepsilon_0, E)$.

Let the primary energy spectrum have the form $[\partial N(E_0)/\partial E_0]\, dE_0$. Then the number of events with a given measured energy $[\partial N(E)/\partial E]\, dE$ can be determined from the following formula:

$$\frac{\partial N(E)}{\partial E} dE = \int_{-\infty}^{\ln \Delta_0} \frac{\partial N(E_0)}{\partial E_0} dE_0 W(\Delta)\, d\ln\Delta = \int_{-\infty}^{\ln \Delta_0} \frac{\partial N(E/\Delta)}{\partial E} dE W(\Delta)\, d\ln\Delta. \quad (1.1)$$

In a similar way, we can treat the deviation of the average values of the parameters of the elementary act (see Section 3).

2.2. Probability Distribution of the Errors of Energy Measurement

The probability distribution $W(\Delta)\, d\ln\Delta$ is conveniently represented in the Gaussian form

$$W(\Delta)\, d\ln\Delta = (d\sqrt{2\pi})^{-1} \exp[-(\ln\Delta)^2/2d^2]\, d\ln\Delta \quad (1.2)$$

This form is convenient because the function (1.2) is symmetric about $\Delta = 1$ and is normalized to unity. In the general case $W(\Delta)$ can be represented as a sum of Gaussian distributions with the appropriate assortment of d and, possibly, shifted relative to $\langle\Delta\rangle = 1$.

The shift of the function $W(\Delta)$ relative to $\langle\Delta\rangle = 1$ implies the existence of a systematic error in the energy determination. The function which takes account of the systematic error has the form /10

$$W(\Delta)\, d\ln\Delta = (d\sqrt{2\pi})^{-1} \exp\left[\frac{(\ln C - \ln\Delta)^2}{2d^2}\right] d\ln\Delta. \quad (1.2a)$$

The quantity C shows how much the mean energy is under- or overestimated.

Thus, the results obtained through the use of (1.2) can be easily generalized to other cases.

2.3. Choice of Functions Accounting for the Threshold of Event Selection

We shall consider three special cases.

1. The selection is based on a parameter that depends on energy.

$$\text{Let } P = P_0 E_0^s. \text{ Then } P = P_0\left(\frac{E}{\Delta}\right)^\beta,\ \Delta^\beta = \frac{P_0}{P}E^\beta.$$

If the threshold value of P is P_{min}, then $\Delta_0 = (P_0/P_{min})^{1/\beta}E$, and

$$\ln\Delta_0 = \frac{1}{\beta}\ln\frac{P_0}{P_{min}} + \ln E. \qquad (1.3)$$

2. Special case: selection made according to true energy $E_0 > \varepsilon_0$,

$$\ln\Delta_0 = \ln\frac{E}{\varepsilon_0}. \qquad (1.4)$$

A similar dependence arises if showers in a photoemulsion are selected according to the energy of the electromagnetic cascades,

$$\ln\Delta_0 = \ln k\frac{E}{\varepsilon_0}. \qquad (1.5)$$

3. Dependence of the selection parameter on energy has the form $P = P_0 \ln E_0$.

Then

$$\ln\Delta_0 = \ln E - \frac{P_{min}}{P_0}. \qquad (1.6)$$

3. Average Measured Characteristics of the Elementary Act

3.1. Power Dependence on Energy

Measurement of the characteristics of an elementary act, the true dependence of which on energy is described by the power function /11

$$x_0 = aE_0^s, \qquad (1.7)$$

leads to an average measured value $\langle x \rangle$ in the form [5, 5a]:

$$\langle x \rangle = aE^s \frac{\exp\left[(s-\gamma+1)^2 \frac{d^2}{2}\right][1+\Phi(q_1)]}{\exp\left[(1-\gamma)^2 \frac{d^2}{2}\right][1+\Phi(q_2)]}; \tag{1.8}$$

$$q_1 = (s-\gamma+1)\frac{d}{\sqrt{2}} + \ln \Delta_0 / d\sqrt{2}; \tag{1.9}$$

$$q_2 = (1-\gamma)\, d/\sqrt{2} + \ln \Delta_0 / d\sqrt{2}, \tag{1.10}$$

where $\Phi(q)$ is the Gaussian integral

$$\Phi(q) = \frac{2}{\sqrt{\pi}} \int_0^q e^{-t^2} dt. \tag{1.11}$$

Proof:

$$\langle x \rangle = \frac{\int_{-\infty}^{\ln \Delta_0} (d\sqrt{2\pi})\, AE_0^{-\gamma}\, dE_0\, aE_0^s \exp[(\ln \Delta)^2 / 2d^2]\, d \ln \Delta}{\int_{-\infty}^{\ln \Delta_0} (d\sqrt{2\pi})\, AE_0^{-\gamma}\, dE_0 \exp[(\ln \Delta)^2 / 2d^2]\, d \ln \Delta} =$$

$$= aE^s \frac{\int_{-\infty}^{\ln \Delta_0} \Delta^{\gamma-1-s} \exp[(\ln \Delta)^2 / 2d^2]\, d \ln \Delta}{\int_{-\infty}^{\ln \Delta_0} \Delta^{\gamma-1} \exp[(\ln \Delta)^2 / 2d^2]\, d \ln \Delta}.$$

The latter expression is easily integrated. As a result, we obtain the desired formula (1.8).

3.2. Measurement of the Number of Particles

The number of particles in the interval of measured energies E, E + dE is described by Eq. (1.1), using (1.2a): /12

$$\frac{dN}{dE} = \int_{-\infty}^{\ln \Delta_0} AE_0^{-\gamma} dE_0 d\sqrt{2\pi} \exp\left[-\frac{\ln (C - \ln \Delta)^2}{2d^2}\right] d \ln \Delta =$$

$$= C^{\gamma-1} AE^{-\gamma} \exp\left[\frac{(\gamma-1)^2 d^2}{2}\right] \frac{[1+\Phi(q_2)]}{2}. \tag{1.12}$$

In the limiting case of a very low threshold or high energies,

$$\frac{dN}{dE} = AE^{-\gamma} C^{\gamma-1} \exp\left[\frac{(\gamma-1)^2 d^2}{2}\right], \tag{1.13}$$

i.e., the spectrum has the correct slope, but the absolute intensity is overestimated by a factor $C^{\gamma-1}\exp[(\gamma-1)^2 d^2/2]$.

3.3. Measurement of the Coefficient of Inelasticity

The averaged measured coefficient of inelasticity $<K>$ is expressed in the following form [5, 5a]:

$$<K> = K_0 \frac{\exp\left[(\gamma-2)^2 \frac{d^2}{2}\right][1+\Phi(q_3)]}{\exp\left[(\gamma-1)^2 \frac{d^2}{2}\right][1+\Phi(q_2)]}, \qquad (1.14)$$

where K_0 is the true inelasticity, $q_3 = d^{-1}\ln\Delta_0 - (\gamma-2)d$; q_2, see Eq. (1.10).

3.4. Measurement of the Average Multiplicity

The average multiplicity n_s is calculated from (1.8) in the region of energy where the dependence of n_s on energy is determined by a power function (see Chapter V).

3.5. Logarithmic Dependence of the Investigated Variable on Energy (Measurement of the Dispersion of the Angular Distribution σ and, Possibly the Multiplicity n_s)

Let $<\sigma_{true}> = \sigma_0 \ln E_0 + Q$; then in the limiting case of a very low threshold for the selection of events ($\ln\Delta_0 \to \infty$) we have

$$\begin{aligned} <\sigma_{meas}> &= \sigma_0 \ln E + Q - d^2\sigma_0(\gamma-1) = \\ &= <\sigma_{true}> - d^2\sigma_0(\gamma-1), \end{aligned} \qquad (1.16)$$

where σ_{true} and σ_{meas} are the true and measured values of the variable σ.

3.6. Conclusions

All this shows that, because of the specific form of the energy spectrum of the cosmic radiation, there arises a number of effects that distort the average characteristics of the interaction. The degree of distortion is determined by the magnitude of the dispersion of the errors in the measurement of the energy in individual cases d^2, the exponent of the power law of the energy spectrum, and the selection threshold. Figures 1--3 show the results of a calculation of the meas-

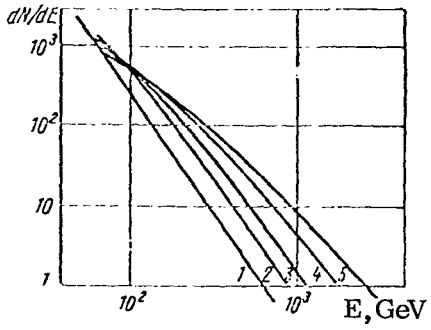

Figure 1. Distortions of the Energy Spectrum Due to Errors in the Measurement of Energy.

1 - true spectrum (d = 0); 2 - d = 0.75; 3 - d = 1.00; 4 - d = 1.30; 5 = 1.60.

ured characteristics with definite assumptions about the character of the true dependences

$$K_0 = 1, \quad \gamma = 3 \text{ and } n_s = n_s^0 E^{1/4}$$

and for different values of the dispersion and the energy threshold for selection. The minimum deviations of the average measured quantities occur near the threshold, and the maximum deviations are in the region where the threshold is of no consequence. In this region the energy dependences acquire their true form. The energy at which the threshold ceases to have effect is many times greater than the threshold value.

Thus, the question of the systematic errors of experimental results is resolved /14 if the mean square error of the measurement of energy by the applied method is known.

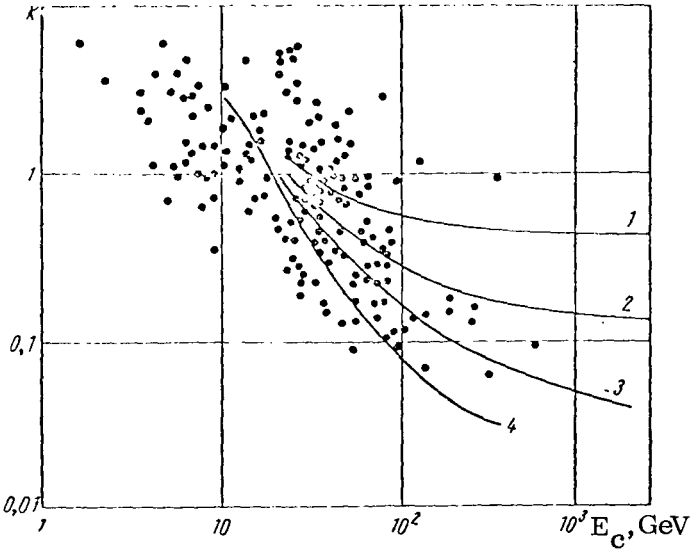

Figure 2. Deviations of the Coefficients of Inelasticity Due to Errors in the Measurement of Energy.

1 - d = 0.75; 2 - d = 1.00; 3 - d = 1.30; 4- d = 1.60; points experimental [6].

4. The Case When the Dispersion d^2 Depends on Energy

In this case the function $W(E, E_0)$ is not homogeneous. If d depends on energy, the energy dependences will deviate not only near the threshold for the selection of events, but also in the entire region of energy where d varies. /15

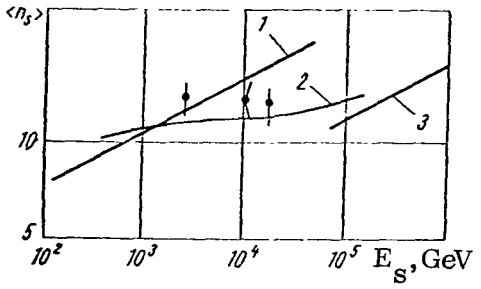

Figure 3. Deviations of the Multiplicity Due to Errors in the Measurement of Energy.

1 - $n_s \sim E^{1/4}$; 2 - calculation from Eq. (1.8); d = 1.6; 3 - calculation with no selection threshold, d = 1.6.

The deviations of the energy spectrum for this case were considered by Rozental and Shestakov [7]. The function $W(E, E_0)$ was chosen in the form of the normal distribution (1.2), but the dispersion $d^2 = \sigma^2/n_s$ depended on energy. The form of the dependence was chosen in accordance with the predictions of Landau's hydrodynamic theory:

$$\sigma^2 = \frac{1}{2} \ln \frac{E_0}{2m}; \qquad (1.17)$$

$$n_s = n_s^0 (E_0/m)^{1/4}; \qquad (1.18)$$

where $n_s^0 \sim 1.5$--2.0, and m is the mass of the particle.

The calculations showed that under these assumptions the magnitude of the exponent was very strongly affected. If the true value of γ was 2.8, then the measured value was 3.5. In a practical measurement of spectra the scale of energy is broken up into a number of intervals. If the exponent of the spectrum is determined at two points E_1 and E_2, then the experimental value of γ is related to the true value by the following relation:

$$\gamma_{exp} = \gamma_{true} - \frac{\gamma_{true} + 1}{2} \cdot \frac{E_1 - E_2}{E_1 E_2} \qquad (1.19)$$

In order that the measured exponent should not differ from the true one, it is necessary that the condition $|E_1 - E_2| \ll E_1$ be fulfilled. However, the interval $E_1 - E_2$ cannot be small, since it is necessary to provide sufficient statistical accuracy.

The determination of the energy spectrum of muons from the distribution of collisions in ionization chambers was also studied in [7]. In this case $W(E, E_0)$ is determined by the geometry of the chamber. For a spherical chamber the au-

thors indicate the following form for the connection between E and E_0 in individual cases: /16

$$W(E, E_0) = \begin{cases} \frac{8}{9} \cdot \frac{E}{E_0^2} & 0 < E < \frac{3}{2} E_0; \\ 0 & E > \frac{3}{2} E_0. \end{cases} \tag{1.20}$$

If the angular distribution of muons is independent of energy, then the exponent of the spectrum does not vary. For a spherical chamber this conclusion is valid also for a dependence of the angular distribution of muons on energy, whereas for flat chambers the exponent increases.

The inverse problem is also discussed in [7]. One can ask, how do you find the true spectrum $\partial N/\partial E_0$, if the function $W(E, E_0)$ and the experimental energy spectrum F(E), measured with sufficient accuracy, are known? The solution to this problem has the form

$$\frac{\partial N}{\partial E_0} = \sum_{i=0}^{\infty} b_i H_i(E_0);$$
$$b_i = \frac{d^{2n-1}}{2^i i!} \cdot \frac{\partial^n}{\partial E_0^n} F(E_0), \tag{1.21}$$

where $H_i(E_0)$ is a Hermite polynomial.

In the special case when the distribution is

$$W(E, E_0) = \begin{cases} a \text{ for } E - a < E < E_0 + a; \\ 0 \text{ for } E < E_0 - a;\ E > E_0 + a, \end{cases} \tag{1.22}$$

we have

$$\frac{\partial N}{\partial E_0} = -2a \frac{d}{dE_0} \left\{ \sum_{i=0}^{\infty} F[E_0 + (2i+1)a] \right\}. \tag{1.23}$$

5. Distortion of the Distributions

Until now, we have been considering the distortion of the average characteristics of the interaction. Obviously, the distributions of the measured quantities will also be distorted. Lohrmann [8] has considered this question in the case of distortion of the distribution of transverse pulses due to errors in measuring the energy of the secondary particles.

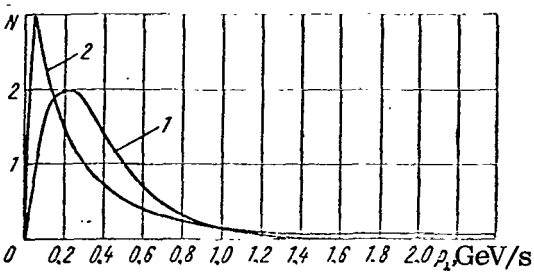

Figure 4. Distortion of the Distributions of Transverse Pulses in Using the Castagnoli Method for Energy Determination.

1 - measured distribution (d = 1.3);
2 - true distribution.

The energy of secondary particles in a nuclear interaction in the region of high energies is frequently determined from the angular distribution of tertiary β-mesons in the showers created by the secondaries. As is shown in Chapter II, this method has a marked dispersion d^2. Using the same approach as in the calculation of the average characteristics (see Section 3), we find the distribution of the measured transverse pulses: /17

$$N'(p'_\perp)\,dp'_\perp \sim \frac{dp_\perp}{p'_\perp} \times$$

$$\times \int_{p_\perp=0} p_\perp \exp\left[-\frac{p_\perp}{p_0} - \ln\left(\frac{p_\perp}{p'_\perp}\right)^2 \Big/ 2d^2\right] dp_\perp. \qquad (1.24)$$

It was assumed that the true distribution of $p_\perp$ has the form

$$N(p_\perp)\,dp_\perp \sim p_\perp \exp\left[-\frac{p_\perp}{p_0}\right] dp_\perp;$$

$$\langle p_\perp \rangle = 2p_0 = 0.38 \text{ GeV/s}. \qquad (1.25)$$

The results of the calculation of the distribution $N'(p'_\perp)dp'_\perp$, together with the true distribution, are shown in Fig. 4. The average measured value $\langle p'_\perp \rangle$ is overestimated by a factor of 1.8, and there appear cases of very high values of $p'_\perp$, whereas the true distribution is practically broken off at 1.5 GeV/s.

CHAPTER 2

KINEMATIC METHODS FOR THE MEASUREMENT OF PARTICLE ENERGY

1. Coordinate Systems

1.1. Definitions

We shall use Roman letters to label the different coordinate systems: laboratory system--L; system with a center of inversion--C; mirror--M; reflex--R; symmetric--S. All variables referred to a given system, with the exception of the laboratory system, will be labeled with the corresponding letter; variables in the laboratory system will be unlabeled. /18

The use of a system in which a given event possesses the maximum degree of symmetry greatly facilitates the solution of a physical problem. Let us consider these systems.

a. System with center of inversion (C-system). In a system with a center of inversion the sum of the momenta of colliding particles equals zero:

$$P_{1c} + P_{2c} = 0. \tag{2.1}$$

In this system the total energy of collision (the sum of the total energies of the colliding particles) has a minimum value.

b. Symmetric system (S-system). In the study of cosmic rays with the aid of Wilson chambers or photoemulsions only charged particles are observed. Hence for the symmetrization of the phenomenon one has to consider a system in which the sum of the momenta of the secondary charged particles is zero:

$$\sum_{i=1}^{n_s} P_{is} = 0. \tag{2.2}$$

Obviously, the sum of the total energies of the secondary charged particles in this case is a minimum. The symmetric system coincides with the inversion

system if the angular and momentum distribution of the neutral and charged particles are the same. /19

c. Laboratory system (L-system). In this coordinate system we have the instruments with which the elementary act is observed. In the majority of cases the target is at rest or has a small energy in this coordinate system. If there is a collision of a primary particle with a free nucleon, the latter can be considered to be at rest in the L-system. However, if the nucleon-target is part of a nucleus, it possesses a definite momentum and energy (the Fermi motion of nucleons in a nucleus).

If the Lorentz factor of a primary nucleon in the L-system is γ_0, then in a system fixed to the nucleon-target this Lorentz factor is changed by an amount

$$\frac{\Delta\gamma_0}{\gamma_0} \approx \frac{P_F}{m_p} \cos\theta_F. \qquad (2.3)$$

The Fermi momentum P_F is close to 200 MeV; hence the maximum change in γ_0 is $|\Delta\gamma_0/\gamma_0| \approx 0.2$. The Lorentz factor of the primary particle in the L-system will be symbolized by γ_0, the velocity by β_0.

d. Mirror system (M-system). The mirror coordinate system is fixed to the primary particle. In this system the primary particle is at rest and the target particle falls into it with velocity $-\beta_0$ and Lorentz factor γ_0.

e. Reflex system (R-system) [10]. The relax system moves relative to the C-system with the same velocity as the L-system, but in the opposite direction. Since the velocity of the L-system in the C-system is $-\beta_c$, the velocity of the R-system in the C-system is β_c. The relative velocity of the R- and L-systems, obviously, is equal to $\beta_{RL} = 2\beta_c/1 + \beta_c^2)$, and the corresponding Lorentz factor is $\gamma_{RL} = 2\gamma_c^2 - 1$. From the definition of the R-system it follows that its parameters are identical for particles of any mass, since it depends only on the rate of motion relative to the C-system and is not fixed to the moving particle. In the case of collision of particles of identical mass the reflex system coincides with the mirror system.

1.2. The Relation Between the Characteristics of Particles in the Different Systems.

We present some formulas for the transformation of variables most frequently encountered in practice from one coordinate system to another. /20

a. Transformation of angles. The transformation of the angle of departure of the i-th particle in a transition from the C-system to the L-system is

carried out according to the formula

$$\tan\theta_i = \sqrt{1-\beta_c^2}\,\frac{\sin\theta_{ic}}{\cos\theta_{ic}+\frac{\beta_c}{\beta_{ic}}} = \frac{1}{\gamma_c}\cdot\frac{\sin\theta_{ic}}{\cos\theta_{ic}+\rho_{ic}}. \qquad (2.4)$$

Here $\rho_{ic} = \beta_c/\beta_{ic}$, θ_i is the angle in the L-system, θ_{ic}, β_{ic} are the angle and velocity in the C-system, and β_c and γ_c are the velocity and Lorentz factor in the C-system relative to the L-system. This formula facilitates the transformation into any other coordinate system, if use is made of the appropriate values for the Lorentz factor and velocity. For example, transition to the reflex system is accomplished with the very same Lorentz factor as in the L-system, but the velocity β_c has the opposite direction. Consequently,

$$\tan\theta_{iR} = \frac{1}{\gamma_c}\cdot\frac{\sin\theta_{ic}}{\cos\theta_{ic}-\rho_{ic}}. \qquad (2.5)$$

Transition from the L-system to the reflex system:

$$\left.\begin{aligned}\tan\theta_{iR} &= \frac{1}{\gamma_{RL}}\cdot\frac{\sin\theta_i}{\cos\theta_i-\rho_{iRL}};\\ \rho_{iRL} &= \beta_{RL}/\beta_i.\end{aligned}\right\} \qquad (2.6)$$

Then, using the values

$$\beta_{RL} = \frac{2\beta_c}{1+\beta_c^2} \quad \text{and} \quad \gamma_{RL} = 2\gamma_c^2 - 1 \qquad (2.7)$$

(see the definition of the R-system), we find

$$\tan\theta_{iR} = \frac{1}{2\gamma_c^2-1}\cdot\frac{\sin\theta_i}{\cos\theta_i-\frac{2\beta_c}{(1+\beta_c^2)\beta_i}}^{*}. \qquad (2.8)$$

For the usually encountered case, when $\beta_c \sim 1$, we have /21

$$\tan\theta_{iR} = \frac{1}{2\gamma_c^2}\cdot\frac{\sin\theta_i}{\cos\theta_i-\rho_i}; \quad \rho_i = \frac{\beta_c}{\beta_i}. \qquad (2.9)$$

*$2\gamma_c^2 - 1 = \gamma_0$, if the masses of the colliding particles are equal.

If θ_{im} is the angle in the mirror coordinate system, then

$$\tan\theta_{iM} = \frac{1}{\gamma_0} \cdot \frac{\sin\theta_i}{\cos\theta_i - \frac{\beta_0}{\beta_i}}. \tag{2.10}$$

b. Transformation of energies. We have

$$\varepsilon_i = \gamma_c \varepsilon_{ic} (1 + \beta_{ic}\beta_c \cos\theta_{ic}); \tag{2.11}$$

$$\varepsilon_{iR} = \gamma_c \varepsilon_{ic} (1 - \beta_{ic}\beta_c \cos\theta_{ic}); \tag{2.12}$$

$$\varepsilon_{iM} = \gamma_0 \varepsilon_i (1 - \beta_i\beta_0 \cos\theta_i); \tag{2.13}$$

$$\varepsilon_{is} = \gamma_{sc} \varepsilon_i (1 + \beta_{ic}\beta_{sc} \cos\theta_{ic}); \tag{2.14}$$

$$\varepsilon_{iR} = \gamma_{RL} \varepsilon_i (1 - \beta_i\beta_{RL} \cos\theta_i) \approx \gamma_0 \varepsilon_i (1 - \beta_i\beta_c \cos\theta_i). \tag{2.15}$$

c. Transformation of total energy of collision E_0. We have

$$E_0 = E_1 + E_2, \tag{2.16}$$

where E_1 and E_2 are the energies of the first and second colliding particles.

In the L-system

$$E_2 = M_2c^2, \tag{2.17}$$

then

$$E_0 = E_1 + M_2c^2; \tag{2.18}$$

in the C-system

$$E_{0c} = \frac{1}{\gamma_c} E_0; \tag{2.19}$$

in the symmetric system

$$E_{0s} = \gamma_{sc} E_{0c}; \tag{2.20}$$

in the reflex system

$$E_{0R} = \gamma_c E_{0c} = E_0; \tag{2.21}$$

in the mirror system

$$E_{0M} = M_1c^2 + \frac{M_2}{M_1}E_1. \tag{2.22}$$

d. Transformation of the sum of the energies of the secondary particles. /22

$$\sum\varepsilon_i = \gamma_c\sum\varepsilon_{ic}; \tag{2.23}$$

$$\sum\varepsilon_{iR} = \gamma_c\sum\varepsilon_{ic}; \tag{2.24}$$

$$\sum\varepsilon_{is} = \gamma_{sc}\sum\varepsilon_{ic}; \tag{2.25}$$

$$\sum\varepsilon_{iM} = \gamma_0\sum\varepsilon_i(1 - \beta_i\beta_0\cos\theta_i). \tag{2.26}$$

e. Transformation of the coefficient of inelasticity. The coefficient of inelasticity is invariant under Lorentz transformations. For example,

$$K = \frac{\Sigma\varepsilon_i}{E_0} = \frac{\gamma_c\Sigma\varepsilon_{ic}}{E_{0c}\gamma_c} = \frac{\Sigma\varepsilon_{ic}}{E_{0c}}.$$

Similarly,

$$K = K_c = K_s = K_R = K_M. \tag{2.27}$$

It should be noted that in the proof of (2.27) the summation was carried out over all secondary particles (charged and neutral). Under these conditions the S- and C-system coincide.

f. Transformation of the total energy of the charged particles. According to the definition of the S-system, the sum of the momenta of the charged particles in it equals zero. If in this system the sum of the momenta of the neutral secondary particles is nonzero, it does not coincide with the C-system. In this case the energy of the secondary particles can be expressed in terms of the energy in the symmetric system with the aid of the following expressions (the summation is carried out over the charged particles):

$$\sum_{n_s}\varepsilon_{ic} = \gamma_{sc}\sum_{n_s}\varepsilon_{is}; \tag{2.28}$$

$$\sum_{n_s}\varepsilon_i = \gamma_c\gamma_{sc}(1 + \beta_c\beta_{sc})\sum_{n_s}\varepsilon_{is}; \tag{2.29}$$

$$\sum_{n_s}\varepsilon_{iR} = \gamma_c\gamma_{sc}(1 - \beta_c\beta_{sc})\sum\varepsilon_{is}. \tag{2.30}$$

The corresponding coefficients of inelasticity are equal ($\alpha_\pm$ is the inelasticity determined with respect to the charged particles, and the summation is /23

over the charged particles):

$$\alpha_{\pm s} = \frac{1}{\gamma_{sc}} \cdot \frac{\Sigma \varepsilon_{is}}{E_{oc}}; \tag{2.31}$$

$$\alpha_{\pm c} = \gamma_{sc} \frac{\Sigma \varepsilon_{is}}{E_{oc}}; \tag{2.32}$$

$$\alpha_{\pm} = \gamma_{sc}(1 + \beta_c \beta_{sc}) \frac{\Sigma \varepsilon_{is}}{E_{oc}}; \tag{2.33}$$

$$\alpha_{\pm R} = \gamma_{sc}(1 - \beta_c \beta_{sc}) \frac{\Sigma \varepsilon_{is}}{E_{oc}}. \tag{2.34}$$

If $\beta_c \beta_{sc} = 0$, the S-system coincides with the C-system, and

$$\alpha_{\pm s} = \alpha_{\pm c} = \alpha_{\pm} = \alpha_{\pm R} = \alpha_{\pm M}.$$

If $\beta_c \beta_{sc} > 0$, i.e., the direction of motion of the symmetric system in the C-system coincides with the direction of motion of the C-system in the L-system, then

$$\alpha_{\pm} > \alpha_{\pm c} > \alpha_{\pm s} > \alpha_{\pm R} > \alpha_{\pm M}. \tag{2.35a}$$

In the opposite case ($\beta_c \beta_{sc} < 0$),

$$\alpha_{\pm M} > \alpha_{\pm R} > \alpha_{\pm c} > \alpha_{\pm s} > \alpha_{\pm}. \tag{2.35b}$$

g. Interrelation of the Lorentz factors of the different systems.

$$\gamma_c = \frac{M_1 \gamma_0 + M_2}{\sqrt{2\gamma_0 M_1 M_2 + M_1^2 + M_2^2}}. \tag{2.36}$$

In the relativistic case ($\gamma_c \gg 1$ and $M_1 \gamma_0 \gg M_1, M_2$), we have

$$\gamma_c = \sqrt{\frac{E_1}{2M_2}}. \tag{2.37}$$

If the masses of the colliding particles are the same ($M_1 = M_2$), then

$$\gamma_c = \sqrt{\frac{\gamma_0 + 1}{2}}; \quad \gamma_0 = 2\gamma_c^2 - 1. \tag{2.38}$$

In a highly relativistic case ($\gamma_0 \gg 1$) /24

$$\gamma_c = \sqrt{\frac{\gamma_0}{2}}, \quad \gamma_0 = 2\gamma_c^2. \tag{2.39}$$

The Lorentz factor of the R-system in the L-system is

$$\gamma_{RL} = 2\gamma_c^2 - 1.$$

In the case of collision of particles of identical mass $\gamma_{RL} = \gamma_0$. The Lorentz factor of the M-system relative to the L-system is $\gamma_{ML} = \gamma_0$. The Lorentz factor of the S-system relative to the C-system can be related to the coefficients of inelasticy:

$$\frac{\alpha_\pm + \alpha_{\pm R}}{2\sqrt{\alpha_\pm \alpha_{\pm R}}} = \frac{1}{\sqrt{1-(\beta_c\beta_{sc})^2}} \approx \frac{1}{\sqrt{1-\beta_{sc}^2}} = \gamma_{sc} \qquad (2.40)$$

for $\beta_c \approx 1$.

In the collision of identical particles, the reflex system coincides with the mirror system. Then we arrive at the formula first obtained by Zatsepin [11] and used in [12]:

$$\gamma_{sc} = \frac{\alpha_\pm + \alpha_{\pm M}}{2\sqrt{\alpha_\pm \alpha_{\pm M}}}. \qquad (2.41)$$

The relation of the Lorentz factors of the other systems with each other can be obtained with the aid of the formula for combining Lorentz factors. If γ_{12} is the Lorentz factor of the first system relative to the second and γ_{23} is that of the second system relative to a third, then

$$\gamma_{13} = \gamma_{12}\gamma_{23} \pm \sqrt{\gamma_{12}^2 - 1}\sqrt{\gamma_{23}^2 - 1}. \qquad (2.42)$$

2. Estimate of the Energy of Collision From the Angular Distribution of the Created Particles [13-16]

2.1. The Half-Angle Method [14]

The formula for transformation of angles from the C- to the L-system (2.4) is often used to determine the Lorentz factor γ_c that appears in it. Thereby, a number of methods develop which are based on measurements of the angles of departure of secondary charged particles in the laboratory system of coordinates. /25

In case the energies of the created particles and the energy of the primary particle are large ($\beta_c \sim \beta_{ic} \sim 1$), we may assume that $\rho_{ic} = 1$. Then Eq. (2.4) simplifies to

$$\tan\theta_i = \frac{1}{\gamma_c}\operatorname{tg}\frac{\theta_{ic}}{2}. \qquad (2.43)$$

A second simplification is that in the C-system it is assumed that the scattering of the secondary charged particles is symmetrical. Then the angle $\theta_c = \pi/2$ separates one half of the particles from the other in the C-system. In the L-system there will also be a corresponding angle containing half the particles, $\theta_{1/2}$. Hence

$$\tan\theta_{1/2} = \gamma_c. \tag{2.44}$$

The elegance of this method in the framework of the assumptions made does not require comment. One can increase the statistical material for the determination of γ_c in an individual case if one introduces, in general, a harder combing out of the detailed correspondence of the departure angles of the particles forward and backward in the C-system, i.e., if one assumes that each particle with angle θ_{ic} corresponds to a particle with angle $\pi - \theta_{ic}$. If θ_f is the angle in the L-system and there is a fraction f of the particles inside a cone bounded by the angle θ_f, then

$$\gamma_c^2 = \operatorname{ctg}\theta_f \operatorname{ctg}\theta_{1-f}. \tag{2.45}$$

2.2. Basic Assumption of the Method

The assumption of symmetry is valid only when the charged and neutral particles are separately symmetrical in the C-system. Since only charged particles are observed in an experiment, as a rule, this condition cannot be checked (see Chapter IX). Therefore Eqs. (2.44) and (2.45) give the possibility of obtaining only the Lorentz factor of the S-system γ_s. The assumption $\beta_{ic} = \beta_c = 1$ is also very infrequently fulfilled. If $\rho_{ic} < 1$, i.e., $\beta_{ic} < \beta_c$, two values of θ_{ic} correspond to one value of θ_i. This leads to a mixing of the particles of the front and back cones.

2.3. The Castagnoli Method [16]

The method put forward by Castagnoli is based on the same hypotheses as the half-angle method, except that all the registered particles are employed in the determination of the Lorentz factor; hence there are fewer statistical errors in this method. /26

If we take the logarithm of (2.4), we obtain

$$\log\tan\theta_i = -\log\gamma_c + \log\frac{\sin\theta_{is}}{1+\cos\theta_{is}}. \tag{2.46}$$

Summing the left and right members of (2.46) over all charged particles and assuming symmetry of scattering of charged particles, we find

$$\log\gamma_s = -\frac{1}{n_s}\sum_{i=1}^{n_s}\log\tan\theta_i = -\langle\log\tan\theta_i\rangle. \tag{2.47}$$

In a number of papers attempts have been made to introduce corrections that take into account assumptions about the equality of the velocities of secondary particles in the symmetric system, [10, 15-17]. To this end, Castagnoli et al., [16] Boos and Takibaev, [15] Imaeda et al., [17] Shen and Kaplon, [10] and others have given attention to the energy distribution of secondary particles.

The calculation of the velocity distribution of pions in the symmetric system leads to the appearance in Eq. (2.47) of an additional term lg C.

$$\log \gamma_s = -\langle \log \tan \theta_i \rangle + \frac{1}{n_s} \sum U(\cos \theta_{is} \beta_{is}), \tag{2.48}$$

where

$$U(\cos \theta_{is} \beta_{is}) = \frac{\log (1 - \cos^2 \theta_{is})}{(\beta_e/\beta_{is}) + \cos \theta_{is} - 1}.$$

In order to present Eq. (2.48) in more symmetric form, we can introduce the correcting factor C

$$-\log C = \frac{1}{n_s} \sum_{i=1}^{n_s} U(\cos \theta_{is} \beta_{is}). \tag{2.49}$$

If $d^2n/d\varepsilon_s d\cos\theta_s$ is the angular and energy distribution of the secondary particles in the symmetric system, then /27

$$-\log C = \int_0^\infty d\varepsilon_s \int_{-1}^{+1} \frac{d^2n(\cos \theta_{is}, \varepsilon_{is})}{d\varepsilon_s d \cos \theta_{is}} U(\cos \theta_{is} \beta_{is})\, d \cos \theta_{is}. \tag{2.50}$$

The angular and energy distribution of particles must be taken from experiment or based on the theory of multiple creation of particles.

2.4. Statistical Error of the Castagnoli Method

The statistical error of the Castagnoli method is $\sigma/\sqrt{n_s}$. It follows from Eq. (2.47) that in the study of angular distributions it is convenient to use as an argument the quantity $x_i = \log \tan \theta_i$. Landau [18] was the first to call attention to this. We shall call the distribution of particles with respect to the x coordinate the x representation. It is obvious that the differential angular distribution of secondary charged particles in the scale $\log \tan \theta_i$, i.e., $dn/dx = d \log \tan \theta$, has center of inversion located at the point $\langle x \rangle = -\log \gamma_s$. The accuracy of determination of this inversion center depends on the number of particles and the dispersion

σ^2 of the angular distribution in the x representation:

$$\Delta \log \gamma_s = \left[\frac{<(x_i - <x_i>)^2>}{n_s}\right]^{1/2} = \left(\frac{\sigma^2}{n_s}\right)^{1/2}. \quad (2.51)$$

This is the theoretical accuracy of determination of $\log \gamma_s$ in the case when the deviations of x_i from $<x_i>$ have a statistical character, whereas the accuracy of determination of the angles θ_i is rather great. If the departures of the particles are correlated, the error in determining γ_s increases.

An interesting property of the x representation is that the transition from one energy γ_s' to another γ_s'' is related simply to the shift of the entire distribution along the x axis by an amount $\log(\gamma_s''/\gamma_s')$ for $\rho_{is} = 1$). Hence in the scale of x it is convenient to compare the angular distributions of the secondary particles for different energies. For this, the distributions for different energies are constructed in the coordinates

$$X = x - \log \gamma_s = \log \gamma_s \tan\theta. \quad (2.52)$$

By these same methods one normalizes the energies of different events for the study of their total angular distribution.* /28

If the angular distribution in the symmetric system is isotropic, then in the scale of x it is rather well described by a Gaussian curve with halfwidth 0.39 (see Chapter IX). For this halfwidth and a multiplicity of secondary particles of the order of ten the statistical error of the Castagnoli method equals $\sigma/\sqrt{n_s} = 0.12$, and

$$d = 2\frac{\sigma}{\sqrt{n_s}} \ln 10 = 0.55. \quad (2.53)$$

2.5. Method of Duller and Walker [13]

The integral F representation gives another way for a graphic determination of the quantity $\log \gamma_s$. If the angular distribution of secondary charged particles is isotropic in the symmetric system and F is the fraction of particles included in the angular interval $0 - \theta_s$ in the symmetric system, then

$$\log \frac{F}{1-F} = 2 \log \gamma_s + 2 \log \tan \theta_F. \quad (2.54)$$

*See also [19] about the properties of the x representation.

In the plane $\log\frac{F}{1-F} = f(x)$ we find a straight line intersection the axis of abscissas at $\log \gamma_s$. This method gives the same value for γ_s as the Castagnoli method. The assumption of isotropic scattering of particles is not obligatory. In the case of a different form for the angular distribution the integral representation (2.54) will not be represented by a straight line or its slope will be different. A value of ρ_{is} different from unity leads to similar changes. However, the point of intersection of the curve with the abscissa axis is determined by the symmetry of the dispersion of the particles

$$\frac{F}{1-F} = 1.$$

3. Calibration of the Castagnoli Method

3.1. Method

The deviation of the quantity γ_s determined by the Castagnoli method from the Lorentz factor γ_c of the C-system occurs because of failure of the assumption that $\rho_i = 1$ due to statistical fluctuations and the difference between the symmetric and C-systems. Hence, in order to elucidate the real accuracy of the Castagnoli method, it is necessary to know that the actual value of γ_c and to compare it with that determined from the angular distribution of the charged particles. The distribution of the deviations of γ_s from γ_c makes it possible to determine the mean square error d and the systematic error C (see Chapter I). /29

3.2. Utilization of Data Obtained in Accelerators

Measurements have shown that the mean square error d greatly exceeds the theoretical value (2.51). Figure 5 shows the distribution of $E_s = (2\gamma_s^2 - 1)mc^2$ for the case of the interaction of 30-GeV protons with a nuclear photoemulsion, [20]. To obtain the distribution interactions with $N_h \leq 5$ were selected, which in the majority of cases corresponds to nucleon-nucleon collisions. Very frequently the energy is overstated or understated by a factor of ten, particularly for showers with $n_s \geq 3$. /30

An analogous investigation was made by Lim [21] for primary pions with energy 17 GeV and also by Shen and Kaplon [10] for the collision of protons with nucleons at 28.5 GeV and of pions with nucleons at 17 GeV. In the latter work particles departing at angles of $\theta < 1°$ in the L-system for the case of p = N collisions and $\theta < 1.4°$ for π-N were excluded. This is necessary in order to exclude the primary particle which after interaction retains more than 70% of its initial energy, since the determination of γ_s is based on the angular distribution of newly created particles. /31

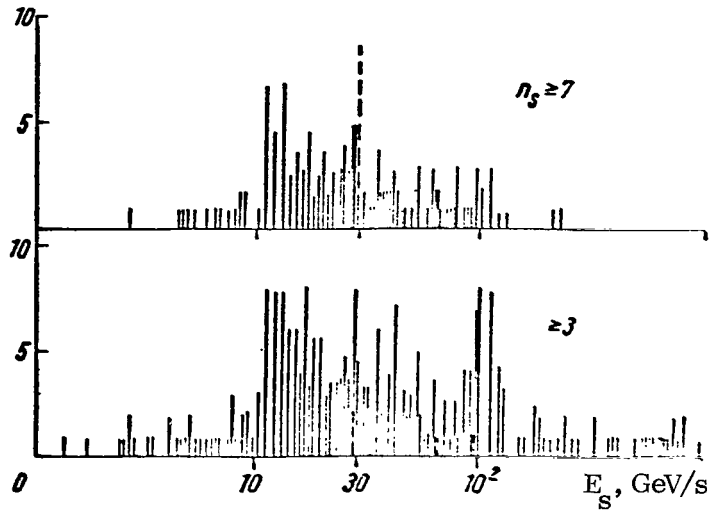

Figure 5. Distribution of E_s for the Interaction of Protons of Energy 30 GeV in a Photoemulsion With $N_h \leq 5$.

The results of Shen and Kaplon are shown in Fig. 6a, b. The distributions obtained are asymmetric, but if the symmetric part is separated out, the approximate value of d is found to be equal to 1 (instead of the theoretical value $d = 2\sigma \ln 10/\sqrt{n_s} = 0.55$ for cases of isotropic angular distribution of particles in the symmetric system). The average value of γ_s is 6.15, which is 1.6 times greater than γ_c (i.e., $C = 1.6$).

For the pion-nucleon interaction ($n_s \geq 4$), $d = 0.7$ and $C = 1.6$, which also exceeds the theoretical estimate.

3.3. Calibration According to Results Obtained from Cosmic Rays

At cosmic energies the mean square deviation d is twice as large as the theoretical value $2\sigma \ln 10/\sqrt{n_s}$. A large amount of material has been accumulated in cosmic ray investigations for the determination of d and C. Using a total absorption spectrometer, Lal et al., [22] studied the distribution of the ratio E_s/E_0 (E_0 is the energy measured by the spectrometer). At an energy of 60 GeV the magnitude of d is 1.5.

Using the results of [12] and [23], achieved with the aid of an ionization calorimeter and a Wilson chamber, the distribution of $\log \gamma_s/\gamma_c$ in the energy region 100--200 GeV was investigated. This distribution is sketched out in Fig. 7. It can be approximated by a Gaussian distribution with $d \sim 1.35$. Lohrman et al., [24] constructed the distribution of E_s/E_0, determining E_0 by the relative scattering method (see Chapter IV). At nucleon energies of about 250 GeV, $d = 1.35$.

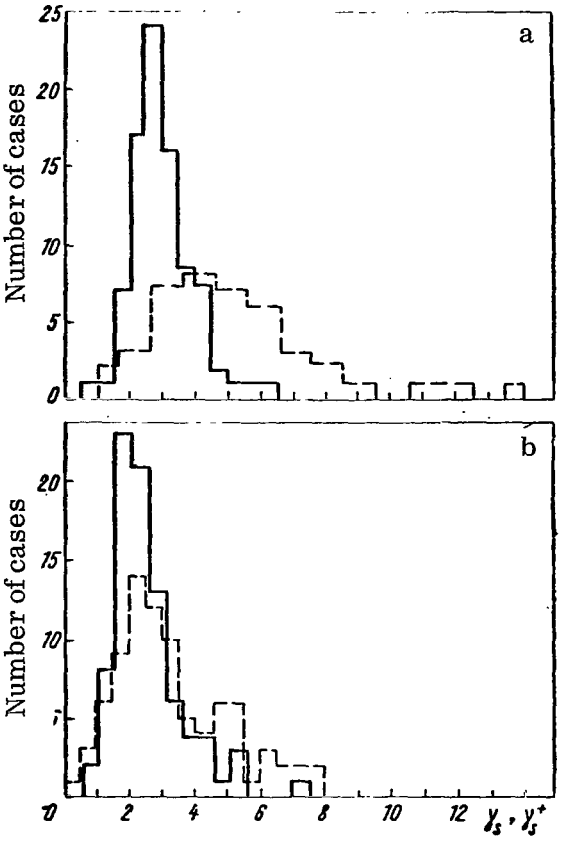

Figure 6. Distribution of γ_s (dashed line) and γ_s^+ (solid line) About the True Value γ_c:

a) for p-N Interactions With Energy 28.5 GeV in a Photoemulsion; b) for π-N Interactions at 17 GeV.

Finally, in the region of still higher energies ($E_0 \sim 10^3$ GeV), Abraham et al., [25] by observing the fragmentation of a primary nucleus with Z = 15, obtained the distribution of $\log\gamma_s$ for an almost monoenergetic beam of nucleons (see Fig. 7b). This distribution gives the value $d \sim 1.25$. /32

On the basis of these results, it is possible to conclude that the Castagnoli method has a significant dispersion d^2 that depends little on energy. The numerical value of d is within the limits 1.1 to 1.5, which is more than twice as high as the statistical error. This discrepancy is due to the asymmetry of the dispersion of charged particles in the C-system, i.e., in the final analysis, to definite correlations in the departure of the particles. The Fermi momenta of nucleons in the nucleus (see Section 1) also contribute to an increase in the deviation, and the scatter in the measured values of energy reaches 10%. /33

3.4. Systematic Errors: On the Average, Energy is Overestimated

To evaluate the quality of a method it is insufficient to know the mean square error. It is also necessary to take into account the possibility of a systematic error in the measured energy. In an experiment this systematic error can be detected only in case the true value of γ_c is determined by an independent method.*

An investigation of the question of systematic errors has been carried out by many authors [26]. To determine the correction factor C, the results of the determination of γ_s with no account taken of the term log C [see Eq. (2.49)] were

*To avoid misunderstanding, we note that this systematic error in energy has no relation to the overestimation of average energy due to the sharp drop in the spectrum of the generating particles (see Chapter I).

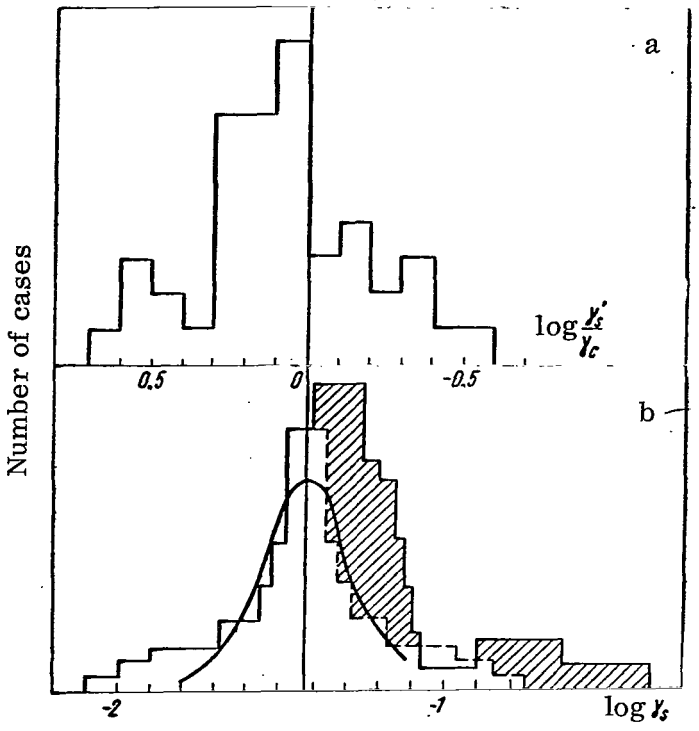

Figure 7. Distribution of the Quantity $\log\gamma_s/\gamma_c$:

a) for Interactions of Nuclear-Active Particles in LiH [12]; b) for the Family No. 1115 [25] (Continuous Histogram). The Hatched Portion is supposed to be Due to Nucleons That Have Experienced Interactions During Fragmentation, Which are not Taken Into Account in Estimating the Energy of the Primary Nucleus. The Smooth Curve Corresponds to a Distribution With Half-width ± 0.16.

compared with the known energy of the primary particles. It was found that the energy was on the average overestimated, i.e., C > 1. The experimental value of C in various experiments differs somewhat. In the work of Shen and Kaplon mentioned above C ~ ~ 1.6 ($N_h = 0.1$).

In another accelerator experiment, [27] C = 1.13. Using cosmic rays, Lohrman et al., [24] found C = 1.6 for events with $N_h > 5$.

In a number of papers the magnitude of C was calculated by the Monte Carlo method or from formulas analogous to (2.49), and different assumptions were made about the distribution of transverse momenta and departure angles of the secondary particles.

Settles and Huggett [26] calculated C by the method of statistical testing at energy of the primary particle of E_0 ~ ~ 3000 GeV. They considered an isotropic angular distribution and distribution of $d\Omega/\sin\theta_s$ and Gaussian and asymmetric distributions of $p_\perp$. It was found that the magnitude does not depend much on the choice of angular distribution, but changes from 1.4 to 1.7 in going from a Gaussian to an asymmetric distribution of $p_\perp$. The magnitude of the dispersion of the distribution of $\log\gamma_s$, on the other hand, depends more strongly on the form of the angular distribution than on the distribution of $p_\perp$. Shen and Kaplon [10] in calculating C considered two distributions /34

$$f(p_\perp) = \delta(p_\perp - \langle p_\perp\rangle); \qquad (2.55)$$

$$f(p_\perp) = \frac{2}{a^2} p_\perp \exp\left(-\frac{p_\perp^2}{a^2}\right) dp_\perp;$$
$$\langle p_\perp\rangle = \frac{\sqrt{\pi}}{2} a = 0.35 \text{ GeV/s}. \qquad (2.56)$$

With the distribution of $p_\perp$ in the form (2.55), C turned out to be 1.07. If instead of $< p_\perp >$ one used the distribution (2.56), then C = 1.18.

The authors also calculated a correction under the assumption that 25% of all secondary particles are K-mesons. If $< p_\perp >$ for k-ons is the same as for pions, then C = 1.20.* Table 1 gives other experimental and calculated data on the magnitude of C.

TABLE 1. EXPERIMENTAL AND CALCULATED VALUES OF C

C	Remarks	Reference
1.4	Photoemulsion, $7 < E_0 < 100$ GeV/nucleon	28
1.49	Photoemulsion, experiments with pions and protons in accelerators	29
1.55	Photoemulsion, accelerators	30
1.4		31
1.4--1.6	Calculated, Landau spectrum of secondary particles	32
1.4--2.0	Calculated, Heisenberg theory	16

3.5. Dependence of C on the Size of the Target Nucleus

In collisions with heavy nuclei, as a result of secondary interactions or mass increase of the target, the departure angles of secondary particles in the L-system increase and the experimentally found values of C decrease. Thus, for the case of collisions with heavy nuclei ($N_h > 5$), Lohrman observed an underestimation of energy in the L-system by a factor of 1.8 ($C \approx 0.75$), whereas for $N_h < 5$, $C \approx 1.3$. Erofeeva et al., [34] found that the factor C was close to 1 for collisions of nucleons with carbon nuclei and much less than one for collisions with aluminum nuclei. /35

*Imaeda and Shah [33] also considered the effect of distributions of transverse momenta on the magnitude of C. For different distributions of p the magnitude of C varied from 1.09 to 1.7. This quantity is sensitive to the fraction of heavy particles in the secondaries, since they have a higher momentum $p_\perp$ on the average (see Chapter VII).

3.6. Distortion of Observed Characteristics

In many cases, the Castagnoli method gives an inadmissably large distortion of the experimentally observed characteristics. If we substitute into the formulas of Chapter I the dispersion values 1.2—1.6 characteristic of the Castagnoli method and an energy threshold for event selection $\varepsilon_0 > 50$ GeV,* we find that /36 threshold effects are important up to energies a hundred times greater than the threshold value.

If the true dependence of the multiplicity on energy has the form $n_s = n_s^0 E_0^{1/4}$, then in the experiment, because of the reasons given in Chapter I, there appears a region of apparent saturation of multiplicity extending to energies of the order of 10^4 GeV. For these same reasons the energy spectrum of nuclear-active particles studied by the Castagnoli method in photoemulsions has a power dependence less than the true one. Figure 8 serves as an illustration of this, as well as the experimental results taken from [35]. Thus, the Castagnoli method is not suitable for the measurement of spectra, coefficients of inelasticity in the laboratory system of coordinates, the multiplicity etc., (see Figs. 1, 4, 8).

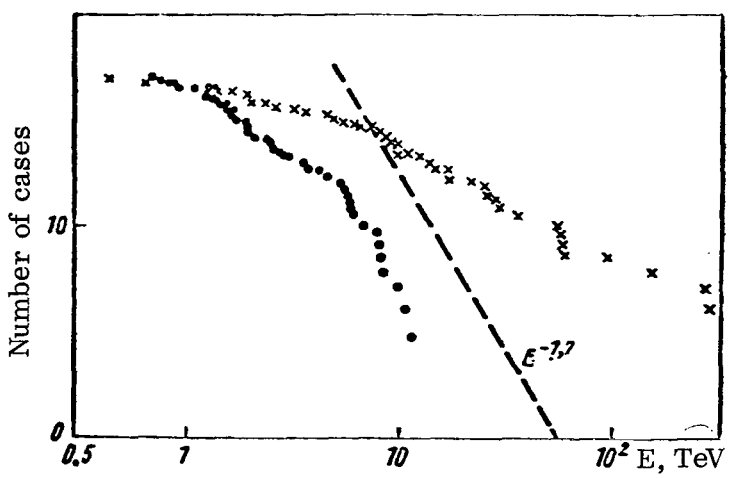

Figure 8. Spectrum of Primary Particles Obtained in a Measurement of Energy by the Castagnoli Method (crosses); Spectrum of Electron-Photon Cascades (points); Expected Spectrum of Primary Particles [35] (dashed line).

*This is the typical threshold value for photon cascades in photoemulsions.

4. Further Development of Kinematic Methods for Energy Determination

In recent years, along with criticism of the Castagnoli method, there have been attempts to avoid some of the assumptions of the method. However, almost all of these amount to the establishment of average corrections that do not eliminate all the errors. The basic problem is the large dispersion d^2.

A successful attempt to overcome these difficulties, which leads to a sharp reduction of the dispersion d^2, was undertaken by Shen and Kaplon [10].

a. Assumptions. The authors started from the fact that the principal errors of the Castagnoli method spring from two assumptions: $\rho = 1$ and the symmetry of particle scattering in the C-system.

Shen and Kaplon decided to replace these assumptions with others that were more general experimentally. They started from the facts that usually one measures only charged particles in the L-system, the transverse momentum does not depend on departure angle and on particle energy, and the mean energy of pions in the C-system is 0.5 GeV, i.e., the condition $\beta_c/\beta_{ic} = \rho_{ic} \approx 1$ is approximately fulfilled.

b. Mathematical formulation of the method. The treatment is carried out /37
in several coordinate systems: L, S, C and R (see Section 1). The Fermi motion of nucleons in the nucleus is not taken into account. In the method of Shen and Kaplon the starting relation for the determination of γ_c is not the formula for the transformation of angles, as in the Castagnoli method, but the formula for the transformation of energies (see Section 1).

Comparing the symmetric and laboratory systems [Eq. (2.28)], we find

$$\gamma_c = \frac{1}{\gamma_{sc}(1+\beta_c\beta_{sc})} \cdot \frac{\Sigma\varepsilon_i}{\Sigma\varepsilon_{is}} \tag{2.57}$$

(for notation, see Section 1).

Using the constancy of transverse momentum, it is possible to express ε_i and ε_{is} in terms of $< p_\perp >$ and the departure angles of the particles θ_i and θ_{is}. Then, to the accuracy of terms

$$\sim \frac{1}{8}\left(\frac{m_\pi c}{<p_\perp>}\right)^4 \Sigma \sin^4\theta_i$$

we obtain

$$\gamma_c = \frac{\gamma_s^+}{\gamma_{sc}(1+\beta_c\beta_{sc})}, \tag{2.58}$$

where

$$\gamma_s^+ = \left(\frac{1+\zeta}{1+\zeta^+}\right)\frac{\Sigma \csc\theta_i}{\Sigma \csc\theta_{is}}; \tag{2.59}$$

$$\zeta = \frac{1}{2}\left(\frac{m_\pi c}{\langle p_\perp\rangle}\right)^2 \frac{\Sigma \sin\theta_i}{\Sigma \csc\theta_i}; \tag{2.60}$$

$$\zeta^+ = \frac{1}{2}\left(\frac{m_\pi c}{\langle p_\perp\rangle}\right)^2 \frac{\Sigma \sin\theta_{is}}{\Sigma \csc\theta_{is}}. \tag{2.61}$$

Thus, to determine γ_c it is necessary to know the angular distribution in the laboratory and symmetric coordinate systems and the magnitude of β_{sc}(or γ_{sc}).

c. Calculation of the deviation of $\langle \rho_{is} \rangle$ from 1. We shall approximate the angular distribution in the symmetric system by

$$f(\theta_s)\,d\theta_s = A_n \sin^n\theta_s \sin\theta_s d\theta_s \tag{2.62}$$

$$f(\theta_s)\,d\theta_s = A_m \cos^m\theta_s \sin\theta_s\, d\theta_s.$$

It is obvious that ζ and $\Sigma\csc\theta_{is}$ in Eq. (2.59) depend on n or m for the chosen form of the angular distribution. To determine n and m one can use the experimentally observed magnitude of σ^2, the dispersion of the angular distribution. In the special case $\rho_{is} = 1$, the dispersion σ^2 is a Lorentzian invariant. However, in the general case it depends on ρ_s. Hence one can establish the connection between n, m, σ and ρ_s. Assuming that the velocities β_{is} have a sufficiently narrow distribution, we may say

/38

$$\rho_{is} = \langle \rho_{is} \rangle = \left\langle \frac{1}{\beta_{is}} \right\rangle = \langle \rho \rangle.$$

If the function of the angular distribution g(x) = g(log tan θ) corresponds to the functions f(θ_s) [the connection is established in Eq. (2.4)], then

$$\sigma^2 = \int (x - \langle x \rangle)^2 g(x)\, dx.$$

The results of the calculation of σ as a function of $\langle \rho \rangle$ for different n and m are shown in Fig. 9, [10].

From (2.4) we can determine

$$\sum \operatorname{ctg}\theta_i = \gamma_s \sum \frac{\beta_i/\beta_{is}}{\sin\theta_{is}} = \gamma_s \langle \rho_{is} \rangle \sum \csc\theta_{is} = \\ = \langle \rho_{is} \rangle \left(\frac{1+\zeta}{1+\zeta^+}\right) \sum \csc\theta_i . \tag{2.63}$$

Consequently,

$$\langle \rho_{is} \rangle = \left(\frac{1+\zeta^+}{1+\zeta}\right) \frac{\Sigma \operatorname{ctan}\theta_i}{\Sigma \csc\theta_i} . \tag{2.64}$$

By calculating σ from the experimental data, it is possible to find the values of n or m (see Fig. 9) preliminarily for $\langle \rho \rangle = 1$. This gives the possibility of computing ζ^+ and the first approximation of $\langle \rho \rangle_1$ from Eq. (2.64).

Repeating the procedure with the value found for $\langle \rho \rangle_1$ leads to new values of n (or m). Thus, by iteration, we can find sufficiently accurate values of n or m. We then have the possibility of determining ζ and γ_s^+ with account taken of the deviation of $\langle \rho \rangle$ from 1. If the asymmetry of the showers is not taken into account, i.e., assuming that the symmetric system coincides with the C-system, then $\beta_{sc} = 0$ and $\gamma_c = \gamma_s^+$. Therefore, the quantity γ_s^+ may be considered as the next approximation to the true value γ_c in comparison with the Castagnoli method. /39

The advantages of the second approximation are illustrated in Fig. 6, where the distributions of γ_s and γ_s^+ about the true value γ_c are compared for the case of the interaction of protons with nucleons at 28.5 GeV. The distribution of γ_s^+ was found to be much narrower than the distribution of γ_s.

d. Calculation of the motion of the symmetric system. There still remains an error connected with the assumption of symmetry of the showers with respect to charged particles in the C-system. In general, asymmetry in the C-system /40 arises if the symmetric system oves relative to the C-system with velocity $\beta_{sc} \neq \neq 0$. According to Shen and Kaplon, this velocity can be found in the following way.

Consider the coefficients of inelasticity α determined from the charged particles in the L- and R-systems (see Section 1). According to Eq. (2.40),

$$\frac{1}{\sqrt{1-(\beta_c\beta_{sc})^2}} = \frac{1+\alpha/\alpha_R}{2\sqrt{\alpha/\alpha_R}} .$$

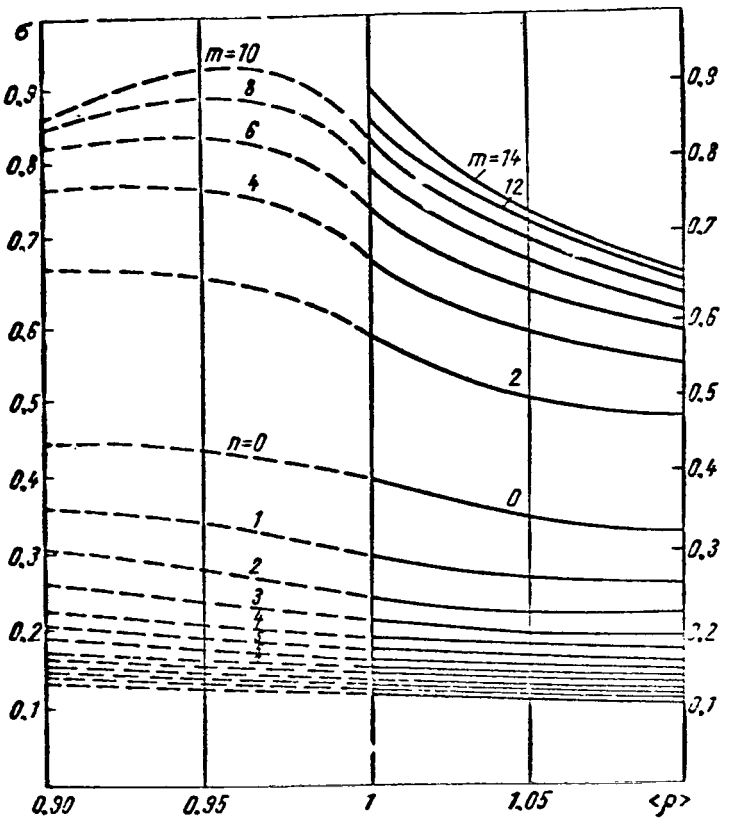

Figure 9. Relation Between the Angular Distribution Parameter σ, the Anistropy Index of the Angular Distribution (m or n), and the Average Velocity of Secondary Particles in the Symmetric System $< \rho >$.

The quantities α and α_R are expressed in terms of parameters measured in the L-system

$$\alpha \approx <p_\perp> (1 + \zeta) \Sigma \csc \theta_i. \tag{2.65}$$

Since the Lorentz factor of the R-system relative to the L-system is $\gamma_{RL} = 2\gamma_c^2 - 1$ (see Section 1) and the velocity $\beta_{RL} \approx 1$, then

$$\alpha_R = (2\gamma_c^2 - 1) <p_\perp> (1 + \xi) \Sigma \tan \frac{\theta_i}{2}; \tag{2.66}$$

$$\xi = \frac{1}{2} \left(\frac{m_\pi c}{<p_\perp>} \right)^2 \frac{\Sigma \sin \theta_i}{\Sigma \tan \theta_i / 2}; \tag{2.67}$$

$$\frac{\alpha}{\alpha_R} = \frac{a}{2\gamma_c^2 - 1}; \tag{2.68}$$

$$a = \left(\frac{1+\zeta}{1+\xi}\right)\frac{\Sigma \csc \theta_i}{\Sigma \tan^2 \theta_i/2}. \tag{2.68a}$$

Hence it is easy to show that

$$\beta_c\beta_{sc} \approx \beta_{sc} = \pm \frac{2\gamma_c^2 - 1 - a}{2\gamma_c^2 - 1 + a} \tag{2.69}$$

[see Eq. (2.40)]. We have $\beta_c\beta_{sc} > 0$ for $\alpha > \alpha_R$ (forward asymmetry) and $\beta_c\beta_{sc} < 0$ for $\alpha < \alpha_R$ (backward asymmetry).

e. Determination of γ_c for $<\rho> \neq$ and $\beta_{sc} \neq 0$. The formulas given below are suitable for practical application. Finding γ_c reduces to the following.

1. Determine the angular distribution of the secondary particles in the laboratory system from experiment. /41

2. Calculate γ_s^+ and $<\rho>$ by the method set forth in c and d above. Table 2 gives the quantity $(\text{cosec } \theta_s)^{-1}$, necessary for calculating γ_s^+ and ρ, as a function of m and n.

3. Calculate a from (2.68a).

4. Calculate α/α_R from (2.68) and determine the sign of β_{sc} from (2.69). In this, γ_c is considered equal to γ_s^+.

TABLE 2. DETERMINATION OF $1/<\text{cosec } \theta_s>$ [10] FROM VALUES OF n OR m.

n	$\frac{1}{<\csc\theta_s>}$	m	$\frac{1}{<\csc\theta_s>}$	n	$\frac{1}{<\csc\theta_s>}$	m	$\frac{1}{<\csc\theta_s>}$
0	0,6366	0	0,6366	7	0,9396	14	0,2023
1	0,7854	2	0,4244	8	0,9462	16	0,1970
2	0,8488	4	0,3335	9	0,9513	18	0,1807
3	0,8836	6	0,2410	10	0,9556	20	0,1721
4	0,9054	8	0,2587	11	0,9592	22	0,1646
5	0,9204	10	0,2352	12	0,9623	24	0,1580
6	0,9313	12	0,2171				

Commas represent decimal points.

5. Find the quantity

$$\delta = \langle \rho \rangle - 1 = \zeta^+ - \zeta - (\zeta^+)^2 - \frac{\Sigma \tan \theta_i/2}{\Sigma \csc \theta_i}. \tag{2.70}$$

6. If $\beta_{sc} > 0$, then for $\delta < 0$, $\gamma_c = \gamma_s^+$;

$$\gamma_c = \begin{cases} \gamma_s^+/(1 + \beta_c \beta_{sc}); & 0 \leqslant \delta < 0.02 \\ \frac{1}{2}\left[\frac{\gamma_s^+}{1 + \beta_c \beta_{sc}} + \frac{\gamma_s^+}{1 + \beta_c \beta_{sc}}\right]; & 0.02 \leqslant \delta < 0.04 \\ \frac{\gamma_s^+}{\gamma_{sc}(1 + \beta_c \beta_{sc})}; & 0.04 \leqslant \delta < 0.08. \end{cases} \tag{2.71}$$

If $\beta_{sc} < 0$, then for

$$\gamma_c = \begin{cases} \frac{\gamma_s^+}{1 + \beta_c \beta_{sc}}; & \delta < -0.01 \\ \frac{\gamma_s^+}{\gamma_{sc}(1 + \beta_c \beta_{sc})}; & -0.01 \leqslant \delta < 0 \\ \frac{\gamma_s^+}{\gamma_{sc}(1 + \beta_c \beta_{sc})}; & 0 \leqslant \delta < 0.02 \\ \frac{1}{2}\left[\frac{\gamma_s^+}{\gamma_{sc}(1 + \beta_c \beta_{sc})} + \frac{\gamma_s^+}{1 + \beta_c \beta_{sc}}\right]; & 0.02 \leqslant \delta < 0.04 \\ \frac{\gamma_s^+}{1 + \beta_c \beta_{sc}}; & 0.04 \leqslant \delta < 0.08. \end{cases} \tag{2.72}$$

The authors remark that successive approximations for the determination of β_{sc} might not converge,* but owing to the small size of β_{sc} we can be limited to the first approximation, by substituting $\gamma_c = \gamma_s^+$ into Eq. (2.69).

The results of the application of this method for the determination of γ_c in an accelerator are shown in Fig. 6, from which it follows that the method of Shen and Kaplon is effective, at least, for energies $\sim$ 30 GeV. This method does not eliminate the totality of sources that lead to the smearing of the distribution of

*The absence of convergence in successive approximations in finding β_{sc} engenders the thought that this procedure is not always reliable. The principal virtue of the method is the calculation of the deviation of $\langle \rho \rangle$ from 1 in each interaction.

the measured value of γ_c about the true one. In particular, Fermi motion of nucleons in the nucleus leads to broadening of the curve.

As seen from Fig. 6, the error in determining γ_c allowing for $<\rho> \neq 1$ and for motion of the symmetric system relative to the C-system, equals $\sim$ 20%. A comparison of the accuracy of the various methods of determining energy will be made in the next chapter.

5. Measurement of the Primary Energy From the Total Energy of the Charged and Neutral Particles

This method is based on the following assumptions.

1. The transverse momenta of the secondary particles are independent of their departure angles and the energy of the primary particles ($<p_\perp> = 0.35$ GeV).

2. The inelasticity is independent of energy:

$$K = \delta(K - \langle K \rangle).$$

a. Determination of E_0 from the energy of the secondary charged particles. /43

In this case it is assumed that

$$n_{\pi\pm} = 2n_{\pi^0}. \tag{2.73}$$

Then

$$E_0 = 1.64 \langle p_\perp \rangle \frac{\Sigma \csc \theta_i}{\langle \alpha_\pm \rangle} \tag{2.74}$$

where the coefficient 1.64 takes into account the contribution of π^0 mesons and neutral K mesons. The dispersion of errors of this method depends on the fulfillment of relation (2.73) in the individual cases and on the fluctuations of the inelasticity $\alpha_\pm$. The distribution of errors was studied in [10], and it was found that for $\alpha_\pm = 0.35$ there was an overestimation of the mean value of the energy in the C-system by a factor of 1.8.

The halfwidth of the distribution was 30% greater than in the Castagnoli method.

b. Determination of energy from the total energy of charged and neutral particles. In rare cases it is possible to measure simultaneously the energy conveyed to charged and neutral particles. This makes it possible to avoid the

assumption (2.73) and to use the following expression for the determination of energy:

$$E_0 = \frac{\langle p_\perp \rangle \Sigma \csc \theta_i + \Sigma \varepsilon_\nu}{\langle K \rangle}. \qquad (2.74a)$$

This method is somewhat better than the former, since its dispersion is determined only by fluctuations of the total coefficient of inelasticity K.

6. Measurement of the Energy of Primary Nuclear Fragments

6.1. Disintegration of a Primary Nucleus

It is possible to eliminate the errors associated with the sharp drop in the spectrum of cosmic radiation if one studies the interactions of nucleons, α-particles, and heavier fragments that arise in the disintegration of primary nuclei at the moment of interaction.

Kaplon et al., [36] noted that the process of disintegration of primary nuclei (fragmentation) can be treated as a process of evaporation in the mirror system. Then in the L-system all fragments will have almost identical energies per nucleon. /44

The character of nuclear disintegration depends on nuclear size. A nucleus of average atomic weight (C, N, O, F) frequently breaks up into its constituent nucleons (in 30--40% of the cases). The number of cases in which three or more fragments with $Z \geq 2$ arise does not exceed 5--8%. In the interaction of heavy nuclei ($Z \geq 10$), 25% of the cases give rise to more than three fragments. Total disintegration of the nucleus is observed in less than 20% of the cases [37]. In large photoemulsion piles one sometimes observes a whole cascade of successive interactions of the nucleus and the products of its fragmentation. An example of such an event is the cascade registered in an 80-liter pile flown at an altitude of 40 km for 38 h [38]. In this case (Fig. 10) there is a stepwise splintering off of fragments--nucleons and α-particles--with an energy of about 1300 GeV/nucleon from nucleus of $Z \approx 15$. /45

6.2. Methods of Determining the Energy of Fragments

The equality of fragment energy makes it possible to use several methods to determine it.

a. Method of relative scattering. The method of measuring multiple scattering at high energies is applied only in cases of very long tracks. However, even here false scattering and different kinds of noise set limits to the use of this method. The limit can be moved out to the region of higher energies if one measures the relative scattering of particles moving in almost parallel paths and at a very small distance (tens of microns) from each other. In this case, the effect of the various interferences (false scattering, distortion, etc.) is reduced.

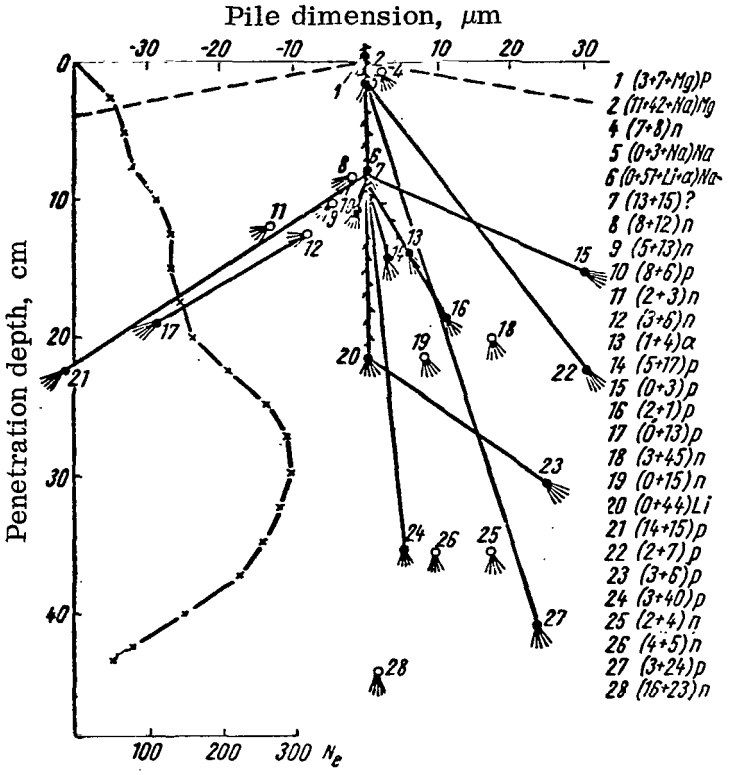

Figure 10. Successive Disruption of a Primary Nucleus with Z ≈ 15 and Energy About 1300 GeV/ /nucleon. The Events are Labeled Serially by Number and are Listed at the Right. The Dotted Line Corresponds to a Spreading Angle of 10^{-3} rad. The Curve on the Left Represents the Electromagnetic Cascade Developing in the Emulsion (N_e is the Number of Electrons in an Area of 600 x 600 μm^2).

Since in the disintegration of primary nuclei of high energy the emission angles of the fragments are very small, the method of relative scattering can give good results. This method was used by Lohrman et al., [37]. Energies in hundreds of GeV/nucleon were measured. The accuracy of the method depends on the length of the measured tracks and the spacing between them. The average accuracy of determining energy amounts to 30%, which corresponds to a mean square error d ≈ 0.25 (see Chapter I).

b. Determination of energy from the emission angle of α-particles [36]. Let β_0 be the velocity of the primary particle, β_θ the velocity of a fragment particle emitted at angle θ in the L-system. With the subscript M signifying

a variable in the mirror system (M-system) associated with the primay nucleus, we have /46

$$\tan\theta = \frac{1}{\gamma_0} \cdot \frac{\sin\theta_M}{\cos\theta_M + \frac{\beta_0}{\beta_M}} \tag{2.75}$$

Since in the rest system of the primary nucleus the products of its fragmentation are dispersed isotropically, the fraction of particles emitted into a solid angle $d\Omega$ is $-d\cos\theta_M$, and the average value $< \tan^2\theta >$ is determined by

$$<\tan^2\theta> = -\frac{1}{2\gamma_0^2}\int \frac{\sin^2\theta_M\, d\cos\theta_M}{(\cos\theta_M + \beta_0/\beta_M)^2} = \\ = \frac{2}{3}\cdot\frac{1}{\gamma_0^2}\cdot\frac{\beta_M^2}{\beta_0^2}. \tag{2.76}$$

If among the fragments we consider only α-particles with an average energy in the M-system of

$$<\varepsilon_\alpha>_M = \frac{1}{2} m_\alpha \beta_M^2. \tag{2.77}$$

then

$$<\tan^2\theta_\alpha> = \frac{4}{3}\cdot\frac{<\varepsilon_\alpha>_M m_p^2}{E_0^2 m_\alpha^2}, \tag{2.78}$$

where E_0 is the energy of the primary particle in the L-system.

At high energies we have $< \tan^2\theta_\alpha > \approx < \vartheta_\alpha^2 >$. The average energy of the evaporated α-particles in the M-system approaches 10 MeV; hence

$$\sqrt{<\theta_\alpha^2>} = \frac{0.56}{E_0}. \tag{2.79}$$

Practically no α-particles with energy > 30 MeV are encountered among the fragmentation products. Hence the maximum emission angle of α-fragments [see Eq. (2.78)] is

$$\theta_{max} \simeq \frac{0,12}{E_0}. \tag{2.80}$$

It is easy to find that the fraction of α-particles concentrated within the limits of the angle $<\theta^2>^{1/2}$ is close to 0.42.

Equations (2.79) and (2.78) can be used to determine E_0. If the relation (2.78) is represented in the form /47

$$\langle\theta_i^2\rangle^{1/2} = \frac{B}{E_0} \qquad (2.81)$$

the quantity B can be determined experimentally by a comparison of the energy measured from the scattering and from the angle $\langle\theta_\alpha^2\rangle^{1/2}$. Such a comparison [28] has corroborated Eq. (2.79). The quantity B turned out to be 0.060 ± 0.006 for primary nuclei of medium atomic weight and 0.055 ± 0.006 for heavy ones.

Since the energies of the α-particles in the rest system of the primary nucleus are distributed across the spectrum, the values of E_0 determined from Eq. (2.79) have a scatter around the true value. Figure 11 shows the distribution of energies calculated from (2.79) about the values of energy determined by the multiple scattering method for the same particles. The mean square error of this method is d = = 0.27.

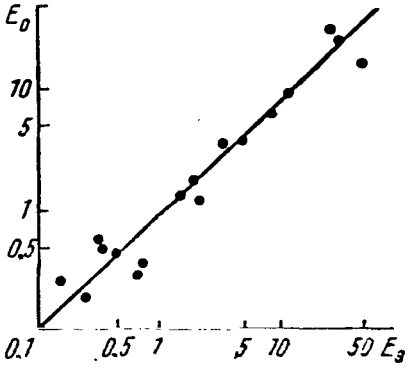

Figure 11. Distribution of Energies E_θ Calculated From Eq. (2.79) About the "True" Values E_0 (Measured by the Multiple Scattering Method.

c. Estimate of energy from the emission angle of protons. Substituting the magnitude of the energy of evaporated protons [$(E_p)_M$ = 12 MeV] into (2.76), we find

$$\langle\theta_p^2\rangle^{1/2} = \frac{0.12}{E_0}. \qquad (2.82)$$

However, in contrast to the α-particles, besides the evaporated protons from the disruption of nuclei there also arise recoil protons having energies in the hundreds of megaelectron volts (in the mirror system). On the average, in a collison of the primary nucleus with a nucleus in the emulsion, about half if its nucleons participate in the interaction (see Chapter V). /48 Therefore the distribution of the measured values of the energy about the true value E_0 is several times wider than in the case of α-particles.

d. Determination of the energy of the fragments by the Castagnoli method. Since the secondary fragments of one nucleus have the same energy per nucleon, the distortion of the characteristics of their interaction associated with the form of the spectrum of the cosmic radiation (see Chapter I) does not appear. Among the protons that are products of nuclear disintegration, about half also have almost identical energies. Hence, in determining the energy of the fragments and the individual nucleons it is possible to use the kinematic methods considered in Sections 2--4.

The accuracy of the Castagnoli method increases in this case by a factor $n^{1/2}$ (n is the number of fragments). If we select out cases of the interaction of the nucleus with an individual nucleon in the emulsion, then among the disintegration products there will be a small number of recoil nucleons (one or two), and hence almost all the nucleons will have the same energy in the laboratory system. The collision of a primary nucleus with an individual nucleon can be distinguished by the low multiplicity of pion production (see Chapter V).

If the distribution of newly created particles in the C-system is sufficiently broad (close to isotropic), the newly created particles are well separated from the protons (if the latter have an energy less than 30 MeV in the mirror system).

The use of the Castagnoli method gives the possibility of determining the energy not only of charged, but also of neutral nuclear fragments.

6.3. Some Examples of the Determination of the Energy of the Fragments

Lohram et al., [37] studied the interactions of nucleons and α-particles that were products of the disruption of nuclei. Energies in the hundreds of GeV were measured by the method of relative scattering.

Table 3 gives the results of the determination of energy by the Castagnoli method for the rich family of fragments No. 1115, which is sketched out in Fig. 10, [38, 39]. In order to improve the conditions of applicability of the Castagnoli method, only interactions of fragments with $5 < n_s < 25$ were used. /49

TABLE 3. ENERGY DETERMINATION OF A FAMILY OF FRAGMENTS BY THE CASTAGNOLI METHOD

No. of the interaction	Type of interaction	$\log \nu_c \pm \frac{\sigma}{\sqrt{n_s}}$	σ
1115—14	(5+17) p	1,41±0,15	0,64
1115—27	(3+24) p	1,33±0,16	0,77
1115—19	(0+15) n	1,30±0,17	0,65
1115—10	(8+6) p	1,61±0,39	0,94
1115— 9	(5+13) n	1,31±0,17	0,62
1115— 8	(8+12) n	1,42±0,16	0,57
1115—21	(14+15) p	0,89±0,24	0,87
1115—23	(3+6) p	1,55±0,38	0,92
1115—22	(2+7) p	1,38±0,30	0,73
1115—28	(16+23) n	1,28±0,13	0,64
1115—12	(3+6) n	1,59±0,49	1,21
1115— 4	(7+8) n	0,65±0,25	0,71

Commas represent decimal points.

The primary nucleus and its multi-charged fragments experience seven interactions in the pile. In each of the interactions nucleons split off from the nucleus. In all, 17 protons arose this way. These protons move inside a cone with an angle less than 10^{-3} rad and form the clear stem of the shower. Within this cone there are nine interactions evoked by protons and ten by neutrons. Since up to one half of the nucleons of the primary nucleus participate in the collision, it is necessary for an estimate of the energy of the primary particle to use only half of the most energetic particles (see Fig. 7). Then it turns out that the energy of the primary nucleus is E_0 = 1300 GeV/nucleon.

To check this value we can use (2.82) and determine the expected emission angle of nucleons with the given energy E_0. In the experiment it is found that a certain fraction of the nucleons is actually emitted at zero angle; however,

many move off at quite large angles. Evidently, these latter have taken part in collisions. Thus, the principal information about the energy in this case is obtained by the Castagnoli method.

It should be noted that the particles flying in the stem of the shower produced as a result of the disruption of the nucleus are assumed to be nucleons from a priori considerations. If at high energies the hydrodynamic mechanism of formation of new particles is active (Landau theory), then there may be pions among the fastest particles in the stem of the shower. /50

CHAPTER 3

THE IONIZATION CALORIMETER METHOD

1. Idea of the Method

The ionization calorimeter method, with various modifications, has been widely applied in recent years. /50

In a sufficiently large block of dense material a particle of high energy, as the result of successive interactions, is able to transfer all of its energy to the secondary particles. In a dense material only a negligible part of this energy is carried off by muons and neutrinos. By means of the whole chain of processes the principal fraction is transferred to secondary electrons, protons, nuclear fragments, and other ionizing particles. These particles are rather quickly absorbed, and in the end their energy is expended in heating up the material. Consequently, in a thick layer of material all the energy of the primary particle turns into heat. Here there exists an analogy with the calorimetric method of measuring energy or work. However, the direct measurement of the quantity of evolved heat in a large block of material is impossible. The following circumstance relieves the situation.

Before turning into heat, the energy of the particle is expended mainly in the ionization of atoms, and in the formation of one pair of ions the same specific amount of energy W is always used up, regardless of the nature and energy of the particle causing the ionization. Hence, by measuring the number of pairs of ions formed in the block of material, it is possible to determine the energy E_0:

$$E_0 = WI_0 = \int_0^\infty I(x)\,dx. \qquad (3.1)$$

Here I(x)dx is the ionization at depth x in layer dx. The ionization can be measured by known methods (ionization chambers, proportional counters, scintillators). /51

The union of the calorimetric principle with ionization methods of measuring energy is reflected in the name of the method--the ionization calorimeter. This method was proposed by Grigorov and first used by him [40].

The calorimetric principle nevertheless remains the basic one in the method, i.e., the total absorption of the primary particle and its products in a block of material. Thus we have the builder of one of the instruments based on this principle calling it a total absorption spectrometer [41].

2. Fundamental Processes in the Absorber of an Ionization Calorimeter

2.1. Introduction

At the present time it is well known that in a collision of a nuclear-active particle of high energy with a nucleus a certain fraction of the energy of the α--particle is transferred to secondary π^0 mesons. These π^0 mesons decay and give the initial electromagnetic cascade. The remaining energy is transferred to charged π mesons, K mesons, nucleons, and nuclear fragments. As a result, in a single act a small amount of energy is transferred to strongly ionizing particles, and this amount does not depend on the energy of the generating particle [42]. In light materials it is $E_d = 400$ MeV, and in heavy materials it can reach $E_d \sim 1$ GeV. Thus, in the region of interest almost all the energy of the primary particle after its first collision is divided among π^0 mesons and nuclear-active particles. In heavy materials the quantity $\Sigma\varepsilon_{\pi^0}/E_0 = \alpha_0$ can approximate 1/3, and consequently in a small number of successive acts the energy of the particle is transferred to the electron-photon component. This process continues until the energy of the most energetic of the secondary particles drops to 1 GeV. All the remaining energy is borne away by strongly ionizing particles. It /52
is impossible to know a priori at just what depth this will occur, since this depends on unknown details of the process of nuclear collision and is subject to fluctuations. Thus, the nuclear cascade curve will be represented as a superposition of a number of successive electromagnetic cascades and splashes of ionization from strongly ionizing particles, and the principal part of the ionization will be created by electrons. In individual cases, strong fluctuations in the form of the nuclear cascade can be observed if among the secondaries there is a small number of particles of high energy. But if the energy is more or less distributed uniformly among a large number of secondary particles, smooth cascade curves will be observed, inasmuch as the large number of secondary cascades must average out. Such a smooth curve is obtained if we sum over many individual cascades, even if they strongly fluctuate in form.

2.2. Calculation of an Average Cascade

The average cascade may be easily calculated, if we start from the simple phenomenological picture of a nuclear collision described earlier and do not consider the transfer of energy to strongly ionizing particles [43].

If the number of photons with energies from ε to $\varepsilon + d\varepsilon$, arising from the decay of π^0 mesons in a layer dx, equals $n_\gamma(\varepsilon, x)d\varepsilon dx$, then the number of electrons at depth x_0 is determined by

$$dn_e = \int_0^{E_0} \{\mathcal{P}(\varepsilon, x_0 - x)\}\, n_\gamma(\varepsilon, x)\, d\varepsilon dx/\lambda. \tag{3.2}$$

where λ is the interaction path.

Here $\{\mathcal{P}(\varepsilon, x_0 - x)\}$ is the cascade curve for the primaty photon with energy ε. The function $\{\mathcal{P}(\varepsilon, x_0 - x)\}/\varepsilon$ depends very weakly (logarithmically) on energy. Hence we may write

$$dn_e \approx \frac{dx}{\lambda} \cdot \frac{\{\mathcal{P}(<\varepsilon>, x_0 - x)\}}{<\varepsilon>} \int_0^{E_0} \varepsilon n_\gamma(\varepsilon, x)\, d\varepsilon. \tag{3.3}$$

The quantity described by the integral is obviously the total energy of all photons originating in layer dx:

$$\int_0^{E_0} \varepsilon n_\gamma(\varepsilon, x)\, d\varepsilon = \varepsilon_{\pi^0}(x). \tag{3.4}$$

It can be calculated from the formula

$$\varepsilon_{\pi^0}(x)\frac{dx}{\lambda} = \left[S_n(x)\frac{\alpha}{\lambda_n} + S_\pi(x)\frac{\beta}{\lambda_\pi}\right] dx, \tag{3.5}$$

where $S_n(x)$ and $S_\pi(x)$ are the fluxes of nucleon and pion energy, and α and β are the fractions of energy transferred to the π^0 mesons by nucleons and pions, respectively; λ_n and λ_π are the interaction paths of nucleons and pions. The total number of electrons observed at depth x_0 is

$$n_e(x_0) = \int_0^{x_0} \varepsilon_{\pi^0}(x)\, \frac{\{\mathcal{P}(<\varepsilon>, x_0 - x)\}}{<\varepsilon>} \frac{dx}{\lambda} \sim I(x_0). \tag{3.6}$$

The fluxes of nucleon and pion energy (if it is assumed that the fraction $\alpha = (1/3)K$ of the energy of all pions is transferred to π^0 mesons) are determined

from the equations (K is the total coefficient of inelasticity)

$$\left.\begin{aligned} dS_n = -\frac{KS_n dx}{\lambda_n};\ dS_\pi = \left(\frac{2}{3}KS_n\frac{1}{\lambda_n} - \frac{\beta}{\lambda_\pi}S_\pi\right)dx; \\ S_n(x=0) = (1-K)E_0;\quad S_{\pi^\pm}(x=0) = \frac{2}{3}KE_0; \\ S_{\pi^0}(x=0) = \frac{1}{3}KE_0. \end{aligned}\right\} \qquad (3.7)$$

consequently,

$$\left.\begin{aligned} S_n(x) = (1-K)E_0 e^{-\frac{Kx}{\lambda_n}}; \\ S_\pi(x) = \frac{2}{3}\cdot\frac{KE_0}{\left(\frac{K}{\lambda_n}-\frac{\beta}{\lambda_\pi}\right)}\left\{\left(\frac{1}{\lambda_n}-\right.\right. \\ \left.\left.-\frac{\beta}{\lambda_\pi}\right)e^{\frac{-\beta x}{\lambda_\pi}} - \frac{1-K}{\lambda_n}e^{\frac{-Kx}{\lambda_n}}\right\} \end{aligned}\right\} \qquad (3.8)$$

Figure 12 shows the variation of the energy flux of the nuclear-active component with depth, calculated from Eq. (3.8) for various values of K (β was taken equal to 1/3, and $\lambda_\pi = \lambda_n$). Substituting these expressions into Eq. (3.6), we find $n_e(x_0)$ by numerical integration for different K (Fig. 13).

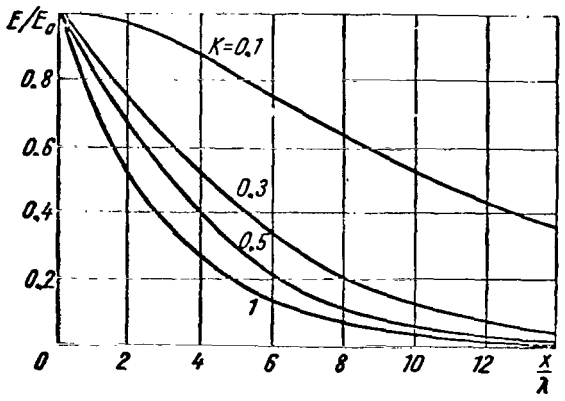

Figure 12. Variation of the Energy Flux of the Nuclear Component With Depth [Eq. (3.8)]. The Numbers on the Curves Correspond to Different Coefficients of Inelasticty K.

The form of the electron-nuclear cascade (3.6) depends on the relation between the length of the interaction path and the t-unit. The greater the ratio λ/t, the stronger the form of the nuclear cascades fluctuates. /55

2.3. Effect of Strongly Ionizing Particles

Strongly ionizing particles have a large effect on the form of the nuclear cascade. All the preceding considerations do not take this into account. However, the simplest estimates show that the role of strongly ionizing particles should be important. This leads to the energy flux of the nuclear-active component being absorbed more rapidly than given by Eq. (3.8) and Fig. 12 [44].

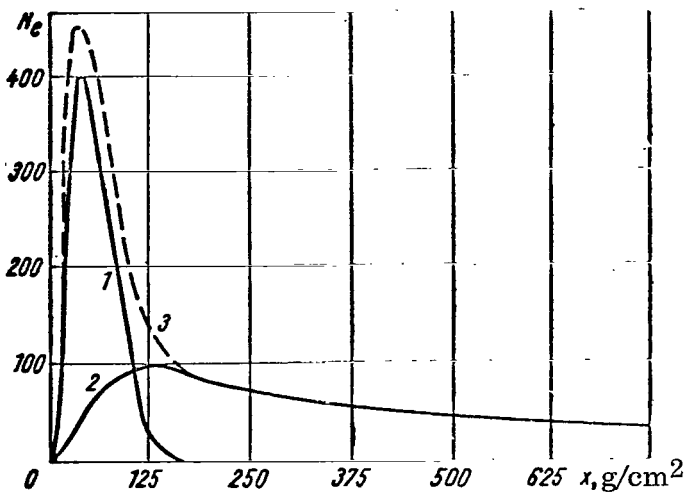

Figure 13. Variation of Number of Electrons N_e With Depth in an Electron-Nuclear Cascade, Developing in Lead:

1) for Electrons Arising in the First Interaction; 2) for Electrons From Subsequent Interactions; 3) Total.

Of interest is the data on the fraction of energy transferred to strongly ionizing particles in the entire cascade. This estimate was first made for iron by Raman Murthy et al.,[41] with a total absorption spectrometer and a gas Cerenkov counter at an energy of about 40 GeV. It turned out that the energy measured by their apparatus was only half of the expected amount. Since the organic scintillators used in this work were not very effective in registering strongly ionizing particles (see Section 3.5), the difference is evidently due to an error in counting these particles. Thus, at 40 GeV approximately 55% of the energy is transferred to strongly ionizing particles.

At higher energy this fraction can be obtained from experiment, if one adduces the results of ionization calorimeter measurements. For this we return to the formulas in (3.8). The energy flux of the nuclear component S(x) equals (for $x \gg 1$ and $K \sim 1$)

$$S(x) \approx \frac{2}{3} E_0 e^{-\frac{\beta x}{\lambda}} \tag{3.9}$$

(without accounting for strongly ionizing particles).

Taking into account the energy $\varepsilon_{si}(x)$ given up to strongly ionizing particles in a layer of material from 0 to x, we obtain a different dependence of energy flux on depth:

$$S'(x) \approx \frac{2}{3} E_0 e^{-\frac{\beta x}{\lambda}} - \varepsilon_{si}(x). \tag{3.10}$$

At energies much greater than 10^9 eV, the path of absorption of energy flux /56 is significantly greater than the path of ineraction, since in each act, an account of the charge independence of the secondary pions being produced, only a portion of the energy (borne off by π^0-mesons) irreversibly disappears from the nuclear component. When the flux of fast nucleons and pions decreases to zero, the remaining low-energy pions (with $E_0 \leq 10^9$ eV) can in one act dissipate all of their

energy by forming strongly ionizing particles. This happens at some point x_1. After this point absorption of the energy flux will proceed faster than for $x < x_1$.

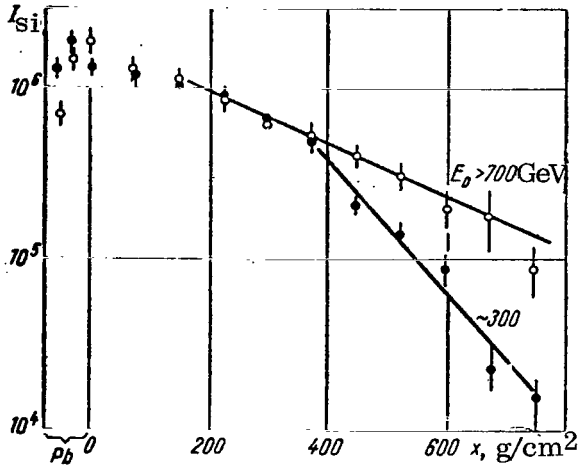

Figure 14. Variation of Ionization With Depth in Iron.

This point is determined by the relation $S'(x_1) = 0$, i.e.,

$$\varepsilon_{Si}(x_1) = \frac{2}{3} E_0 e^{\frac{-\beta x_1}{\lambda}} \qquad (3.11)$$

Point x_1 must be determined from experiment by a measurement of the absorption curve of the average nuclear cascade. In Fig. 14 are shown curves of the variation of ionization with depth in iron for $200 \leq E_0 < 500$ GeV ($x_1 \sim 400$ g/cm^2) and $E_0 \geq 700$ GeV ($x_1 \geq$ ≥ 700 g/cm^2) [44]. In the first case $\varepsilon_{si}/E_0 = 0.25$, and in the second $\varepsilon_{si}/E_0 \leq 0.15$.

2.4. Number of Nuclear Splittings in a Cascade N_{ns}

According to data from photoemulsions [42], the average energy expended in the formation of a single nuclear splitting in a collision with iron nuclei may be estimated as $E_d \sim 800$ MeV independently of the energy of the primary particle.* Then the number of primary nuclear splittings arising in the entire cascade at different energies is ε_{si}/E_d (see Table 4). /57

2.5. Energy of Neutrinos and Muons

The energy expended in the formation of neutrinos and muons is negligibly small. Postively charged pions of low energy are not able to cause nuclear splittings; hence they decay with the transmittal to a neutrino in the final analysis of 3/4 of their rest energy. The fraction of the energy borne off by neutrinos is

$$\frac{\varepsilon_\nu}{E_0} = \frac{3}{4} \cdot \frac{m_\pi c^2}{E_0} n_\pi.$$

*If this energy exceeds 1 GeV.

The number of slow pions n_π does not exceed 5% of the number of emitted protons n_g of corresponding energy [45]. Then the total number of slow mesons is

$$n_\pi \sim 0.05 N_{\text{ns}}\, n_g \quad (n_g = 2)$$

The neutrino energy calculated in this way is given in Table 5. The same table gives the energy borne away by fast muons arising from the decay of π-mesons of high energy:

$$\frac{\varepsilon_\mu}{E_0} = \frac{1}{E_0} \int_{m_\pi c^2}^{\varepsilon_{\max}} n_\pi(\varepsilon_\pi)\, \varepsilon_\pi \frac{\lambda}{c\tau_0 \gamma_\pi}\, d\varepsilon_\pi =$$

$$= \frac{\lambda}{c\tau_0} \cdot \frac{m_\pi c^2}{E_0} \int n_\pi(\varepsilon_\pi)\, d\varepsilon_\pi = \frac{m_\pi c^2}{E_0} \cdot \frac{\lambda}{c\tau_0} N_\pi .$$

Here N_π is the total number of high-energy pions. Assuming that this is /58
equal to the total number of primary splittings, we arrive at the results given in Table 5.

TABLE 4. NUMBER OF PRIMARY NUCLEAR SPLITTINGS IN A CASCADE

E_0, GeV	40	300	1000
$N_{\text{ns}} = \frac{\xi_{si}}{E_d}$	25	100	200

TABLE 5. ENERGY BALANCE IN A DENSE SUBSTANCE

E_0, GeV	40	300	1000
ε_{π^0}/E_0, %	44	75	85
ε_{si}/E_0, %	55	25	15
ε_ν/E_0, %	1	0.3	0.2
ε_μ/E_0, %	0.3	0.1	0.1

All the preceding estimates were made for iron, but because of the weak dependence of the parameters used on the atomic number of the substance, these estimate are also valid for other elements in the middle of the periodic table. These are the elements of greatest interest as absorbers in calorimeters [46].

2.6. Energy Balance in a Dense Substance with Average Atomic Number

The estimates of the preceding section give the possibility of considering the role of the various channels through which flows the energy of a primary particle incident on a dense absorber (see Table 5).

3. Constructional Features of a Calorimeter

The principal physical parameters of a calorimeter are: 1) thickness of the absorber x_0; 2) thickness of the layers between detectors Δx_i; 3) linear vertical dimension 1; 4) type of ionization (energy)detectors; 5) area.

The pattern of development of the nuclear cascade, which was the subject of a previous paragraph, is the basis for choosing the optimum parameters for the calorimeter. In doing this one must consider both the requirements of sufficiently accurate energy measurement and practicality. The latter condition /59
means a minimum allowable number of ionization detectors and consequently a minimum absorber thickness. From the point of view of the physical experiment one would like to have the maximum light grasp possible. Other conditions being equal, this is obtained with a choice of a minimum vertical dimension for the calorimeter. All of these conditions impose a limitation on the choice of material for the absorber. Calculations show [46] that at particle energies $E_0 \sim 1000$ GeV the thickness of the absorber in the calorimeter should be not less than 5 nuclear path lengths (~ 700 g/cm^2 of iron). The ionization detectors are spaced equally every 5--6 cascade units of the substance, if one is studying primary particles with energies ≥ 200 GeV. At lower energies the thickness of the layers needs to be reduced to 2--3 cascade units [41]. Elements in the middle of the periodic table are the best materials for the absorber: iron, copper, tungsten. The favorable relation between the lengths of the t-unit and the interaction path in these substances and the high density permit the construction of a calorimeter with a minimum number of detector rows (10--15) and a minimum geometrical height, which is essential for high light grasp.

When it is necessary to study the dynamics of the development of nuclear or electronic cascades, it is desirable to have a considerably greater number of detector rows and a thinner layer of material between them [47].

The choice of copper, brass, or iron as the absorber is also expedient for another reason. In the majority of cases, the body of the ionization detector is made of brass or iron. Hence the use of these same materials in the absorber precludes the appearance of transitional effects. The use of lead filters would lead to transitional effects from lead to iron. The magnitude of this transitional effect for the maximum of an electronic cascade was calculated in [48]. When scintillators or Cerenkov counters are used as detectors marked transitional effects arise even when iron filters are used. As detectors, one may use proportional counters [49], ionization chambers [40], Cerenkov counters [50], and /61
scintillators [41].

Ionization chambers are most often used. Organic scintillators miscount to a considerable degree the ionization from strongly ionizing particles, and Cerenkov counters register only relativistic particles. In the latter case it is necessary to take into account marked transitional effects.

In studying interactions of particles of high energy in the lower atmosphere, it should be kept in mind that the particles frequently fall into the apparatus in groups. The spacing between the particles in a group depends on their energy.

In order to distinguish cases of incidence of single particles and groups of particles, it is necessary to have detectors of small size. The diameter of the electron-photon cascade in iron is several centimeters. Hence for best resolving power, one needs detectors several centimeters in size. Usually the ionization chambers have tubes 4--10 cm in diameter and are arranged in adjacent

rows in mutually perpendicular directions. This system make it possible to distinguish the stems of showers from particles with energy $\sim$ 100 GeV. At energies of the order of 1000 GeV the average spacing between the particles of a group is several centimeters, and in many cases it is impossible to resolve individual particles.

The situation arising with the use of Cerenkov counters and scintillators is even more complex. These detectors do not give information about the quantity of stems and their direction of motion, unless one uses a very large number of photomultipliers.

Figure 15 shows the typical constructional details of various calorimeters.

4. Accuracy of the Energy Determination

4.1. Experiments

The principal methodological question is the question of the mean square error of the energy determination d. /62

The error distribution can in principle be determined by the experimental calibration of the calorimeter using particles of known energy. The particle energy must be measured by some accurate independent method.

In Section 2 we mentioned the results of a group of Indian authors, who calibrated a total absorption spectrometer with protons of about 40 GeV energy [41]. The protons were selected by a gaseous (air) Cerenkov counter set up above the calorimeter. This counter, under the conditions of the experiment, registered π-mesons beginning from an energy of 6 GeV and protons from 43 GeV. Since the principal portion of the flux of charged nuclear-active particles are protons, then in the energy region about 43 GeV one expects an increase in the fraction of cases when a shower in the calorimeter is accompanied by operation of the Cerenkov counter. It was found that a change in the effectiveness of the counter set in, apparently, at 20 GeV, and not at 43 GeV. The possible reasons for this were discussed earlier (see Section 2.5). This result, which is evidence of a large deficiency in energy measurement with scintillator dectectors, cannot be extended to ionization detectors. In addition, as was pointed out above, in order to estimate the accuracy of a measurement of energy it is necessary to know the distribution of the probability of occurrence of a given error. Thus, at the present time the problem of an absolute calibration of a calorimeter remains unsolved.

4.2. Possible Errors

For this reason we have to take another approach and, starting from the experimental results obtained in calorimeters, try to determine the distribution of errors in the energy measurement in an indirect way. For this purpose it is necessary to measure or calculate all possible errors and their distributions. The

energy of particles falling down into the calorimeter is

$$E_0 = W\int_0^\infty I(x)\,dx.$$

62

From this it is clear that in the energy measurement the error δE_0 is the sum of several errors... /63

a. Systematic errors. These errors affect the average value of the measured energy. They occur on account of an inaccurate value of the quantity W, the loss of low-energy particles unable to create ionizing particles, expenditure of energy in overcoming the coupling forces between nucleons in nuclei, etc.

b. Extrapolation errors. Since the block of material in the calorimeter has a finite thickness, there is an error associated with the exit of a portion of the energy from the calorimeter. This error is

$$\delta E_1 = W\int_{x_0}^\infty I(x)\,dx. \qquad (3.12)$$

It also leads to a systematic underestimation of the energy on the average. However, unlike the errors mentioned earlier, this one is in many cases equal to zero, since for a sufficient thickness x_0 the majority of cascades die out at $x < x_0$. For very great thicknesses x_0 δE_1 can be made as small as desired.

c. Interpolation errors. The calorimeter has a finite number of ionization (energy) detectors arranged at discrete levels. Therefore the integral in Eq. (3.1) has to be replaced by the sum

$$\int_0^{x_0} I(x)\,dx \to \sum_{i=1}^{N} I_i \Delta x_i. \qquad (3.13)$$

If all layers are the same, the sum is $\Delta x\sum_{i=1}^{N} I_i$. Obviously, this replacement leads to an error which can be decreased by using a more accurate interpolation formula. However, even Eq. (3.13) gives a very small error (less than 5%), since the nuclear-cascade curves are quite smooth.

Besides the purely mathematical inaccuracy there is also an error associated with physical reasons and also due to the discrete arrangement of the detectors. This error arises on account of the important role of strongly ionizing particles, which because of their small path are seldom registered but yield a strong ionization in the chambers. Thus the energy can be not only underestimated, but also overestimated. Fluctuations arising from this source can be reduced by increasing the number of detectors. The average value of the error is zero if one uses ionization chambers as detectors. /64

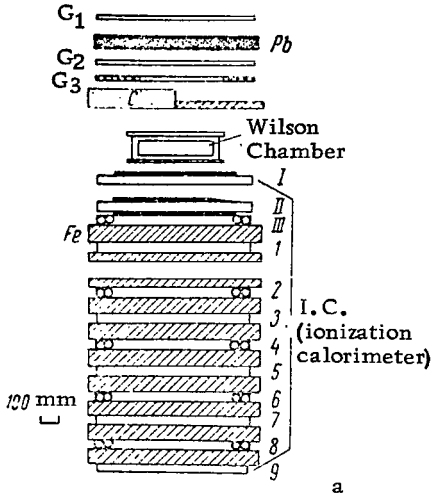
G1
Pb
G2
G3
C
Wilson
Chamber
I
II
III
Fe
1
2
3
4
5
6
7
8
9
I.C.
(ionization
calorimeter)
100 mm

a

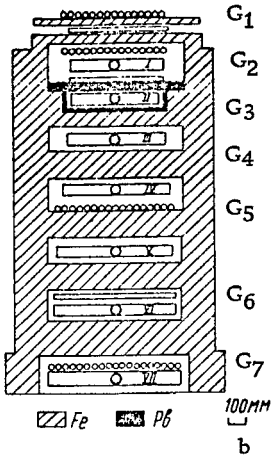
G1
G2
G3
G4
G5
G6
G7
Fe
Pб
100MM

b

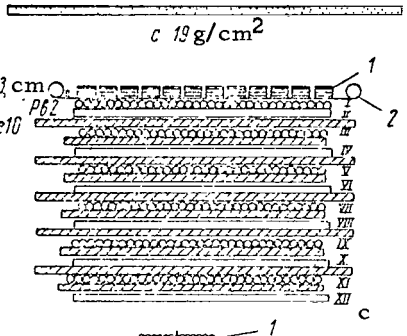
c 19 g/cm2
Pб3 cm
Pб2
Fe10
1
2

c

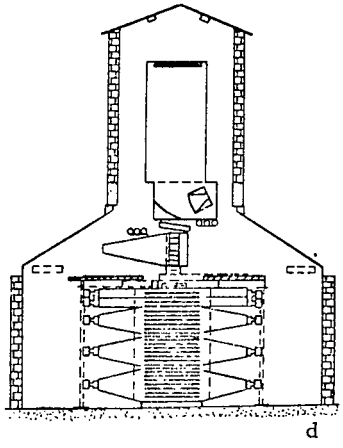

d

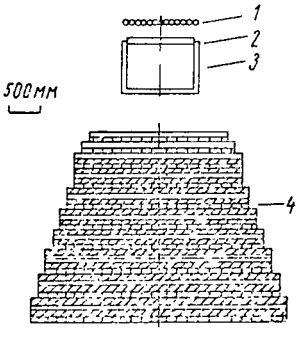
1
2
3
500MM
4

e

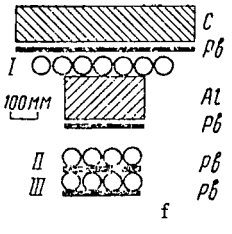
C
Pб
I
100MM
Al
Pб
II
III
Pб
Pб

f

4.3. Extrapolation Error

An extrapolation error can arise if an electronic-nuclear cascade which has developed in the calorimeter does not succeed in becoming absorbed in it. Then the energy is carried away by a large number of low-energy particles. This means that the variation of energy flux with depth can be described by average characteristics even in individual cases and in each case a correction can be determined. The correction is small for particles with $E_0 \sim 10^{11}$ eV, if the calorimeter has a thickness $x_0 \geq 700$ g/cm^2.

It has been shown [44] that an electronic-nuclear cascade is absorbed according to the law $e^{-x/L}$, where $L \sim \lambda$ of 2λ. Hence the correction in individual cases is

$$\delta E_2 = W \int_{x_0}^{\infty} I_N e^{\frac{-x_0-x}{L}} dx = W I_N L = W I_N \quad (1 \text{ to } 2)\lambda \tag{3.14}$$

(I_N is the ionization in the last row of the calorimeter).

When $E_0 < 10^3$ GeV, cases in which the cascade is not successfully absorbed are rare, and the quantity I_N is usually small. Hence the indeterminacy of the correction does not much effect the measurement of E_0.

It is still necessary to take into account the possibility of the exit from the calorimeter of particles that retain a significant portion of the primary energy and have not undergone an interaction within it. A calculation of this [46b] shows that at 300 GeV 92% of the avalanches are absorbed up to $x = 5\lambda$, and at 10^{12} eV, about 77%; in the majority of cases, the energy escaping from a calorimeter of thickness $x_0 = 5\lambda$ does not exceed several percent.

Figure 15. Typical Constructions of Working Calorimeters (G_i--Rows of Counters):

a) Ionization Calorimeter in Combination With a Wilson Chamber and a Godoscopic Arrangement of Counters [23]; b) Calorimeter With Cerenkov Counters as Detectors [50]; c) Ionization Calorimeter in Combination With Photoemulsion Layers (Method of Controlled Photoemulsions) [52]; 1) Photoemulsions; 2) x-Ray Film; d) Total Absorption Spectrometer (TAS) With Scintillators as Detectors. The Apparatus Includes a Gaseous Cerenkov Counter and a Wilson Chamber [41]; e) Ionization Calorimeter With a Large Wilson Chamber in a Magnetic Field [51]; 1) Geiger Counters; 2) LiH Filter; 3) Wilson Chamber; 4) Ionization Calorimeter; f) Arrangement for Measuring "Impact Ionization [53].

4.4. Systematic Underestimation of the Energy

Systematic underestimation of the energy can occur on account of its transfer to fast muons and neutrinos, as well as to slow neutrons which are already in no condition to create ionizing particles. Significant amounts of energy are expended in overcoming the binding forces between nucleons in nuclei.

The energy transferred to muons and neutrinos was estimated in Section 2.5. The binding energy and the energy of slow neutrons can be determined by going back to the results of the investigation of nuclear fragmentations with the aid of photoemulsions. On the basis of the data of Powell et al., [45] it is possible to compile the energy balance of nuclear fragmentations (Table 6). In doing this it is necessary to take into account that the number of "black" tracks N_b is on the average twice as great as the number of "gray" ones N_g, and 1/3 of the black tracks are formed by α - particles. Secondary stars are created by neutrons with energies in the hundreds of megaelectron volts, and gray tracks rarely arise in them. /65

Assuming that the energy of splitting an iron nucleus $E_d = 800$ MeV, we obtain $N_g = 2$. At an excitation energy $\sim$ 100--150 MeV the number of black tracks $N_b' = 3$. Consequently, the energy of the secondary star is 110 MeV. Considering the total energy of the neutrons produced, which is 165 $N_g = 330$ MeV, we find that the number of secondary and tertiary stars should be on the average three for every primary. Thus, the total number of stars in the calorimeter is $4N_{ns}$. From the table it also follows that the measured energy amounts to 60% of the total energy of strongly ionizing particles, whereas 40% is lost. At an energy of 300 GeV the lost energy amounts to 10% of the total, and at 1000 GeV it is $\leq$ 6%. /66

4.5. Measurement of the Energy of Strongly Ionizing Particles

It is obvious that on the average all the energy of the strongly ionizing particles is measured correctly. In fact the energy measured by the ionization chambers is

$$\nu \frac{R_{\text{eff}}}{\Delta x} \varepsilon_{si} \frac{\delta}{R_{\text{eff}}} \cdot \frac{\Delta x}{\delta} = \nu \varepsilon_{si}, \qquad (3.15)$$

where ε_{si} is the energy of strongly ionizing particles in one splitting; $R_{\text{eff}}/\Delta x$ is the probability of the registration of a splitting by the chamber (R_{eff} is the effective path of the products of the splitting); δ/R_{eff} is the fraction of the energy of the splitting developed in the working volume of the chamber with quantity of gas δ; ν is the number of nuclear fragmentations in a layer Δx; $\Delta x/\delta$ is the coefficient of conversion from ionization in the chamber gas to ionization in the layer Δx (interpolation!). On the basis of Table 6 it is possible to estimate the magnitude of the fluctuations of the measured energy due to inaccuracy of interpolation. Cal-

TABLE 6. ENERGY BALANCE OF NUCLEAR FRAGMENTATIONS

Energy expended	Energy, MeV	Remarks
a. Primary		
In fast protons forming gray tracks	165 N_g	Measured
In neutrons corresponding to fast protons	165 N_g	Further expended in the formation of secondary stars
In evaporated protons and α-particles	13 N_b = 26 N_g	Measured
In evaporated neutrons	8 N_b = 16 N_g	Possibly lost
In the transformation of the bond of nucleons and α-particles in the nucleus	48 N_g	Lost
Total	420 N_g = 800	
b. Secondary		
In evaporated protons and α-particles	13 N_b' = 117	Measured
In evaporated neutrons	8 N_b' = 72	Possibly lost
In the binding of nucleons in the nucleus	18 N_b' = 162	Lost
Total	39 N_b'	

culation shows [46b] that the principal contribution to this is brought in by α-particles and evaporated protons. Protons with energies in the hundreds of gigaelectron volts (gray tracks in the photoemulsions) are registered with high efficiency and practically do not contribute to the fluctuations associated with interpolation error [46b].

4.6. Accuracy of the Calorimetric Energy Measurement

Summarizing, we conclude that all the possible errors which can occur in the measurement of energy with an ionization calorimeter lead, on the average, to an underestimation of the energy and to relatively small fluctuations about the average value of the measured energy. /67

Table 7 shows the ways in which energy escapes from observation in an ionization calorimeter (for a material thickness $x \gg 5\lambda$).

TABLE 7. PERCENTAGE OF ENERGY NOT REGISTERED BY THE CALORIMETER

Type of energy	Energy of the primary particle, GeV		
	50	300	1000
Binding energy and energy of slow neutrons	22	9	6
Energy of neutrinos	1	0.3	0.2
Energy borne off by fast muons	0.3	0.1	0.1
Total	23.3	9.4	6.3

In this distribution we have not taken into account the Fermi motion of the nucleons in the nucleus and fluctuations of the fraction of energy transferred to strongly ionizing particles in the individual acts. Although the fluctuations can be large, nevertheless they evidently do not affect the character of the curve in Fig. 16 very much. This results from the rather high efficiency of registration of fragmentations by the ionization calorimeter. However, when scintillators and particularly Cerenkov counters are used as detectors, fluctuations of the energy of the strongly ionizing particles in individual acts play an important role.

The distribution obtained for Δ shows that it can be approximately described in a logarithmic scale by a Gaussian shifted by an amount $\lg\Delta_0 \sim 0.1$ relative to $<\Delta> = 1$ and having a mean square deviation $d \sim 0.1$. If the Fermi motion is taken into account, the quantity d increases to 0.13. Thus the condition of applicability of this apparatus in cosmic ray investigations ($d^2 \ll 1$) is fulfilled quite well. /68

5. The Hazards of Event Selection

In the preceding section it was shown that in the case of an ionization calorimeter with absorber thickness $\sim 5\lambda$ the magnitude of d is small, and consequently the form of the energy spectrum of the cosmic radiation has little effect. However, in calorimetric measurements, particularly when the thickness is diminished, a unique effect appears that is associated with the selection of events which differ because of fluctuations by short avalanches.

Let, for example, a calorimeter register all events that develop in its absorber an amount of energy greater than or equal to E. Then the number interactions registered by a calorimeter with absorber thickness x_0 equals

$N(E, x_0)dE$ $(x_0 > \lambda)$:

$$N(E, x_0)\,dE = \int_E^\infty N(E_0)\,dE_0 W(E, E_0, x_0)\,dE. \qquad (3.16)$$

Here $N(E_0)dE_0$ is the spectrum of particles incident on the calorimeter and $W(E, E_0, x_0)dE$ is the probability that an energy E will be developed in the layer x_0. The spectrum is $N(E_0)dE_0 = AE_0^{-\gamma}dE_0$ (see Chapter XII). Hence if W depends only on E/E_0 = and not on E_0, /69

$$N(E, x_0)\,dE = AE^{-\gamma}dE \langle \delta^{\gamma-1}(x_0) \rangle. \qquad (3.17)$$

Actually, as was shown in Section 4, the function $W(E, E_0, x_0)dE$ does depend on E_0. Then

$$N(E, x_0)\,dE \approx AE^{-\gamma}dE \langle \delta^{\gamma-1}(x_0, E_0) \rangle. \qquad (3.18)$$

This means that, in the first place, the calorimeter preferentially selects events when in layer x_0 the maximum possible energy is liberated, and in the second place, there is a distortion of the energy spectrum of the incident particles due to the dependence of $\langle \delta^{\gamma-1} \rangle$ on E_0.

Table 8 presents experimental data on the ratio of the energy registered by calorimeters of various thicknesses to that registered by a calorimeter of

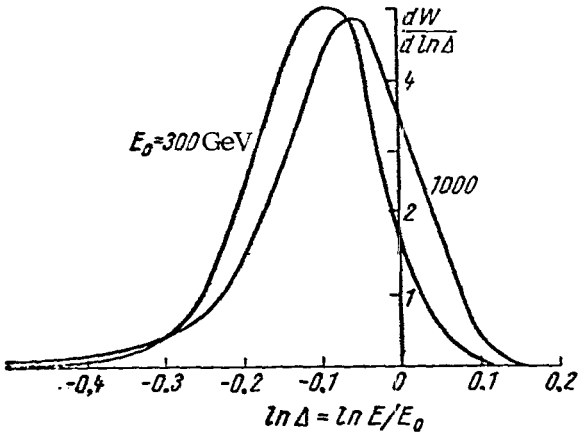

Figure 16. Distribution of Errors in the Measurement of Energy With a Calorimeter.

TABLE 8. RATIOS OF ENERGIES REGISTERED BY CALORIMETERS WITH DIFFERENT ABSORBER THICKNESS

Thickness of Fe absorber x_0, g/cm²	$\langle E \rangle$=220 Gev		$\langle E \rangle$=1300 Gev	
	$\langle \delta \rangle$	$\langle \delta^2 \rangle$	$\langle \delta \rangle$	$\langle \delta^2 \rangle$
75	0.17	0.04	0.03	0.01
150	0.44	0.24	0.35	0.17
225	0.61	0.43	0.53	0.33
300	0.76	0.62	0.63	0.46
375	0.85	0.74	0.75	0.59

Commas represent decimal points.

thickness 800 g/cm^2 of iron, $\delta = E(x)/E(800)$. It is obvious that the selection effect decreases with increasing x_0.

If we go to very small thicknesses x_0, when in the layer x_0 there occurs, as a rule, one interaction, then

$$N(E, x_0)\,dE = AE^{-\gamma}dE < x_0^{\gamma-1} > w(x_0), \qquad (3.19)$$

where $w(x_0)$ is the fraction of energy transferred in a single act to the electronic-photon component. Obviously, if α_0 is independent of energy, the apparatus will correctly measure the energy spectrum.

Usually in instruments of this type one uses a layer of light material (e.g., carbon) as a target and two rows of ionization chambers under thin layers of lead for the registration of the electron-photon cascade [54, 56]. The name "impact" has been given to such instruments. Of course, it is possible to determine with them only some average effective energy, and in an individual case it is possible to indicate only the lower limit of the energy, equal to E. /70

6. Comparison of Different Methods of Energy Determination

Table 9 gives a comparison of the accuracy of energy determination by different methods.

TABLE 9. COMPARISON OF VARIOUS METHODS OF ENERGY DETERMINATION

Method	C_1	d	Remarks
Castagnoli	2.0	1.3 to 1.6	Accuracy of method increases with increasing n_s; for collisions with nuclei, C_1 is less than two
Based on constancy of $< p >$ and on inelasticity	3.2	1.8	C_1 depends on assumption about $< \alpha_\pm >$

TABLE 9. (continued)

Method	C_1	d	Remarks
Energy determined from the emission angle of α-fragments	1.0	1.27	The value given refers to the case when the number of α-fragments in the shower ≥ 3
Relative scattering	1.0	0.25	At energies $\lesssim$ 100 GeV. Accuracy becomes poorer as energy increases
Shen and Kaplon	1.0	0.23	Method verified at accelerator energies
Calorimetric (ionization chambers used as detectors)	0.75 0.90 0.95	0.15 0.15 0.15	50 Gev 300 GeV 1000 GeV For an absorber thickness $x_0 = 5\lambda$

In the second column is given the value of the quantity C_1, which determines the average energy discrepancy in the laboratory coordinate system. If $C_1 > 1$ the energy is overestimated; in the opposite case it is underestimated, i.e., $E = C_1 E_0$, where E is measured and E_0 is true in the laboratory coordinate system. /71

The third column gives the mean square deviation of the measured value of the energy from the true value

$$d = \sqrt{\langle (\ln E - \ln E_0)^2 \rangle}.$$

In what follows, we shall regard methods of energy determination for which $d^2 \ll 1$ as "reliable". The results obtained by such methods will be given preference in the analysis of experiments.

PART II

INTRODUCTION

Before we go on to an analysis of the experimental material, we shall make a few general observations of a methodological character. /72

1. Besides the energy of the primary particle, the determination of which was the subject of Part I, the question of the masses of the colliding particles is important in any description of the process.

The nature of the primary particle, as a rule, is specified by the experimental conditions. Thus, in satellite experiments the primary particles may be protons or heavier nuclei, and it is easy to distinguish these by their ionization properties. In the lower atmosphere the picture is more complicated. The heavy particles have practically disappeared, but secondary particles appear: neutrons, pions, K mesons, etc. At high energies protons, K mesons, and pions are practically indistinguishable by ionization. Thus, only the absence of charge on the primary particle will give evidence of its nucleonic nature, whereas the nature of charged primary particles is not determinable.

The question of the nature of the target particle is not always successfully resolved in a well-defined way.

In experiments with photoemulsions we have to use a probability-type approach, because of their complex composition. From a priori considerations it has been proposed [30, 45, 57] that the interactions in which the number of gray and black tracks (N_h) is zero or one occur in the collision of a nucleon with a nucleon. If $N_h \leq 5$, the target particle is considered to be a light nucleus; if $N_h > 5$ (or 8 in some papers) the target nucleus is a heavy one. Sometimes, to increase the statistics, cases with N_h equal to two or three are also considered to arise from the collision of a nucleus with a nucleon. The accepted criterion for isolating nucleon-nucleon interactions is not reliable.

In its passage through the photoemulsion a primary particle collides mainly with bound nucleons, which is not taken into account in this criterion. /73

In experiments with apparatus in which a Wilson chamber is used to register secondary interactions, the nature of the target particle is better defined. In this case a filter-generator of a homogeneous substance is placed above the chamber. The average number of nucleons in the nucleus involved in the collision can be determined for nuclei heavier than hydrogen from the formula

$$\langle n \rangle = \frac{2}{3} \cdot \frac{A - (2A^{1/3} - 1)^{3/2}}{(A^{1/3} - 1)^2}$$

where A is the atomic weight of the target nucleus.

For a generator made of LiH, $\langle n \rangle = 1.4$, for graphite, $\langle n \rangle = 2$, etc.

2. Direct information about the interaction is obtained from measurement of the energies (ε_i), momenta (p_i), and emission angles (θ_i) of the secondary particles. In order to have the possibility of uncovering the dynamics of the interaction, it is necessary to transform from the quantities measured in the experiment to the characteristics that depend on the impact mechanism. The multiplicity and momentum spectra of the secondary particles, the coefficients of inelasticity and the angular distributions, the transverse momenta $p_\perp$ and the four-dimensional transfrred momenta Δ are such characteristics. At this stage of investigation, we shall treat them as fundamental. This is a consequence both of the experimental potentialities and of the ideas about the mechanism of creation of the particles that have been invented by existing theories of the interaction. The possibility is not precluded that as we penetrate deeper into the unknown, new parameters may be found that will overshadow the current ones or take their places beside them.

In cosmic ray experiments the individual approach to the events under investigation is a decisive factor. Hence, the principal problem of the experimenter should be to obtain all the possible parameters of an individual interaction. However, owing to the paucity of statistical material, particularly at high energies of about 10^3 GeV, one has to average over the registered events and determine the average parameters of the interaction ($\langle n \rangle$, $\langle k \rangle$, $\Sigma f(\theta_i)$, $\langle p_i \rangle$, etc.) instead of their distributions. Later, the dependence of the average interaction parameters on the energy of the primary particle and the various correlations between the parameters are investigated. / 74

However, obtaining the average characteristics sometimes leads to a concealment of the main features of the interaction or even to the appearance of false effects, if suitable precautions are not taken in the averaging process. Such effects in averaging over the energy spectrum of the primary particles were analyzed in Part I. As an example, we can give here the situation with the average value of the coefficient of inelasticity for pion-nucleon interactions, which is set forth in detail in Chapter VIII.

An average value of $\langle \alpha_0 \rangle \sim 0.5$ is obtained in averaging events with very small or very large coefficients of inelasticity.

Events with coefficients of inelasticity equal to the average value are practically absent.

A similar picture is obtained in the study of angular distributions. The total angular distribution of the secondary particles turns out to be symmetric. However, this symmetry is usually the result of adding together angular distributions that are asymmetric in the forward direction and asymmetric in the backward direction (see Chapter IX).

These examples show that before one does the averaging, he should obtain all possible characteristics of the individual events and average only events that similar individual characteristics.

3. It is obvious that a different kind of distribution over the individual characteristics, and not their average values, gives us much more information for the explanation of the interaction mechanism. Obtaining such distributions is the basic, but unfortunately not always solvable, problem.

The next step in the analysis of the experimental material is the study of the correlations between the different distributions.

Although the remarks above are obvious, they are not always taken to heart. Sometimes, in the analysis of experiments we shall be able to discern such defects and expose them. /75

CHAPTER 4

THE INTERACTION CROSS SECTION

1. The Study of Interaction Cross Sections at High Energies

1.1. Definitions

We distinguish two types of particle interaction—elastic and inelastic, and this requires the introduction of the corresponding effective cross sections. Collisions of particles with nucleons are called inelastic if new particles are created thereby. Cases of scattering (including those with charge transfer) are elastic. The interaction of a nucleon with a nucleus is somewhat more complicated. Only that process in which the primary particle is scattered by a nucleus as a whole should be strictly elastic (coherent scattering). There is also the quasi-elastic (incoherent) scattering of the primary particle by individual nucleons of the nucleus. As a result of quasi-elastic collision, one or several δ-nucleons are emitted from the nucleus, and the nucleus goes to pieces.

Experiments by Belletini et al. [58] have shown that during elastic scattering by a nucleus the square of the four-dimensional transferred momentum $|t|$ exceeds 0.02 $(\text{GeV/c})^2$ only rarely, and the scattering angle θ is usually less than $7 \cdot 10^{-3}$ rad. Quasi-elastic scattering takes place at $\theta > 7 \cdot 10^{-3}$ rad, when the recoil nucleon obtains enough energy to overcome the binding forces in the nucleus. The kinetic energy of the recoil nucleon is determined from the relation

$$T = \frac{|t|}{2} \text{ GeV},$$

which gives about 10 MeV for $\theta = 7 \cdot 10^{-3}$ rad and $|t| = 0.02$ $(\text{Gev/c})^2$. The distribution of the quantity $|t|$ in the case of quasi-elastic scattering by a nucleus should coincide with distribution for elastic scattering by an individual nucleon. Using [58a], in which proton-proton scattering was studied, and taking p-p are p-n scattering to be the same, Belletini et al. [58] obtained the dependence of

the cross section of quasi-elastic scattering on $|t|$

$$\frac{d\sigma}{d\omega} = N(A)\frac{(p\sigma_{pp})^2}{(4\pi\hbar)^2}\exp(-c\,|\,t\,|), \tag{4.1}$$

where σ_{pp} is the total cross section of a nucleon-nucleon collision, $p\sigma_{pp}/4\pi\hbar$ is the amplitude of forward scattering in a p-p collision, and N(A) is the effective number of nucleons in a nucleus with atomic weight A that participate in incoherent scattering. In other words, quasi-elastic scattering by a nucleus A coincides with scattering by N(A) independent nucleons. /76

Using for the constant c in Eq. (4.1) the numerical value obtained from experiments on p-p scattering at 19.3 GeV, the differential cross section of incoherent scattering can agree with experiment if we take

$$\frac{d\sigma}{d\omega} = N(A)\,11e^{-10\,|\,t\,|}\ \text{b/sr},$$

and

$$N(A) = 1.6A^{1/3}.$$

The latter relation shows that the cross section of inelastic scattering increases slowly with increasing atomic number of the target nucleus.

In the majority of cosmic experiments the incoherent quasi-elastic interaction is not registered, since thick filters that absorb δ-nucleons are used as targets.

Usually the fact of an interaction is established from the appearance in the target of two or more secondary particles or from the electron-photon cascade which is developed in a special lead filter. In the latter case a certain minimum transfer of energy to π^0-mesons is required. The required inelasticity, especially in the region of high energies, can be extremely small ($\sim$ 1%), and inelastic interactions are recorded rather well.

In those experiments where thin targets are used, quasi-elastic interactions are also partially registered. The results of different experiments may not agree because of different contributions by incoherent scattering.

1.2 Interaction Path

Instead of the interaction cross section, the interaction path λ is used in cosmic rays. The interaction path is equal to the distance in which the number of particles that have not undergone an interaction is reduced e times. It is obvious that λ is simply related to σ: /77

$$\lambda = \frac{1}{\sigma n}. \tag{4.2}$$

Here λ is measured in centimeters and σ in square centimeters, and n is the number of nuclei per cubic centimeter. It is often more convenient to measure λ in grams per square centimeter, which permits elimination of the density of the substance in which the path is measured:

$$\lambda\left[\frac{z}{c.u^2}\right] = \lambda\ [c.u]\ \rho\left[\frac{z}{c.u^3}\right] = \frac{\rho}{zn} = \frac{Am_p}{z}, \tag{4.2a}$$

where A is the atomic weight, m_p is the proton mass, and ρ is the density of the substance.

1.3. Geometric cross section

Physicists rather frequently use the concepts of geometric cross section σ_0 and of geometric path λ_0 corresponding to it. These concepts arose from the idea that the nucleon was a sphere with radius r_0. Then the geometric cross section $\sigma_0 = \pi r_0^2$. Because of the close packing of nucleons in the nucleus, the geometrical cross section of a nucleus with atomic weight A is

$$\sigma_0 = \pi r_0^2 A^{2/3}, \tag{4.3}$$

and the geometric path

$$\lambda_0 = \frac{m_p A^{2/3}}{\pi r_0^2}. \tag{4.4}$$

In experiments with particles of low energy the radius of the nucleon r_0 has been found to be equal to 1.4 F. Therefore in the older literature the calculated geometrical cross sections had extremely high values. The smaller values obtained in experiment were interpreted to be the result of a certain "transparency" of the nucleon [59].

The experiments of Hofstadter [60] on the determination of the electromagnetic form factor of the nucleon showed that the density of material in the nucleon smoothly decreases within a certain interval of distances from the center of the nucleon. In this connection it is possible to determine only some effective radius of the nucleon, which was found to be equal to $(<r_0^2>)^{1/2} \sim 1.2$ F. The presence of a semitransparent edge on the nucleon results in a variation of the cross section with the atomic number of the nucleus. In fact, the region where the nucleus is semitransparent plays a relatively smaller role as the nuclear size increases, and the dependence of cross section on A should be faster than $A^{2/3}$. /78

1.4. Connection between nucleon-nucleon and nucleon-nucleus cross sections

In the limiting case of high energies it is easy to establish the relation between the cross sections of nucleon-nucleon and nucleon-nucleus interactions based on the form factor of the nucleus.

If the wavelength of the incident particle is so short that the properties of the nuclear material change little within it, then the nucleus can be considered as a continuous medium with a density distributed according to some law $\rho(r)$, where r is the distance from the center of the nucleus. Then

$$\sigma_A = 2\pi \int_0^\infty \left\{ 1 - e^{-2\sigma_1 \int_0^\infty \rho_A \left(\sqrt{b^2+s^2}\right) ds} \right\} b\,db, \tag{4.5}$$

where b is the collision parameter of the incident particle, and σ_1 is the cross section of the interaction of the primary particle with an individual nucleon. /80

The density distribution of the nuclear substance in a nucleus of atomic weight A, $\rho_A(r)$ can be obtained from Hofstadter's experiments [60]. Figures 17 and 18 show the dependence of λ or σ_A on the magnitude of the cross section σ_1 [61]. With the aid of these graphs it is possible to determine the elementary cross section σ_1 from the measured interaction cross section of nuclei. It should be remembered, however, that the nuclear form factors are obtained in electron scattering experiments. The form factors of nuclei for nuclear-active particles may be different. For example, Belletini et al. [58] observed that the radius of a lead nucleus was 0.5 F larger than that given by Hofstadter's experiments.

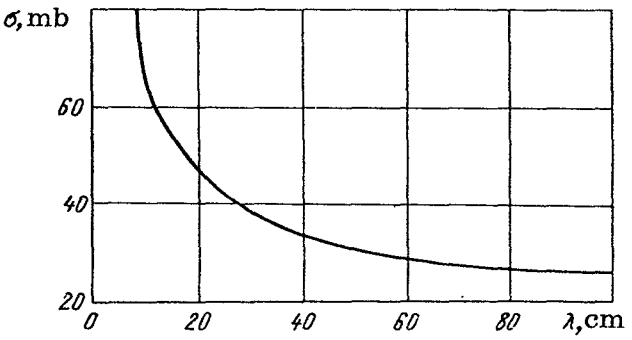

Figure 17. Relation Between the Total Effective Elementary Interaction Cross Section σ and the Interaction Path in an Emulsion λ [60].

2. Experimental Methods for the Study of Cross Sections

2.1. Basic formula

At the basis of all methods for the determination of interaction paths in cosmic rays lies the formula

$$N = N_0 \exp[-x/\lambda], \tag{4.6}$$

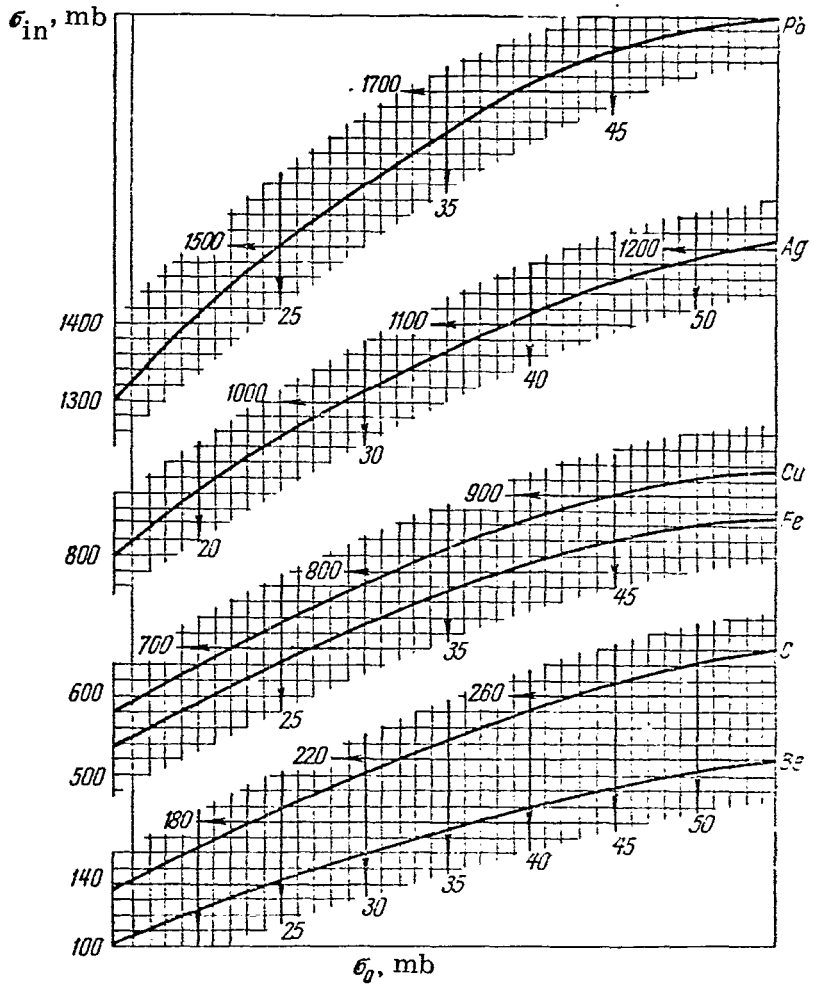

/79

Figure 18. Relation Between the Total Effective Elementary Interaction Cross Section and the Cross Section of Inelastic Interaction With Nuclei for Various Substances [61].

where N is the number of particles passing through a layer x without interaction.

2.2. Beam extraction methods

The beam extraction method is the most reliable. This method requires an apparatus consisting of the following elements (Fig. 19):

A—An arrangement for isolating the primary particle. For measurements in the atmosphere systems of hodoscopic counters are used, which make it possible separate a single particle from the showers;

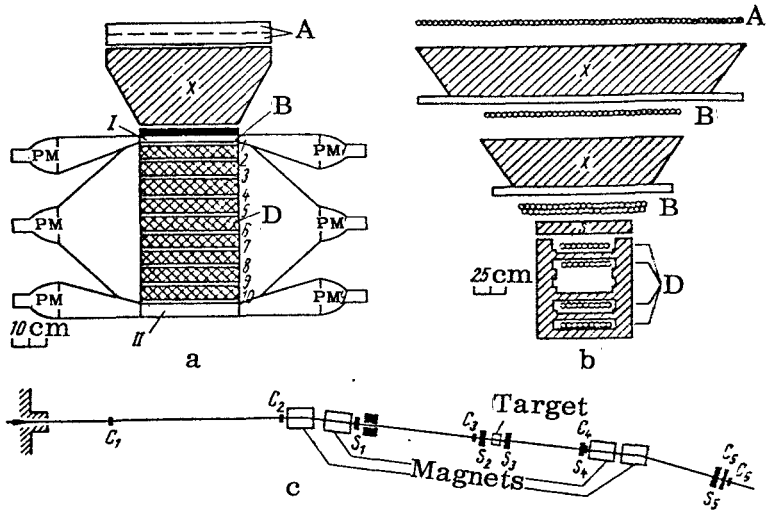

/81

Figure 19. Apparatus for the Measurement of the Effective Cross Section in Cosmic Rays by the Beam Extraction Method:

a) after Basilov et al. [62]; b) after Bozoki et al. [58]; C_1—C_6, scintillation counters; S_1—S_5, spark chambers with sound registration. The target is placed between chambers S_2 and S_3.

X—A filter made of the substance under investigation, of thickness x;

B—Hodoscopic counters or proportional counter for isolating the particles hat pass through the layer x without interaction;

D—The interaction detector. This detector may include:

a) counters under thick layers of material for observation of cases when several penetrating particles are observed in the interaction (if their number exceeds three, this corresponds to an average energy of primary particles of about 20 GeV);

b) ionization chambers arranged in two rows with a lead separator (in this case events with transfer of a definite energy to photons are registered);

c) an ionization calorimeter (the energy is measured directly);

d) spark chambers (showers are observed in the chamber; the energy of the primary particles is estimated from the multiplicity).

The probability of registering an interaction with the detector is w_d. The number of events registered by the apparatus with filter x equals

$$N_1 = N_0 w_d e^{-x/\lambda}. \qquad (4.7)$$

In the measurement process the filter X is periodically taken away. The number of events without the filter is /82

$$N_2 = N_0 \omega_d. \tag{4.8}$$

Therefore

$$\lambda = \frac{x}{\ln N_2/N_1} \tag{4.9}$$

2.3. Distribution of interaction points

The distribution of interaction points with depth gives the possibility of determining λ. To this end ionization calorimeters or photoemulsion piles and chambers of sufficient thickness are used. If the thickness of the emulsion layer or the quantity of material in the calorimeter were infinitely large, then this method would make it possible to construct the entire curve (4.6) directly and thereby determine λ.

However, in practice the thickness of the material in the calorimeter is limited to several interaction path lengths, and in the photoemulsions to one. Hence the effectiveness of registering interactions depends on the depth (a portion of the interactions occurring at the bottom is lost, since the energy of the particle cannot be completely evolved).

In photoemulsions, abondoning the possibility of determining energy, interactions are sampled only from the first cascade. Events which take place closer than 5 to 10 t-units from the end of the pile are lost, since the cascade cannot develop.

In this case we consider the so-called potential length R', i.e., the path of the particle from its entrance to its exit from the pile.

It was shown in [64] that it is necessary to take a quantity 10-15 cm smaller as the potential length, in order to allow for the ineffectiveness of the last layers of the emulsion. Of course, this quantity will vary somewhat depending on the energy of the photons creating the cascade. The estimate of the interaction path is made by the method of maximum probability. In its application to photoemulsion work this method was considered by Bartlett [65], who introduced the function S'(λ): /83

$$S' = S + \frac{1}{6}\rho(S^2 - 1);$$

$$S = \sum_{i=1}^{n}\left\{-1 + \frac{l_i}{\lambda} + \frac{R_i}{\lambda}\left[\exp\left(\frac{R_i}{\lambda}\right) - 1\right]^{-1}\right\} A^{-1}; \tag{4.10}$$

$$\rho = \sum_{i=1}^{n}\left\{2 - \left(\frac{R_i}{\lambda}\right)^3 \exp\left(-\frac{R_i}{\lambda}\right)\left[1 + \exp\left(-\frac{R_i}{\lambda}\right)\right]\right.$$

$$\times \left[1 - \exp\left(-\frac{R_i}{\lambda}\right)\right]^{-3}\Big\} A^{-1};$$

$$A = \left\{\sum_{i=1}^{n}\left[1 - \left(\frac{R_i}{\lambda}\right)^2 \exp\left(-\frac{R_i}{\lambda}\right)\left(1 - \exp\left(-\frac{R_i}{\lambda}\right)\right)^{-2}\right]\right\}^{1/2}$$

where n is the total number of interactions; l_i is the distance from the point of entry to the point of interaction of the i-th particle; R_i is the potential path length ($R_i = R_i' - 15$ cm) for the i-th particle.

If the most probable value of the interaction path is λ, then $S'(\lambda) = 0$. The standard deviation is then equal to

$$\sqrt{\langle \Delta\lambda^2 \rangle} = (\lambda - \hat{\lambda}) S'(\lambda) = \pm 1.$$

In practice this amounts to constructing the dependence of S' on $1/\lambda$ and to extracting the value of $1/\lambda$ corresponding to S' = 0.

Another approach is possible when an ionization calorimeter is used. In this case the energy is well estimated for events beginning in the upper layers. But if the interaction should occur in the bottom of the calorimeter, a portion of the energy cannot be evolved in the block of material and in choosing events according to the rule $E > E_{min}$ some of the events will be lost. This effect is easily allowed for. If a cascade beginning at depth x_0 has a chance to evolve a fraction of energy δ, $\delta + d\delta$ with probability $w(\delta, x)d\delta$, then the number of events with a point of interaction located at a depth greater than x registered by the calorimeter, is given by the formula [66]

/84

$$n(>x, >\varepsilon_{min}) = \int_x^R \int_{\varepsilon_{мин}}^{\infty} \frac{Ae^{-x/\lambda} dE' dx}{E'^{\gamma}\lambda} \int_0^{\infty} \delta^{\gamma-1} w(\delta, x)\, d\delta =$$

$$= \frac{A}{\gamma \varepsilon_{min}^{\gamma}} \int_x^R e^{-x/\lambda} \frac{dx}{\lambda} \int_0^{\infty} \delta^{\gamma-1} w(\delta, x)\, d\delta.$$

Consequently

$$\frac{n(>x, >\varepsilon_{min})}{n(>0, >\varepsilon_{min})} = \frac{\int_x^R \langle \delta^{\gamma-1}(x) \rangle e^{-x/\lambda} \frac{dx}{\lambda}}{\int_0^R \langle \delta^{\gamma-1}(x) \rangle e^{-x/\lambda} \frac{dx}{\lambda}} \qquad (4.11)$$

Here R is the thickness of the calorimeter (equivalent of the potential length), and γ is the index of the differential energy spectrum of the particles at the level of observation. This index is close to 3 on mountaintops (2000-5000 km). Hence to calculate $n(> x, > \varepsilon)$ as a function of depth, it is possible to utilize the data of Table 9, which gives the quantity $\langle \delta^2 \rangle$ as a function of x.

2.4. Method of comparing the interaction paths in two substances

In a number of papers (e.g., [67]), in order to elminate the primary beam, the ratio of the interaction path in various substances to that in lead was measured. For this a plate of the substance under investigation was placed in a Wilson chamber and under it plates of lead. The number of showers begun in lead n_{Pb} and in the investigated substance n_i was compared: /85

$$\frac{n_i}{n_{Pb}} = \frac{(1 - \exp[-x_i/\lambda_i])}{\exp[-x_i/\lambda_i]\,(1 - \exp[-x_{Pb}/\lambda_{Pb}])} \left(\frac{E_{Pb}}{E_i}\right)^{\gamma-1} \qquad (4.12)$$

The last factor appears because the showers from the i-th substance and those from the lead differ. Hence choosing the showers according to an arbitrary criterion (e.g., multiplicity) leads to a difference of the average energy of registered particles.

The energies E_{Pb} and E_i are evaluated from the angular distribution, which renders this method insufficiently conclusive. Evidently, the error arising because of this is lessened if an intercomparison of paths is made in different light substances, e.g., Li, C. Al [67].

2.5. Observation of solitary protons at the bottom of the atmosphere

If at a depth x in the atmosphere one samples nucleons which have not undergone interaction in the overlying air layers, then a comparison of their intensity with the intensity at the outer edge of the atmosphere gives the possibility of determining λ from formula (4.6) [68-70].

An air shower accompanying a nucleon serves as an indicator of an interaction that has taken place. Hence, by measuring at level x the intensity of nucleons without air accompaniments, it can be assumed that this is the same as the intensity of noninteracting nucleons.

Actually, in a number of cases the air shower is absorbed in the atmosphere and does not arrive at the level of observation. Hence the observed intensity of solitary nucleons is too high, and this method gives only an upper estimate of the interaction path. In addition, the probability of missing the accompaniment reduces with increasing energy, and the spectrum of solitary protons will be steeper for this reason.

3. Results of Experiments on Cross Sections*

/86

3.1. General remarks

Results of investigations of inelastic cross sections of the interaction of nucleons with nuclei at cosmic energies have been obtained by the various methods described in the preceding section.

Inelastic cross sections (or absorption cross sections) have been determined in accelerators at energies of the order of 20 GeV both by the method of "poor geometry" and from the difference between the total and elastic cross sections.

In the latter case the system of particle detectors shown in Fig. 19 has been used [58] Belletini et al. [58] have shown that for heavy nuclei this method gives the same results as the method of poor geometry used earlier by Ashmore et al. [71]. However, for light nuclei the method of poor geometry gave values of cross section that were too low (in Be by 25%, in C by 17%).

3.2. Cross section of the interaction of nucleons with lead nuclei

The cross section of the interaction of nucleons with lead nuclei equals 1800 mb and is independent of energy. Tables 10 and 11 give the results of the measurements of cross sections in lead at various energies. For convenience, the values of the cross sections and of the inelastic interaction paths are given.

The cross section of the interaction of nucleons with lead nuclei lies in the interval 1760—1800 mb. Within the limits of twice the statistical error the cross section of the interaction of nucleons with nuclei varies by less than 15% in the interval from 1 to 10^5 GeV.

TABLE 10. AVERAGE VALUES OF CROSS SECTIONS OF THE INTERACTION OF NUCLEONS WITH LEAD NUCLEI FOR VARIOUS ENERGY INTERVALS

Energy interval, GeV	Inelastic interaction cross section, mb	Interaction path g/cm^2	Remarks
1—10	1760	—	Accelerators
10—100	1770 ± 30	197 ± 3	Accelerators
	1850 ± 100	188 ± 10	Cosmic Rays
10^2—10^3	1310 ± 220	192 ± 20	"
10^3—10^5	1790 ± 140	195 ± 15	"

/87

3.3. Cross section of the inelastic of nucleons with carbon nuclei

At accelerator energies the cross section of inelastic interaction of nucleons with carbon nuclei has been studied by the methods of good and poor geometry. The latter method almost completely eliminates the quasi-elastic interaction. The cross section of inelastic col-

*A large amount of reference material on effective cross sections of elastic and inelastic interactions from very low to cosmic energies is given in the monograph of V. S. Barashenkov [61].

TABLE 11. CROSS SECTION OF THE INTERACTION OF NUCLEONS WITH LEAD NUCLEI

Energy, GeV	Interaction cross section, mb	Path, g/cm^2	Remarks	Ref.
1.4	1727±45	202±5	Accelerators	[72]
2.8	1630±75	214±10	"	[73]
3.0	1930±300	180±30	"	[74]
4.0	2050±13	170±2	"	[75]
5.0	1670±79	203±8	"	[76]
8.3	1713±66	197±6	"	[77]
17	1740±90	200±10	"	[78]
20	1750±50	199±6	"	[58]
23	1810±60	192±4	"	[79]
23.3	1750±30	199±3		
24.0	1820±50	191±5	"	[71]
20	2150±100	162±8	Cosmic Rays	[80]
30	1550±130	225±18	"	[81]
150	1810±570	192±40	"	[82]
400	1800±250	194±24	"	[83]
$3\cdot10^3$	1730±170	201±17	"	[84]
$4\cdot10^3$	1910±300	182±25	"	[84]
$7\cdot10^4$	1810±380	192±34	"	[85]

lision, measured by the method of poor geometry [71], was found to be equal to (218 ± 2) mb, and by the difference between the total cross section and the cross section of elastic coherent scattering (254 ± ± 4) mb. /87

In cosmic rays, the method of beam extraction has been used for the measurement of inelastic cross sections. In the experiments of Rubtsov et al. [86] at 600 GeV (Table 12), the interaction was fixed from the electron-photon cascade. The result agrees with the data taken at 20 GeV [71]. The possibility is not excluded that in using the electromagnetic cascade for identification of the interaction the cross section is somewhat underestimated if π^0-mesons do not arise in all inelastic interactions. It is not easy to estimate the size of this effect at the present time; presumably, it is not large. /88

In the work of Bolotov et al. [82] the cross section of the interaction of neutrons with carbon nuclei was studied with the aid of a spark chamber. Events were selected on the basis of the appearance of two particles in the chamber. The result is close to the preceding one. A similar event selection, but using gas discharge counters was employed by Bozoki et al. [81]. They worked with primary neutrons of about 30 GeV in energy, i.e., very close to the interval of accelerator energies. They obtained an interaction cross section of 256 ± 15 mb, which corresponds with experiments with good geometry in an accelerator. It is possible that their experimental set-up (Fig. 19b) more effectively registered quasi-elastic scattering than other cosmic ray experiments. /89

Comparing the results of these experiments, we find that the cross section of the inelastic interaction of nucleons with carbon nuclei is independent of energy from 20 to 1000 GeV.

Other authors [62] came to a different conclusion. Preliminary data obtained with the "Proton" satellites show that the cross section of the interaction of protons with carbon nuclei increases somewhat from 221 ± 3 mb at 24 GeV to 256 ± 15 mb at about 1000 GeV. This work was done by the beam extraction method, and registration of the interaction required the passage through the detector of two charged particles. The detector, a scintillation counter, was placed under a layer of lead, which gave the possibility of registering cases when there were

TABLE 12. INELASTIC CROSS SECTION OF THE INTERACTION OF NUCLEONS WITH CARBON NUCLEI

Eo,GeV	σ, mb	λ, g/cm^2	Ref.	Remarks
2.2	260 ± 6	77 ± 2	[87]	Acceleration
2.8	230 ± 12	88 ± 5	[73]	"
5.0	235 ± 16	85 ± 6	[76]	"
8.3	218 ± 8	92 ± 4	[77]	"
20	254 ± 4	79 ± 1	[58]	Cross section includes incoherent scattering
32	256 ± 15	78 ± 4	[63]	Cosmic Rays
20	257 ± 33	78 ± 9	[67]	"
24	221 ± 3		[62]	Cross section does not include incoherent scattering
60	237 ± 4		[62]	
150	220 ± 70	91 ± 30	[82]	Cosmic Rays
170	242 ± 3		[62]	"
400	$220 \pm {}^{40}_{70}$		[83]	"
510	270 ± 5		[82]	"
600	$220 \pm {}^{20}_{26}$	$91 \pm {}^{12}_{8}$	[86]	"
1100	256 ± 15		[62]	"

only π^0-mesons among the secondary particles. This system nevertheless miscounted some of the interactions, specifically reactions of the type

/88

$$p + n = \pi^+ + n + n;$$

$$p + p = \pi^+ + n + p.$$

Experiments in an accelerator at an energy of 27 GeV showed [30] that in the interaction of protons with light nuclei of an emulsion there is only one charged particle in the final state in 10% of the cases. As the primary particle energy increases the fraction of cases with $n_s = 1$ decreases, since the average multiplicity increases. Thus, some part of the change in cross section with energy in the "Proton" experiments can be attributed to this effect. However, the situation remains unresolved due to the impossibility of obtaining agreement among the absolute values of cross sections obtained in different experiments.

In what follows we shall use a cross section of inelastic interaction equal to 255 mb as the most probable value.

/90

3.4. Interaction path in air

The interaction path in air is 85 g/cm^2. In experiments carried out under the direction of Grigorov [68, 70], as well as Zatsepin [69], the lower limit possible values of the inelastic interaction cross section was determined from measurements in air (for method, see Section 2). The results of this work are given in Table 13.

At energies less than 10^3 GeV, the results presented in Table 13 can be correlated with the idea that the cross section is constant in the energy interval from 20 to 10^3 GeV. However, for E_0 of the order of 10^4 GeV, the lower limit of the possible values of the cross section measured in [68] is 20% greater than the cross section in the interval 20 to 10^3 GeV. Such a change could have arisen on account of a four- or fivefold error in the intensity measurement of because of an increase

TABLE 13. LOWER BOUNDARY OF POSSIBLE VALUES OF THE INTERACTION CROSS SECTION IN AIR (in mb)

E_0, GeV			Refs.
10^2	10^3	10^4	
≥ 235	≥ 285	≥ 337	[68]
—	$\geq 280 \pm 15$	$\geq 283 \pm 15$	[69]

in the index of the spectrum of the primary protons at energies $E_0 > 10^3$ GeV (see Chapters XII and XIII).

The magnitude of the cross section of the interaction of nucleons in air can be estimated on the basis of measurements of their absorption path length L, using the formula $\lambda = L(i - <\beta^{\gamma-1}>)$, where β is the fraction of energy remaining with the nucleon after collision, and γ is the exponent of the differential energy spectrum.

The absorption path is 110 g/cm^2 in the energy interval 10^2—10^3 GeV. The magnitude of $<\beta^{\gamma-1}>$ is in the interval 0.25—0.35 (see Chapter XII). From this /91 we find $72 < \lambda < 90$, i.e., $\sigma = 274 \pm 30$ mb, $\lambda = 83 \pm 9$ g/cm^2. This value corresponds with the cross section in carbon $\sigma_c \sim 245 \pm 27$ mb, which agrees with other results and with accelerator data.

In the region of energies greater than 10^4 GeV, estimates of interaction cross sections are made using results of the study of wide atmospheric showers. The upper limit of the interaction cross section may be obtained from data on the height dependence or the angular distribution of wide atmospheric showers, which give an absorption path length of 140 g/cm^2, i.e., the upper limit of the interaction path.

The lower limit of the interaction path depends on assumptions about the mechanism of shower development. Hence the values obtained are included in a rather wide interval. According to data of Vernov et al., [88]

$$65 \leqslant \lambda \leqslant 140 \text{ g/cm}^2,$$
$$120 \leqslant \sigma \leqslant 360 \text{ mb}.$$

3.5. Dependence of the inelastic interaction cross section on atomic number

Figure 20 gives the results of measurements of cross sections of the interaction of nucleons with various nuclei [58, 61, 63, 83, 84].

In an accelerator at 20 GeV, the cross section of inelastic interaction was obtained by a single method for a wide selection of atomic nuclei [58]. In this case the dependence of cross section on atomic number has the form $\sigma \sim A^{2/3}$ (for $A > 12$). For $A \leq 12$, the dependence has an irregular character.

The figure gives averaged data obtained in cosmic rays and in an accelerator. In calculating the averages results with large statistical errors were included.

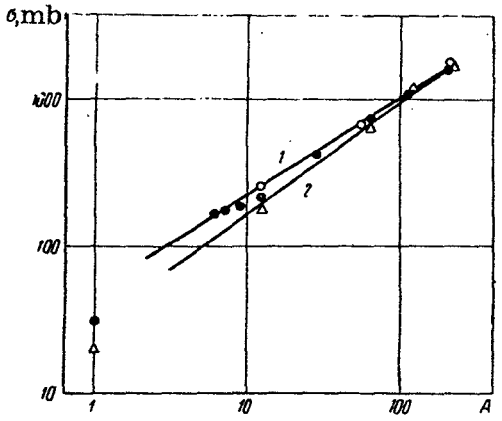

Figure 20. Cross Section of the Inelastic Interaction of Pions and Nucleons With Various Nuclei:

●-results of measurement of the nucleon-nucleus cross section in an accelerator [58] ○-the same from cosmic ray measurements; Δ-cross sections of the pion-nucleus interaction; 1—dependence $\sigma \sim A^{2/3}$; 2—$\sigma \sim A^{3/4}$.

Figure 20 shows that in the interval of A from 16 to 208, the points lie well on the straight line corresponding to the dependence $\sigma \sim A^{2/3}$.

Usually, deviations of the dependence of the cross section from the $A^{2/3}$ law (see Section 1) are associated with a decrease in the transparency of heavy nuclei. /92

The quantity N(A) (see Section 1.1) introduced by Belletini et al., [58] is equal to the number of nucleons in a nucleus, a collision with which (nucleons) does not lead to creation of new particles. Consequently, the ratio $N(A)/A = 1.6\,A^{2/3}$ emerges as a better measure of the transparency of a nucleus, in the opinion of the authors of [58], then the usual formula

$$T = 1 - \frac{\sigma}{\pi R^2}, \qquad (4.13)$$

where T is the transparency, R is the nuclear radius determined from scattering, and σ is the inelastic interaction cross section. The magnitude of the transparency for various nuclei is given in Table 14.

In cosmic rays, nuclear transparencies have been studied by Askowith and Sitte [67]. They determined the cross section of inelastic interaction of nucleons with nuclei by the method of comparing the number of interactions in various substances and in lead [Eq. (4.12)]. If we recalculate the results of these authors using the presently known values of λ_{Pb} and the exponent of the energy spectrum $\gamma - 1 = 1.7$ (see Chapter XII), we find the following values of cross section of 20 GeV: $\sigma_{Li} = 180^{+20}_{-30}$; $\sigma_C = 275^{+40}_{-30}$; $\sigma_{Al} = 425 \pm 45$ mb. Using the values of the nuclear radius from [58], we obtain the transparencies given in the first row of ble 14. /93

The question of the dependence of cross section on atomic weight of the nucleus has attracted the attention of both theorists and experimentalists in connection with the study of the asymptotic behavior of cross sections. In [89] the asymptotic relation between the total cross sections of nucleon-nucleon σ_{NN} and nucleon-nucleus σ_{NA} interactions was obtained:

$$\sigma_{NN}\sigma_{AA} = (\sigma_{NA})^2, \qquad (4.14)$$

TABLE 14. TRANSPARENCY OF SEVERAL NUCLEI AT 20 GeV.

Element							Refs.
Li^6	Li^7	Be^9	C^{12}	Al^{27}	Cu^{63}	Pb^{208}	
0,47	0,43	0,41	0,25	0,15	0,16	0,09	[58]
—	0,51+0,03		0,25±0,10	0,22±0,05	—	—	[67]

Commas represent decimal points.

which is satisfied by the following dependences of cross section on atomic number:

$$\sigma_{NA} = A\sigma_{NN} \quad \text{and} \quad \sigma_{AA} = A^2\sigma_{NN}. \tag{4.15}$$

Such a dependence signifies an increase in transparency and nucleonic radius in the limiting case of high energies.

The experimental data that has been considered show that up to energies of 10^4 GeV, a dependence like (4.15) is not approached. If it were, the interaction path in all substances would tend to the same limit /94

$$\lambda_\infty = \frac{m_p}{\sigma_{NN}}, \tag{4.16}$$

where m_p is the proton mass, and σ_{NN} is the cross section of a nucleon-nucleon collision.

Gell-Mann and Udgaonkar [90] considered the question of the asymptotic behavior of the inelastic cross sections σ_{NA} and found that in the case of a complex nucleus the cross section satisfies (4.15) with allowance made for the "shadow correction". This correction is proportional to $1/\ln E_0$. Table 15 are presented the numerical estimates of the dependence of the quantity $\sigma_{NA}/\pi R_A^2$ on energy for two nuclei (R_A is the radius of nucleus A).

Thus, a 25% change in cross section sets in only at energies of the order of 10^6GeV, and the asymptotic limit is practically unattainable.

3.6. Interaction path of nucleons in an emulsion

Nuclear emulsions have an extremely complex composition. Table 16 gives the number of nuclei of the basic components for two types of emulsion (in order to obtain the number of nuclei per cm^3 it is necessary to multiply the numbers in the second and third columns of the table by 10^{22}).

TABLE 15. DEPENDENCE OF THE EFFECTIVE CROSS SECTION OF INELASTIC PROCESSES ON ENERGY AND ATOMIC NUMBER

Atomic number	Energy, GeV				Asymptotic limit
	10	10^2	10^4	10^9	
12	0,98	1,1	1,22	1,23	2,29
216	1,05	1,14	1,24	1,32	6,00

Commas represent decimal points.

The composition of the compared emulsions is very similar. /95

The last column of the table gives the calculated fraction of cases of interaction of the nucleon with the different nuclei. In calculating the total cross section the results of measurement of cross section of nuclei in [58] were used. The probability of collision of a nucleon with a free proton in the emulsion is very small (less than 3%).

In 74% of the cases, a collision with heavy nuclei takes place. Using the data of Table 16, one finds that the interaction path of nucleons in an emulsion should be equal to 30 cm.

Recently, the experimental data obtained in photoemulsions was analyzed by Daniel et al., [64] as well as by others [91, 92]. The results are given in Table 17.

TABLE 16. CHEMICAL COMPOSITIONS OF NUCLEAR PHOTOEMULSIONS AND THE PROBABILITY OF INTERACTION OF NUCLEONS WITH THE VARIOUS NUCLEI OF THE EMULSION

Probability of interaction	Emulsion		Chemical element
	G-5	NIKFI-R	
H	3,37	2,93	0,026
C	1,36	1,39	0,106
N	0,29	0,37	0,031
O	1,02	1,06	0,092
Br	1,02	1,02	0,343
Ag	1,02	1,02	0,400

Commas represent decimal points.

The interaction path in emulsions at accelerator energies is greater than that calculated on the basis of data on the composition of emulsions ($\lambda = 30$ cm).

The source of this discrepancy may be the difference in the methods of measuring cross sections employed in [58 and 64]. If one uses a dependence of cross section on A in the form $\sigma \sim A^{2/3}$ in calculating the interaction path in an emulsion [64], one gets $\sigma = 34$ cm.

3.7. Cross section of the nucleon-nucleon interaction /96

Direct measurements of the cross section of the inelastic nu-

TABLE 17. INTERACTION PATH OF NUCLEONS IN AN EMULSION AT VARIOUS ENERGIES

E_0, GeV	λ, cm	Method	Refs.
6—23	35.5±0.5	Accel., exam. along tracks	[64]
170	41±10	Cosmic Rays	[24]
500—10^3	26±9	Examination along tracks	[91]
10^3	$27\pm^{14}_{7}$	Cosmic Rays	[93]
		Dist. of interaction points	
$3\cdot10^3$	$22\pm^{10}_{6}$	"	[92]

cleon-nucleon interaction have been achieved at the present time only in accelerators with the aid of hydrogen targets or bubble chambers.

Averaged data in the interval 10-20 GeV give for the total cross section of the interaction $\langle\sigma_{pp}\rangle = 39.5 \pm 0.3$ mb [94]. Considering that the elastic cross section in this energy region is 9 mb [61], we obtain $\langle\sigma_{in}\rangle = 30.5 \pm 0.5$ mb. Cocconi [95] reports a value close to this: 34 ± 3 mb from bubble-chamber data and 31 ± 2 mb from counter experiments. In cosmic rays the cross section of the inelastic interaction with hydrogen nuclei has been determined from the difference of the number of interactions in paraffin and graphite blocks. Bozoki et al., [63] measured the cross section of the nucleon-nucleon interaction in cosmic rays. At energies of 30 GeV, $\sigma_{pp} = 35 \pm 11$ mb and 60 GeV, $\sigma_{pp} = 34 \pm 12$ mb. This same method is used in the "Proton" satellites [62].

To obtain the magnitude of the nucleon-nucleon cross section in the region of very high energies it is possible to use Eq. (4.5) and the graphs in Figs. 17 and 18, which relate the inelastic cross sections on nuclei with the total nucleon-nucleon cross section.

At accelerator energies this method may be checked directly. For this, we compare the nucleon-nucleon cross sections calculated from Eq. (4.5), starting from recent measurements of the inelastic cross section on different nuclei [58], with the cross section of the nucleon-nucleon collision from measurements in hydrogen bubble chambers ($\sigma_{NN} = 39.5$ mb). The results of this comparison are given in Table 18.

The difference between the average calculated value of the nucleon-nucleon cross section and the true one does not exceed 10% and is completely explained by the anomalously high magnitude of the cross section in beryllium. If we consider only nuclei that are heavier than beryllium, the difference does not exceed 3%.

Thus, there is hope of obtaining the correct value of the nucleon-nucleon cross section even from measurements on nuclei at very high energies. For this we use the values of cross sections at the highest energies. The results are given in Table 19. /97

The average value of the total nucleon-nucleon cross section differs little from that observed at energies attainable in accelerators.

4. Cross Section of the Interaction of Mesons with Nuclei

4.1. Pion-nucleon interactions

The pion-nucleon interaction cross section is less than the nucleon-nucleon cross section. Measurements made in accelerators with bubble chambers give for the total pion-nucleon interaction cross section a value which can be approximated from the formulas [61] (kinetic energy T > 10 GeV).

$$\left.\begin{aligned}\sigma_{\pi^- p} &= (23.6 \pm 0.9) + \frac{8.3 \pm 3.5}{T^{1/2}};\\ \sigma_{\pi^+ - p} &= (21.6 \pm 0.8) + \frac{9.3 \pm 3.4}{T^{1/2}}.\end{aligned}\right\} \qquad (4.17)$$

For experiments with cosmic particles energies $E_0 \gg 10$ GeV play a role, i.e., the asymptotic values of Eqs. (4.17). The difference noted in [61] between the asymptotic values for π^+- and π^--mesons is therefore practically nonexistent in cosmic rays.

TABLE 18. COMPARISON OF CALCULATED CROSS SECTIONS (in mb) OF NUCLEON-NUCLEON INTERACTIONS WITH MEASURED VALUES

Cross section	Target nucleus					Nucleons
	Be	C	Al	Cu	Pb	
Measured, inelastic interaction	227	254	472	850	1750	31
Calculated, total nucleon interaction	60	42,5	38,5	39,0	44,5	Average 44,5

Commas represent decimal points.

The inelastic cross section is calculated as the difference between the total and elastic cross sections. The latter varies insignificantly (from 5 to 4 mb) in the region of energies ~ 10—20 GeV. Consequently, the inelastic interaction cross section of pions with nucleons is close to $\sigma_{\pi p} = 20$ mb. The cross section of the inelastic nucleon-nucleon interaction is $\sigma_{pp} = 30$ mb; hence, $\sigma_{pp}/\sigma_{\pi p} = 1.5$.

4.2. Cross section of the interaction of pions with nuclei

Figure 20 shows the dependence of the cross section of the inelastic interaction of pions with nuclei at energies of 10—30 GeV. This dependence is somewhat stronger than for nucleons and can be approximated for $A \geq 12$ by $\sigma_{\pi A} \sim A^{0.8}$. The smaller values of the cross sections of the interaction of pions with light nuclei is easy to understand, in view of the small magnitude of the cross section of pion-nucleon interaction.

At higher energies, information about pion interaction cross sections is very fragmentary.

All available results have been obtained by the photoemulsion method for secondary particles originating in electron-nuclear showers; 80% of such particles are pions.

The average inelastic interaction path of pions in an emulsion is [93] /99

$$\lambda = (35{,}9 \pm 2\ 9)\ \text{cm} \quad 50 < E_0 < 300\ \text{GeV};$$
$$\lambda = (41 \pm 7)\ \text{cm} \quad 1 < E_0 < 100\ \text{GeV}[92];$$
$$\lambda = \left(37 \pm {}^{5}_{4}\right)\ \text{cm} \quad 10^3 < E_0 < 10^4\ \text{GeV}[53].$$

A path length of $\lambda = 37\ {}^{+4}_{-5}$ cm corresponds to a total π-nucleon cross section of $\sigma_{\pi p} = 29\ {}^{+11}_{-7}$ mb. These magnitudes are close to those observed in accelerators. Consequently, the cross section of π-emulsion and π-nucleon collisions is essentially invariant at energies from 10 to 10^4 GeV.

TABLE 19. CALCULATED TOTAL NUCLEON-NUCLEON CROSS SECTION AT COSMIC ENERGIES

Substance	Energy	Measured nucleon-nucleus cross section, mb	Calculated total nucleon-nucleon cross-section, mb
Pb	10^3—10^5	1790 ± 140	$52 \pm {}^{?}_{19}$
Fe	10^2—10^3	710 ± 50	$29 \pm {}^{6}_{5}$
C	10^2—10^3	220 ± 20	$34 \pm {}^{4}_{6}$
Emulsion	$>10^3$	$\left[\lambda = \left(27 \pm {}^{14}_{7}\right)\text{cm}\right]$	$70 \pm {}^{\infty}_{46}$
Average			$46 \pm {}^{?}_{6}$

4.3. Interaction path of pions in air

The interaction path of pions in air is 125 g/cm^2. By interpolation in Fig. 18 it is possible to obtain the cross section of the inelastic interaction of pions in air at an energy of several GeV. This cross section corresponds to a path $\lambda_\pi = 102$ g/cm^2. At higher energies the interaction path is determined from the asymptotic value of the elementary cross section $\sigma_{\pi p}$ (4.17) and the graphs in Fig. 18. As a result, we obtain the dependence of λ_π on energy represented in Fig. 21. A similar calculation was carried out in [96]. In both cases the asymptotic values of the interaction paths are close to 125 g/cm^2. Thus, the interaction cross section of pions in air should be considered to be smaller than for protons:

$$\sigma_{p,A=14} = 285\ \text{mb}, \quad \lambda_p = 85\ \text{g/cm}^2;$$
$$\sigma_{\pi,A=14} = 194\ \text{mb}, \quad \lambda_\pi = 125\ \text{g/cm}^2.$$

Certain data obtained in an accelerator [97] support this. In this work, the interaction cross section of pions with nuclei was investigated in a bubble chamber /100

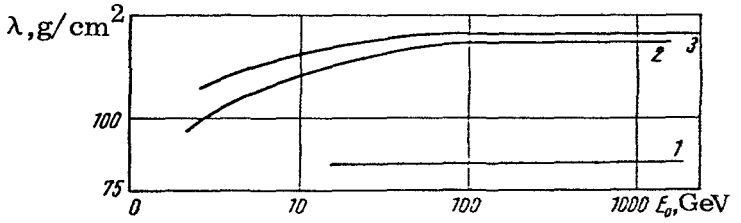

Figure 21. Interaction Paths of Nucleons (1) and Pions in Air (2—From the Graph in Fig. 18; 3—From [96].

filled with a mixture of propane (68%) and Freon (32%). The number of nucleons in the average nucleus was $\langle A \rangle = 12.3$. The results obtained are presented in Table 20.

4.4. Cross section of the interaction of K-ons with nucleons and nuclei

There is no information about the cross section of the interaction of K-ons at energies greater than 20 GeV. The experimental data on the dependence of total cross section on energy at E > 10 GeV can be approximated by the expression [61]

$$\sigma_0(E) = (18.0 \pm 1.3) + \frac{12.4 \pm 4.8}{E^{1/2}} \text{ mb.}$$

The elastic cross section evidently tends to a constant value of 3—4 mb. Consequently the cross section of inelastic K-on—nucleon interaction must be close to 14—15 mb.

Using the graphs in Fig. 18, it is possible to calculate the cross section of the inelastic collision of K-ons with nuclei, which is approximately equal for carbon to 160, for iron to 600, and for lead to 1400 mb. The interaction path of k-ons in air calculated from these data is close to 140 g/cm^2.

5. Interaction Paths of Primary Nuclei

5.1. Interaction path of nuclei in an emulsion

One of the first investigations of the interaction path of primary nuclei in an emulsion was made by Bradt and Peters [98]. For the calculation of the cross section of the collision of a nucleus A_1 with a nucleus A_2 they used the formula

$$\sigma_{A_1 A_2} = \pi r_0 (A_1^{1/3} + A_2^{1/3} - 1.17). \qquad (4.18)$$

For A_1, $A_2 > 12$ this expression is valid with deviations of ±15%, if r_0 is taken equal to 1.45 F. /101

The majority of measurements of the inelastic interaction paths of heavy nuclei have been made in the region of relatively low energies per nucleon, where the intensity of these nuclei is not too small. The interaction path of α-particles has been measured up to energies $\sim 10^3$ GeV. The results of measurements of the interaction paths of nuclei with $Z \geq 3$ and α-particles in emulsions at various energies are given in Tables 21 and 22.

Evidently, the inelastic interaction path does not vary with energy. The interaction path of the deuteron in an emulsion is 16.2 ± 1.4 cm [103].

Aditya [103] used the available data on the interaction paths of various nuclei in an emulsion to determine the effective radius of the nucleon, assuming that the nucleus can be represented as a rough disk. According to this model, the interaction cross section of two nuclei (incident nucleus of radius R and target nucleus or radius r_i) is

$$\sigma_i = \pi (R + r_i)^2. \qquad (4.19)$$

The radius of the nucleus is expressed by the formula $R = r_0 A^{1/3}$. These relations permit the calculation of λ_i as a function of r_0 and the dimensions of the primary particle A. Hence, experiment gives the possibility of finding r_0, if the dependence of λ on A is measured. The experimentally determined radius r_0 varies somewhat from 1.13 F for $3 \leq Z \leq 5$ to 1.07 F for $Z \geq 20$. For light primary nuclei, e.g., He^4, D^2, H^1, large deviations from the expected value of λ_i /102

TABLE 20. CROSS SECTION OF THE INTERACTION OF PIONS WITH NUCLEI, MEASURED IN A PROPANE-FREON CHAMBER [97]

Energy, GeV	Inelastic interaction cross section, mb
6.1	193±7
11.6	187±7.5
18.1	186±8.6

TABLE 21. INTERACTION PATHS OF NUCLEI WITH $Z \geq 3$ IN EMULSIONS AT ENERGIES OF 1.5—40 GeV (in cm)

Z=3–5 <A>=8	Z=6–9 <A>=14	Z>10 A>20	Z>20 A>40	Refs.
16,1±5,1	15,6±1,6	9,6±1,3		[99]
		9,4±1,4	7,0±1,4	[100]
13,5±1,6	13,6±1,0	9,6±1,3	9,2±1,8	[101]
13,2±2,8	13,2±1,0	10,9±2,9		[45]
13,4±1,4	13,0±0,9	11,5±1,1	9,2±2,1	[37]
15,5±1,8	13,4±1,0	11,0±1,3		[102]
14,2±1,2	13,6±0,7	10,2±0,8	8,4±1,2	[103]
Weighted averages				
14,9±0,8	13,9±0,5	10,9±0,5	8,7±0,5	

Commas represent decimal points.

TABLE 22. INTERACTION PATHS OF α-PARTICLES IN EMULSIONS

E_0, GeV/nucleon	λ_α, cm	Refs.	E_0, GeV/nucleon	λ_α, cm	Refs.
6	$20,5\pm2,2$	[104]	40	$18,1\pm2,3$	[37]
8	$18,4\pm4$		166	27 ± 7	[24]
10	$19,7\pm2,4$	[37]			
12	$17,5\pm1,0$	[105]	300	$29,2\pm{}^{11}_{6}$	[107]
20	$19,7\pm2,0$	[106]	500	$25,8\pm{}^{20}_{8}$	[108]
20	$20,2\pm1,7$	[37]	$3\cdot10^3$	$18,0\pm{}^{9}_{6}$	[62]

Average value $18,7\pm0,6$

Commas represent decimal points.

TABLE 23. INTERACTION PATH OF HEAVY NUCLEI IN CARBON

Z	λ, g/m^2	Calculated from Eq. (4.19)	Calculated from Eq. (4.18)
6—9	$21,6\pm1,9$	20,9	24,2
$\geqslant10$	$15,5\pm1,7$	15,9	16,9
10—16	$15,7\pm2,1$	17,5	18,9
16—19	$13,9\pm4,4$	14,7	15,3
$\geqslant20$	$15,5\pm4,2$	12,9	13,0

Commas represent decimal points.

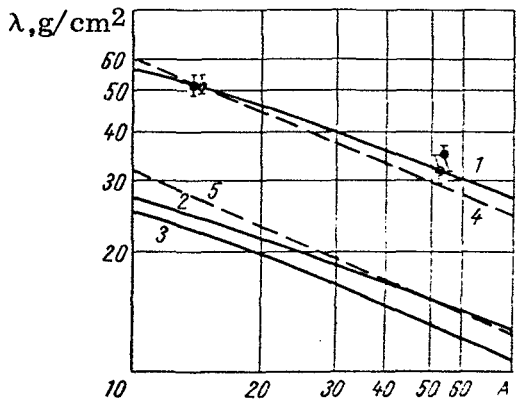

Figure 22. Calculation of Interaction Paths λ of Nuclei in Various Substances.

Calculation from Eq. (4.19): 1—for an emulsion; 2—for air; 3—for celluloid. Calculation from Eq. (4.18): 4—for an emulsion; 5—for air [109a].

are observed. In fact, a nucleon radius of 1.1 F gives $\lambda_1 = 25.5$ cm, and not 36 cm, the experimental value (see Section 3).

The experimental value of the cross section of inelastic p-p interaction leads to $r_0 = 0.5$ F. If in calculating σ from Eq. (4.19) we assume a nucleon radius of 0.5 F, then for all primary nuclei with $Z \geq 3$, we obtain $r_0 = 1.16 \pm \pm 0.03$ F. The deviation from Eq. (4.19) for light nuclei is explained by their structure. The radius of the most compact organized system of α-particles is $r_0 = 1.04$ F, and of the most loosely organized system—the deuteron—1.62 F.

5.2. Interaction paths of primary nuclei in carbon

Badhwara et al., [109] investigated the interaction paths of heavy nuclei in carbon at primary energies $\sim$ 16.8 GeV/nucleon. The results of these measurements are given in Table 23. /103

The authors state that the rough disk model [see Eq. (4.19)] gives somewhat better agreement with experiment than Eq. (4.18).

5.3. Interaction path of nuclei in air

Using Eq. (4.19) it is possible to calculate the interaction path in air for various nuclei. The results are given in Fig. 22.

CHAPTER 5

MULTIPLICITY AND NATURE OF SECONDARY PARTICLES

1. Introduction

1.1. Electron-nuclear showers

Electron-nuclear showers were discovered by Soviet physicists under the direction of Veksler and Skobeltsin in 1949 [110]. The principal feature of these showers is the multiple creation of secondary nuclear-active particles, mostly pions. Neutral pions, which have a lifetime of 10^{-16} s, decay and initiate the electron-photon cascades. These are the basic processes in cosmic rays. /104

Microphotographs of electron-nuclear showers registered in photoemulsions are shown in Fig. 23 [111]. The first thing that comes to our attention is the high multiplicity of secondary particles.

At an early stage of the investigation there arose a discussion about whether the formation of particles was due to multiple collisions with several nucleons of a nucleus. The famous star of Shein [112], which now decorates many books, gave serious proof of the multiple character of meson production. In this star, 14 secondary particles originate simultaneously in a nucleon-nucleon collision.

1.2. Classification of secondary particles

The multiplicity of particles of a given kind may serve as one of the physical characteristics of the interaction process, e.g., the number of pions, K mesons, protons. However, in the majority of cases, the nature of the particles cannot be identified, and so one often turns to a phenomenological classification based on differences in ionizing ability.

By studying nuclear collisions in emulsions sensitive to relativistic particles, Brown et al., [113] introduced a classification of secondary particles using measurements of the density of grains in the tracks of particles in the emulsion. They deemed it sufficient to consider three groups of tracks.

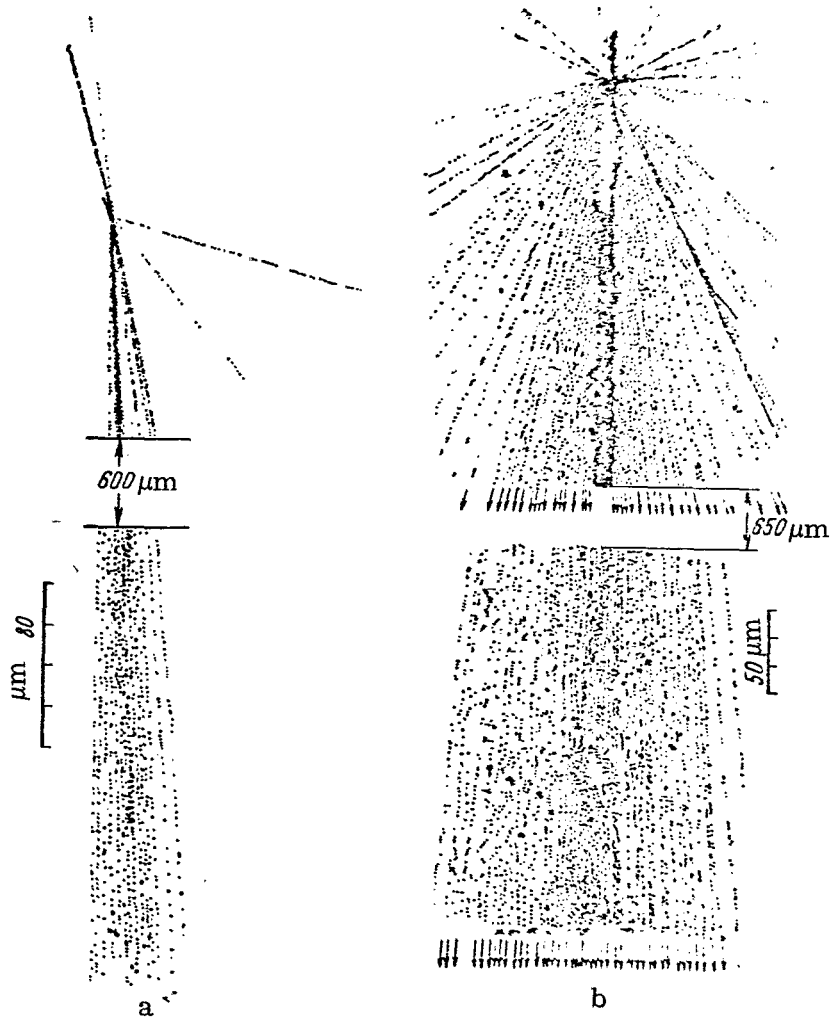

/105

Figure 23. Microphotographs of Electron-Nuclear Showers in Photoemulsion [111]:

a—shower type (2 + 3 + 40)p; b—shower type (6 + 9 + 330)Z; $Z \approx 20$.

First, there are tracks created by strongly ionizing particles. The density of grains in this case $G > 1.4g_{min}$, where g_{min} is the density of grains in a track created in the emulsion by a particle with unit charge and with kinetic energy close to the intrinsic mass. The number of such tracks in each star is symbolized N_h. /106

Strongly ionizing particles leave tracks of two types: "gray", for which $1.4g_{min} \leq G \leq 6.8g_{min}$, and "black", when $G > 6.8g_{min}$. The number of rays

in the stars is symbolized N_g and N_b, respectively. These groups of tracks are distinguished by the fact that two maxima are observed in their distribution over G—in the region $1.5—2g_{min}$ and at $15g_{min}$.

Finally, "thin" tracks with $G < 1.4g_{min}$ are created by relativistic (shower) particles. The number of such particles in a shower is symbolized n_s.

Later, this classification was made more complicated. For nucleon-nucleon and pion-nucleon collisions the following groups of particles are considered [114]: n, the total number of secondaries; n_s, the number of shower tracks. They correspond to π-mesons with energies T > 60 MeV, protons with energies T > 400 MeV, etc., (T is the kinetic energy); n_p, the number of fast recoil protons (T > > 400 MeV); $n_{\pi^\pm}$, the number of charged pions with T > 60 MeV; $n_{X^\pm} = n_s - n_p - n_{\pi^\pm}$ is the number of particles other than pions and protons; n_c, the number of newly created charged particles (T > 60 MeV); $n_c = n_s - n_p$.

2. Strongly Ionizing Particles

2.1. Average number of strongly ionizing particles

At a high energy of the primary particle, strongly ionizing particles are formed as the result of nuclear fragmentation or the formation of recoil nucleons. The products of nuclear fragmentation have been studied mainly by the photoemulsion method. Here it is particularly important to mention the basic work of Powell and his colleagues. A survey of the results of these authors is given in [45].

The average number of strongly ionizing particles does not depend on the energy of the primary. Jain et al., [115] analyzed the dependence of N_h on the energy of the primary particle in the interval from several GeV to the maximum energies studied in cosmic rays, which exceed 10^3 GeV. In the region below 1 GeV, $<N_h>$ decreases and reaches 3 at 100 MeV. The results of various measurements are summarized in Fig. 24. This figure demonstrates the practically complete constancy of $<N_h>$ in the interval from 10 to 10^3 GeV for stars created both by protons and by pions. At cosmic energies the data for pions were obtained from observation of interactions of secondary particles. /107

2.2. Features of the differential distribution of N_h

The differential distribution of N_h in stars created by protons in accelerator experiments is shown in Fig. 25 [116]. The results were obtained by looking for stars along the tracks of primary particles. This method gives the possibility of finding all stars, including $N_h = 0$. In cosmic-ray investigations, when one often has to look over the area of a photoemulsion, stars with small $N_h = 0$, 1 may be

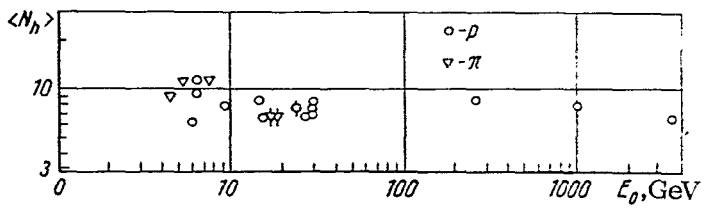

Figure 24. Average Number of Strongly Ionizing Particles as a Function of the Energy of the Primary.

lost. It is better to measure the distribution of N_h for stars originating from primary nuclei. Such a distribution is given also in Fig. 25 [116]. The difference is that the group of events with N_h from 4 to 6 is more clearly expressed in the spectrum from primary nuclei. This result is in complete agreement with the conclusions of Powell et al., [45] who also found a maximum in the distribution for $N_h > 5$ for primary nuclei with energies of 3 GeV/nucleon. These authors explain the appearance of the maximum by the more complete (compared with protons) disruption of the light nuclei of the photoemulsion by the primary nuclei. /108

In those cases when there is a disruptive interaction of the primary nucleus, i.e., when fragments with $Z > 2$ are not observed among the secondaries, the average number of black tracks is found to be extremely large [37]. Then two maxima at $N_h \sim 4$ and $N_h \sim 18$ are found, which correspond to almost complete fragmentation of a light target nucleus and considerable disruption of a heavy one.

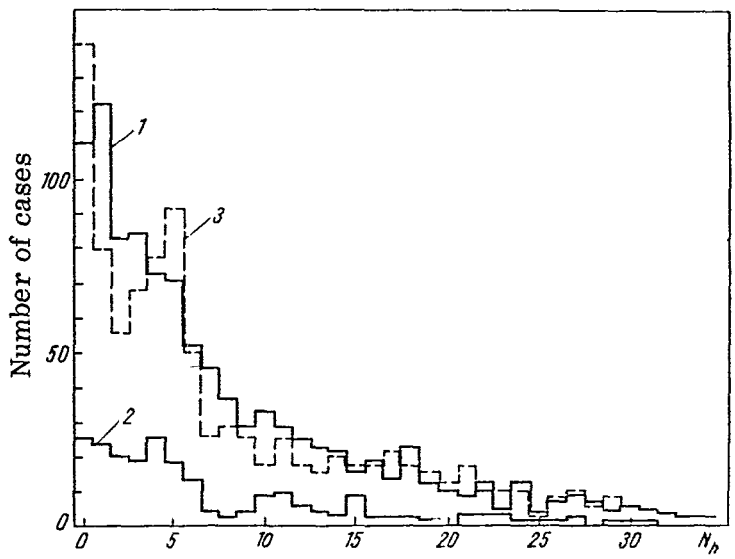

Figure 25. Differential Distribution of N_h in Stars Produced by Protons:

1—at accelerator energies; 2—in cosmic rays; 3—from the primary nuclei of cosmic rays.

If the primary nucleus is only partially broken apart and there are coarse fragments among the products, the distribution of stars over N_h has a different character [37]. The number of stars rapidly decreases with increasing N_h and the most probable value is $N_h = 0$.

2.3. Criterion for the selection of interactions with different nuclei

A common property of all these distributions is the presence of a "step" at $N_h = 6$, which systematically appears in almost all experiments. This step can /109
obviously be explained by the contribution of nuclei of the group C, N, O at $N_h \leq \leq 6$. Nevertheless, the role of interactions with heavy nuclei is significant even for a small number of strongly ionizing particles. In the region $N_h \leq 6$, the distribution contains about half of all the events. From Table 16 it follows that at a light nucleus there occurs only 1/4 of the whole cross section of an "effective" nucleus of the emulsion. Hence about 50% of all events with $N_h \leq 6$ occur at heavy nuclei. The majority of events with $N_h = 0, 1$ also occur at nuclei heavier than hydrogen. The total number of observed interactions with $N_h = 0$ and 1 reaches 17%, whereas the expected number of collisions of a nucleon with a free proton amounts to at most only 3%.

All the same, the criterion of selection of nucleon-nucleon collisions $N_h \leq \leq 1$ is widely used. Less scrupulous authors apply an even more liberal criterion: $N_h \leq 3$ and $N_g \leq 1$. They start from the premise that a small number of strongly ionizing particles means a weak excitation of the target nucleus. The nucleus in this case does not affect the interaction process, and the latter will resemble a nucleon-nucleon one, although the Fermi motion of nucleons in the nucleus creates a 20% indeterminacy in the energy of collision in the L system.

In choosing nucleon-nucleon collisions according to $N_h = 1$, it is usual to exclude stars that have recoil fragments or nuclei. The mass of the target m_t, the magnitude of which should be less than the mass of the nucleon, may serve as an additional criterion.

It is noted that the extraction of a neutron leaves a radioactive nucleus behind, whereas extraction of a proton leaves a stable one. This, in principle, gives the possibility of distinguishing proton-neutron from proton-proton collisions. However, it is not always easy to detect the decay electron.

The choice of interactions with $N_h \geq 8$ automatically excludes cases of weak excitation of a heavy nucleus. Therefore, by studying only cases with $N_h \geq 8$ it is impossible to obtain all the properties of the interaction with heavy nuclei. The absence of good criteria for the selection of interactions with different nuclei compels us to use the generally accepted ones: a) nucleon-nucleon interaction, $N_h \leq 2$

or $N_h = 0, 1$; b) collision with C, N, O nuclei ($\langle A \rangle = 14$), $2 < N_h \leq 5$; c) collision with heavy nuclei, $N_h \geq 6$ or $N_h \geq 7$.

2.4. Nature of strongly ionizing particles and their properties

Gray tracks are formed mainly by recoil protons. In the region of cosmic energies the number of recoil protons does not depend on the energy of the primary particles. The average energy of particles forming gray tracks in emulsions likewise is independent of the primary energy [117]. This energy is 165 MeV. According to the data of [46], the fraction of strongly ionizing pions is not large and amounts to 0.005 per interaction. Such pions, evidently, are formed as a result of the retardation of fast pions due to secondary collisions in a nucleus, since their number is proportional to the product $n_s N_h$. Slow π^+-mesons originate more rarely than π^--mesons. /110

Black evaporative tracks are formed by protons and deuterons with energies less than 25 MeV, by slow α-particles, etc., [118]. The fraction of evaporated particles of different kind depends on the dimensions of the target nucleus. In the fragmentation of heavy nuclei, the fraction of α-particles amounts to 30%, and in the fragmentation of light ones it reaches 50% of the total number of particles [119]. The fraction of deuterons and tritium nuclei is also considerable ($\sim 0.3 n_p$) [120]. Heavy fragments are rarely emitted. It is obvious that the probability of emission of fragments in the distruption of nuclei by protons equal the probability of fragmentation of high-energy primary nuclei in hydrogen (see Section 4). This problem has been investigated by Waddington [116].

The average energy of evaporated particles depends on their nature. For singly charged particles this energy is 8—10 MeV, for α-particles 16 MeV, and for neutrons 3—4 MeV.

In conclusion it remains to be said that the emission of evaporated particles occurs isotropically [45]. Gray tracks are usually more or less collimated in the direction of motion of the primary.

3. Multiplicity of Relativistic Particles n_s /111

3.1. Factors of importance in the measurement of multiplicity

At first sight it seems that the determination of the average multiplicity of relativistic particles should not encounter any difficulties using modern techniques. This is not so, however. Although in each individual case the number of particles in a shower can be counted rather accurately, it is difficult to determine the average value of the number of particles in cosmic experiments. The reasons for this are the following.

1. The multiplicity depends on energy. Hence the problem of determining the energy of the primary particle aggravates the situation.

2. The multiplicity depends on the size of the target nucleus. The absence of reliable criteria for distinguishing interactions with different nuclei in a photoemulsion makes the result inconclusive.

3. $\langle n_s \rangle$ can depend on the nature of the primary particle.

These factors have made the problem of determining the average multiplicity at different energies extremely involved and the results are contradictory.

3.2. Dependence of multiplicity on the size of the target nucleus

It is rather obvious, but not unambiguous, that an indication of the size of the target nucleus is the number of strongly ionizing particles produced in its fragmentation. Hence the presence of a correlation between n_s and N_h should be evidence of a dependence of n_s on the mass number of the nucleus A. /112

Table 24 brings together some typical data on the dependence of $\langle n_s \rangle$ on N_h.

TABLE 24. DEPENDENCE OF THE MULTIPLICITY OF SHOWER PARTICLES $\langle n_s \rangle$ on N_h

Primary particle	E_0, GeV	$N_h \leq 2$ $N_h = 0$	$N_h < 5$ $N_h \leq 5$	$N_h > 5$ $N_h > 7$	Refs.
Protons	9	—	5,0±0,1	6,0±0,3	[121]
Nucleons	>40	—	5,35±0,3*	6,4±0,5**	[122]
Nucleons	250	8,8±1,9	10±1,9	16,5±3,4	[24]
Nucleons	2700	6,4±2,5	12,2±3,1	17,4±4,0	[123]
Nucleons	3500	15±5	20±3,5	23±6,5	[124]
α-particles	160	—	14,7±4,2	31±10	[24]

*Interactions in carbon.
**Interactions in copper.
Commas represent decimal points.

Using the criteria for the selection of interactions with various nuclei (Section 2), we constructed the dependence of n_s on $\langle A \rangle$, assuming that for light nuclei $\langle A \rangle = 14$ and for heavy ones $\langle A \rangle = 94$ (Fig. 26). All the results were normalized to $\langle n_s \rangle = 16$ at $\langle A \rangle = 94$. The dependence obtained can be approximated by the expression $\langle n_s \rangle = n_s^0 A^{0.15 \pm 0.06}$

Lohrman et al., [24] and Friedlander [125] arrived at the same conclusion earlier. In determining the dependence on A, a broad range of energies was used, among them extremely small energies. This result is not contradicted by the consequences of hydrodynamical theory, which predicts a dependence of the form $n_s \sim$ $\sim A^{0.19}$. The applicability of hydrodynamical concepts at 9 GeV is doubtful, and this agreement with hydrodynamics may be accidental.

3.3. Dependence of multiplicity on energy

a. Theoretical predictions—These are:

$$n_s \sim E_0^{1/4}; \quad n_s \sim E_0^{1/4}; \quad n_s \sim \ln E_0.$$

The investigation of the energy dependence of n_s is of great interest from the point of view of selection of a theoretical model for the interaction process. /113

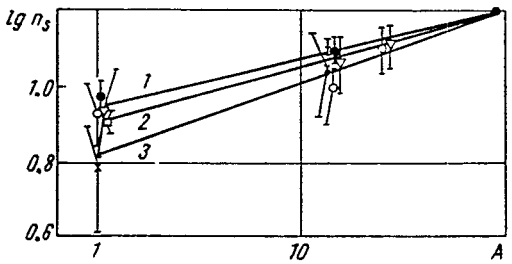

Figure 26. Dependence of Multiplicity on Mass Number:

1 — $n_s \sim A^{0.12}$; 2 — $n_s \sim A^{0.15}$; 3 — $n_s \sim A^{0.19}$.

The hydrodynamical theory of Landau [18] and the statistical theory of Fermi [126] predict a dependence of the type $n_s \sim E_0^{1/4}$ at energies greater than 100 GeV. A stronger dependence, close to $n_s \sim E_0^{1/3}$, is obtained in the statistical theory with allowance made for isobaric states [127].

The Heisenberg theory [128] gives an even stronger dependence $n_s \sim E_0^{1/2}$ or $E_0^{1/2}(\ln E_0)^2$. The completely peripheral model developed first by Amati et al., [129] predicts a logarithmic growth of n_s with energy. A similar dependence is characteristic of other peripheral models.

Thus, these few models already give a rather wide range of dependences of n_s on energy. However, any quantitative difference among them appears distinctly only at energies $E_0 \gtrsim 10^3$ GeV.

Each of the theories has a specific energy limitation. For example, strictly speaking, the Landau theory is applicable only at very high energies, whereas the peripheral models are applicable at lower energies. Hence the possibility is not excluded that one will observe different dependences of n_s on E_0 at different energies. In addition, in a certain energy region events of different types can exist simultaneously. This still further complicates the picture.

Unfortunately, information about the magnitude of $\langle n_s \rangle$ at high energies is fragmentary and not always valid (see point b). The principal task of an experiment is the accumulation reliable data.

b. The attempt to select reliable data.—For the determination of the dependence of n_s on energy, we selected papers satisfying the following criteria:

1) the energy of the primary particle is determined sufficiently reliably (see

Chapter III, Section 6, Reliable Methods); 2) the results compared were obtained through the use of identical criteria for event selection; 3) the nature of the primary particle was accounted for.

We shall consider the results collected in this fashion to be reliable. /114

For the comparison we shall also make use of other materials, obtained mainly in photoemulsions during energy determination by the Castagnoli method.

c. Dependence of $\langle n_s \rangle$ on energy: logarithmic or power-law?—Fig. 27 we show the theoretical dependences of $\langle n_s \rangle$ on energy (curves 1, 2 and 3), together with the reliable experimental data. The results used pertain almost exclusively to nucleon-nucleon interactions. The theoretical curves were normalized so that they agreed with experiment at an energy of about 25 GeV. Curves 1 and 3 practically coincide over the energy interval from 25 to 150 GeV.

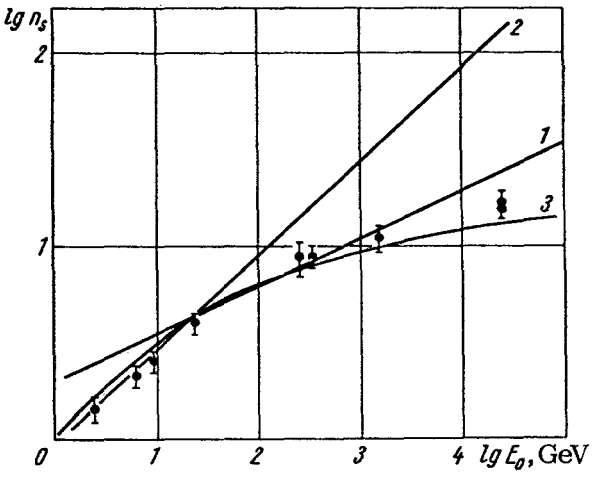

Figure 27. Dependence of Multiplicity n_s on Energy on a Log-Log Plot:

$1 - n_s \sim E^{1/4}$; $2 - n_s \sim E^{1/2}$; $3 - n_s \sim \ln E$.

As a result we obtain the following analytical representations of the functions:

$$\begin{aligned} &1)\ n_s = 2\,(E_0/M)^{1/4};\\ &2)\ n_s = 0.91\,(E_0/M)^{1/2};\\ &3)\ n_s = 3.2\lg(E_0/M). \end{aligned} \qquad (5.1)$$

The experimental material used for comparison with these expressions is listed in Table 25. /115

It follows from Fig. 27 that in the region of accelerator energies (E_0 < 30 GeV) the experimental dependence of n_s on energy can be represented by the functions (5.1) (functions 2 and 3), whereas at high energies it is difficult to make a choice between curves 1 and 3. Experiments at very high energies would be of decisive value.

For the region of energies less than 60 GeV, Malhotra [130] proposed the following approximate formula for the dependence of multiplicity on energy (E_0 in GeV):

$$\langle n_s \rangle = 0{,}95 E_0^{0{,}46}. \qquad (5.2)$$

TABLE 25. "RELIABLE" EXPERIMENTAL DATA ON MULTIPLICITY IN NUCLEON-NUCLEON INTERACTIONS

Energy of primary nucleon, GeV	Type of interaction or method of event selection*	n_s	Remarks	Refs.
3,5	p-N-emulsion	$1,5 \pm 0,2$	Accelerator	[131]
6,2	$N_h \leqslant 1$	$2,28 \pm 0,16$	"	[132]
9,0	p-N-emulsion	$2,59 \pm 0,16$	"	[133]
23,5	p-p	$4,1 \pm 0,6$	"	[134]
24,0	p-p	$4,0 \pm 0,1$	"	[135]
250	p-N-emulsion	$8,8 \pm 1,9$	Relative scattering	[24]
300	p LiH	$9,0 \pm 1,0$	Calorimeter	[136]
1300	p-nucleus	$(18 \pm 3,0)$	Castagnoli method	[91]
1300	p-N	$(11 \pm 2,0)$	in nuclear disintegration**	
12 300	$N_h \leqslant 1$	17 ± 1	Three cases***	[91]
12 300	$N_h \leqslant 5$	16 ± 3	Eight cases****	[91]

*In the majority of cases the selection of nucleon-nucleon interactions was more rigorous than was considered earlier.

**The case of fragmentation of the primary nucleus was used to determine $\langle n_s \rangle$. From the author's [91] value of $\langle n_s \rangle$ for the emulsion, the average multiplicity for the nucleon-nucleon interaction was determined with the aid of Fig. 26.

***Specifically, three cases from the disintegration of fragment No. 1010 [91].

****The same, but converted to the nucleon-nucleon interaction with the aid of Fig. 26.

The multiplicity of newly created particles $\langle n_s \rangle$ can be described by the function /116

$$n_c = 0,63E^{0,52}. \tag{5.3}$$

The valid experimental data in the interval of energies from several GeV to 10^4 GeV satisfy the nearly logarithmic law

$$\langle n_s \rangle = 2,9 \log (E_0) + 0,03E_0^{1/2}. \tag{5.4}$$

In the region of high energies this result is based on a single point at $E_0 = 1.2 \times 10^4$ GeV, from which one can judge its reliability. At this energy the average multiplicity calculated from Eq. (5.1) (function 1) is 1.5 times greater than that given by experiment. This difference cannot have any decisive value, since the statistical uncertainty of the experiment is too great.

Thus, in the energy region $E_0 > 100$ GeV, the question of whether the dependence of $\langle n_s \rangle$ on energy is logarithmic or power-law remains open.

3.4. Dependence of $\langle n_s \rangle$ on energy in the interaction of nucleons with nuclei

Table 26 gives the results of the determination of $\langle n_s \rangle$ in the interaction of high-energy nucleons with emulsion nuclei.

The energy dependence of $\langle n_s \rangle$ derived from this table is the same as that for nucleon-nucleon collisions. In the region of lower energies, the increase of multiplicity is evidently faster.

3.5. Dependence of $\langle n_s \rangle$ on energy as measured by the Castagnoli method /117

We now consider the results obtained when the energy of the primary particle is measured by the Castagnoli method.

Sanko, Takobayev, and Usik [137] analyzed 92 cases of the interaction of nucleons with $N_h \leq 2$. The energy was determined from the angular distribution of the secondary particles. They found that in the interval of variation of γ_s from 7 to 70 and higher ($E_0 > 10^4$ GeV in the latter case), $\langle n_s \rangle$ remains constant within the limits of experimental error. The same result was obtained by Malhotra [130]. The universal collection of results they collected of the determination of $\langle n_s \rangle$ for $N_h \leq 2$ leads to a value of $\langle n_s \rangle = 16.3 \pm 1.6$, constant in the energy interval 2.8×10^3 to 1.8×10^4 GeV. These results were presented in Fig. 3 together with the expected dependence of $\langle n_s \rangle$ on the measured energy with the errors of the Castagnoli method accounted for. In the calculation it was assumed that the threshold for event selection in photoemulsion work is at energy of 100 GeV. This value is typical for selection of interactions in electromagnetic cascades. It follows from the figure that the saturation of multiplicity observed in [130] and [137] can be explained by methodological effects.

TABLE 26. DEPENDENCE OF AVERAGE MULTIPLICITY ON ENERGY FOR COLLISION OF NUCLEONS WITH NUCLEI WITH $N_h \geq 0$

E_0, GeV	$\langle n_s \rangle$	Refs.
250	12.9 ± 1.8	[24]
1 300	18.1 ± 1.5	[39, 91]
12 000	24 ± 4	[91]

3.6. Determination of the average multiplicity of pions from the number of high energy photons

McCusker and Peak [138] find a logarithmic depencence of $\langle n_s \rangle$ on energy somewhat like that of (5.4). To determine $\langle n_s \rangle$ at the highest energies ($\sim 3 \times 10^4$ GeV) the results of the measurement of multiplicity of photons in the interaction of primary particles with carbon nuclei are used [139]. In order to

convert to the nucleon-nucleon collision, the authors reduced the experimental results by a factor of 1.5.*

The method of determining multiplicity from the number of photons consists of the following. With the aid of photoemulsion chambers with a carbon target, groups of photons from the interaction of primary particles with carbon nuclei are registered. /118

Those events are selected in which the total energy of the photons exceeds the specified threshold value.** The energy of the primary particle is assumed equal to

$$\langle E_0 \rangle = \langle K \rangle \sum E_\gamma , \qquad (5.5)$$

where <K> in different papers is taken equal to a value between 5 and 6 (see Chapter VI, Section 5). Photons with energies less than 50 GeV escape from observation, and corresponding corrections have to be introduced. These corrections must take into account photons of low energy emitted within the limits of the same angles in the L system as high-energy photons, as well as photons emitted backwards in the S system. The first correction, according to the estimates of the authors of [139] and [140], amounts to about 20%, and the second is estimated from the assumption of symmetry in the C system.

The Lorentz factor of the C system is found from the energy E_0 determined by formula (5.5) assuming a nucleon-nucleon collision. A certain arbitrariness in choice of <K> leads to errors in the estimate multiplicity. According to data of [139], the used of the limiting values <K> = 5 or <K> = 10 changes $\langle n_{\pi^0} \rangle$ by less than 10%. The number of charged pions is determined from the assumption of isotopic invariance. The results obtained by this method are presented in Table 27.

It is impossible to compare directly these results with the data in Table 25 and Fig. 27, for two reasons. Firstly, this method gives no possibility of allowing for the contribution of K-mesons, and, secondly, in a number of cases it is not possible to establish the nature of the primary particle. /119

The first reason, abviously, lowers the total multiplicity. If a portion of the registered events is evoked by primary nuclei, the multiplicity will turn out too high. Thus, a certain methodological indeterminacy comes about. With this allowed for, the data of Table 27 agree with the approximate formula (5.4).

In a number of papers the authors insist that the multiplicity increases with energy like $E_0^{1/4}$ [91], [141]. We have already remarked that it is practically

---

*From Fig. 26, this coefficient is 1.4.

**The energy of the photons is measured by the methods considered in Chapter VI.

TABLE 27. MULTIPLICITY OF π-MESONS, DETERMINED BY THE NUMBER OF PHOTONS IN GROUPS

/118

$\langle \Sigma E_\gamma \rangle$, GeV	$\langle E_0 \rangle = 7 \langle \Sigma E_\gamma \rangle$	$\langle n_{\pi^\pm} \rangle$	Multiplicity in nucleon-nucleon collision*	Refs.
1600	$11 \cdot 10^3$	16 ± 2	11 ± 1.5	[139]
1600	$11 \cdot 10^3$	25 ± 5	18 ± 3.5	[140]
4000	$28 \cdot 10^3$	27 ± 5	19 ± 3.5	[140]
6000	$42 \cdot 10^3$	27 ± 3.5	19 ± 2.5	[139]
6700	$47 \cdot 10^3$	$\sim 35 \pm 10$	25 ± 7.0	[140]

*Multiplicity determined from Fig. 26.

impossible to distinguish this dependence from the logarithmic one over a wide energy range. And, in the region of high energy, where experimental data are very scarce, it is necessary to exercise caution in using the results of the investigation of generation on nuclei. These results require the introduction of significant corrections, and this is not always kept in mind.

3.7. Dependence of multiplicity on the mass of the excited system

/119

From the point of view of the fireball model, the majority of pions is from a strongly excited system that does not include baryons. The mass of such a system $\mathfrak{M}$, generally speaking, can be different. The question arises, how is multiplicity connected with mass [142]? The magnitude of $\mathfrak{M}$ is rather simply determined in the case of the formation of one excited center [11]. Let two colliding nucleons transfer to the excited system energies $K_1 E_c$ and $K_2 E_c$, respectively (E_c is the energy of the nucleons in the C system). Then the mass of the excited agglomerate is

$$\mathfrak{M} = \frac{2E_c}{c^2} \sqrt{K_1 K_2}. \qquad (5.6)$$

An attempt to determine the dependence of n_s on $\mathfrak{M}$ experimentally was undertaken in [143]. The mass of the fireball was determined from (5.6), and the validity of the model with the generation of one fireball was assumed. The linear dependence of n_s on $\mathfrak{M}$ so obtained is not particularly surprising, since it reflects the approximate constancy of the energies of the pions in the C system, in the narrow interval of primary-particle energy considered. The approximate value of the mass of the conglomerate $\mathfrak{M}$ may be obtained from the formula

/120

$$\mathfrak{M} \approx \frac{3}{2} n_s \langle \varepsilon_{s\pi} \rangle, \qquad (5.7)$$

and at not very high energies there is little difference between the S and C systems.

4. Secondary Particles Produced in the Collision of Nuclei and Their Multiplicity

4.1. Fragmentation

In the interaction of heavy primary nuclei of high energy with nuclei, protons, the products of disintegration of the primary nucleus, are present among the thin tracks formed by the secondary particles. It is necessary to account for this in determining $\langle n_c \rangle$, for which the number of protons n_p is subtracted from the measured number n_s, where

$$n_p = Z_0 - \sum_{f>2} Z_f . \qquad (5.8)$$

Here Z_0 is the charge of the primary nucleus and Z_f is the charge of the secondary fragment, equal to two or more. The ionizing ability of these fragments is great, and they do not enter into the number of thin tracks in the emulsion. However, they are quite easily distinguishable from the gray and black evaporative tracks, since they are sharply collimated in the direction of motion of the primary nucleus [see Eq. (2.8)].

The probability of formation of fragments of a primary nucleus increases with its size. Table 28 gives the fraction of cases in which some number or other of fragments with $Z \geq 2$ is formed in the interaction of primary nuclei in an emulsion (averaged result [37], [100], [102].

TABLE 28. AVERAGE FRACTION OF FRAGMENTS WITH $Z \geq 2$ PER INTERACTION

Charge of the primary nucleus	Total No. of cases	Number of fragments with $Z \geq 2$			
		0	>1	>2	>3
6÷9	565	0,36±0,03	0,64±0,04	0,26±0,02	0,05±0,01
10	259	0,19±0,03	0,81±0,06	0,49±0,05	0,26±0,03

Commas represent decimal points.

/121

Let us define the fragmentation parameter P_{ij} as the average number of fragments of type j produced in the fragmentation of a primary nucleus of type i. We divide the primary and secondary nuclei into several groups depending on their charge and introduce the generally accepted notation (Table 29).

The distribution of P_{ij} for various primary nuclei with $E_0 > 7.5$ GeV/nucleon and for various targets is given in Table 30.

Selection of events in an emulsion by the criterion $N_h \leq 1$ gives a significant percentage of collisions with separate nucleons (free or bound). Hence the data in the first line of Table 30 can be considered as the fragmentation parameter for hydrogen [37].

4.2. Average multiplicity of mesons created in the interaction of α-particles with nuclei

The multiplicity of secondary, newly created particles in the interaction of α-particles with nuclei is, on the average, twice as great as in the interaction of nucleons. For the determination of the number of generated particles n_c in the interaction of primary nuclei it is necessary to exclude the protons arising as the result of nuclear disintegration from the observed number of secondaries n_s.

TABLE 29. NOTATION FOR THE VARIOUS GROUPS OF NUCLEI

Nucleus	Charge	Notation
He	2	α
Li, Be, B	3—5	L
C, N, O	6—9	M
—	⩾10	H } S
—	⩾20	VH

For a primary nucleon the correction is not large ($n_p = 0.5$ on the average). If a primary α-particle interacts, in many cases $n_p = 2$.

Investigation of n_c for primary helium nuclei has shown a significant dependence of this quantity on the degree of excitation of the target nucleus, as in the case of nucleons. Thus, for $N_h \leq 5$, $\langle n_s \rangle = 14.7 \pm 4.2$, and for $N_h > 5$, this quantity reaches 31 ± 10 (for $E_0 = 165$ GeV) [24]. These magnitudes are, generally speaking, twice as great as for nucleon-nucleus collisions at the same energies.

4.3. Other nuclei: $\langle n_s \rangle$ is proportional to Z /123

For the analysis one can use the data of [146]. These data contain 25 interactions of primary nuclei with $Z \geq 2$ and 14 interactions of secondary fragments with $Z \geq 2$.

The principal portion of these events had an energy exceeding 1000 GeV (determined from the total energy of the secondary charged particles).* The results are given in Table 31.

In spite of the limitations of the statistical material, a sharp increase in $\langle n_c \rangle$ with increasing charge of the primary nucleus is clearly seen. The somewhat smaller than expected value of $\langle n_s \rangle$ for the group H (the last line of the table), is explained by a fortuitous circumstance—the lower energy per nucleon for this group of nuclei.

*In the majority of cases the energy transferred to the charged particles exceeded 1000 GeV.

TABLE 30. FRAGMENTATION PARAMETERS P_{ij}

i	Material	j				
		H	M	L	α	Refs.
H	Emulsion ($N_h \leq 1$) . . .	0.31 ± 0.07	0.40 ± 0.09	0.10 ± 0.03	1.61 ± 0.20	[37, 100]
	Emulsion	0.31 ± 0.04	0.33 ± 0.04	0.14 ± 0.03	1.30 ± 0.09	[144]
	Carbon.	0.27 ± 0.05	0.30 ± 0.05	0.23 ± 0.05	1.31 ± 0.15	[109]
	Air	0.17 ± 0.03	0.29 ± 0.04	0.26 ± 0.04	1.34 ± 0.12	[143a]
	Polyethylene	0.27 ± 0.06	0.16 ± 0.05	0.36 ± 0.07	1.41 ± 0.19	[143a]
	Teflon	0.10 ± 0.04	0.28 ± 0.07	0.32 ± 0.08	1.37 ± 0.18	[143a]
	Celluloid	0.27	0.34	0.16	1.16	[109a]
M	Emulsion ($N_h \leq 1$) . . .	—	0.10 ± 0.03	0.35 ± 0.04	1.42 ± 0.11	[37, 100]
	Emulsion	—	0.19 ± 0.02	0.21 ± 0.02	0.93 ± 0.06	[144, 145]
	Carbon.	—	0.09 ± 0.03	0.29 ± 0.04	1.05 ± 0.11	[109]
	Air	—	0.11 ± 0.02	0.24 ± 0.03	1.00 ± 0.08	[143a]
	Polyethylene	—	0.09 ± 0.02	0.30 ± 0.04	0.90 ± 0.08	[143a]
	Teflon	—	0.13 ± 0.03	0.19 ± 0.04	0.93 ± 0.12	[143a]
	Celluloid	—	0.04	0.26	0.78	[109a]
L	Carbon.	—	—	0.13 ± 0.06	0.48 ± 0.11	[109]
	Air	—	—	0.15 ± 0.05	0.51 ± 0.08	[143a]
	Polyethylene	—	—	0.17 ± 0.07	0.87 ± 0.15	[143a]
	Teflon	—	—	0.17 ± 0.07	0.54 ± 0.12	[143a]

TABLE 31. DEPENDENCE OF AVERAGE MULTIPLICITY ON THE PRIMARY NUCLEUS

/123

Primary nucleus	$\langle n_s \rangle$	$\langle n_c \rangle$	Event selection	No. of cases
α	37 ± 6	35 ± 6	All	24
α	16.4 ± 4	14 ± 4	$N_h = 0; 1$	8
α	13 ± 3	11 ± 3	$N_h = 0, 1$, except for the two cases with highest and lowest n_s	6
α	8	8	All, but the x-particle was conserved after interaction	2
C, Li, B, Mg	131 ± 55	125 ± 55	All	7
C, Li, B, Mg	—	—	All, but nucleus conserved	0
H	61	55—60	All	9
H	16 ± 4	16 ± 4	All, but nucleus completely or almost completely conserved after interaction	4
H	~ 100	~ 90	All, but nucleus completely disintegrated into nucleons and fragments	5

The increase of $\langle n_c \rangle$ with increasing size of the primary nucleus is considerably greater than with increasing size of the target nucleus for nucleon-nucleus collisions. This implies that the observed interactions of primary nuclei belong to the nucleus-nucleus type.

/124

The change of $\langle n_c \rangle$ with increasing size of the primary nucleus was investigated by Coghen et al., [123]. In all, 11,000 tracks in 104 showers created by α-particles and 37 by heavy nuclei were registered. The interactions chosen were those in which $N_h \geq 7$, $\gamma_c > 23$, and the primary nucleus completely disintegrated.

In this case $\langle n_c \rangle / A = 16$. Within the limits of one standard error the magnitude of n_c was included between 14 and 20 for the α-nuclear collisions and between 12 and 20 for the primary heavy nuclei.

In those cases when only small fragments come out of the nucleus, the ratio $\langle n_c \rangle / \Delta A$, where ΔA is the change in charge of the primary nucleus, is determined. The average value of this quantity for a primary-particle energy of $\sim 1.3 \times 10^3$ GeV/nucleon was obtained by Abraham et al., [38]. For events chosen according to the rule $N_h \leq 5$ (light nuclei in emulsion), $\langle n_c \rangle / \Delta A \geq 8.6 \pm 1.7$, and for $N_h > 5$ (bromine and silver nuclei), $\langle n_c \rangle / \Delta A \geq 17.1 \pm 1.6$. These values are only slightly smaller than those observed for nucleon-nucleus collisions (Table 21). Thus, this result is evidence for the independent behavior of the nucleons entering into the composition of the primary nucleus during the interaction of the latter with nuclei of the photoemulsion. According to the data of these same authors,

TABLE 31. DEPENDENCE OF AVERAGE MULTIPLICITY ON THE PRIMARY NUCLEUS /123

Primary nucleus	$\langle n_s \rangle$	$\langle n_c \rangle$	Event selection	No. of cases
α	37 ± 6	35 ± 6	All	24
α	16.4 ± 4	14 ± 4	$N_h = 0; 1$	8
α	13 ± 3	11 ± 3	$N_h = 0, 1$, except for the two cases with highest and lowest n_s	6
α	8	8	All, but the x-particle was conserved after interaction	2
C, Li, B, Mg	131 ± 55	125 ± 55	All	7
C, Li, B, Mg	—	—	All, but nucleus conserved	0
H	61	55—60	All	9
H	16 ± 4	16 ± 4	All, but nucleus completely or almost completely conserved after interaction	4
H	~ 100	~ 90	All, but nucleus completely disintegrated into nucleons and fragments	5

The increase of $\langle n_c \rangle$ with increasing size of the primary nucleus is considerably greater than with increasing size of the target nucleus for nucleon-nucleus collisions. This implies that the observed interactions of primary nuclei belong to the nucleus-nucleus type. /124

The change of $\langle n_c \rangle$ with increasing size of the primary nucleus was investigated by Coghen et al., [123]. In all, 11,000 tracks in 104 showers created by α-particles and 37 by heavy nuclei were registered. The interactions chosen were those in which $N_h \geq 7$, $\gamma_c > 23$, and the primary nucleus completely disintegrated.

In this case $\langle n_c \rangle / A = 16$. Within the limits of one standard error the magnitude of n_c was included between 14 and 20 for the α-nuclear collisions and between 12 and 20 for the primary heavy nuclei.

In those cases when only small fragments come out of the nucleus, the ratio $\langle n_c \rangle / \Delta A$, where ΔA is the change in charge of the primary nucleus, is determined. The average value of this quantity for a primary-particle energy of $\sim 1.3 \times 10^3$ GeV/nucleon was obtained by Abraham et al., [38]. For events chosen according to the rule $N_h \leq 5$ (light nuclei in emulsion), $\langle n_c \rangle / \Delta A \geq 8.6 \pm 1.7$, and for $N_h > 5$ (bromine and silver nuclei), $\langle n_c \rangle / \Delta A \geq 17.1 \pm 1.6$. These values are only slightly smaller than those observed for nucleon-nucleus collisions (Table 21). Thus, this result is evidence for the independent behavior of the nucleons entering into the composition of the primary nucleus during the interaction of the latter with nuclei of the photoemulsion. According to the data of these same authors,

the quantity $<\Delta A/A>$ reaches 1/2, i.e., on the average about half of the nucleons of the primary nucleus participate in the collision.

It should be mentioned that the obtained dependence of $<n_c>$ on A, in the form

$$<n_c> \approx <n_s^0> A^{1/2} \tag{5.9}$$

does not contradict the predictions of the hydrodynamic theory, [18] according to which /125

$$<n_c> \sim A^{0.75}. \tag{5.10}$$

in a collision of identical nuclei. The difference between the exponents in (5.9) and (5.10) is not so large that it cannot be explained away on the basis of the methodology of the experiment (inaccurate determination of ΔA for high values of A, collision of nonidentical nuclei).

5. Multiplicity of Secondary Particles in the Collision of Pions with Nuclei

5.1. Average value of the multiplicity

The average value $<n_c>$ is the same for pion-nucleon and nucleon-nucleon interactions. This conclusion is based on results obtained in accelerators.

In the region of energy less than 40 GeV, the dependence of $<n_c>$ on energy of the primary pions can be represented in the form [130].

$$<n_c> = 0.95E_\pi^{0.49}, \quad 4 < E_\pi < 40 \text{ GeV}. \tag{5.11}$$

The number of particles created n_c for the case of a primary pion was determined from the formula $n_c = n_s - n_p$, since at high energies the recoil proton can become relativistic. The magnitude of n_p was taken as 0.5. In Chapter VI it is shown that in many cases the primary pion is "conserved" and it is necessary to exclude it from n_c, since it existed in its initial state. One can expect that the number of such pions equals 0.5—0.7 on the average, per interaction. Then

$$<n_c> \approx 0.95E_\pi^{0.49} - 0.5. \tag{5.12}$$

The dependence obtained differs little from the dependence for nucleon-nucleon collisions, and this is also true of the quantity $<n_c>$ itself.

Identification of the primary particles in cosmic rays is not always successful. Hence, in the study of the interactions of pions at high energies one makes use of the secondary particles arising in nuclear collisions. About 80% of these particles are pions; the remainder are K-mesons and others. In all these cases the determination of the primary energy is unreliable. Two methods are usually employed: the Castagnoli method and the method of the constancy of the transverse momentum of the secondary particles (see Chapter VI). Neither of these methods can give good results for the energy of the individual particles. /126

As shown in Chapter IX, one frequently observes in the interaction of pions cases of anomalously narrow angular distribution with a low multiplicity. In such cases the energy is overestimated several times, which leads to an increase in the contribution of low-energy pions in the region of high measured energies and to an underestimation of $\langle n_c \rangle$.

Farrow et al., [9] compare the dependence of $\langle n_c \rangle$ on energy for primary pions in those cases when the energy is determined by Castagnoli method or from the emission angle under the condition $\langle p_\perp \rangle = 0.4$ GeV/s. It was found that in the first case $\langle n_s \rangle$ has almost the same value over the entire interval from several GeV to 100 GeV. The second method leads to an increase of $\langle n_s \rangle$ of 3.5 times. The latter result gives average values of $\langle n_s \rangle$ that are close to the values obtained in accelerators, which is evidence of the definite advantages of the method of estimating the energy from $\langle p_\perp \rangle$. However, measurements with a Wilson chamber in a magnetic field [136] have shown that low-energy pions, for which $p_\perp$ is several times smaller than the average, are often emitted at small angles.

It is probable that these effects can explain the observed saturation of the multiplicity of secondary shower particles in the energy intervals from 50—5000 GeV [147] and 160—1150 GeV [130]. The entire interval lies in the region of unreliable energy measurements. Since the methodology serves to overestimate the energy, one might expect that the minimum energy of the considered range is distorted the least. Hence the value $\langle n_s \rangle = 10.3 \pm 2.0$ found in [130] at 160 GeV seems to be close to the true value. (The corresponding value for nucleons $\langle n_s \rangle = 9.$) The selection of events in this case was not very rigorous. All events with $N_h \leq 3$ were used.

Koshiba [91] reports a value of $\langle n_s \rangle = 12.7 \pm 0.9$ for collisions of pions with emulsion nuclei. The energy, estimated from the angular distribution, was $\langle E_\pi \rangle = 470\ ^{+90}_{-60}$ GeV. For reasons considered earlier, this energy is overestimated. /127

Gould et al., [92] investigated the energy dependence of $\langle n_s \rangle$ for secondary interactions. The pion energy was determined from formula (6.2). The multiplicity increases from $\langle n_s \rangle = 1.3$ at $\langle E_\pi \rangle = 2.8$ GeV to $\langle n_s \rangle = 6.7$ at $\langle E_\pi \rangle = 37$ GeV.

Earlier, this group had concluded that $\langle n_s \rangle$ was constant in the interaction of pions with nuclei in the interval of energies from 50 to 5000 GeV: $\langle n_s \rangle = 11.1 \pm \pm 0.4$ [147].

Since all of these results are based on unreliable energy methods, it seems premature to make any conclusion about the independence of $\langle n_s \rangle$ on energy in the region above 160 GeV.

Thus, at energies less than 160 GeV, the dependence of $\langle n_s \rangle$ on energy for pions is the same as for nucleons, and the average values $\langle n_s \rangle$ differ little.

5.2. Interaction of pions with nuclei

The investigation of the interaction of pions with nuclei can throw light on the mechanism of the processes which go on inside the nucleus when a nuclear-active particle passes through it.

If during the collision of a particle with a nucleus a cascade of consecutive interactions occur within it (intranuclear cascade process), then a marked difference in multiplicity in the collision of pions and nucleons with nuclei should be observed, since the probability of repeated interaction of pions in a nucleus is 1.6 times less than nucleons (see Chapter IV). The average multiplicities in collision of pions and nucleons with nuclei should also be in the same ratio. There are several papers in which the multiplicity $\langle n_s \rangle$ in the interaction of pions and nucleons with nuclei is determined. Table 32 gives the results of the measurement of $\langle n_s \rangle$ in a photoemulsion at accelerator energies. The quantity $\langle z \rangle$ is the ratio of the average multiplicities $\langle n_c \rangle$ for the collision of pions and nucleons with nuclei and nucleons: /128

$$\langle z_\pi \rangle = \frac{\text{multiplicity in a pion-nucleus interaction;}}{\text{multiplicity in a pion-nucleon interaction}}$$

$$\langle z_p \rangle = \frac{\text{multiplicity in a nucleon-nucleus interaction,}}{\text{multiplicity in a nucleon-nucleon interaction}}$$

and n_c for the interaction of pions and nucleons with nucleons is calculated from the formulas (5.10) and (5.11).

If one compares the magnitudes of $\langle z_\pi \rangle$ and $\langle z_p \rangle$ for $N_h \geq 0$ or $N_h \leq 5$, it is found that they differ somewhat, and $\langle z_\pi \rangle$ is less than $\langle z_p \rangle$. From the point of view of the model of consecutive collisions, the difference at small energies cannot be large. In this region of energy a relatively strong dependence of $\langle n_s \rangle$ on E_0 is observed, and consequently repeated interactions of a nucleon in a nucleus give a small addition to the multiplicity.

It should also be considered that in a collision with heavy nuclei the difference in $\langle z \rangle$ should diminish, since in heavy nuclei pions, as well as nucleons, can in-

TABLE 32. THE MAGNITUDE OF $\langle z \rangle$ FOR VARIOUS TYPES OF INTERACTION

Primary particle	E_0, GeV	Type of event, N_h	$\langle n_c \rangle$ experiment	$\langle n_c \rangle$ for N-N interaction	$\langle z \rangle$	Refs.
π^-	5,4	$\geqslant 0$	1,9±0,1	2,18	0,87±0,05	[115]
	16,3	$\geqslant 0$	4,5±0,1	3,7	1,21±0,03	[115]
	17	$\geqslant 8$	6,2±0,4	3,8	1,60±0,15	[148]
p	6,3	$\geqslant 0$	2,9±0,05	2,2	1,32±0,02	[115]
	9	$\leqslant 5$	4,75±0,1	2,6	1,82±0,05	[121]
	28	$\geqslant 0$	6,3±0,1	4,6	1,40±0,07	[115]
	9	$\geqslant 8$	5,5±0,3	2,6	2,10±0,15	[121]

Commas represent decimal points.

teract repeatedly (see the third and last lines of Table 32, for $N_h \geq 8$). Note that the magnitude of $\langle n_c \rangle$ from [148] in the table depends on the assumption that $n_\pi^+ = n_\pi^-$. Because of the conservation of the primary pion (see Chapter VI) the number of positively charged mesons can on the average be less than the number of negative ones, and consequently $\langle z_\pi \rangle$ for $N_h \geq 8$ is overestimated. /129

Thus, in the interaction of pions with nuclei there appears to be a weaker dependence of $\langle n_c \rangle$ on A compared to the nucleon-nucleus interaction. This may mean that the pion participates less actively in the development of the intranuclear cascade than the nucleon.

The difference of the average multiplicities for interactions of pions and nucleons with nuclei might show up more clearly at cosmic energies. This question has been investigated by Farrow et al.,[9] Brisbout et al.,[149] and Gould et al., [92].

Investigating the interactions of secondary particles in emulsions, they found a sharp difference in the average multiplicities for pionic and nucleonic interactions in the same interval of measured energies: $\langle n_s \rangle = 23.6$ for nucleons with energies of the order of 1000 GeV, and $\langle n_s \rangle = 13.6$ for secondary particles with energies of the order of 600 GeV [147]. In the region of lower measured energies $50 < E < 300$ GeV, the multiplicities equal $\langle n_s \rangle = 20.8$ and 10.5 respectively for nucleons and pions [149]. In the interval from 3 to 35 GeV the cosmic experiments give results like those in accelerators: $\langle z_\pi \rangle = 1.2 \pm 0.1$ for registration of stars with $N_h \geq 0$.

Thus, the difference in $\langle n_s \rangle$ for pions and nucleons at high energies is extremely large. Somewhat different experimental data are reported in [124], the

authors of which found that the magnitude of $\langle n_s \rangle$ for secondary interactions is the same independently of the presence of charge on the secondary particle producing the shower. If it is considered that among the neutral secondary particles neutrons must be present, then this result could indicate an identical multiplicity for pionic and nucleonic interactions. In this work, the energy, measured by the Castagnoli method, amounted to 160 GeV on the average, and $\langle n_s \rangle \sim 10$. This magnitude corresponds to the multiplicity of pionic interactions and is half as large as $\langle n_s \rangle$ for collisions of nucleons with nuclei [149]. Another pecularity of this experiment is the absence of a dependence of $\langle n_s \rangle$ on N_h, i.e., on the size of the target nucleus (at least for events with $n_s \geq 5$, $\langle z \rangle \approx 1$).

All these results can be brought into agreement with the conclusions of [9], [92] and [149], if it is assumed that among the neutral secondary particles the majority consists of kaons and they interact the same as pions. /130

In [124], the magnitude $\langle z \rangle \approx 1$ was obtained by a comparison of two groups of showers, selected according to the rule $N_h \leq 5$ and $N_h > 5$. Since both groups of events were registered under the same conditions, the conclusion about the absence of an increase of $\langle n_s \rangle$ with increase in A in secondary interactions does not depend on errors in the energy measurement.

All the preceding results have 15—20% statistical certainty. Thus, in the collision of mesons with nuclei the multiplicity of secondary particles $\langle n_s \rangle$ depends weakly on the dimensions of the nuclear targets.

Because of the uncertainty in the energy measurements, it is difficult to compare $\langle n_s \rangle$ for interactions evoked by pions and nucleons. It was remarked earlier that at high energies the magnitude of $\langle n_s \rangle$ for pions may be underestimated. Hence the difference in the multiplicity of secondary particles in pionic and nucleonic collisions with nuclei is less than the twofold difference registered in [9], [92] and [149]. A ratio of the average multiplicities equal to 2 is difficult to explain solely on the basis of the difference of cross sections of pion-nucleon and nucleon-nucleon interactions, if this difference remains the same as it is at energies less than 30 GeV.

6. Distribution of the Multiplicity

6.1. Theoretical predictions

Additional information about the difference between the interactions of pions and nucleons can be obtained by studying the distribution of the multiplicity about the average value $\langle n_s \rangle$.

The hydrodynamical theory of Landau predicts an extremely narrow distribution of the fluctuations of n_s about its average value. The width of this distri-

bution depends on a parameter of the theory—the radius of the initial volume. The probability of the appearance of a given number of particles $W_n(n)$ (n is the total number of newly created particles) obtained by Mur and Rozental [150] is distinguished by a very fast decrease in probability as the number of particles decreases (by several orders of magnitude for a change in n by a factor of 2). The width of the distribution is markedly increased if one considers only charged particles. Obviously, it is just this special case that is easiest to compare with experiment. /131

The theoretically expected distribution of n_s for the case of a nucleon-nucleon interaction at $E_0 \sim 1000$ GeV is shown in Fig. 28. For comparison of this result with experiment it is necessary to obtain a considerable collection of cases of nucleon-nucleon interaction at the specified energy. This task has not been completed as yet. Hence it is necessary to find characteristic features of the theoretical distribution which do not require knowledge of the entire curve for checking purposes. One of these features is the absence of showers with small multiplicity.

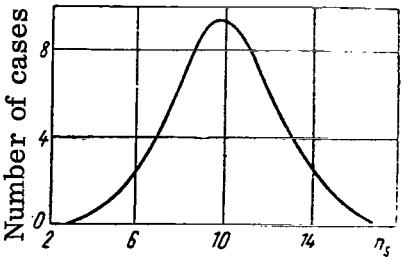

Figure 28. Distribution of n_s Expected From Hydrodynamic Theory for the Nucleon-Nucleon Collision at $E_0 \sim 10^3$ GeV [150].

The theory predicts that at an energy of 1000 GeV there should be practically no events with $n_s \leq 3$, and $n_s \leq 6$ should be observed in only 5% of the cases.

In experiment it is frequently possible to establish a lower limit to the energy of the interaction. Using such events it is possible to find out whether the theoretically predicted frequency of appearance of small values of n_s is contradicted or not. Usually in cosmic rays one observes nucleon-nucleus interactions. However, this does not seriously affect the checking process, since collisions with the complex nucleus lead only to an increase in n_s [150].

6.2. Experimental determination of the distribution of n_s

The mean square deviation from $\langle n_s \rangle$ is large and reaches 0.5 to 0.6 times $\langle n_s \rangle$. This problem has been studied sufficiently rigorously only for a beam of particles of fixed energy, i.e., in accelerators. However, by virtue of the weak growth of $\langle n_s \rangle$ with energy it is possible to investigate flucuations also in cosmic rays, using reliable experiments. /132

In accelerator experiments the mean square deviation $\sigma_\pi = 0.6 \langle n_s \rangle$ for pions and is almost the same value for nucleons.

Interactions of pions and nucleons with heavy nuclei ($N_h > 5$) give a wider distribution of n_s, particularly in the case of primary nucleons with energies of 28 GeV. At low energies (of the order of 6 GeV) the dispersion in the interaction with nuclei increases slightly. This result qualitatively corroborates the conclusions made earlier.

In the region of high energies, estimates of the fluctuations in n_s were made by Fowler and Perkins, [151] who determined the magnitude $\sigma_p(n_s) \sim \sim \langle n_s \rangle/2$. It is true that in this case the mean square deviation σ could have been somewhat overestimated on account of the underestimation of the range of energies selected by the Castagnoli method.

Malhotra [130] obtained the same result using a similar method (Fig. 29). For nucleon-nucleon interactions ($N_h \leq 2$) with an energy (Castagnoli) in the interval from 1 to 50 GeV the mean square deviation $\sigma_p = 1/2 \langle n_s \rangle$. In this distribution events with $n_s < 6$ are definitely present in an account greater than 5%. Coghen et al., [123] analyzed 175 showers produced by nucleons in a photoemulsion (100-liter pile, selection by electromagnetic cascades). For $\gamma_s > 23$ a distribution of n_s for events with various N_h was obtained (Fig. 30), in which separate maxima, corresponding to $\langle n_s \rangle \sim 16$, $\langle n_s \rangle \sim 32$, etc., are noticeable. These maxima are particularly sharp for $N_h > 8$. If further investigations confirm this result, it will be evidence of the existence of successive collisions of the primary nucleon in the target nucleus. In this work cases with $n_s > 7$ were chosen, and it was impossible to establish the presence of showers with small n_s. /134

6.3. On the existence of events with small n_s at high energies

In all cosmic experiments at high energies there is a strong discrimination against interactions with small n_s. The only exceptions are those investigations where the search for interactions is carried out in electron-photon cascades or in cases of disruption of the primary nuclei, when tracks are followed.

In an examination of [146] (search for showers in electron-photon cascades), we found that for $\Sigma E_\gamma > 1000$ GeV, two out of fifteen cases have $n_s \leq 5$.

In the work of Lohrman et al., [24] the minimum energy, determined from scattering, is close to 100 GeV. Among 52 events, 8 were observed with $n_s \leq 5$.

Finally, Abraham, et al., [38] estimated the energy of primary particles from nuclear disruption and at energies $\geqslant 10^3$ GeV observed a significant percentage of events with $n_s \leq 6$ (see Fig. 9). In the family No. 1115 (nucleon energy 1300 GeV) there are five events with $n_s \leq 5$ out of 13 cases of collision of nucleons

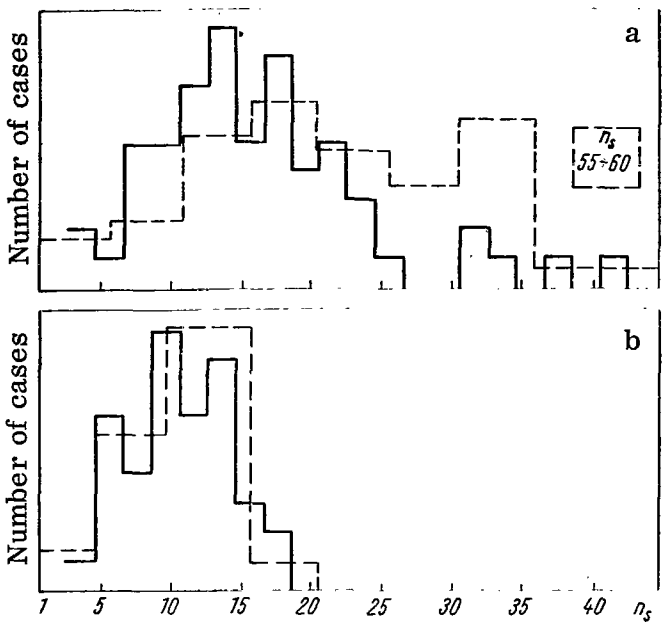

Figure 29. Distribution of the Mulitplicity of Charged Particles:

a—for nucleon-nucleus; b—for pion-nucleus collisions. Solid histogram—results of [130]; dashed—from [147].

with light nuclei ($N_h \leq 5$). Among other families of showers with even higher energy observed in this work, the ratio of the number of cases with $n_s \leq 6$ to the total number of interactions is

$$\frac{W(n_s \leqslant 6)}{W(n_s > 1)} = \frac{4}{9}.$$

The average value of the ratio for all events equals 0.4 ± 0.15. This is many times greater than can be explained by the hydrodynamic theory [150]. Since in this case the predictions of theory are rather specific, it may be concluded that at energies $\sim$ 1000 GeV there exist processes that are distinct from hydrodynamical ones and that lead to small values of the multiplicity of charged particles. Reliable information is practically nonexistent in the region of higher energies. Koshiba [91] presents a case of the interaction of a nucleus with energy 12,000 GeV (No. 1010). The nucleon fragments of this nucleus engage in eight interactions with light nuclei, and among them only one has $n_s = 6$ and in the remaining cases n_s is greater. /135

6.4. Distribution of n_s in showers of high energy produced by primary pions

Figure 29 shows the distribution of n_s for collision of primary and secondary particles with nuclei of an emulsion according to the data of [130] and [147].

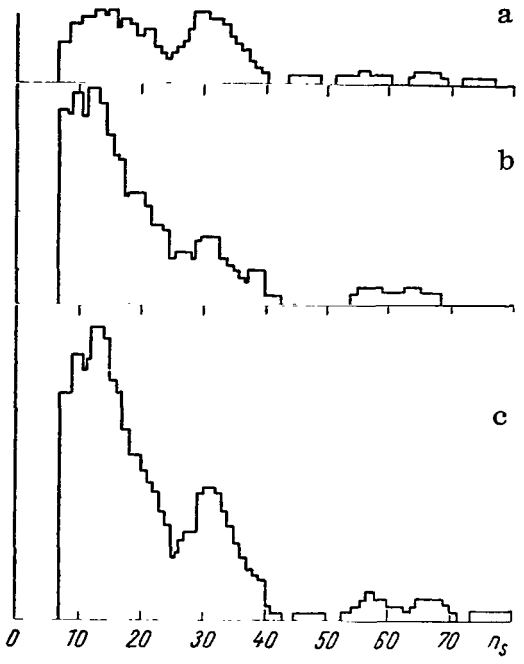

igure 30. Distribution of n_s for vents With $\gamma_s > 23$ and Various N_h: $N_h>8$ (58 cases); b – $N_h\leq 5$ (117 cases); c – $N_h>8+N_h\leq 5$ (175 cases).

It is completely obvious that the distribution of n_s in pionic interactions is approximately 1.5 times narrower, i.e., $\sigma_\pi \sim \langle n_s \rangle/3$ [147] or $\langle n_s \rangle/3.4$ [130].

It should, however, be kept in mind that secondary showers (assuming that they are produced by pions) pertain to smaller energies than primary ones. Malhotra finds that the average energies of primary and secondary showers in the laboratory coordinate system differ by a factor of 15 (γ_s by 2.4).

It was noted earlier that the average values $\langle n_s \rangle$ for pion and nucleon events evidently do not differ very much. The difference in the mean square deviations is probably explained by the fact that in a given case nucleon- and pion-nucleus interactions are considered. If nucleons form better developed cascades in the nucleus, then the multiplicity in such cascade cases is enhanced, [147] and the distribution will be wider than for pions. In the region of energies attainable in accelerators, this effect should be less pronounced, since the dependence of n_s on energy is xtremely sharp, and the growth of n_s as a result of repeated collisions is weaker. he calculation of the intranuclear cascade process carried out by Artykov et al., /136 52] allowing for the experimental dependence $n_s(E_0)$ and the difference in cross ctions of π-p and p-p collisions shows that at energies in the tens of GeV such model agrees with experiment.

All of this inevitably leads us to the conclusion that the average value $\langle n_s \rangle$ r primary pions in collision with nuclei should be less than in nucleon-nucleus llisions (at least, in collisions with average-sized nuclei), which corroborates e results of Section 5.

5. Distribution of n_s in the collision of nuclei with nuclei

The distribution of n_s for the collision of primary nuclei with nuclei is wid- than for nucleon-nucleus collisions. Figure 31 shows the distribution of n_s r collisions of α-particles with nuclei [153]. This distribution has a halfwidth $\approx \langle n_s \rangle$. The smooth curve indicates the expected distribution for the case

when on the average two nucleons simultaneously, but independently, interact. Thus, as a rule, more than one nucleon of the primary nucleus participates in the collision, which agrees with the conclusions of Section 4.

7. Nature of the Secondary Particles

/37

7.1. Formation of pions, kaons, and hyperons in showers

At all investigated energies, π-mesons are more frequently produced than other particles. This conclusion was reached quite some time ago. The survey of Perkins [57] analyzed the results obtained up to 1958. It was found that the ratio of the number of charged pions to the total number of charged particles in a shower equals 0.82 ± 0.05.

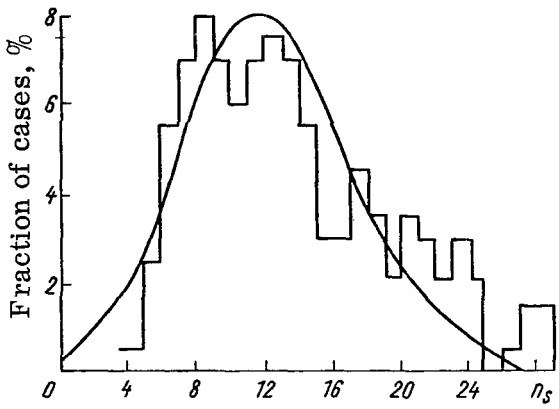

Figure 31. Distribution of n_s for Collision of α-Particles With Nuclei of Photoemulsion.

Only in rare cases is the investigation of the nature of secondaries in high-energy showers made possible by direct measurement of the mass of the secondary particles. In the majority of cases such measurements are applied only to particles of the wide cone.

Kim [154] investigated 22 cases of the interaction of cosmic particles (principally protons) with light nuclei of an emulsion ($N_h \leq 2$). The energy of the primaries was measured by the Castagnoli method and, evidently, amounted to $\sim 10^3$ GeV on the average. By the method of comparison of multiple scattering and ionization he succeeded in determining the masses of 82 particles. Table 33 presents the mass distribution of the measured particles, their emission angles, and the average moments in the symmetric coordinate system.

From Table 33 it is possible to determine the probability of formation of strange particles and the ratio of the number of kaons and pions at high energy. If it is assumed that in the given experiment nucleon-nucleon interactions are observed, then the number of kaons emitted forward and backward ought to be the same. Hence the number of kaons per interaction is about 1.6, and the number of hyperons is close to 0.1. The ratio of the number of kaons to the number of pions $P^{\pm}$ and to the total quantity of mesons $Q^{\pm}$ also can be estimated from Table 33:

/138

$$P^{\pm} = \frac{W_{K^{\pm}}}{W_{\pi^{\pm}}} = 0{,}34 \pm 0{,}10; \quad Q^{\pm} = \frac{W_{K^{\pm}}}{W_{\pi^{\pm}} + W_{K^{\pm}}} = 0.25 \pm 0.06.$$

If these relations hold also for the unidenfied particles, then this is one of the few valid results at high energies, since the nature of the particles was determined directly from measurements of their masses.

TABLE 33. SECONDARY PARTICLES, THEIR MOMENTA, AND EMISSION ANGLES

Secondary particles	$\theta_s > 175°$		$\theta_s < 175°$	
	No. of cases	p_s, GeV/s	No. of cases	p_s, GeV/s
π	7	7,4	46	1
K	9	13.7	9	1,4
p	10	27	—	—
Y	1	—	—	—
Total . . .	27	—	55	—

TABLE 34. PARTIAL CROSS SECTION OF π^--p COLLISION FOR DIFFERENT CHANNELS OF FORMATION OF KAONS IN mb.

Reaction channel	Energy, GeV			
	4,7	7—8	10,0	16,0
$K+Y$	1,11	—	1,45±0,57	1,32±0,15
$K+\bar{K}$	0,57	1,6±0,4	1,97±0,25	2,21±0,25

Commas represent decimal points.

The results given in Table 33 definitely indicate that the ratio P depends significantly on the emission angle of the particles. Heavy particles are emitted primarily at small angles. For the interval of angles 175—180°, P $\sim$ $\sim$ 1, whereas for smaller angles (175—90°), P $\sim$ 0.2. Only in 5% of the cases is a kaon created in company with a hyperon. The situation is different at energies less than 30 GeV. In the interaction of pions with energy from 6 to 16 GeV, the probability of formation of kaons together with antiparticles or with hyperons are comparable. In work with artificially accelerated particles the frequencies of different reaction channels are expressed in the form of partial cross sections normalized to the total interaction cross section. Table 34 gives /139 the cross sections for the channels of the following reactions [155]:

$$\pi^- + p \to K + Y + \text{pions};$$

$$\pi^- + p \to K + \bar{K} + \text{pions}.$$

For the p-p interaction with energy 24 GeV [156] the partial cross section of the channel KY equals 3.1 ± 0.3 mb. In order to compare this experiment with cosmic ray experiments, we compute the number of hyperons per inelastic interaction. This number is n(Y) = 0.1 ± 0.01. This includes all hyperons, both charged and neutral.

In Kim's experiments [154] the same value is obtained for charged hyperons, if one takes the collision to be symmetric. However, the statistical accuracy is insufficient to make any kind of conclusion. A more definite comparison can be made with respect to kaons.

Table 35 gives the results of the determination of the number of particles of different kind in showers created by protons.

TABLE 35. AVERAGE NUMBER OF PARTICLES OF DIFFERENT KIND IN SHOWERS FROM PRIMARY PROTONS AND PIONS

Average No. of particles	Energy of p-p interaction, GeV			
	9 [159]	14 [160]	1000* [164]	16
$\langle n_s \rangle$	3,59±0,20	4,07±0,20	12,0	3,6
$\langle n_c \rangle$	2,41±0,15	2,83±0,20	11,0	3,4
$\langle n_p \rangle$	1,18±0,10	1,24±0,04	1,0	0,15
$\langle n_\pi \rangle$	2,24±0,14	2,53∓0,19	8,3	3,5
$\langle n_K \rangle$	0,17±0,10	0,30±0,06	2,7	0,13
$\langle n_K \rangle / \langle n_\pi \rangle$	0,076	0,12	0,32	0,04
$\langle n_K \rangle / \langle n_c \rangle$	0,07	0,10	0,25	0,04

*It was assumed that the ratio of pions and kaons among the undentified particles was the same as for the identified ones.

Commas represent decimal points.

According to the data of Slavatinskiy et al., [157] the fraction of strange particles does not exceed 6% at 200 GeV. In the last column are given the results for π-p interactions at 16 GeV. From this table it follows that the fraction of kaons grows significantly from 10 to 1000 GeV.

Analyses of the nature of secondary particles with velocities in the interval $0.34 < \beta < 0.7$ were carried out by Hoffman et al., [148] and Garbovska [158]. The particles producing showers in this case were pions with energy 17 GeV and protons with energy 24 GeV, and the heavy nuclei of a photoemulsion served as the target. The results, from which it follows that kaons and hyperons are relatively rarely emitted with velocities in this interval, are presented in Table 36. /14

7.2. Various methods of determination of the fraction of kaons

We now consider other methods of determining the fraction of kaons. At not very high energies a widely applied method is the comparison of the number of π^0-mesons, found by counting the electron-positron pairs, with n_s. Since the average number of nucleons among the secondary relativistic particles is considerably smaller than the number of kaons and pions (see Section 7.1.), we have the ratio

$$R = \frac{n_{\pi^0}}{n_s} \simeq \frac{n_{\pi^0}}{n_{\pi^\pm} + n_{K^\pm}}.$$

If $n_{\pi^0} = 1/2 n_{\pi^\pm}$, it is easy to determine the ratio of the number of charged kaons to the total number of charged newly created particles /141

$$Q^\pm = n_{K^\pm}/n_{K^\pm} + n_{\pi^\pm} = 1-2R.$$

The ratio R, averaged over many data [57], [161], [162] is 0.41 ± 0.03. Consequently, $Q^{\pm} = 0.20 \pm 0.06$.

This result pertains to energies of 10^3—10^5 GeV. Allowing for the probable overestimation of the energy in these cases, * we shall assume that it is valid, at least, to $\langle E_0 \rangle \sim 10^3$ GeV.

TABLE 36. IDENTIFICATION OF SECONDARY PARTICLES WITH VELOCITIES $0.34 < \beta < 0.7$

Secondary particles	No. of particles per interaction	
	Pions with energy 17 GeV	Protons with energy 24 GeV [158]
Pions	0,6±0,2	0,3±0,1
Kaons	0,3±0,1	0,1±0,1
Hyperons	0,1±0,1	—
Protons	3,0±0,4	3,7±0,5
Deuterons and tritons	1,0±0,2	1,0±0,4
Total	5,0±0,6	5,1±0,6

Commas represent decimal points.

Data for high and low energies are compared in Table 37. It follows from this table that the fraction of charged kaons $Q^{\pm}$ at low energies rather rapidly rises and then remains almost constant over a wide energy interval to $E_0 \gtrsim 10^3$ GeV.

The observation of secondary interactions in a photoemulsion also gives the possibility of estimating the fraction of kaons among the secondary particles. This time we define the quantity

$$Q^0 = \frac{N^0}{N^{\pm}}. \qquad (5.13)$$

TABLE 37. DEPENDENCE OF $Q^{\pm}$ AND Q^0 ON ENERGY

Energy, GeV	Type of interaction	$Q^{\pm}$	Q^0	Refs.
2	p-$\bar{p}$	0,01	—	163
9	p-p	0,07	—	159
14	p-p	0,10	—	160
25	p-Al	0,13	—	164
10^3	p-, n-, α-Emulsion nucleus	0,25±0,06	0,23±0,04	165
10^3	p-, n-Emulsion nucleus	0,2±0,06	0,22±0,02	154

Commas represent decimal points.

Here N^0 and $N^{\pm}$ are the number of interactions of high energy created by neutral and charged secondary particles, respectively. Among the secondary neutral particles we have kaons and baryons (principally neutrons), and among the charged

*The energy was determined by the Castagnoli method.

secondary particles we have kaons, pions, and baryons (protons). If the number of protons n_p and neutrons n_n is not large, then /142

$$Q^0 = \frac{N^0}{N^\pm} = \frac{n_{K^0}}{n_{K^\pm} + n_{\pi^\pm}}. \quad (5.14)$$

Usually, however, one allows for the contribution of nucleons, assuming that the overcharge coefficient $\eta \approx 0.5$ and $N_p = N_n = 0.5$. Consequently,

$$Q^0 = \frac{N^0 - 0,5}{N^\pm - 0,5}. \quad (5.15)$$

This quantity can be measured not only in photoemulsions, but also in Wilson chambers. In the latter case, about half of the K^0 mesons decay without providing any secondary interactions. Hence the ratio Q^0 measured in a Wilson chamber Q^0_{WC} is smaller than that measured in photoemulsions:

$$Q^0_{WC} = 0.16 \pm 0.07 \quad \langle E_0 \rangle \sim 100 \text{ GeV}[162];$$

$$Q^0_{em} = 0,22 \pm 0.02 \quad E_0 > 10^3 \div 10^4 \text{GeV}[45, 57, 64, 91, 124].$$

Thus the number of secondary charged and neutral kaons is the same. Over a wide energy interval the total fraction of kaons with respect to all particles produced is

$$\frac{n_K}{n_c} = \frac{n_K}{n_s - 1} = 0.25 \pm 0.03.$$

To estimate the fraction of kaons among particles with energy higher than specified for very high primary energies indirect methods have been employed, based on a comparison of the observed intensity of photons and muons with that calculated on the basis of some fraction of kaons or other [165]. As a result the authors arrived at the conclusion that up to 2×10^4 GeV the fraction of kaons does not exceed 40%. This conclusion is strengthened if it is realized that kaons have on the average a higher energy than pions (see Chapter VI), and the role of kaons at an energy higher than that given will be even less (Chapter XII, Section 5).

7.3. Other information about processes of formation of secondary particles /143

In the literature there is little information about the dependence of the cross section for the formation of kaons on A, as well as about the creation of nucleon-antinucleon pairs at high energies.

Bowen et al., [166] as well as Apishev et al., [167] investigated the cross section for the generation of "strange" particles in the collision of pions and protons with nuclei. At 1.5 and 2.8 GeV/s, as well as in cosmic rays, the cross section for generation of strange particles varies as $A^{2/3}$.

Several years before Peter [168] had proposed the hypothesis that in the region of high energies the most energetic particle is the hyperon. On the basis of this hypothesis he was able to explain a number of characteristics of the atmospheric radiation. However, the positive excess of muons in the high-energy region contradicts this hypothesis [169].

TABLE 38. FRACTION OF HEAVY PARTICLES AT VARIOUS DISPERSION TEMPERATURES OF THE SYSTEM

kT, in units of $m_\pi c^2$	$\frac{n_K}{n_\pi}$	$\frac{n_N}{n_\pi}$	$\frac{n_\Lambda}{n_\pi}$
1	0,23	0,06	—
1,5	0,43	0,27	0,13
2	0,57	0,56	0,33
3	0,73	1,04	0,78

Commas represent decimal points.

As far as the generation of antinucleons in cosmic rays is concerned, it is known only that their role is not large. In the region of energies attained in accelerators, the fraction of antinucleons does not exceed a few tenths of a percent.

7.4. Comparison with theoretical results

The features of the generation of heavy particles have been compared with theory more than once. Belenkiy [170] pointed out that the hydrodynamical theory decribes the basic features of this process well (for $kT \sim m_\pi c^2$). The fraction of particles of different mass arising in collisions of the hydrodynamic type is determined, on the one hand, by the statistical weight of the various states, and, on the other, by the dispersion temperature of the system (Table 38).

In certain papers it is assumed that the dispersal of the excited agglomerate (fireball) in the multicenter model should also be treated statistically or hydrodynamically [142]. Then the results presented in the table are also applicable to the fireball model.

CHAPTER 6

ENERGY SPECTRA OF SECONDARY PARTICLES

1. Methods of Measuring the Energy of Secondary Charged Particles

1.1. Photoemulsions

The most accurate method is the determination of $p\beta$ from multiple scattering in photoemulsions. The applicability of this well known method at high energies is limited by the necessity of having long tracks. As is known, [45, 166, 167] the quantity

$$p\beta = \frac{k_0 Z\sqrt{t}}{\langle \alpha_t \rangle},$$

where p and β are the momentum and velocity of the particle; Z is its charge; t is the length of the cell in which the scattering is measured; $\langle \alpha_t \rangle$ is the average angle of multiple scattering; k_0 is the scattering constant, almost independent of the length of cell t and the particle velocity, but different for different substances. In photoemulsions $k_0 \approx 25$—30 MeV-deg/$(100\ \mu m)^{1/2}$. If we go to a standard cell ($t = 100\ \mu m$), $\alpha_{100} = \alpha_t(10/t^{1/2})$, and

$$p\beta = \frac{k_0}{\langle \alpha_{100} \rangle}. \qquad (6.1)$$

For small values of β, the quantity $p\beta$ is equal to twice the energy, and for large values ($\beta \to 1$), to the momentum.

The errors of the method come from statistical error and noise, and the limiting measurable momentum increases with cell length like $t^{3/2}$. Hence it is desirable to have a large cell length for the measurement. But if the track length is small, then the statistical accuracy is reduced as the cell becomes

larger. In favorable cases it is possible to measure momenta to several tens of GeV/c by this method.

This limit can be exceeded when two or more particles produced in one interaction move very close to one another and in almost parallel paths. Then one measures the relative scattering of two particles, which significantly decreases the role of distortion and various kinds of noise and makes it possible the raise the limit of measureable energies.

Lohrman et al., [24] determined the energy of the disintegration products of multi-charged nuclei by relative scattering at energies in the hundreds and even thousands of GeV. The measurement in the case of fragmentation is facilitated by the fact that the measured particles have close to the same momenta (see Chapter V). The average angle of relative scattering (in degrees per 100 μm) is obviously made up of the scattering angles of the two particles in question:

$$\langle(\alpha_{100})_{rel}\rangle = \frac{1.4k_0}{p\beta}.$$

The energies of pions produced in a shower differ very greatly. Hence, to carry out the measurements it is necessary to choose the most energetic pion and assume its track is rectilinear. The scattering of the remaining particles is measured relative to the fastest pion, the energy of which cannot be measured in this case. The method of multiple scattering is applied mainly to measure the momentum of the particles of the external cone which are emitted backwards in the C system and have less energy in the laboratory system.

Thus, in interactions with energy greater than 100 GeV it is only rarely possible to measure the energy of all secondary particles. As a rule, the energies of the several particles of the inner (narrow) cone that are emitted in the forward direction remain unmeasureable.

Most widely used is the $p_\perp$ method, which is based on the experimental fact that in the first approximation the average transverse momentum of secondary pions is independent of the emission angle of the particle and the energy of the primary (see Chapter VII).

In this case the energy of a particle emitted at angle θ_i is

$$E_{\theta_i} = \frac{\langle p_\perp \rangle c}{\sin\theta_i}. \qquad (6.2)$$

The errors in determining E_θ come from the following sources:

a. In individual cases $p_\perp$ has a broad distribution about the average, which leads to considerable errors in the magnitude of E_θ;

b. $\langle p_\perp \rangle$ is different for particles of different mass;

c. $\langle p_\perp \rangle$ slowly increases with energy;

d. $\langle p_\perp \rangle$ is evidently reduced at very small angles;

e. $\langle p_\perp \rangle$ may be different for collisions of different type (e.g., in peripheral and central).

The merit of this method is its simplicity.

Sometimes the problem arises of determining the average energy of the secondary particles $\langle E_\theta \rangle$ in interactions of a specific type. Then

$$\langle E_\theta \rangle = \frac{\sum_{i=1}^{n} \langle p_\perp \rangle c \csc \theta_i}{n}. \qquad (6.3)$$

Since n and θ_i can be measured rather well, the principal error in determining $\langle E_\theta \rangle$ is associated with the assumption about the constancy of $\langle p_\perp \rangle$.

The error arising from the third source (c) can be reduced, since in the majority of cases the energy of the primary is known (at least in order of magnitude). This makes it possible to allow for the change of $\langle p_\perp \rangle$ with energy.

If the angular distribution of kaons and pions is the same, the error due to the difference in $\langle p_\perp \rangle$ for two types of particles is not large, since the fraction of kaons does not exceed 25% (see Chapter V).

The situation is worsened somewhat if kaons and pions are distributed differently [154, 160].

The biggest error should arise due to particles emitted at low angles, which give the principal contribution to $\Sigma \operatorname{cosec}_i$. Among them are particles with very small $p_\perp$. For example, in [136], in a Wilson chamber with magnetic field and in showers with energies in the hundreds of GeV, particles are encountered which are emitted at angles in the neighborhood of 1° with momenta that are ten times smaller than predicted by formula (6.2). In cases of showers with no particles at very small angles, Eq. (6.3) gives a rather good approximation. In two-thirds of the cases a deviation of less than 1.5 times is observed, and in the remainder the deviation does not exceed a factor of 2 [5].

In emulsion piles of sufficiently large size it is sometimes possible to track the secondary particles up to their interaction. Then it is possible to use the Castagnoli method to determine the energy of high-energy secondaries. Since the spectrum of the secondary particles has a drop-off, this method leads to an overestimation of the average energy (see Chapter I and [8]).

1.2. Wilson chamber

The application of magnetic fields in emulsion work has become possible as the result of the realization of supermagnets.

Pulsed magnetic fields of intensity up to 200 kG permit the measurement of momentum up to 20 GeV/c with an accuracy of up to 15—20% [148, 158, 171]. Such experiments are still only possible in accelerators due to the pulsed nature of the magnetic field and the small volume in which it is established. Under these conditions it is possible to measure all the secondary charged particles. The problem of realizing supermagnets (based on superconducting materials) for cosmic investigations is an urgent one. For the present we have to be satisfied with moderate magnetic fields ($\sim$ 10 kG) with Wilson chambers. The maximum measurable momentum is then the same as in accelerator experiments, i.e., 20—30 GeV/c in the best case [172]. At the present time, events investigated in cosmic rays are at energies of 100 GeV, and a considerable number of the fastest secondary particles are unmeasurable. In [136], where the limiting measurable momentum reached 12 GeV/c, the energy of about 10% of the particles remained unknowned.

Thus, at cosmic energies it is impossible in many cases to obtain complete information about the momenta of the secondary particles.

2. Determination of Photon Energy

2.1. Determination of photon energy from the number of particles in a circle of a certain size

A convenient method for the measurement of the energy of individual photons and electrons was proposed by Pinkau [173]. In this method one uses the dependence of the number of electrons N found in a circle of radius R about the shower axis at a specified distance from the point where the primary photon appears, on the product ER (if $R \ll t_0$, where t_0 is the length of the cascade unit).

A calculation of the function $N(< R) = f(ER, t)$ was made by Nishimura and Kidd [146] for photoemulsions and by Fowler et al., [174] for emission chambers with alternate layers of heavy material. The corresponding curves for lead are given by Buya et al., [175].

In practice, the determination of photon energy reduces to counting the number of electrons included in a circle of radius R at a depth t and comparing the number obtained with theoretical curves.

Fowler et al., [174] compared theoretical and experimental results. The energy of the primary electrons was determined by the method of multiple scattering or from the emission angle of photons from the decay of π^0-mesons. Minikawa et al., [176] compared the emission angles of photons from the decay of π^0-mesons, calculated from measurement of the cascade energies, with those observed experimentally. In three cases studied, the calculated and measured angles differed by less than a factor of 2.

This same method can also be used at high energies, when the density of darkening is high and counting of individual particles impossible. Usually in these cases one used a calibrated photometer [177]. The accuracy of these methods to determine photon energy is close to 30% [178].

Sometimes, in the case of extremely high density in the center, one proceeds differently: he measures the number of electrons in a ring included between radii R_1 and R_2, which are chosen such that indivudual tracks can be resolved in a given distance [178]. The results obtained are compared with calculations for the function

$$N(<R_2) - N(<R_1).$$

It should, however, be realized that the majority of calculations completed in the so-called stem approximation pertains to distances $R \ll t_0$. Pinkau [173] estimated the distances at which this approximation is valid and found that in the case of emulsion cameras with $t_0 \sim 6$ mm (tin + emulsion), the stem approximation is valid up to 200 μm at 5 t-units and at energies ~ 100 Gev, and at 10^4 GeV deviation can already occur at 25 μm.

At a depth of 10 t-units this approximation can be used out to 600 μm at 100 GeV and 200 μm at 10^4 GeV.

2.2. Determination of photon energy from the number of particles at the maximum of the electromagnetic cascade

Another widely used method of estimating the photon energy in a shower is based on the determination of the number of electrons at the cascade maximum:

$$N_m = \frac{k(E)}{\sqrt{\ln \frac{E_0}{\beta}}} \cdot \frac{E_0}{\beta}.$$

Calculations of the number of particles at the maximum based on cascade theory were made not long ago by the moment method in work by Ivanenko et al. [179]. To measure the total number of particles in a cascade in photoemulsions is difficult, since a considerable number of electrons are found at large distances from the axis, where there is a strong background effect.

2.3. Determination of photon energy from the emission angles of electron-position pairs

The energy of the components of an electron-position pair can be found by the multiple scattering method. In the region of energies less than 1 GeV, the accuracy of the method is greater than 30%. At higher energies, the relative scattering method is used, if the distance between the tracks is less than 20 μm. Good results are obtained up to 40 GeV [180].

The photon energy can be estimated from the opening angle of the electron-positron pair. If the energy is divided equally between the electron and positron, then the most probable opening angle of the pair is [181]

$$\omega = \frac{4mc^2}{E_\gamma}. \tag{6.4}$$

In the case of unequal division of energy, one puts a factor, not very different from unity, in the formula. The average value of the photon energy is

$$< E_\gamma > = 4mc^2 \left\langle \frac{1}{\omega} \right\rangle. \tag{6.5}$$

Friedländer [182] proposed the use of the projection φ of the angle instead. To check this possibility be measured the energy of 100 photons produced from photons with energies of 7.3 and 9 GeV from the scattering of the pair components as well as from the formula

$$< E_\gamma > = \frac{< k >}{\varphi},$$

where the experimentally determined quantity $K = 1.64 \pm 0.29$.

The quantity log k has a Gaussian distribution with average value 0.091 and mean square deviation of 0.37.

The energy spectra of photons measured by this method were found to be close to the true ones (measured by scattering).

At photon energies $\geqslant 10^3$ GeV the emission angles of the pair components $\omega \leqslant 10^{-6}$ rad, and it is practically impossible to measure them. The distance between the particles becomes so small that the effect mentioned by Chudakov [183] comes in, wherby there is a reduction in ionization in those portions of the path of the pair in which the distance between the electron and positron is less than the radius of interaction. Then the electric field of the two unlike charges diminishes with distance faster than the field of a single charge. As a consequence of the gradual divergence of the pair components the ionization tends to its limiting value, i.e., to two-fold ionization. /151

The growth of ionization with distance from the point of appearance of the pair was calculated by Chudakov [183]. It is given in Fig. 32 for several opening angles ω. The angles ω are connected with the photon energy by (6.4). By studying in an experiment the dependence of ionization on distance from the point of creation of the pair, it is possible in principle to estimate the photon energy.

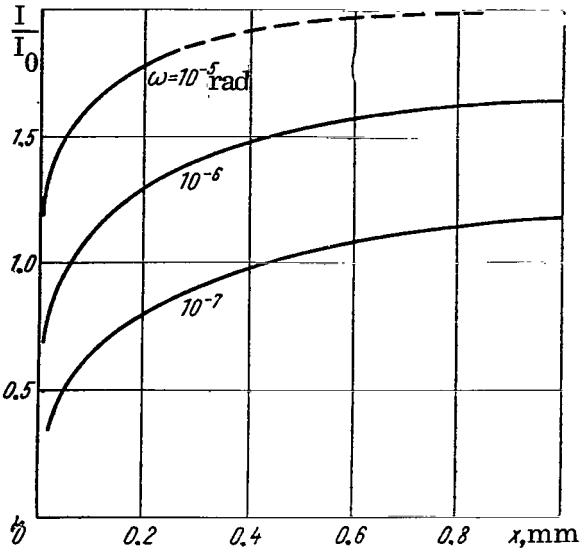

Figure 32. Dependence of Ionization Produced by Pair Components on the Distance to the Point of Pair Formation for Different Opening Angles [183].

2.4. Determination of total photon energy

When it is sufficient to know the total energy of all photons produced, the measurement is more conveniently carried out with ionization chambers, which give the possibility of determining the number of electrons at the cascade maximum. In this it is necessary to have several series of ionization chambers, since the energy spectrum of photons in nuclear interactions fluctuates from case to case and the position of the maximum is shifted. Usually in such measurements lead is used as a photon converter, since it has a short t-unit and relatively long path length of nuclear interactions. This reduces the probability of secondary interactions in the filters and thereby reduces the contribution to the photon energy from secondary cascades. /152

Ionization chambers are usually made of steel or brass, which leads to the appearance of a transition effect from lead in the chamber material. The magnitude of this effect can be calculated theoretically [48] (Fig. 33). In the measurement of the total number of particles it is necessary to introduce the appropriate corrections. In principle, one can make chambers from lead and in this way eliminate this transition effect. However, in this case the role of strongly ionizing particles — the products of nuclear fragmentations—sharply increases, and this will cause an overestimation of the photon energy. In chambers of steel or brass nuclear fragmentations which give a significant contribution to ionization are observed in 15% of the cases. Sometimes nuclear fragmentations imitate photon cascades with an energy of 100 GeV. With a primary particle energy of 300 GeV the contribution of strongly ionizing particles to the measured ionization reaches 10-20% on the average.

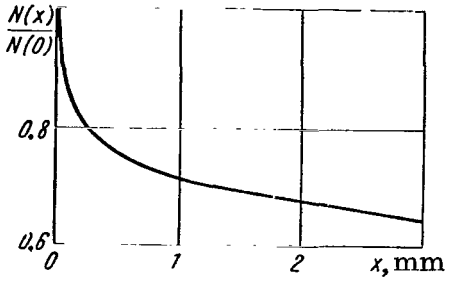

Figure 33. Transition Effect From Steel or Brass to Lead [48].

At the cost of an increase in the transition effect, it is possible to get rid of strongly ionizing particles completely, if Cherenkov counters are used instead of ionization chambers [50]. Transition effects have to be taken into account by means of a factor of 2 to 3, since the thickness of the material in the counters reaches 10 g/cm^2. An intermediate position is occupied by scintillators, [41, 62] in which strongly ionizing particles are registered with less effectiveness than relativistic ones. The thickness of scintillators can be less than that of Cherenkov counters. /153

2.5. Method of controlled emulsions

The method of controlled emulsions was suggested by Grigorov et al. [184] It gives the possibility of utilizing the merits of both photoemulsions and electronic methods. The practical realization of this idea consists of the following (see Fig. 15, c).

Three of four layers of photoemulsion are placed under lead absorbers having a thickness of several t-units. Below are arranged two rows of ionization chambers or an ionization calorimeter. Registration of pulses in the ionization chambers permits selection of events of the required energy and finding, from the arrangement of triggered chambers, the place in the emulsion where a given cascade has transpired. The photoemulsion makes it possible to determine the energy of the individual photons in the cascade, if the shower originates in a special target above the apparatus located at such a distance from the photoplates that the individual photons are able to diverge over a sufficient distance. The energy of the photons is determined by the methods explained in Sections 2.1 and 2.2.

This method not only facilitates the search for events of high energy, but with the aid of chambers gives the possibility of controlling the determination of energy in the photoemulsion. Obviously, the ionization counters in this case measure the total energy of all photons. The use of a calorimeter permits determination of the energy of the primary particle.

Detection of a primary photon by use of photoemulsions is possible only when its energy exceeds 50-100 GeV. Figure 34 is a sketch of a shower found by the controlled photoemulsion method [184]. /154

Photons of high energy are most effectively registered; however, as the energy increases there is a danger that the cascades from individual photons will begin to overlap. Secondary interactions of nuclear-active particles in the lead covering the photoemulsions can also create some difficulty.

Ionization chambers permit the determination of the point of occurrence of a shower to within several centimeters. In order to increase this precision, one

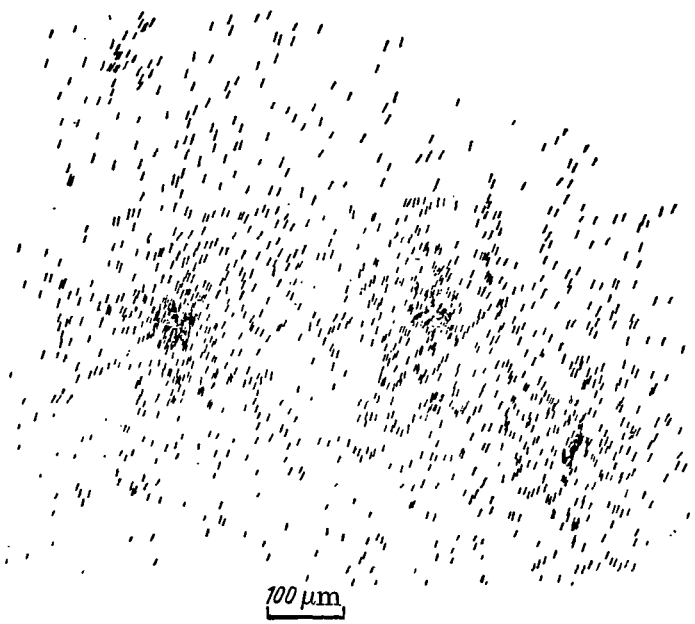

Figure 34. Sketch of a Shower Registered by the Method of Controlled Photoemulsions [184]. Three Stems of Electron-Photon Cascades are Distinctly Visible.

can use x-ray plates below the photoplates [185]. Electron-photon showers leave smeared spots in x-ray film. The coincidence of spots in two plates separated by a layer of material serves as a sufficient guarantee that the spots were not accidental.

The method of controlled photoemulsions possesses a significant advantage /155
over other photoemulsion methods, since it gives the possibility of measuring the energy of the primary particle with an ionization calorimeter.

2.6. Emulsion chambers

Recently, the emulsion chamber method, [176, 178, 186, 187] proposed by Kaplon et al., [188] has received wide application. Typical examples of this type of apparatus are shown in Fig. 35. A target, in which the nuclear interactions are produced, and a detector, made up of emulsion layers with metal plates of lead, tungsten, or tin between them, are the basic elements. The energy of the photons creating cascades in the detector is determined by the methods set forth in Sections 2.1 and 2.2. To facilitate the search for showers, /156
x-ray films are frequently employed in addition to the emulsions. With the aid of this method, investigations of photons have been carried out at very different heights—from mountains to the limits of the atmosphere [176, 177, 187] etc.

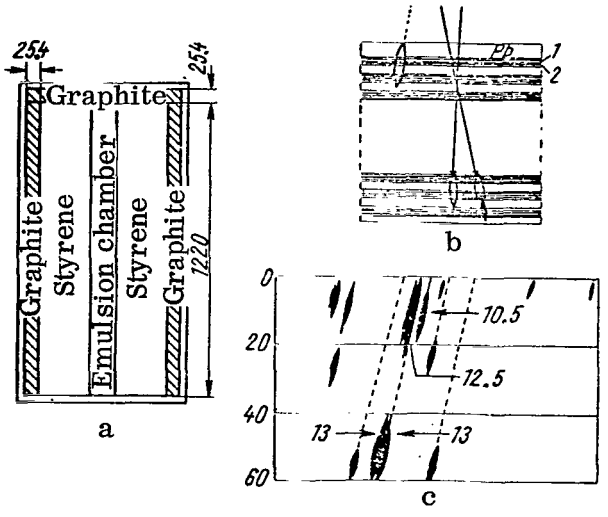

Figure 35. Typical Constructions of Emulsion Chambers:

a—for Investigations Close to the Limits of the Atmosphere; b—for Investigations on Mountains: 1—Nuclear Photoemulsions; 2—X-ray Plates; c—Pattern of the Passage of a Family of Electron-Nuclear Cascades Through the Emulsion Chamber Shown in b. The Numbers Near the Cascades Give Their Energy in TeV. On the Vertical Axis-Lead Thickness in Number of t-Units.

3. Energy Spectra of Secondary Particles in the Laboratory Coordinate System

3.1. Introduction

The energy spectra of secondary particles in the L system, even in the first approximation, cannot be considered without allowing for the distribution of the cosmic radiation with respect to energy. There are two approaches.

First, one can study the energy spectrum of secondary particles averaged over the entire spectrum of the primaries. This approach does not require knowledge of the energy of the primary particles, but it gives only indirect information about the elementary act of interaction.

Second, one can study the energy distribution of pions, kaons, nucleons, and other particles formed at a specific energy of a primary particle of known nature. The latter problem is methodologically more complex, but gives direct information about the elementary act. The features of the energy spectra, such as the presence of secondary particles comparable in energy with the primaries, their nature, the form of the spectrum and its dependence on the nature of the primary particle, give material for the comparison with various theories and models of multiple production.

Reliable information about the spectra of secondary particles in the act of generation is supplied principally by accelerators. At cosmic energies one is able to measure only certain sections of the spectrum. The high-energy portion is determined from photon families, the low-energy from charged pions. Nevertheless, the principal features of the energy distribution can be obtained even in cosmic rays, in spite of the limitations of the methods of measuring energy.

3.2. Spectra of secondary pions in the interaction of nucleons /157

The energy spectra of secondary particles in the interaction of nucleons with nucleons and nuclei can be approximated by an exponential law. This fact was first established by Cocconi et al [189]. To approximate the energy spectrum in the L system they proposed the following formula:

$$N(p)\,dp = \frac{2N_{\pi}\,p\,(p^2+m_{\pi}^2)^{1/2}}{T\,(p^2+m_{\pi}^2+p_0^2)}\left\{\exp\left[-\frac{(p^2+m_{\pi}^2)^{1/2}}{T}\right]+\right.$$
$$\left.+\exp\left[-(p^2+m_{\pi}^2)^{1/2}\left(\frac{1}{T}+\frac{\pi}{p_0}\right)\right]\right\}dp, \qquad (6.6)$$

where T is the average energy in the laboratory coordinate system, and $p_0=\frac{1}{2}<p_{\perp}>=0.18$ GeV/c. At E_0 = 30 GeV, T = 3.75 GeV = 0.124 E_0 GeV. Equation (6.6) easily reduces to a form that does not depend explicity on the primary energy E_0,

$$N(p)\,dp = Ae^{-u/u_0}\,du, \qquad (6.7)$$

in the region of momenta $p^2 \gg p_0^2$. Then u = pc/E, and $u_0 = T/E_0$ turns out to equal ~ 0.124.

At the present time there is a considerable amount of effort devoted to the study of the form of the energy spectrum in the L system. We shall examine certain of these results obtained in accelerators at rather high energies.

In the work of De Marko Trabucco et al. [190] interactions of protons of energy about 25 GeV were studied in a hydrogen bubble chamber. These authors investigated the energy spectrum of secondary pions, kaons, and hyperons. In Fig. 36 the spectrum of pions from this work is compared with the spectrum from the work of Garbovska et al. [158] on the interaction of 24-GeV protons with heavy nuclei of an emulsion. In the same figure is plotted the energy spectrum of π^0-mesons arising in the action of 9-GeV protons [191]. In the latter work, done by Friedlander et al., photons were selected with emission angles $\leqslant 5°$. The spectra are plotted in semi-logarithmic coordinates and for convenience have been reduced to the form (6.7). Cocconi's spectrum (6.6) is plotted in the same figure (curve 4).

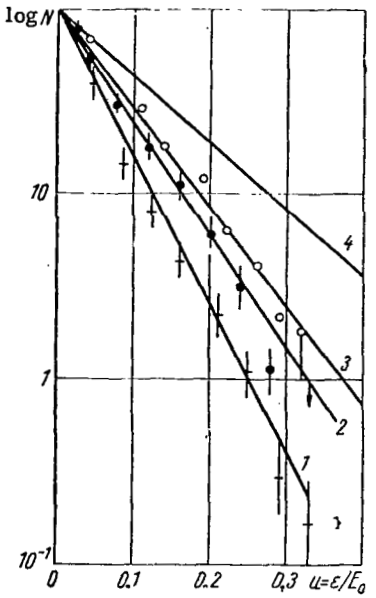

Figure 36. Integral Energy Spectra of Pions Formed by Protons in Interaction:

1—With Heavy Nuclei of the Photoemulsion; 2—With Hydrogen Nuclei [190]; 3—Spectrum of π^0-Mesons Emitted at an Angle Less Than 5°; 4—Cocconi Spectrum (Eq. (6.7)).

It is seen from Fig. 36 that the integrated spectra of pions created in the interaction of primary protons are approximated by an exponential. The difference in spectra 1 and 2 is evidently due to the use of different targets. Spectrum 1, from the interaction of protons with heavy nuclei, is softer than spectrum 2 for proton-proton collisions. The spectrum of π^0-mesons 3 was obtained on averaged-sized nuclei of the photoemulsion. However, in this case, the spectrum of π^0-mesons was determined at very small angles, i.e., the most energetic π^0-mesons were selected. It is completely natural that the spectrum of these particles should turn out to be harder than that of the others. The magnitudes of u_0 are equal respectively to 0.05, 0.07, and 0.08 for spectra 1, 2, and 3.

Thus, the energy spectrum of pions softens in going from nucleon-nucleon to nucleon-nucleus collisions and becomes harder when the particles selected are emitted at small angles.

The last result is also confirmed in other work. Dekkers et al. [192] observed a very strong dependence of the energy spectrum of pions on emission angle in the interval from 0 to 5.7°.

Fidecaro et al. [193] studied the spectrum of photons emitted at various angles in the L system after the collision of a proton with energy 23.1 GeV with a beryllium target. The spectra obtained can be approximated by (6.7) with $u_0 = 0.1$ for angles 1.75 and 3° and 0.06 for an angle of 6°. In a proton-proton collision, u_0 is close to 0.1 for $\theta = 1.75°$, but $u_0 = 0.04$ at 10° and 0.02 at 27°.* /159

Thus, numerous data indicate the exponential character of the integral spectrum of pions produced in proton-proton or proton-nucleus collisions.

3.3. Spectrum of secondary protons of high energy

The spectrum of protons is harder than that of pions. In Fig. 37 is shown the spectrum of protons from [158]. This spectrum was obtained as the

*If the differential spectrum of π^0-mesons can be represented by an exponential dependence, then in the region of photon energies $E_\gamma \gg m_\pi c^2$, the integral spectrum of photons is practically indistinguishable from the spectrum of π^0-mesons.

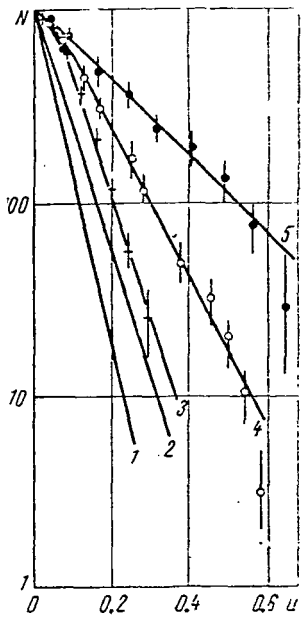

Figure 37. Integral Energy Spectra:

1—Pions in P-Nucleus Interactions [158]; 2—Pions in P-P Collisions [190]; 3—Kaons (in P-P Collision) [190]; 4—Protons in P-Nucleus Interactions [158]; 5—Hypersons in P-P Collision [190]. The Energy of the Primary Particle is About 25 GeV.

difference between the spectra of positive and negative charged particles. The exponent $u_0 = 0.14$, which is twice as large as u_0 for the pion spectrum.

In [190] interactions were chosen in which hypersons were formed. The energy spectrum of these hypersons is shown in the same figure, and in the interval $0 < u \leqslant 0.5$ is described by an exponential with $u_0 \sim 0.2$, which is also considerably greater than for the spectrum of pions under the same circumstances.

Note that in the pion spectrum there are practically no particles with energies in excess of 30% of the primary, whereas the baryon spectrum extends out to $u \geqslant 0.6$. /160

The spectrum of secondary protons in interactions with heavy nuclei is steeper than in proton-proton collisions, which indicates a difference in the coefficients of inelasticity (see Chapter 8).

Figure 37 also gives the spectrum of kaons from [190]. The slope of the straight line in the region $u \geqslant 0.1$ is the same as for pions, but the average energy of the kaons is somewhat greater than that of the pions.

3.4. Differential energy spectra of secondary particles

The differential distribution of secondary particles with respect to energy for energy 24-30 GeV was studied in [21, 158, 190, 192, 193]. The energy spectra for pions, kaons, hyperons, and protons in the L system are shown in Fig. 38. They were all obtained for p-p or p-nucleus collisions at proton energies of 24-30 GeV.

An analysis of the form of the spectra with the aim of deriving an approximate formula was carried out by Aly et al. [194, 195]. They found the momentum distribution by an indirect method with the assumption of no correlation between $p_\perp$ and the emission angle. The authors used a transverse momentum distribution in the form of (7.7) (Chapter 7) and the measured angular distribution for the collision of π-mesons with momentum (16 GeV/c) and of nucleons (14 and 30 GeV/c) with nucleons. To this end they considered interactions in an emulsion with $N_h = 0$ and 1, as well as data on the collision of protons with beryllium nuclei at 30 GeV. The approximation of the differential momentum spectrum proposed by the authors has the form (for $E_0 \approx 30$ GeV) /161

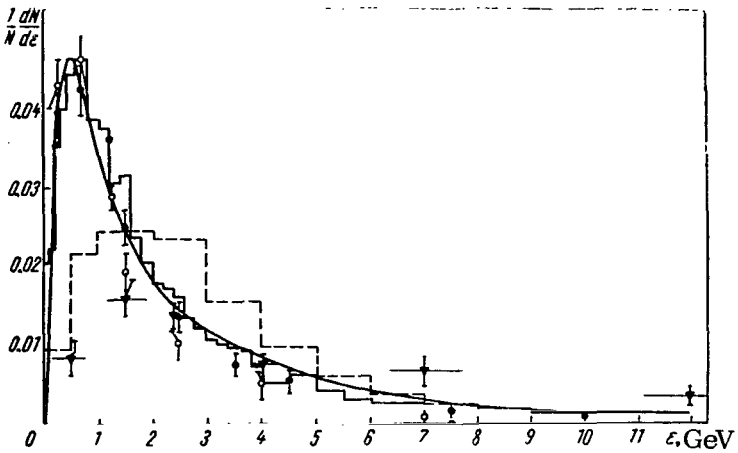

Figure 38. Differential Energy Spectra:
●—of Pions; O—of Kaons; ▼—of Protons and --- of Hyperons in the L System.

$$N(p)\,dp = N_0 e^{-\lambda/p^{\mu}} \frac{1}{p^2}\left(1 - \frac{1}{(10p)^{\mu}}\right)dp, \qquad (6.8)$$

where

$$\lambda = 3.6 \text{ and } \mu = 0.17.$$

This distribution differs markedly from those represented in Fig. 38 by a large number of high-energy particles. The reason for this discrepancy may be that in the given paper the nature of the secondary particles was not analyzed, and the distribution obtained needs to be compared with the total energy distribution of all the secondary particles (see Fig. 38).

Finally, it should be remembered that this result was obtained on the basis of an assumption about the universal character of the distribution of transverse momenta in all interactions, although it is possible that in events of a different type (e.g., for different kinds of secondary particles) this distribution is different. The spectrum of Cocconi et al. [189] (6.6) is evidently a better description of experiment if the magnitude of T is changed in accordance with the values of $u_0 = T/E_0$ specified in Section 3.2.

3.5. Energy spectrum of secondary particles for the collision of pions with nuclei

The spectra of π^0-mesons arising from the collision of primary pions and nucleons with nuclei differ strongly. The results of the measurement of the integral spectra of secondary pions in pion-nucleus collisions are presented in Fig. 39. The spectra was obtained by Hoffmann et al. [148] and pertain to the interaction /162

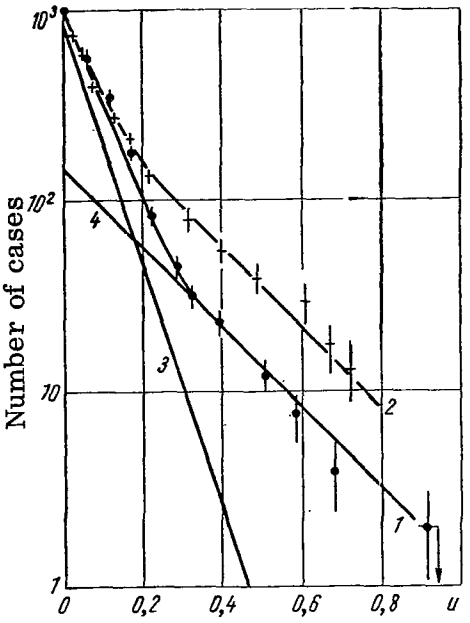

Figure 39. Integral Spectra of Pions in Pion-Nucleus Collisions: 1—π^- [148]; 2—π^0 [191]; 3 and 4—Decomposition of Spectrum into Its Components.

of negative pions with heavy nuclei of the photoemulsion ($N_h \geqslant 8$). The measurements of momenta were made in a magnetic field of 165 kG.

The spectrum observed in this work cannot be represented in the form of a single exponential law. The initial portion of the spectrum for $u<0.3$ falls steeply, but at $u \geqslant 0.3$ the slope of the spectrum changes, and the sloping part can be approximated by an exponential with index $u_0 \gtrsim 0.17$. This value is close to the magnitude of u_0 for secondary nucleons in proton-nucleus or proton-proton collisions.

In the work under consideration secondary negative particles were chosen to construct the spectrum. Consequently, the spectrum contains a certain proportion of kaons, although at energies attained in accelerators considerably fewer negative kaons are formed than positive ones. /163

In order to elucidate whether or not the highest energy part of the spectrum is associated with kaons, we shall turn to [191], where the spectrum of π^0-mesons in the collision of π^--mesons with emulsion nuclei was studied. The most energetic pions are emitted at small angles to the direction of the primary particle. Hence, one might expect that in observation at small angles the high-energy portion of the spectrum is manifested more sharply compared to the large emission angles of π^0-mesons.

This is confirmed by curve 2 in Fig. 39, which gives the spectrum of secondary π^0-mesons at angles less than 5°. In this case the slope of the spectrum in the semi-log plot is determined by the quality $u_0 \approx 0.2$ (for $u>0.15$), which agrees with the value of the exponent for the spectrum of charged pions.

For $u<0.15$ the energy distribution of π^0-mesons coincides with the distribution of negatively charged ones. This fact, that the spectrum of π^0-mesons becomes more inclined at smaller values of u, is evidently explained by the selection of photons emitted at small angles.

Thus, the spectrum of π^0-mesons, as well as the spectra of charged secondary particles, are essentially different in the case of pion-nucleus and nucleon-nucleus collisions.

The integral distribution seen in Fig. 39 (curve 1) can be represented in the form of the sum of the two exponential curves 3 and 4. In this, curve 3 has

almost the same slope as does the spectrum of pions created in proton-nucleus collisions. This evidently means that the mechanisms of generating pions with $u \leqslant 0.3-0.4$ are the same in proton-nucleus and pion-nucleus collisions. Pions that bear away a large part of the primary energy are formed principally in pion-nucleus collisions and almost never in nucleon-nucleus collisions.

But what of the fraction of high-energy pions?

Extrapolation of curve 4 in Fig. 39 to the point u = 0 gives that poins distributed over the inclined branch of the spectrum constitute approximately 1/6 of all pions. It is possible that this estimate is too high, since in the region $u<0.3$ the form of spectrum 4 is obtained by extrapolation. At the energy considered /164
the multiplicity of secondary particles is close to five, and on the average less than one pion responsible for the spectrum 4 is formed per interaction.

If one assumes a break in spectrum 4 at u = 0.3, then the number of high-energy pions is found to be of the order of 0.35 per interaction (minimum estimate). Consequently, analysis of the form of the integral spectra of secondary particles discloses a change in slope of the spectrum of π^-- and π^0-mesons in π^--nucleus collisions in the region $u \sim 0.3$. When $u < 0.3$ a group of particles stands out which have a slope of spectrum the same as that of pions in nucleon-nucleus collions. If one constructs the total spectrum of all secondary particles, in proton-nucleus collisions, this spectrum, as well as the pion spectrum, changes slope at $u \sim 0.3$.

Therefore, the spectra of all secondary particles in pion-nucleus and nucleon-nucleus collisions are qualitatively alike. However, in the case of nucleon-nucleus collisions the high-energy portion of the spectrum is produced by nucleons, and in pion-nucleus interactions, by π-mesons. This conclusion is contradicted by the results of Babu et al. [195a], who studied the spectra of photons arising in a graphite target under the action of 17-GeV pions and 24-GeV nucleons. The spectrum of photons in pion-nucleus interactions was found to be shorter that in nucleon-nucleus interactions (u = 0.07 and 0.14 for pion- and nucleon-nucleus collisions, respectively). The reasons for this disagreement are unclear.

3.6. Conservation of the primary particle

The primary particle is usually conserved after collision. The conclusions of Section 3.5, where it was shown that the most energetic secondary particle is of the same nature as the primary, indicate this.

In the energy range considered ($\sim$ 30 GeV), conservation of energy by the nucleon in nucleon collisions was established first in cosmic rays [196, 197]. Usually the result is formulated like this: collision of nucleons takes place with considerable elasticity (see Chapter 8). Accelerator experiments have shown the validity of this conclusion for the collision of nucleons not only with light, /165
but with heavy nuclei, as well as for pion-nucleus collisions. However, the possible details of this process should be kept in mind. In the collision of a primary proton with a nucleon or nucleus overchanging must exist, i.e. the

secondary nucleon may be both a proton and a neutron (see Chapter 12). In other cases the nucleon may be excited and fly off in the form of an isobar or hyperon. Thus the property under consideration should be considered as the conservation of a baryon as the result of a collision at energies in the tens of GeV.

Similar features should also be observed in the interaction of a pion. The secondary pion may as the result of a collision undergo inelastic overcharging. In other words, in the collision of a π^--meson with a nucleus, the most energetic surviving particle can be a π^--, π^+-, or π^0-meson. The probabilities of the reaction channels:

$$\begin{aligned} &1.\ \pi^- \longrightarrow \pi^- + \text{particles of low energy;} \\ &2.\ \pi^- \longrightarrow \pi^+ + \text{particles of low energy;} \\ &3.\ \pi^- \longrightarrow \pi^\circ + \text{particles of low energy;} \end{aligned} \qquad (6.9)$$

may be different.

Thus, in experiments [158] on the interaction of π^--mesons with nuclei, negative particles are encountered twice as frequently as positive ones among the particles with energies $E > 0.3E_0$. This shows that the probability of the reaction channel in the first case of (6.9) is twice as great as in the second.

4. Experiments in Cosmic Rays

The region of cosmic energies begins at $E_0 > 30$ GeV. However, it is hard to expect a significant change in the properties of the interaction up to 100 GeV, since the energies in the C system at 30 and 100 GeV differ by 1.8 times at most. Hence, phenomena in the region $\gtrsim$ 1000 GeV are the ones of most interest. Unfortunately reliable data on the spectra of secondary pions do not exist in this energy region.

In the energy region $\sim$ 100-200 GeV one uses the Wilson chamber in a magnetic field or the method based on the constancy of the average transverse momentum to determine the energy spectrum of secondary particles in the L system. /166

Aly et al. [194] considered the question of the possibility of determining the spectrum of secondary particles from the magnitude of $\langle p_\perp \rangle$. For this they compared the spectrum determined according to $\langle p_\perp \rangle$ in p-p collision at 300 GeV with the spectrum calculated on the assumption of the constancy of the distribution of $p_\perp$ and the experimental angular distribution. They found a marked difference in the spectra and decided on this basis that it was not possible to use $\langle p_\perp \rangle$ to determine the spectrum. However, it was pointed out earlier that their formula (6.4) does not agree with direct measurements in the 30-GeV region. A comparison of the distribution obtained on the basis of the assumption of the constancy of $\langle p_\perp \rangle$ with direct measurements in the very same energy region can give more reliable information about the applicability of this method.

First, it is necessary to make the following remark. Among the secondary particles in a shower, a surviving nucleon is present, which should be excluded. Otherwise we do not obtain the spectrum of pions. The surviving nucleon bears a significant fraction of the primary energy and is emitted at a relatively small angle. As is shown in Chapter 7, the principal fraction of protons have $p_\perp < 1.5$ GeV/c. Consequently, the majority of conserved nucleons liable to exclusion should depart at an angle $\theta < 1.5/(1 - K)E_0$ (energy in GeV, K is the coefficient of inelasticity). As a minimum we ought to discard protons which as a result of collision have not changed their energy much; then $\theta = 0.05$ rad (3°) at 30 GeV and $\theta = 0.0075$ rad ($\sim 30'$) at about 200 GeV. The number of rejected particles can serve as the criterion for the correctness of selection. For proton-nucleon or proton-nucleus collision the number of excluded particles should be of the order of 1/2 per interaction and not more than 1 in any event.

Guided by these rules, we excluded from the spectrum of the momenta of secondary particles in the work of Aly et al. particles which were emitted at angles less than 2°, and the remaining particles were used to construct the integral spectrum. The spectrum obtained agrees well with the direct measurements [190] (Fig. 40). /167

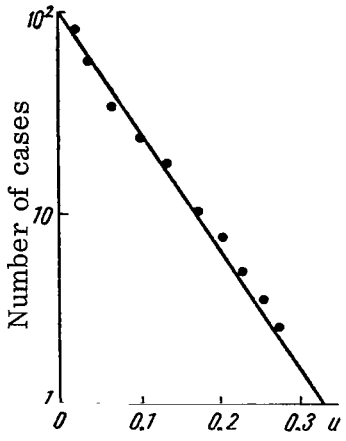

Figure 40. Integral Energy Spectrum Obtained Under the Condition p = Const. Points-Results of Direct Measurements from [190].

Thus, it is possible to expect that the method based on the use of $<p_\perp>$ for the determination of spectra should give correct results also for cosmic experiments.

The energy distribution of secondary particles has been obtained by this method with the aid of an ionization calorimeter and Wilson chamber. The spectra of secondary particles created by neutral and charged primaries were studied individually. If it is assumed that protons and neutrons interact in the same way, then the difference between the two distributions should give the energy spectrum of secondary particles produced by primary pions. The results are shown in Fig. 41, and, in complete agreement with data obtained in accelerators, they show the difference in the secondary spectra for cases of interaction of primary protons and pions. The spectrum of secondary particles created by nucleons is described by an exponential with exponent $u_0 = 0.05$.

At an energy of about 200 GeV, as also at lower energy, nucleons almost never create pions with energies greater than $0.3\ E_0$. Both in accelerator and cosmic ray experiments one frequently observes cases in which the primary pion is conserved. /168

Experiments with a Wilson chamber placed in a magnetic field have the advantage that they make it possible to detect particles emitted at small angles

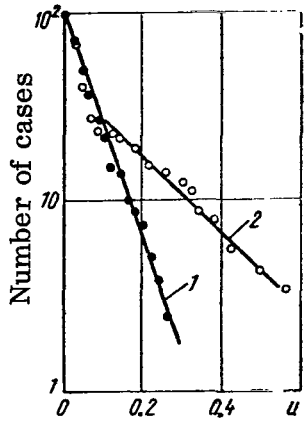

Figure 41. Integral Energy of Secondary Particles at 200 GeV:

1—Primaries Neutral;
2—Difference of the Distributions for Charged and Neutral Primaries.

but having a very low momentum. In the work of Dobrotin et al. [12, 198] such particles were observed in 20% of the showers. They had angles less than 1-2° and momenta one-tenth of that expected from the constancy of $p_\perp$.

Many attempts have been made to elucidate the form of the spectrum of protons of high energy. Usually it was assumed that the particle having the greatest energy is a proton. Its energy was determined from the angular distribution of particles in secondary interactions. This method cannot give reliable quantitative results. Daniel et al. [64], after a similar analysis concluded that in each interaction there is one secondary particle that bears on the average about one-half of the initial energy. The energy of any of the remaining particles almost never exceeds 10% of the primary. Thus, in this case the concluion of Section 3.6 about the conservation of the primary particle after interaction is corroborated. There are certain reservations, however. The authors assumed the most energetic particle to be a nucleon a priori. In fact, this is an extremely grave assumption, since it is impossible to determine the nature of a high-energy particle.

The hydrodynamic theory predicts the existence of a particle that bears away about half of the initial energy, but in the majority of cases the fastest particle is a pion. Hence, the determination of the nature of the secondary particle of highest energy could give valuable information about the validity of hydrodynamic ideas. There is a basis for believing that in nucleon-nucleon collisions such a particle is a nucleon.

In collisions of nucleons with heavy nuclei the situation may be different [199, 200] (see Chapter 8).

The energy spectrum of secondary nucleons of high energy can be measured /169
by studying the distribution of the magnitude of the second maxima of the nuclear-cascade curve in a calorimeter [201, 202]. Examination of the form of individual nuclear cascades shows that a depth distribution with secondary maxima is typical (Fig. 42). It is obvious that they are due to a nuclear-active particle that survives the first interaction. The area bounded by the second maximum S_2 is proportional to the energy of the surviving particle. If S_0 is the area bounded by the entire nuclear-cascade curve, the fraction of the energy of the most energetic particle will be

$$\frac{E_2}{E_0} = \frac{S_2}{S_0}.$$

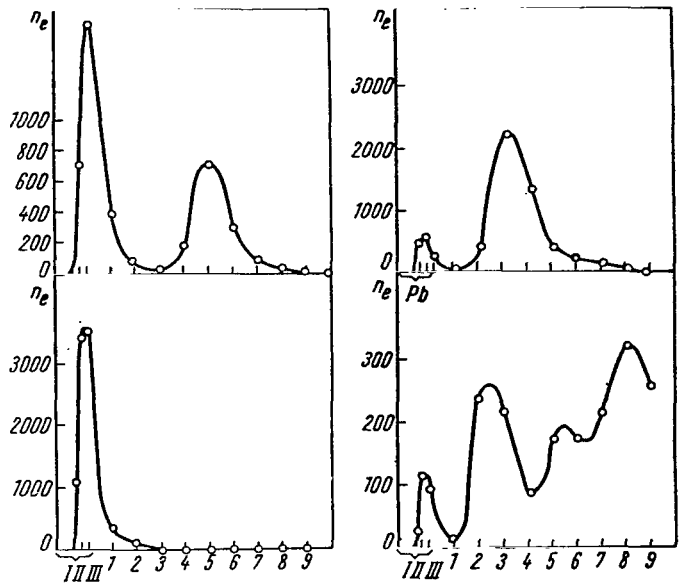

Figure 42. Dependence of Number of Electrons n_e on Depth in the Absorber of the Calorimeter. The Numbers on the Abscissa Axis Denote the Row Number of the Ionization Chambers in the Calorimeter (see Fig. 15a). Rows I, II, and III are Arranged Under Layers of Lead, the Remainder Under Layers of Iron.

The slope of the integral spectrum of secondary particles for the case of cascades initiated in a graphite target is $u_0 = 0.30 \pm 0.05$. Within the limits of experimental error this agrees with the spectrum of nucleons in p-p collision at $E_0 \sim 25$ GeV. /170

In the work of Brook et al. [96] the differential spectrum of the highest energy nucleons arising from the interaction of primary particles with light nuclei was derived on the basis of an analysis of the passage of cosmic radiation through the atmosphere. They chose for this spectrum the following approximate formula:

$$P(u)\,du = -5.9u^{1.43}\ln u\,du.$$

This distribution also describes the results of measurements with a calorimeter [202].

5. Energy Spectra of π^0-Mesons

5.1. Photon families

The energy spectrum of π^0-mesons with respect to photons is studied by the method of controlled emulsions, emulsion chambers, and piles, frequently in combination with x-ray plates.

These experiments have the feature that the investigated interaction occurs not in the detector itself, but in a special graphite target placed at a height of 1.5 m or so above the cascade detector or in the atmosphere over the apparatus. This is necessary in order to give the possibility that the photons formed in the interaction will diverge sufficiently. In practice, it is possible to resolve cascades from photons if the latter traverse the emulsion not less than 50-100 μm apart.

Groups of photons arriving from the atmosphere or from a target and registering simultaneously in the apparatus have acquired the name "photon families." Each photon family forms in the material of the detector an electron-photon cascade, which is registered by the photoemulsion or x-ray film. In the x-ray film is observed a group of spots, the size of which is determined by the energy of the photon. In photoemulsions one can distinguish the individual particles with sufficient magnification. Examples of sketches of showers are shown in Fig. 34.

5.2. Interpretration of photon families

/171

The photons belonging to a family can come from various sources.

First, photons arise directly in the decay of π^0-mesons, and, second, as products of an electron-photon cascade in air. On the basis of the spatial distribution of photons in the family, it is possible in principle to determine the mechanism of their generation [203]. If two photons with energies E_1 and E_2 come from the decay of a π^0-meson, the spacing between them

$$h = H \frac{m_\pi c^2}{\sqrt{E_1 E_2}}, \qquad (6.10)$$

where H is the distance from the point of origin of the π^0-meson to the detector and m_π is the mass of the π^0-meson.

The average spatial distribution of photons of an air shower is characterized by the mean square radius of the shower $\langle R \rangle$ in the plane of the detector

$$\langle R \rangle = A \frac{E_s}{E_{\min}},$$

where E_{min} is the minimum detected energy, and $E_s \approx 21$ MeV is the characteristic energy for electron scattering.

The constant A depends on the age of the shower and in the case of small distances H is of the order of 0.1. The ratio

$$\frac{h}{R} = H\left(\frac{E_{\min}}{\sqrt{E_1 E_2}}\right)\left(\frac{m_\pi c^2}{E_s}\right)\frac{1}{A} \cdots \qquad (6.11)$$

shows that the biggest difference between $<R>$ and h is observed at large magnitudes of H and $\xi = \frac{\sqrt{E_1 E_2}}{E_{\min}}$. For certain values of the parameters H and ξ it is impossible to determine the source of the photons (when $R \sim h$). The mean square radius $<R>$ is conveniently calculated as the weighted mean over the energies

$$<R> = \frac{\Sigma E_i R_i}{\Sigma E_i},$$

where R_i is the distance of the i-th photon from the shower center.

If one observes in the emulsion photons which have undergone cascade multiplication in the atmosphere, then the problem arises of determining the energy of the primary photon that gave birth to the cascade. One can calculate /172 the dependence of $<R>$ on $\frac{\Sigma E_i}{E_0}$ (and on H), where E_0 is the energy of the primary photon. The appropriate dependence for small values of $<R>$ gives $\frac{\Sigma E_i}{E_0} \approx 1$.

5.3. The union of pairs of photons into π^0-mesons [203]

If the photon cascades observed in the emulsion proceeded directly from the decay of π^0-mesons, the distance between the photons from the decay of a single π^0-meson is connected with their energy and height of origin H by the relation (6.10).

To solve the problem of uniting the photons into the pairs that belong to a specific π^0-meson, one attempts to find those combinations of photons which give the same height of shower origin for any selected pair of photons.

The correctness of the joining can be checked by constructing the distribution of the energies of the photons that have been grouped into pairs.

Let the energies of the decay photons be E_1 and E_2, with

$$E_1 > E_2 \text{ and } E_1 + E_2 = E_{\pi^0}.$$

It is known that the energies of decay photons are distributed uniformly in a certain interval determined by the conservation laws. Assuming that the minimum detectable energy is E_{min}, we find

$$\frac{E_1 + E_2}{2} < E_1 < E_1 + E_2 - E_{min}$$

and

$$E_{min} < E_2 < \frac{E_1 + E_2}{2}$$

The quantity constructed from E_1, E_2 and E_{min}

$$\zeta = 2\frac{E_2 - E_{min}}{E_1 + E_2 - 2E_{min}}$$

should be uniformly distributed between 0 and 1.

Some of the photons remain unpaired, since E_2 can be less than E_{min} in the experiment. Then the energy of the π^0-meson is included in the limits from E_1 to $E_1 + E_{min}$. The probability of observing a single photon is $2E_{min}/E_0$. /173

5.4. The energy spectrum of photons

Usually the energy of the primary nuclear-active particle that creates a given family is unknown. Hence, to construct the normalized energy spectrum in an act of generation the energies of the individual photons are related to the total energy of the photons of a given family. Obviously, this procedure cannot give the true shape of the energy spectrum in an act of generation.

If a certain fraction of energy α_0 is transferred to all the photons, it is possible to establish how far the measured spectrum differs from the true one. To this end, in the expression for $u_0 = T/E_0$ (see Eq. (6.7)) we should replace E_0 by αE_0. Consequently, the new value is

$$u_0' = \frac{T}{\alpha E_0} = \frac{1}{\alpha_0} u_0.$$

Even the spectrum normalized to the energy $\alpha_0 E_0$ will be considerably more inclined than the energy spectrum per act. In the selection of events according to electron-photon cascades the principal contribution in this case will be given by events with large α_0 (see Chapter 2). It may be expected that the slope of the spectrum will be changed by a factor of two or three. (If all events are chosen, then $<\alpha_0> \sim 0{,}2$ and $u_0' = 5\ u_0$).

In Chapter 8 it is shown that pions transfer to photons on the average more energy than do nucleons. At mountain heights, where there are particularly many pions in the nuclear component of the cosmic radiation, these latter can give a very big contribution to the number of observed events (see Chapter 12).

According to estimates of Akashi et al. [84], at a depth of 500 g/cm^2 $(45 \pm 20)\%$ of all showers in emulsion chambers occur from primary pions. At greater depths the fraction of pions in the nuclear component increases, and their role in creating families will be still greater. Thus, on mountains photon families come from pions to a considerable degree, whereas in the stratosphere and near the limits of the atmosphere they come from nucleons.

In interpreting the results it should be kept in mind that photons with an energy less than 50-100 GeV are usually not registered, and therefore the number of photons of low energy is underestimated [204]. /174

For convenience in comparing with the spectra considered earlier we shall present the result of the measurement of spectra in families on a semi-log plot, although a log-log plot is used in most of the original papers.

Figure 43 summarizes the data on photon measurements by the method of controlled emulsions in the papers of Babayan et al. [205, 206] and Buya et al. [175], and the data of Akashi et al. [207]. To construct the spectra, showers were chosen in which the total energy of the photons was on the average close to 10^{12} eV or somewhat less. The data was obtained at mountain heights. Within experimental error, the photon spectrum can be expressed by an exponential /175 with coefficient $u_0' \sim 0.1$* (in the given case, $u_i = \frac{(\Sigma\gamma)_i}{\Sigma(E\gamma)_i}$). The similar value of $u_0' = 0.13$ was obtained by Heidbreder and Pinkau [204] for three families with energy of several thousand GeV.

In [206a, 207] many photons were successfully joined into pairs and the spectrum of the π^0-mesons was obtained. In general, this spectrum has the

*The authors approximate the spectra of π^0-mesons and photons they obtained by a power law with exponent 1.50 ± 0.20 (in the region $u > 0.1$ for π^0-mesons).

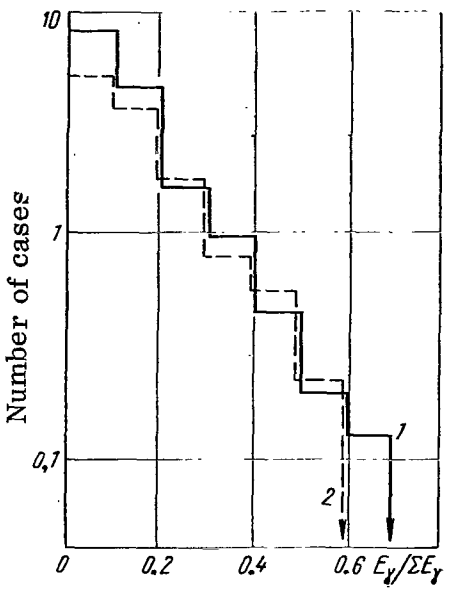

Figure 43. Integral Energy Spectrum of Photons in "Families", Measured at Mountain Heights:

1—From [175, 206]; 2—From [207].

same character as that of the photons, and cases are encountered in which one π^0-meson bears almost all the energy of the family (in two cases out of 15 one π^0-meson carriers more than 70% of the family energy).

Extensive investigations of photon spectra was carried out by a Japanese-Brazilian group working on Mt. Chacaltaya [84] (5200 m above sea level—550 g/cm^2). Their emulsion chambers consisted of nuclear photoemulsions and x-ray plates interspersed with lead, up to 20 t-units in total thickness. The authors obtained spectra of photons in families with energy ΣE_γ from 10^{12} to 50×10^{12} eV. In this energy interval they did not observe a significant difference in the form of the spectra, although at the highest energies ($\Sigma E_\gamma \geqslant 2 \times 10^{13}$ eV) there appeared cases where one of the pions carriers almost all the energy of the family. The average values $\langle E_{\pi^0}/\Sigma E_\gamma \rangle$ does not change with energy: $\langle E_{\pi^0}/\Sigma E_\gamma \rangle = 0.35 \pm 0.03$, if $100 < \Sigma E_\gamma < 1000$ GeV, and $\langle E_{\pi^0}/\Sigma E_\gamma \rangle = 0.33 \pm 0.02$ in the region $\Sigma E_\gamma > 10^4$ GeV.

The particles of highest energy $\Sigma E_\gamma > 2 \times 10^4$ GeV gave several interactions where one of the pions carried a significant portion of the family energy. At energies less than 10^4 GeV, similar cases, according to data of Akashi et al., are rare. However, Fowler [139] and Buya et al. [175] found such events even in the lower energy region down to 100 GeV.

The study of photon families with the aid of emulsion chambers has shown that the normalized spectra of photons in families differ little at mountain heights and close to the limits of the atmosphere. This results does not contradict our conclusions about the considerable difference between the characteristics of the interaction of pions and nucleons.

If the experimental data obtained in accelerators is normalized in the same way as cosmic data, i.e., to the energy transferred to pions, then the difference between the spectra for pion and nucleon collisions will be small.

An investigation of the spectra of photons in families was carried out by Fowler et al. [139] and also by Malhotra et al. [140].

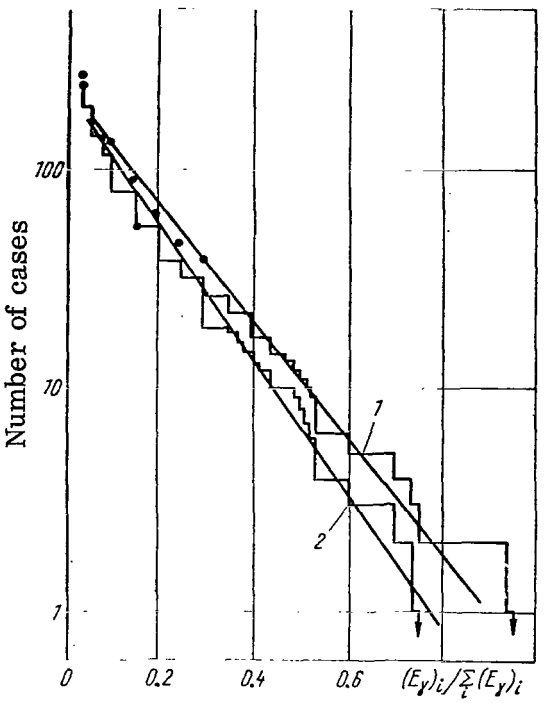

Figure 44. Integral Energy Spectrum of Photons in Families, Measured Near the Limits of the Atmosphere:

1—Number of Photons in a Family $n_\gamma > 2$;
2—$n_\gamma > 4$.

These workers did not observe any significant difference in the form of the normalized spectra of photons for events with total energy $\Sigma E_\gamma > 2 \cdot 10^4$ 400 GeV and 1600 GeV. The summation was carried out over all photons having an energy $E_\gamma \geqslant 50$ GeV and angle $\theta < 10^{-2}$ rad. On the average 90% of the photon energy was contained within these limits. In the region $u' > 0.1$ the observed spectrum is represented by an exponential (Fig. 44) with $u'_0 = 0.175$ for events with the number of photons greater than one and $u'_0 = 0.152$ for $N_\gamma \geqslant 4$. This result is close to that observed on mountains. /177

In the work of Fowler et al. [139] the normalized spectrum of photons was found to depend on energy. For $\Sigma E_\gamma > 3000$ GeV the form of the spectrum is the same as in the work of Malhotra: $u_0' = 0.16 \pm \frac{0.03}{0.02}$; however, at lower energies $u_0' = 0.24 \pm 0.03$. In both investigations the quantity of registered cases was extremely small (several tens of events), and the difference is evidently due to accidental sources.

Thus, up to primary energies of the order of 10^4 GeV the energy spectra of photons and consequently also of pions remain exponential, with the exponent not changing much.

Babayan et al. [206] and Grigorov et al. [52], using the controlled emulsion method in combination with an apparatus of the calorimetric type, succeeded in determining the energy of individual photons in the groups and estimating the energy of the primary particle. They chose events with energy exceeding 10^3 GeV. In all, they published 13 cases of families consisting of more than two photons.

In all cases they determined the energy of the most energetic π^0-meson $(E_{\pi^0})_{max}$, as well as the ratio of the energies of the most energetic particles. The results are presented in Table 39. All the families examined arose in a graphite target placed above the apparatus.

The nature of the particles evoking the electron-nuclear showers was not determined in these experiments. However, based on the aforementioned

TABLE 39. CHARACTERISTICS OF INTERACTIONS REGISTERED BY THE CONTROLLED EMULSION METHOD

E_0, GeV	ΣE_γ	$\alpha_0 = \frac{\Sigma E_\gamma}{E_0}$	N_γ	$(E_{\pi^0})_{max}$	$\frac{(E_{\pi^0})_{max}}{E_0}$	Energy of the most energetic photon, GeV
a) $\alpha_0 > 0.6$						
1 700	1200	0.72	4	680	0.40	680
2 800	2580	0.92	6	1100	0.39	920
3 000	2400	0.80	7	800	0.27	620
3 600	3280	0.90	6	1500	0.42	1500
4 000	2560	0.64	6	1000	0.25	920
5 100	3790	0.74	4	2500	0.49	2000
5 800	4540	0.78	10	1400	0.24	900
6 000	4840	0.81	10	2900	0.48	1920
9 400	5800	0.62	6	5000	0.53	2840
b) $\alpha_0 < 0.6$						
4 700	2300	0.49	9	600	0.13	400
8 600	3510	0.41	14	700	0.08	400
11 500	2300	0.20	8	1100	0.10	800
11 700	3100	0.26	20	500	0.04	440

results of Akashi et al. [84], we must assume that more than half of all registered showers were caused by primary pions. This conclusion will find confirmation later (see Chapter 12). In Chapter 8 it is shown that only in rare cases do nucleons transfer to π^0-mesons more than 60% of their energy in a single act. Hence the results given in Table 38 can be divided into two groups with $\alpha_0 > 0.60$ and $\alpha_0 < 0.60$. Among events with $\alpha_0 > 0.6$ interactions evoked by primary pions should predominate, with $\alpha_0 < 0.6$—by nucleons (see Chapter 8). The properties of these two groups of events with respect to their energy characteristics are essentially different.

In interactions with $\alpha_0 > 0.6$ ($<\alpha_0> = 0.78 \pm 0.03$) the energy of the most energetic π^0-meson averaged over all events is $<(E_{\pi^0})_{max}/E_0> = 0.37 \pm 0.05$. This same quantity in the second group of events ($<\alpha_0> = 0.34 \pm 0.05$) is four times less: $<(E_{\pi^0})_{max}/E_0> = 0.09 \pm 0.02$. The average multiplicity of π^0-mesons in the first group is 3.5 ± 0.35, in the second, 7 ± 1.6. This result agrees with the conclusions in Chapter 5 about the lower multiplicity in pion-nucleus collisions.

Thus, in collisions which can be assumed to be pion-nucleus, the average multiplicity of secondary pions is one-half, and the energy of the most energetic pion is one-fourth as great as in nucleon-nucleus collisions. This means that the spectrum of π^0-mesons produced by pions is harder than the corresponding spectrum from nucleons.

The total energy spectrum over all events can be derived by using the authors' table of average values of the energy of the four photons of highest energy. It can be represented by an exponential with $u_0' = 0.22$. Considering that over all cases /179

$<\alpha_0> \approx 0.65$, the spectrum normalized to the total energy of the primary particle E_0 will have a slope $u_0 = 0.65\, u'_0 \approx 0.15$. However, this result pertains to a mixture of nucleon and pion interactions. To obtain the form of the spectrum for pion and nucleon interactions, one can utilize separately the average energies of the most energetic π^0-meson for these interactions.

Approximating the energy spectrum of secondary π^0-mesons by an exponential law and allowing for the multiplicity difference, we find that for pion-nucleus collisions at 1000 GeV, $u_0 = 0.25 \pm 0.03$, and for nucleon-nucleus $u_0 = 0.05 \pm 0.1$. This agrees with the results of accelerator experiments.

5.5. Average characteristics of the energy spectra of pions in the L system

In calculations of the passage of cosmic radiation through the atmosphere an important quantity is $<n_\pi u^{\gamma-1}>$, where n_π is the number of pions, and γ is the index of the differential energy spectrum of the primary particles (see Chapter 12). The value of γ is close to 3; hence $<n_\pi u^{\gamma-1}> = <n_\pi u^2>$. This parameter can be obtained from the differential distribution of pions with respect to energy in the L system.

From the spectrum measured by Garbovska et al. [158] for interactions of protons with heavy nculei, we find $<n_\pi u^2> = 0.040 \pm 0.015$ (E_0 = 24 GeV). For nucleon-nucleon collisions [190], $<n_\pi u^2>_p = 0.05 \pm 0.01$. For the interaction of pions with nuclei [148], $<n_\pi / u^2>_\pi = 0.13 \pm 0.05$. The spectrum of secondary particles in a pion-nucleon collision [194] leads to a value $<n_{\pi^\pm} u^2>_\pi = 0.18 \pm 0.04$.

The quantity $k = <nu>$ is the coefficient of inelasticity. As will be shown in Chapter 8, its average value does not vary with energy. Since the multiplicity $<n_s>$ increases with energy, the quantity $<u>$ must therefore vary with energy, and consequently $<nu^2>$ may depend on energy. We shall postpone further discussion about the properties of this parameter until Chapters 12 and 13. /180

6. Energy and Momentum Spectra of Secondary Particles in the C System

6.1. Transformation of energy distributions into the C system

Presentation of results in the C system frees the investigated phenomena from the influence of kinematic peculiarities associated with motion of the coordinate system and having no relation to the dynamics of the collision process. Therefore examination of the interaction characteristics in the system of the center of mass of the colliding particles facilitates the comparison of different data, as well as of experiment with theory.

Transformation of the energy distribution from one system to another can be accomplished by means of known transformation formulas [208]

$$\frac{d^2N(p_c, \theta_c)}{dp_c d\Omega_c} = \gamma_c(1 - \beta_c \cos\theta)\frac{d^2N(p, \theta)}{dpd\Omega},$$

where $d\Omega_c$, $d\Omega$ are elements of solid angle; p_c, θ_c and p, θ are related by the usual formulas for the transformation of angles and momenta. It is obvious that it is necessary to have good information about γ_c for this procedure to be successful.

In many cases the form of the distribution $\frac{d^2N(p, \theta)}{dpd\Omega}$ in the laboratory system is unknown. Then one transforms the momenta and angles of the individual particles and constructs the distribution in the C system from this.

6.2. Integral distributions in the C system

In this section we shall compare the results of the determination of integral spectra of secondary particles at different energies. The integral spectra of pions in nucleon-nucleon collisions are shown in Fig. 45 [135, 190, 198, 209, 210].

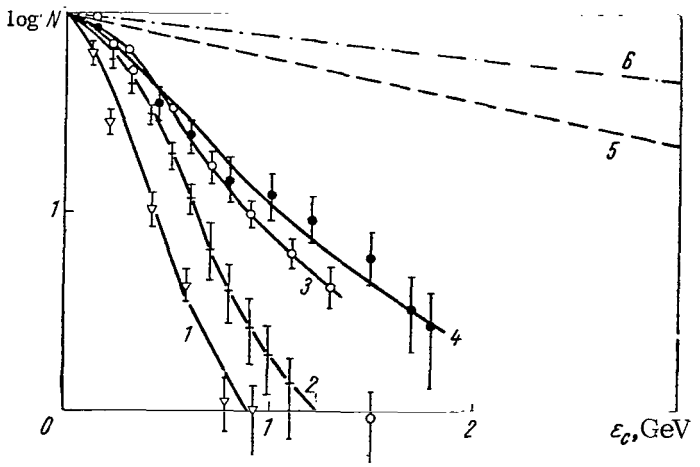

Figure 45. Integral Energy Spectra of Pions in the C System for Different Primary Energies:

1—3, 5 GeV [210]; 2—19 GeV [200]; 3—25 GeV [190, 135]; 4—200 GeV [198]; 5—$\overline{\gamma\Sigma E_\gamma} \simeq 10^4$ GeV; 6—$\overline{\gamma\Sigma E_\gamma} = 2.8 \cdot 10^4$ GeV (5 and 6—from [140].

The pion spectra in p-p collisions at 25 GeV are constructed up to values of the momentum $p_c \sim 2$ GeV/c. The results obtained by Dodd et al. [135] and De Marko Trabucco et al. [190] at energies near 25 GeV are almost the same and are united in Fig. 45. The data of Dobrotin et al. [198] pertains to the symmetric system. However, the velocity of the symmetric system relative to the C system is small ($\gamma_{sc} \sim 1{,}1$), and therefore the spectra in these two systems should not be very different.

In this work the energy of the primary particles (nucleons and pions) was measured with a calorimeter and was in excess of 100 GeV, and the energy of the secondaries was determined in a Wilson chamber from the radius of curvature of the trajectory in a magnetic field. Curves 1 and 2 in Fig. 45 represent spectra of pions in the C system at a momentum of the primary protons of 19 and 3.5 GeV/c. It follows from the graphs that the energy spectrum of pions depends on the energy of the primary particle.

The energy spectra of photons in the C system at an energy 23.1 GeV were studied by Fidecaro et al [193]. There results can be compared with the data of Malhotra et al. [140] at 1600 and 4000 GeV, which were obtained in an emulsion /182
chamber, and the spectrum of photons in the C system was calculated from the energy distribution of photons in the families. The average energy of the primary particles was assumed to be

$$<E> = 7 <\Sigma E_\gamma>.$$

In this case the event selection was by electron-photon cascades and such an energy estimate is bound to be too high (see Chapters 12, 13), leading to errors in the determination of the form of the spectrum in the C system.

The magnitude of the error in determining the energy of individual particles in the C system arising from the use of an incorrect value for E_0 is

$$\left| \frac{\Delta \varepsilon_{ic}}{\varepsilon_{ic}} \right| \sim \frac{\Delta \gamma_c}{\gamma_c}.$$

If γ_c is too high, the energy of particles in the outer cone after transformation /183
into the C system will be greater than the true value, whereas the energy of particles in the inner cone will be too low.

In cosmic ray experiments particles in both the outer and inner cones are analyzed. Measurements of multiple scattering usually are made on particles of the inner cone.

In the photon experiment being considered, they studied mainly inner-cone particles in the L system, and consequently it may be expected that the average photon energy obtained in [140] will be too low in the C system. The results of the comparison of integral photon spectra in the C system at a proton energy of 23.1 GeV, as well as when $\Sigma E_\gamma = 1600$ and 4000 GeV, are shown in Fig. 46. The sharp difference in the spectra in different energy regions indicates the marked growth of the average photon energy in the C system with increasing energy of the primary particle. It is easy to establish the relation between the spectra of π^0-mesons and photons.

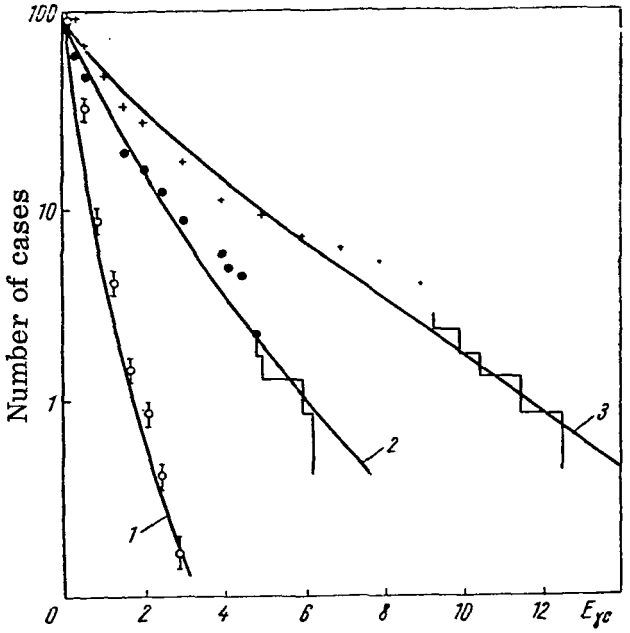

Figure 46. Comparison of Integral Energy Spectra of Photons in the C System for Different Energies of Primary Protons:

1—23.1 GeV; 2—$\Sigma E_\gamma = 1600$ GeV; 3—$\Sigma E_\gamma = 4 \cdot 10^3$ GeV.

If the pion spectrum in the C system has the form

$$\frac{dN_\pi}{d\varepsilon_{\pi c}} = \frac{A}{T_c} \exp\left[-\frac{\varepsilon_{\pi c}}{T_c}\right], \tag{6.11}$$

and $\varepsilon_c \gg m_\pi$, then

$$N_\gamma(>\varepsilon_c) = 2A \int_{\frac{\varepsilon_c}{T_c}}^{\infty} dy \int_y^{\infty} \frac{\exp(-t)}{t}\, dt = 2AEi(\varepsilon_c/T_c), \tag{6.12}$$

(E_i is the integrated exponential function). The photon spectrum calculated from Eq. (6.12) for the case of high energy is indicated in Fig. 46 by the continuous lines. The approximating curves have $T_c = 2.0$ for $<\Sigma E_\gamma> = 1600$ GeV and $T_c = 3.7$ for $<\Sigma E_\gamma> = 4000$ GeV.

In Fig. 45 is plotted the spectrum of π^0-mesons for energies $7<\Sigma E_\gamma>\sim 10^4$ GeV and 2.8×10^4 GeV.

6.3. Differential distributions

The differential distribution of pions in the symmetric system was obtained by Dobrotin et al. [198]. This distribution is shown in Fig. 47 and is described by the Planck formula, except for the high-energy region ($\varepsilon_c \geqslant 0.7$ GeV), /184

$$\frac{dN_\pi}{d\rho_c} = A \frac{(\rho_c)^2}{\exp[(\rho_c/T) - 1]}. \qquad (6.13)$$

For the parameter T the authors give the value (0.7 - 1) m_π.

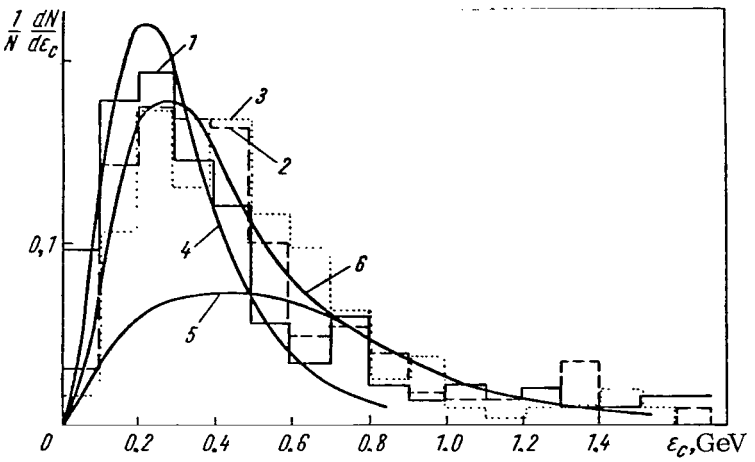

Figure 47. Differential Energy Spectrum of Pions in the Symmetric and C Systems:

1—Spectrum from [198]; 2—[190]; 3—[140]; 4—Spectrum Calculated from Eq. (6.13); 5—Calculation of Hagedorn from Statistical Theory [211, 212] Without Allowing for Isobars; 6—With Account Taken of Isobars (3/2, 3/2).

In the region of accelerator energies the results of experiment are conveniently compared with calculations based on statistical theory. According to the data of [135, 190], the comparison of the differential spectrum in the C system with calculations of Hagedorn [211, 212], who took into account also the contribution of isobars 3/2, 3/2 shows good agreement between theory and experiment.

Differential spectra at 25 and 200 GeV [198] differ very little. Hence the statistical theory is good also for describing the spectrum at 200 GeV. The theory agrees with experiment also in the high-energy portion of the spectrum, whereas Eq. (6.13) describes the distribution only in the region $p_c<0.7$ GeV.

A consequence of the hydrodynamic theory is the presence in the spectrum of very highly energetic particles. At the same time a large number of low-energy particles arise in the interaction. The energy of the fastest particle is proportional to $E_0^{+0.93}$ [150].

Other models, for example the isobaric, can also explain the existence of a particle with energy proportional to E_0. Vinitskiy et al. [213] made a comparison with theory of the energy spectra of photons for the case when particles with energy 100-200 GeV interacted in emulsion. They found that the experimental energy distribution of photons was softer than predicted by the Landau theory, but did not contradict the Heisenberg theory [128] and the spectrum calculated by Milekhin [214].

The Heisenberg theory gives a pion spectrum that obeys the law $1/\varepsilon_\pi^2$ in the region beyond the spectral maximum. Because of limited data it is difficult to distinguish this dependence from an exponential, although many observers [172, 215, 216] report that this form of the spectrum does not contradict experiment.

In several investigated interactions with extremely high energies ($E_s\sim1400$-3800 GeV) [215], the index of the spectrum was found to be close to unity(in the region beyond the maximum). This suggests that at such high energies experiment gives evidence for an equation of state typical of the Landau theory, whereas at lower energies the Heisenberg model is preferable. However, there is not enough experimental material to justify a final conclusion. The position of the maximum of the differential spectrum of pions in the symmetric system varies somewhat with energy. Table 40 gives the position of the maximum of the distribution for various primary energies [215]. The quantity Z is here the fraction /186
of particles which have an energy less than $2m_\pi c^2$:

$$Z=\frac{N_\pi(\varepsilon_c<2m_\pi c^2)}{N_\pi(>0)}.$$

This table shows an obvious shift of the distribution toward the region of high values of the energy $\hat{\varepsilon}_c$ as the primary energy increases.

6.4. Pion-nucleon collisions

Investigations of pion-nucleon interactions done with photoemulsions at $E_0\sim7$ GeV have shown that there are two maxima in the spectra of protons in the C System [217-219]. Statistically both maxima are guaranteed in the limits of a 99% confidence level [219]. The maxima are located in the regions 0.4-0.7 and

TABLE 40. POSITION OF THE MAXIMUM OF THE MAXIMUM OF THE ENERGY DISTRIBUTION OF PIONS $\hat{\varepsilon}_c$ [215]

E_0·GeV	$\hat{\varepsilon}_c$·MeV	z	E_0·GeV	$\hat{\varepsilon}_c$·MeV	z
4.2	180	0.6	150—230	320	0.08
6.2	180	0.5	1400	210	0.25
8.7	260	0.4	2700	380	0.09
10—230	260	0.27	3800	320	0.14

1.4-1.6 GeV/c. To these two groups of nucleons correspond different values of inelasticity in the mirror coordinate system $K_M > 0.5$ and $K_M < 0.5$. A difference also shows up in the multiplicity of secondaries and the angular distributions (see Chapter 8).

In certain papers (e.g., [220]) some doubt has been expressed that two sharp maxima actually exist in the proton spectrum. In particular, it is possible that the appearance of maxima is associated with the difficulty of identifying protons in the intermediate energy region. However, the presence of a correlation between the energy of the recoil proton and other characteristics of the interaction speaks for the existence of two types of interaction independently of the degree of energy separation of the two groups of protons.

6.5. Average energy of secondary pions in the C system

By using the results of the study of pion spectra, it is possible to determine their average energy in the C system.

In the literature [162, 6] there is a very clear expression of the point of view that the average energy of secondary pions in the C system is independent of the energy of the primary particle. This conclusion is quite significant, since important consequences result from it.

If the average energy of pions in the C system $\langle \varepsilon_{\pi c} \rangle$ did not depend on the primary energy, then the inelasticity would decrease with energy: /187

$$K_c = \frac{(n_{\pi^\pm} + n_{\pi^0}) \langle \varepsilon_{\pi c} \rangle}{2\gamma_c Mc^2}. \qquad (6.14)$$

Since n_s increases with energy like $\gamma_c^{1/2}$ or slower, K_c will fall like

$$K_c \sim \frac{1}{\gamma_c^{1/2}}. \qquad (6.15)$$

Later it will be shown that $<\varepsilon_{\pi c}>$ increases with energy and K_c remains constant. Perkins [221], Ohta [222], Matsumoto [215], and Barashenkov [223] have already called attention to this. /188

TABLE 41. MAGNITUDE OF $<\varepsilon_{\pi c}>$ FOR PRIMARY PROTONS

Primary energy, GeV	Type of collision	$<\varepsilon_{\pi c}>$	Remarks	Refs.
2	$p-\bar{p}$	0.39 ± 0.02	Annihilation	[221]
2	$p-\bar{p}$	0.38 ± 0.01	»	[224]
2	$p-N$	0.35 ± 0.02	»	[45]
3	$p-n$	0.33 ± 0.06	»	[225]
5.7	$p-N$	0.35	—	[226]
6.2	$p-p$	0.38 ± 0.02	—	[227]
6.2	$p-N$	0.43 ± 0.05	—	[228]
9	$p-N$	0.42 ± 0.10	—	[229]
19	$p-N$	0.40	—	—
24	$p-C$	0.47 ± 0.04	Photons	[230]
24	$p-p$	0.52 ± 0.01		[135]
23	$p-p$	0.55 ± 0.05	Photons	[193]
25	$pp\to KK+n\pi$	0.42 ± 0.03	—	[190]
25	$pp\to YK+n\pi$	0.54 ± 0.04	—	[190]
26.7	$p-N$	0.48 ± 0.06	—	[230]
20—100	p, $\pi-C$	0.43 ± 0.05	π^0 mesons	[162]
100	p, $\pi-C$	0.47 ± 0.05	γ_c by Castagnoli	[172]
10—200	p — emul	0.42 ± 0.03	γ_c »	[231]
200	p-π — LiH	0.51 ± 0.11	—	[136]
$5\cdot10^3$	p -emul	1.3—1.7	In the center of emission sys.	[232]
10^4	p — C	2.0	Photons. Energy determined from Eq. (6.11)	[178]
$3\cdot10^4$	p — C	3.7		[178]
$3\cdot10^5$	p — air	3.0	Photon families	[139]

Tables 41 and 42 gives the results of the measurement of $<\varepsilon_{\pi c}>$ at different energies. A comparison of the data in these tables shows that there is a certain difference between the average energy of secondary pions for primary particles of different nature. In the case of primary pions $<\varepsilon_{\pi c}>$ is 25 to 30% greater than for primary protons (in the interval 4-25 GeV). The average energy of particles in the C system depends on the nature of the secondary particles much more strongly. Table 43 presents the values of the average momenta of particles /189 of different kind in the C system.

From this table it is seen that the average energy of secondary particles rapidly increases as their mass increases. The average energy of secondary pions in the C system also depends on the multiplicity. At accelerator energies it is shown that the magnitude of $<\varepsilon_{\pi c}>$ has its highest value for the minimum multiplicity n_s.

Table 44 gives some of the results of the determination of $<\varepsilon_{\pi c}>$ for various n_s.

TABLE 42. MAGNITUDE OF $\langle \varepsilon_{\pi c} \rangle$ FOR PRIMARY PIONS

Primary energy, GeV	Type of collision	$\langle \varepsilon_{\pi c} \rangle$, GeV	Remarks	Refs.
4.5	$\pi^- p$	0.45 ± 0.03	—	[233]
4.5	$\pi^- n$	0.40 ± 0.03	—	[233]
6.8	$\pi^- N$	0.52 ± 0.02	Propane chamber	[234]
6.8	$\pi^- N$	0.59 ± 0.02	"	[234]
7.5	$\pi^- N$	0.52 ± 0.02	Emulsion	[235]
7.0	$\pi^- N$	0.50 ± 0.02	—	—
7.3	$\pi^- N$	0.47 ± 0.03	Emulsion	[233]
16.2	$\pi^- p$	0.64 ± 0.02	Hydrogen chamber	[237]
17	$\pi^- p$	0.61 ± 0.02	—	[238]
17	$\pi^- p$	0.67 ± 0.02	—	[238]

TABLE 43. DEPENDENCE OF AVERAGE MOMENTA $\langle P_c \rangle$ ON THE KIND OF SECONDARIES

Energy GeV	Type of collision	Secondary particles	Momentum GeV c/c	Refs.
4.5	$\pi^- p$	π	0.39 ± 0.02	[233]
		p	0.91 ± 0.15	[233]
7.3	$\pi^- p$	π	0.42 ± 0.03	[236]
		p	0.93 ± 0.17	[236]
24	p-p	π	0.47 ± 0.03	[190]
		K^0	0.79 ± 0.01	[190]
		Y	1.89 ± 0.09	[190]

TABLE 44. DEPENDENCE OF $\langle \varepsilon_{\pi c} \rangle$ ON N_S

GeV	Type of collision	Secondary particles	$n_s=2$	$n_s=4$	$n_s=6$	$n_s=8$	$n_s=10$
16	$\pi^- p$	π^-	1.2 ± 0.09	0.63 ± 0.04	0.51 ± 0.03	0.44 ± 0.07	—
		π^+	0.86 ± 0.09	0.64 ± 0.04	0.52 ± 0.03	0.57 ± 0.07	—
24	p-p	π^-	1.35	0.88	0.77	0.61	0.38
		π^+	—	0.58	0.52	0.45	0.20

This information is still lacking in cosmic experiments.

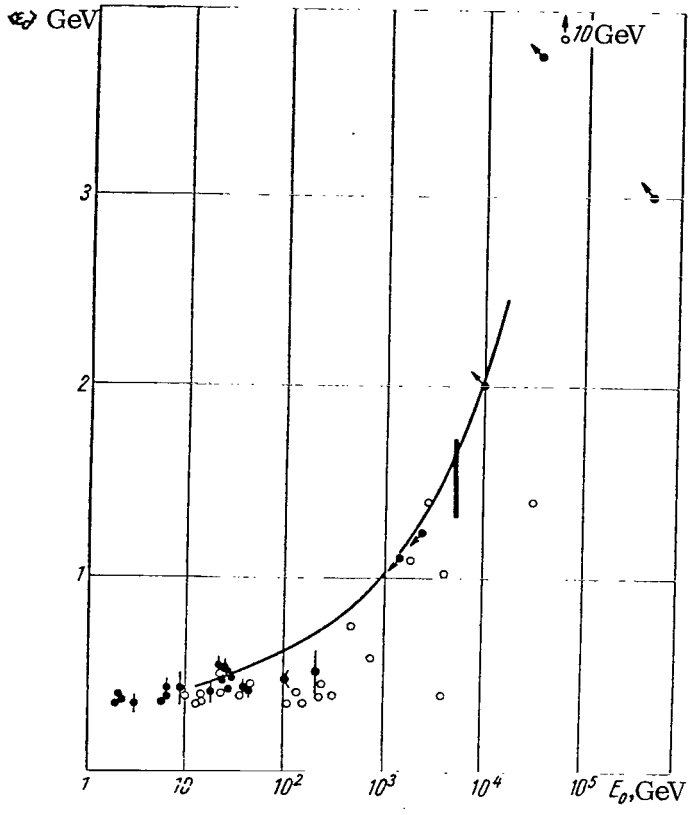

Figure 48. Dependence of the Average Energy of π-Mesons in the C System on the Energy of the Primary Nucleon:

●—Averaged Data; O—Results of Measurements of Average Energies in Individual Showers. Solid Lines Obtained from Eq. (6.14) with the Condition $K_c = 0.5$.

Figure 48 shows the results of the measurement of $<\varepsilon_{\pi c}>$ at different energies. It is seen from the figure that this quantity increases with increasing energy of the primary particle E_0. The observed increase agrees with the presumption of constant inelasticity with changing E_0

$$K = \frac{3}{2} \cdot \frac{n_s <\varepsilon_{1c}>}{2(\gamma_c - 1)} \cdot \qquad (6.16)$$

In Fig. 48 is also plotted the calculated dependence of $<\varepsilon_{\pi c}>$ on E_0 with the assumption that $K_c = 0.5$ and n_s varies according to (5.4). The physical

interpretation of the increase of $\langle \varepsilon_{\pi c} \rangle$ with energy may be different. From the point of view of the hydrodynamic treatment $\langle \varepsilon_{\pi c} \rangle$ is proportional to exp(L/2)

$(L/2)^{1/2} \gg 1$ $\left(L = 0.56 \frac{E}{mc^2} + 1.6\right)$ [239].

In the fireball model it is assumed that the average energy in the agglomerate system is independent of energy, but that the rate of agglomeration increases with increasing primary energy. Such a hypothesis was made, in particular, by Zatsepin [142] and Imaeda [6]. If the center of emission of pions moves relative /191
to the C system with Lorentz factor $\bar{\gamma}$, the pion energy in the C system

$$\langle \varepsilon_c \rangle = \langle \varepsilon_{ce} \rangle \bar{\gamma}.$$

By assumption $\langle \varepsilon_{ce} \rangle = \text{const}$, consequently (see (6.14) and (6.15)),

$$K_c \sim \frac{\bar{\gamma}}{\gamma_c^{1/2}}. \tag{6.15a}$$

Hence, in order that the inelasticity not change with energy, we must have

$$\bar{\gamma} \sim \gamma_c^{1/2}.$$

Such a dependence of $\bar{\gamma}$ on γ_c was obtained earlier by Zatsepin from the assumption of the existence of limiting momenta of pions $p_{c,cr}$ at which they still could form a single system, i.e., a fireball. If the momenta of the pions in the C system $p_c \gg p_{c,cr}$, two fireballs with Lorentz factors $\bar{\gamma} \sim \gamma_c^{1/2}$ can arise [142].

Imaeda [60] used Eq. (8.14) for a calculation of the inelasticity, determining $\bar{\gamma}$ from experimental data (see Chapter 9). It was found that even allowing for $\bar{\gamma}$, the inelasticity decreases with energy, i.e., $\bar{\gamma}$ depends on energy more weakly than $\gamma_c^{1/2}$.

Is the average energy of pions in the fireball system constant? The energy distribution of particles in a meson agglomerate system was obtained in [198]. The energies of the particles processed were measured by deflection in a magnetic field (i.e., $E_i < 12$ GeV). For asymmetric showers the motion of the symmetric system relative to the C system was taken into account. The Lorentz factor of the C system was determined from calorimeter data. The results are given in Fig. 47. The average energy of the mesons in the agglomerate system was found to equal 0.45 GeV for $E_0 \sim 200$ GeV.

In [198] the rate of motion of the agglomerate was determined from the emission symmetry condition for charged particles only. Since the neutral particles were not accounted for, it is impossible to be sure that the system found actually pertains to a special object of the fireball type. A similar criticism can also be applied to [206], where the velocity of the agglomerate was determined only for the emission symmetry of neutral mesons. The average value of the photon energy in the agglomerate system was close to 200 MeV for $E_0 \sim 10^{13}$ eV, which gives $\langle \varepsilon_{\pi^0} \rangle \sim 400$ MeV in agreement with the results at 200 GeV [198]. In this case the velocity of the agglomerate has to be assumed very large. Its Lorentz factor with respect to the C system reaches 20 to 35. The possibility is not excluded that in the selected interactions charged particles are also emitted from the common center (backwards in the C system). They compensate the momenta of the π^0-mesons in the C system, and it is not necessary to assume that the agglomerate has such a high velocity (see Chapter 9, Sources of Asymmetry); then the energy of the π^0-mesons in the agglomerate system will also increase. /192

In [232], in work done with photoemulsions at $E_0 = 5000$ GeV, the energy of pions in the center of emission system was found equal to 1.3 to 1.7 GeV.

Thus, it is not now possible to settle the question of the spectrum and average energy of pions in the fireball system. The principal obstacle to this is the impossibility of reliably establishing the presence of a fireball in individual cases and its velocity by observing only some of the secondary particles (in some experiments charged, on others neutral).

CHAPTER 7

TRANSVERSE MOMENTUM

1. Introduction

A number of reasons explain the interest in investigating the transverse component of the momenta of secondary particles.

First of all, transverse momentum is invariant under Lorentz transformations and, as a parameter of the elementary interaction process, is of particular importance in cosmic ray experiments.

Milekhin and Rozental [240] showed that transverse momenta of secondary particles are sensitive to the mechanism of their formation. It may be expected that investigation of the distributions of transverse momenta will permit elucidation of the mechanisms of production of pions and other particles and answering the question about the role of isobars and statistical processes (pionization) at super-high energies.

In the case of elastic scattering processes the transverse momentum is directly related to such highly important parameters of the collision as the four dimensional transferred momentum t (at small scattering angles $p_\perp = t^{1/2}$) [94]. In addition, the phase of the wave function of a particle undergoing elastic diffraction scattering depends on its transverse momentum [241]. From results of measurements of transverse momenta during elastic scattering it is possible to obtain information about the features of the interaction at high energy.

Several authors [242-245], using the principle of indeterminacy, have attempted to connect the transverse momentum with the region in which the interaction of particles during collision is accomplished.

The transverse momentum distribution and its average value can be obtained in any strong-interaction theory and is of great value for the comparison of experimental results with theory. From these points of view, it is expedient to have reliable information both about the distributions over transverse momentum and about its average value and its dependence on the energy and nature of the primary and secondary particles, on the emission angles of the secondary particles, as well as on other parameters of the interaction.

The distribution of transverse momenta and its average value do not change much as the primary particle energy changes, and in a narrow range of primary energies this change can be neglected. In this case the $p_\perp$ distribution can be used to determine the energy of the secondary particles in those cases when the direct energy measurement is impossible and there is only information about the particle emission angles (see Chapter 6).

2. Distribution of Transverse Momenta

2.1. Methods of determining transverse momentum

In accordance with the definition of transverse momentum $p_\perp = p\sin\theta$, it is necessary to know the total particle momentum p and its emission angle θ.

To measure the total momentum one usually uses one of the following methods, thoroughly described in Chapter 6: a) by the curvature of particle tracks in a magnetic field; b) by multiple Coulomb scattering; c) by electromagnetic cascades from γ-quanta arising in the decay of π^0-mesons; d) from the angle of divergence of the components of the pair (e^+e^-) formed by a γ-quantum from the decay of a π^0-meson; d) by the Castagnoli method—from the emission angles of secondary charged particles. The most reliable data are based on measurements of momenta of secondary particles from the curvature of tracks in a magnetic field, multiple scattering, and electromagnetic cascades from γ-quanta. /194

Determination of the emission angle of secondary particles θ requires first of all information about the direction of motion of the primary particle. In those cases when this direction is known, the minimum angle which can be determined in a Wilson chamber is of the order 10^{-2} rad, and in photoemulsions of the order 10^{-5} rad. But if the direction of the primary particle is unknown, which happens when the primary particle is neutral or when the point of origin of the shower lies outside the limits of the experimental apparatus, then the error in the emission angle of secondary particles becomes significant and is determined by the error in choosing the direction of the primary particle (see Chapter 9).

2.2. Experimental material

Of the large number of experimental cosmic ray experiments we analyzed primarily those in which there were definite data on the energy and nature both of the primary and of the secondary particles [4, 139, 154, 161, 172, 176, 216, 222, 246-250]. The energy of the primary particle was considered specified if it could be measured from the total energy of the secondary particles registered by the apparatus. To such works belong those of [216, 246, 260], which were done with the aid of a Wilson chamber in a magnetic field, in which the momenta of secondary charged particles were measured. The energy of the primary particles in these experiments was not high (less than 200 GeV).

Experiments with emulsion piles [149, 154, 222, 249-251, 259] were included in the examination when the energy of the primary particles could be estimated from the energies of the secondary charged particles measured by multiple or relative scattering.

All events with energy greater than 10^3 GeV were registered in emulsion chambers [139, 176, 252-256] or by the controlled photoemulsion method [257]. In these experiments the energy of the primary particles was determined from electromagnetic cascades from photons or with ionization calorimeters.

Usually in the study of interactions in emulsion chambers it is taken that the energy of the primary particle $E_0 = (7-10)\Sigma E_\gamma$. The coefficient 10 in such an estimate overestimates the primary energy (see Chapter 2). If we take these effects into account, which are associated with the choice of events with high inelasticities α_0, then the energy of the primary particles will be not greater than $6\Sigma E_\gamma$. Below, in the analysis of the dependence of transverse momentum on energy, use will be made of this energy estimate.

In the examined papers we selected data on the transverse momenta of particles of specific nature: neutral pions produced in electromagnetic cascades from photons or by the photons themselves; charged pions identified by the method of multiple scattering or from the sign of charge; neutral secondary particles that produce nuclear interactions.

In addition to the results of experiments with cosmic particles we examined results obtained in accelerators [209, 262-266]. These were used primarily to clarify the dependence of the transverse momenta on the mass of the secondary particles and on the energy of the primaries. Tables 45 and 46 summarize the examined experimental material.

2.3. Forms of the distributions of transverse momenta

The form of the distribution of transverse momenta has been considered in many papers, both in the region of acclerator energies [194, 244, 265, 266, 268] and at energies ~ 100 GeV [269, 270, 268] and higher than 1000 GeV. [154, 195, 268, 271]. In order to analyze the dependence of the $p_\perp$ distribution on the various parameters of the collision (on the energy and nature of the primary particles, on the nature of the secondary particles, on the multiplicity, etc.), the experimental results are best differentiated into groups that bring together events with the same or closely similar properties.

On the other hand, for quantitative estimates it is convenient to find an approximation of the experimental $p_\perp$ distributions in some suitable analytical form that is somehow related with the theories of strong interactions. Usually, the following forms of analytical expressions are analyzed [194, 240, 271, 272].

a. The Planck law describes the momentum distribution of secondary particles obtained in the Fermi-Landau theory [18, 126]:

TABLE 45. RESULTS OBTAINED IN COSMIC RAYS

Type of interaction	Method	$\langle E_0 \rangle$, GeV	$\langle P_\perp \rangle$, MeV	Nature of secondaries and means of determination	Reference
n.a.-Al	W.c.	40	310 ± 10	π^- by sign of charge	[246]
n.a.-C	W.c.	100	307 ± 26	$\pi^\pm$ by ionization and curvature in magnetic field	[172]
n.a.-C	W.c.	100	220 ± 160	$\pi^\pm$ by ionization and curvature in magnetic field	[216]
n.a.-paraffin		200	300 ± 15	π^- by sign of charge	[4]
n.a.-LiH	W.c.	250	340 ± 20	$\pi^\pm$ not identified	[260]
p-nucleus of em.	p.e.p.	200	240 ± 30	$\pi^\pm$ by ionization and scattering	[222]
n.a.-nucleus of em.	p.e.p.	500	$300 \pm ?$	$\pi^\pm$ by ionization and scattering	[248]
N-nucleus of em.	p.e.p.	600	300 ± 50	$\pi^\pm$ by ionization and scattering	[249]
p-nucleus of em.	p.e.p.	1400	316 ± 64	$\pi^\pm$ by ionization and scattering	[250]
n.a.-nucleus of em.	p.e.p.	~3000	300 ± 70	$\pi^\pm$ by ionization and scattering	[154]
n.a.-nucleus of em.	p.e.p.	~3000	306 ± 56	Photons	[251]
n.a.-light nucleus	e.c.	2000	365 ± 30	π^0 by photons	[176]
		5000	407 ± 32		
n.a.-C	c.p.e.	$5 \cdot 10^3$	320 ± 20	π^0 by photons	[257]
n.a.-C	e.c.	7.2×10^3	347 ± 73	π^0 by photons	[252]
n.a.-nucleus in air	e.c.	$4 \cdot 10^4$	300 ± 50	Photons	[253]
			490 ± 80	π^0 by photons	
n.a.-C	e.c.	9.6×10^6	450 ± 160	π^0 by photons	[255]
n.a.-nucleus in air	e.c.	$2 \cdot 10^5$	250 ± 30	Photons	[254]
			530 ± 50	π^0 by photons	
n.a.-heavy nucleus	e.c.	10^6	360 ± 700	Photons π^0 by photons	[267]

Notes: n.a.—nuclear-active particles (π, N, α);
W.c.—Wilson chamber;
p.e.p.—photoemulsion pile;
e.c.—emulsion chamber;
c.p.e.—controlled photoemulsion.

TABLE 46. RESULTS OF EXPERIMENTS IN ACCELERATORS

Type of interaction	Method	$\langle E_0 \rangle$, GeV	$\langle p_\perp \rangle$, MeV/c	Secondary particles	References
p-p	c. p. e.	3,5	111 232	Pions Nucleons	[261]
	c. p. e.	4,2	142 265	Pions Nucleons	[262]
π^--p	Hydrogen chamber	10	300 ± 20 320 ± 10 370 ± 20 470 ± 20 530 ± 30 580 ± 60	π^0 $\pi^\pm$ K^0 Λ^0 $\Sigma^\pm$ Ξ^-	[264]
π^--p	Hydrogen chamber	10	300 390 390	π K p	[155]
p-nucleus $n_s \geqslant 5$	c. p. e.	14	295 ± 16 373 ± 51 394 ± 32	π K p	[160]
p and π with nuclei of p. e.	p. e	17	200 ± 16 220 ± 44 310 ± 34	π K p	[263]
p-p	p. e.	19,8	154 217	π p	[209]
p and π (with light nuclei	W. c. and p. e.	<6 $6 \div 30$	224 ± 4 332 ± 5 306 ± 6 423 ± 9	Pions Baryons Pions Baryons	[266] (averaged data)

$$\rho(p_\parallel, p_\perp)\, d\varphi\, dp_\parallel\, dp_\perp = \frac{1}{N} \cdot \frac{p_\perp\, d\varphi\, dp_\parallel\, dp_\perp}{\left[\exp \frac{\varepsilon}{kT} - 1\right]}, \qquad (7.1)$$

where

$$\varepsilon = \sqrt{\mu^2 c^4 + p_\perp^2 c^2 + p_\parallel^2 c^2}\ ; \quad N = 4\pi (kT)^3 F(a);$$

$$F(a) = a^2 \sum_{n=1}^{\infty} \frac{\mathfrak{B}_2(n, a)}{n}\ ; \quad a = \frac{\mu c^2}{kT}\ ,$$

where $\mathfrak{K}_2$ is a Bessel function of the second kind. After integration of (7.1) over the azimuthal angles φ and the longitudinal momenta $p_\parallel$ we arrive at the $p_\perp$ distribution

$$\rho_p(p_\perp)dp_\perp = \frac{1}{F(a)}\left(\frac{\sqrt{\mu^2c^4 + p_\perp^2c^2}}{kT}\right)\left(\frac{p_\perp}{kT}\right)\times \\ \times\sum_{n=1}^{\infty}\mathfrak{K}_1\left(\frac{n\sqrt{\mu^2c^4 + p_\perp^2c^2}}{kT}\right)\frac{dp_\perp}{kT}, \tag{7.2}$$

where $\mathfrak{K}_1$ is a Bessel function. /199

The average value of the transverse momentum is

$$\langle p_\perp\rangle = \frac{\left(\frac{\pi}{2}\right)^{1/2}kT}{F(a)}\sum_{n=1}^{\infty}a^{3/2}n^{-3/2}\mathfrak{K}_{3/2}(na). \tag{7.3}$$

In the Fermi theory T in (7.2) in understood as the initial temperature of the system in a state of statistical equilibrium, whereas in the Landau theory T is the finite temperature of the system at the moment of its divergence, and the hydrodynamic velocity of the elements of the system is not taken into account.

A calculation of the three-dimensional state of disintegration of a hydrodynamic system was made by Milekhin [272]. The qualitative results are not affected by this; there arise only small quantitative corrections which need to be kept in mind at very high energies of the primary particles (greater than 10^{14} eV).

Unfortunately, the other existing theories of strong interaction do not give definite predictions about the form of the transverse momentum distribution. Therefore the agreement with the Landau theory that is observed in certain cases does not yet mean that it should be given perference.

b. A linear exponential distribution* is obtained from the Planck distribution under the condition $\varepsilon \gg kT$. If in (7.1) we neglect unity compared with $\exp(-\varepsilon/kT)$, the distribution takes the form

*According to accepted terminology, a linear exponential distribution is a distribution of the Boltzmann type, and a quadratic exponential distribution is one of the Rayleigh type. However, the second distribution is frequently called the Boltzmann distribution [266, 271]. Because of this confusion, we shall name these distributions in accordance with the degree of $p_\perp$ in the exponent (linear or quadratic).

$$\rho'(p_\parallel\ p_\perp)\,d\varphi dp_\parallel\,dp_\perp = \frac{1}{N}\,p_\perp \exp\left[-\frac{\varepsilon}{kT}\right] d\varphi dp_\parallel\,dp_\perp. \qquad (7.4)$$

Integrating this expression over φ and $p_\parallel$, we obtain:

$$\rho_L(p_\perp)\,dp_\perp = \frac{p_\perp}{p_0}\exp\left[-\frac{p_\perp}{p_0}\right] dp_\perp; \qquad (7.5)$$
$$p_0 = kT/c; \quad <p_\perp> = 2p_0.$$

c. Quadratic exponential distribution is formally obtained from (7.4) with /200
the assumption $\varepsilon \approx \mu c^2 + \frac{p_\perp^2 + p_\parallel^2}{2\mu}$, which is valid for the non-relativistic case.
It has the form

$$\rho_Q(p_\perp)\,dp_\perp = \frac{2}{p_0^2}\,p_\perp \exp\left[-\frac{p_\perp^2}{p_0^2}\right] dp_\perp; \qquad (7.6)$$
$$p_0^2 = 2kT\mu c^2,$$
$$<p_\perp> = \frac{\sqrt{\pi}}{2}\,p_0.$$

The last two forms of $p_\perp$ distribution may be considered as independent ones, not partaking of any of the thermodynamic significance included in the Planck law.

Thus, based on quantum-mechanical considerations and assuming that the probability of spatial distribution of particles inside the interaction region is described by a wave packet, Takibayev et al. [244] showed that for elastic processes the distribution of $p_\perp$ has the quadratic exponential form

$$\rho_Q(p_\perp) = \frac{1}{2<p_\perp^2>}\,p_\perp \exp\left[-\frac{p_\perp^2}{2<p_\perp^2>}\right]. \qquad (7.7)$$

In this case it is possible to find the rms size of the interaction region (in the plane perpendicular to the direction of motion of the colliding particles):

$$<r^2>^{1/2} = \frac{\hbar}{2}<p_\perp^2>^{-1/2}. \qquad (7.8)$$

2.4. Differential distribution of transverse momenta

Examples of the differential experimental distributions of transverse momenta of secondary pions are shown in Fig. 49 for three energy ranges of the primary particles.

In order to check which of the above described analytical expressions best describes the experiment, we shall present a graphical analysis of the xx distributions. /201

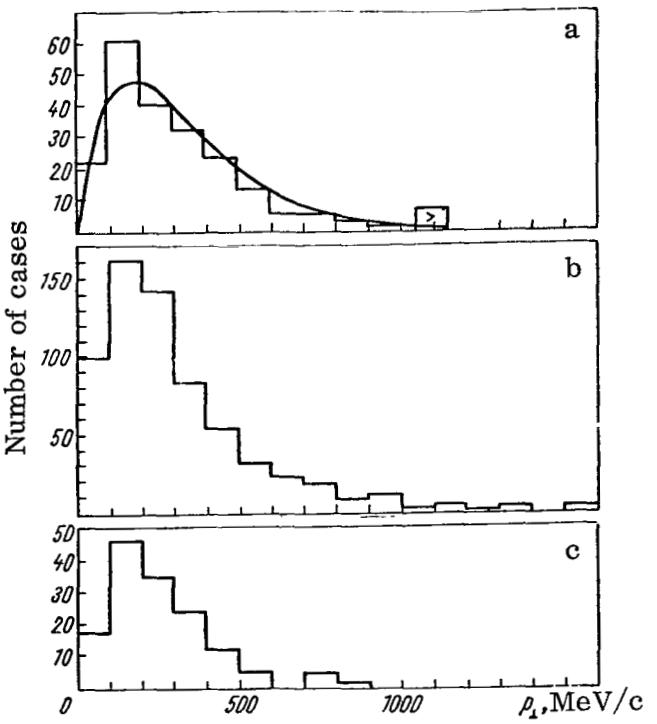

Figure 49. Differential Distributions of Transverse Momenta of Secondary Pions for Three Energy Ranges of Primary Particles:

a—$E_0 > 10^3$ GeV, $\langle p_\perp \rangle_{\pi^\pm, 0} = (370 \pm 6)$ MeV/c [271];

b—$\langle E_0 \rangle = 40$ GeV, $\langle p_\perp \rangle_{\pi^\pm} = (310 \pm 10)$ MeV/c [246];

c—$E_0 = 25$ GeV, $\langle p_\perp \rangle_{\pi^\pm} = (290 \pm 14)$ MeV/c [265].

Consider the integral distributions of transverse momenta. For the linear exponential form we have $F(>p_\perp) = \int_{p_\perp}^{\infty} \rho_\pi(p_\perp) dp_\perp \approx e^{-p_\perp/p_0}$, and for the quadratic exponential distribution, $F(>p_\perp) dp_\perp = \int_{p_\perp}^{\infty} \rho_k(p_\perp) dp_\perp = e^{-p_\perp^2/p_0^2}$. The linear /203

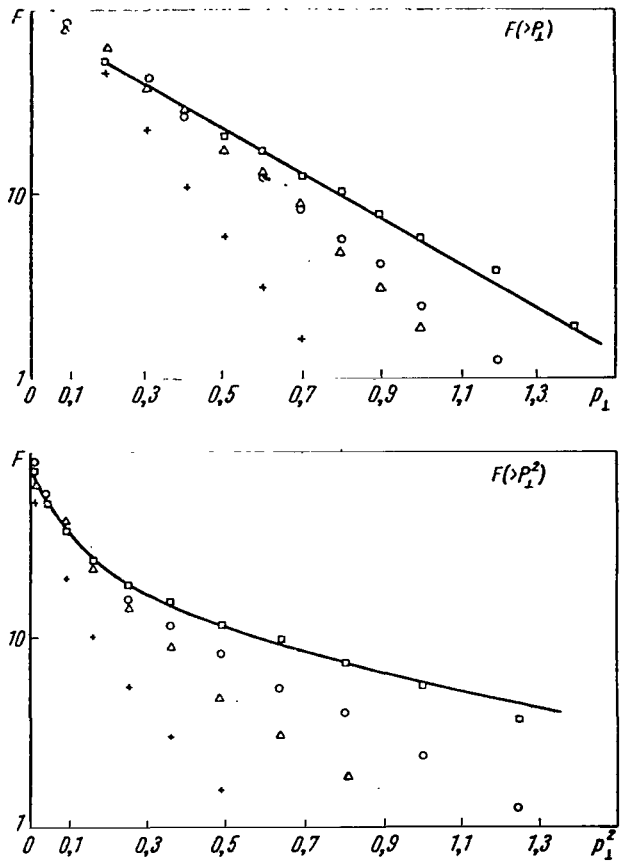

Figure 50. Integral Distributions of Transverse Momenta p of Secondary Pions:

+—$E_0<6$ GeV [266]; △ – $6<E_0<30$ GeV [266]; O—$E_0>10^3$ GeV [271]; □ – $E_0\sim10^6$ GeV [268]; —— —Calculated According to the Landau Theory with Allowance for the Hydrodynamic Velocity of Dispersal of the System $E_0=10^6$ GeV, $T=m_\pi c^2$.

exponential distribution is given by a straight line in coordinates $\lg F(>p_\perp)$ with 10% accuracy, because of the logarithmic term of the form $\log\left(\frac{p_\perp}{p_0}+1\right)$, and the quadratic exponential form by a straight line in coordinates $\log F(>p_\perp^2)$. In Fig. 50 are given the experimental $p_\perp$ distributions for secondary pions in these two representations. The figure caption cites the reference used in constructing the curves.

The results of calculations based on hydrodynamic theory, taken from Milekhin and Rozental [240], are indicated in the figures by solid lines. The theoretical curves pertain to a primary energy $E_0 = 10^{15}$ eV and temperature $T = m_\pi c^2$.

The integral $p_\perp$ distributions for pions obtained experimentally fall well on a straight line in coordinates $\lg F(>p_\perp)$. The experimental results represented in the form $\log F(>p_\perp^2)$ do not give straight lines.

The form of the distribution is practically maintained over the whole range of considered energies (from 6 to 10^6 GeV). Some change in the slope of the integral $p_\perp$ distributions with a change in energy of the primary particles is evidence for a change in the parameters entering into the distribution: the average and most probable values of $p_\perp$.

A similar analysis of $p_\perp$ distributions for secondary pions was made by Fowler and Perkins [268], both in the region of moderate energies 25-300 GeV, and at energies of 10^3 to 10^6 GeV. They concluded that for transverse momenta in the interval 0.1 to 1.5 GeV/c the results are well described by the linear exponential distribution at any primary particle energy (Fig. 51, a, b).

/204

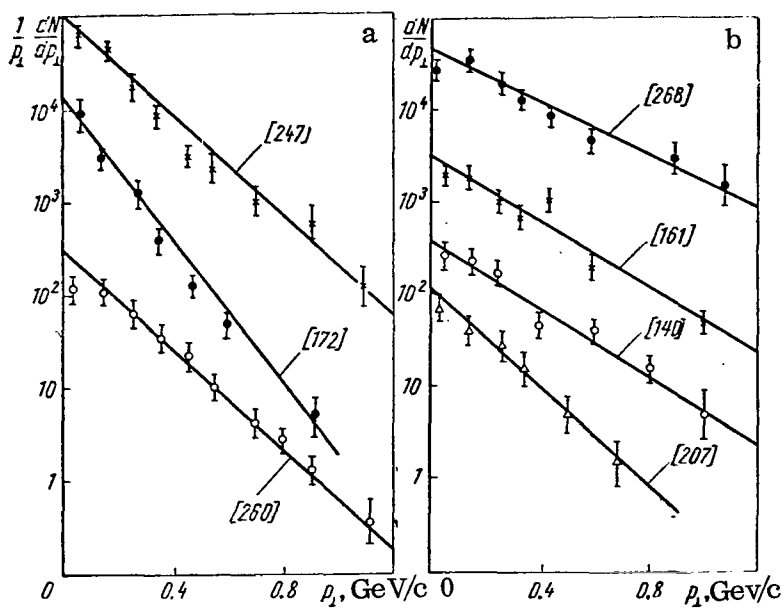

Figure 51. Differential Distributions of Transverse Momenta Obtained in Different Investigations:

a—For Secondary Pions; b—For Photons.

A similar result was obtained by Imaeda et al. [271], who analyzed all three $p_\perp$ distributions considered in the preceding subsection by the method of maximum probability. These authors chose from among the interactions with primary energies greater than 1000 GeV available in world statistics, the transverse momenta of strictly identified secondary particles. The differential distribution of $p_\perp$ obtained by this means is shown in Fig. 49, a, from which it is seen that within the limits of experimental error it agrees with the corresponding curve calculated on the basis of hydrodynamic theory (smooth curve).

The squares in Fig. 50 represent the $p_\perp$ distribution for one case, arising from a primary particle with energy $E_0 \sim 10^6$ GeV and registered in an emulsion chamber by Fowler et al. [268]. The shower contains about 150 photons. The distribution for this shower coincides with the distribution obtained from the Landau theory with allowance for the hydrodynamic velocity of dispersal of the particles (solid curve). Thus, at super-high energies of primary particles the experimental results on $p_\perp$ distributions for pions do not contradict hydrodynamic theory. /205

2.5. Distributions of $p_\perp$ for different particles

A dependence of the form of distributions of transverse momenta on the nature of the secondary particles in the region of moderate energies was observed by Friedlander [266, 273]. The maximum probability method of analyzing the distributions of transverse momenta of secondary pions, kaons, protons, and hypersons showed that the $p_\perp$ distribution for secondary baryons is better described by a quadratic exponential dependence (see Fig. 52). The integral distribution for baryons gives a straight line in coordinates $p_\perp^2$.

Thus a difference is observed in the $p_\perp$ distributions for pions and baryons. The first is described by a linear exponential and the second by a quadratic exponential function. The difference appears also in the average characteristics of these distributions, which is illustrated by Table 47 for two intervals of primary particle energy.

TABLE 47. AVERAGE VALUES OF TRANSVERSE MOMENTA FOR PIONS AND BARYONS

E_0, GeV	Nature of secondary particles	Number of cases	$\langle p_\perp \rangle$, MeV/c	$\sigma_{p_\perp}$*, MeV/c	$\sigma_{p_\perp}/\langle p_\perp \rangle$	Reference
<6	Pions	1241	224 ± 4	151 ± 3	0.675 ± 0.017	[130, 262, 274]
	Baryons	1268	332 ± 5	177 ± 4	0.533 ± 0.017	[262, 274]
6÷30	Pions	1251	306 ± 6	222 ± 4	0.726 ± 0.019	[228, 238, 275—280]
	Baryons	665	423 ± 9	238 ± 6	0.526 ± 0.022	[155, 277, [238, 263, 228, 282]

*$\sigma_{p_\perp}$ — standard deviation.

The observed difference between the distributions of transverse momenta of pions and baryons can be treated in two ways. /207

The first explanation, associated with the recognition of the existence of two different kinds of $p_\perp$ distribution (linear and quadratic), must entail the assertion that pions and baryons arise as the result of different processes.

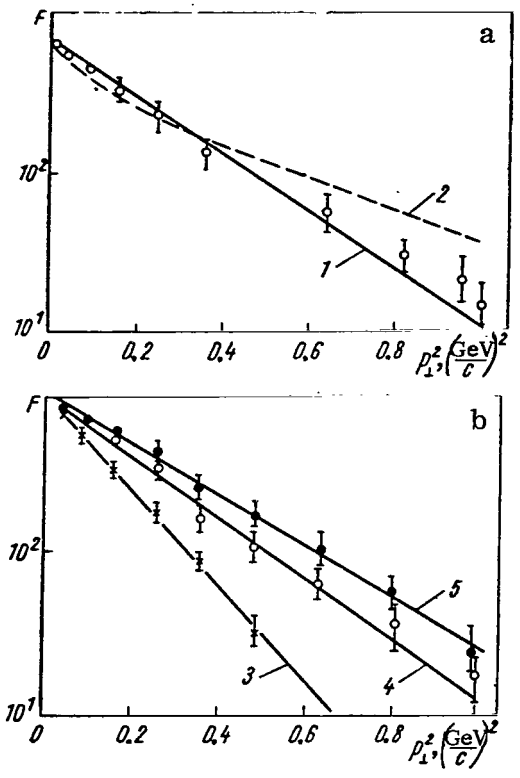

Figure 52. Integral Distribution o. Secondary Baryons with Respect to Transverse Momentum:

a—For Secondary Baryons Formed by Primary Particles with Energies from 6 to 30 GeV; 1—Quadratic Exponential Distribution (7.7); 2—Linear Exponential Distribution (7.5); b—For Secondary Nucleons from Primary Particles; 3—With Energy $E_0<6$ GeV; 4—The Same for Particles with Energy $6<E_0<30$ GeV; 5—The Same for Secondary Hypersons Formed by Particles With Energies From 6 to 30 GeV.

The second approach, proposed by Friedlander [266], is based on the assumption that the quadratic exponential form of the distribution, which describes the $p_\perp$ distribution for baryons, is the basic form. It is acceptable for the description of the distribution of secondary particles of any kind, including pions. Then, since the $p_\perp$ distribution for pions in cordinates $\log F(>p_\perp^2)$ does not fall one one straight line, Friedlander proposes to represent it in the form of a superposition of two lines having different slopes σ_1 and σ_2. In this case one can speak of the existence of two components in the $p_\perp$ distribution for pions. These components must have different sources. If the fraction of one of these components with respect to the other is α, the transverse momentum distribution law for pions will have the form

$$p_K^\pi(p_\perp)\,dp_\perp = p_\perp\,dp_\perp\left\{\frac{1-\alpha}{\sigma_1^2}\exp\left[-\frac{p_\perp^2}{2\sigma_1^2}\right]+\right.$$
$$\left.+\frac{\alpha}{\sigma_2^2}\exp\left[-\frac{p_\perp^2}{2\sigma_2^2}\right]\right\}, \qquad (7.9)$$

and the corresponding integral distribution

$$F^\pi(>p_\perp) = (1-\alpha)\exp\left[-\frac{p_\perp^2}{2\sigma_1^2}\right]+$$
$$+\alpha\exp\left[-\frac{p_\perp^2}{2\sigma_2^2}\right]. \qquad (7.10)$$

If there really are two components in the distribution of the transverse momenta of pions, then the question arises whether both components are present in each act of production, or there are two different processes for the creation of pions.

The same author has shown [273] that there is a better basis for accepting the existence of two different processes for pion production. /208

It is extremely likely that the pattern sketched here really takes place. However, it is not clear to us how well based the initial assumption about the quadratic exponential distribution being the fundamental one is. May not this function be a convenient, but accidental mathematical approximation of some unknown true law?

2.6. Size of the interaction region

In a number of accelerator experiments [238, 244, 245] it has been shown that the distribution of transverse momenta of elastically scattered protons coincides with the distribution for protons arising in inelastic processes. This fact, interesting enough in itself, together with the quadratic exponential form of the $p_\perp$ distribution established for protons, permits us to find the rms dimension of the interaction region not only in the case of elastic but also of inelastic processes [245]. Using (7.8), we find $\langle r^2\rangle^{1/} \sim 0.6$–$0.4$ F for $\langle p_\perp\rangle =$ (330–420) MeV/c.

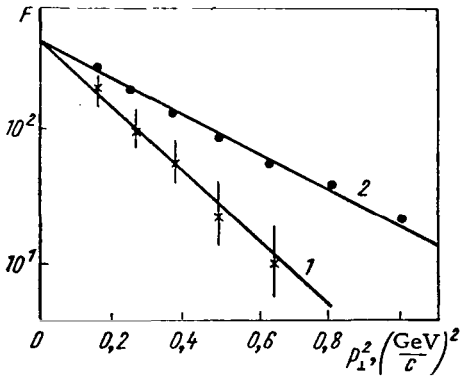

Figure 53. Integral $p_\perp$ Distribution for Pions Formed by Protons (1) and Pions (2); $6<E_0<30$ GeV.

2.7. Dependence of the transverse momentum distribution on the nature of the primary particles

/209

The distribution of the transverse momenta of secondary pions is sensitive to the nature of the primary particles. Figure 53 shows the $p_\perp$ distributions for pions arising from pions and from protons at one and the same energy for the primary particles. The difference in the slopes of the straight lines joining the experimental points is evidence for the dependence of the $p_\perp$ distribution on the nature of the primary particle.

The same tendency to a harder spectrum of secondary pions arising from "primary" pions is also observed in an examination of momenta spectra (Chapter 6).

3. Dependence of the Average Magnitudes of Transverse Momentum on the Energy and Nature of the Colliding Particles

3.1. Dependence of the average value of transverse momentum on energy

In the first approximation it seems that the average value of transverse momentum $p_\perp$ is independent of the energy of the primary particle. Existing experimental data show a very large scatter of the average values at nearby values of the energies of the primary particles. However, a discriminating approach to the available results as manifested in a strict selection of events

with identified secondary particles and with reliable determination of the primary energy, leads us to the conclusion that there is a weak dependence of the average transverse momentum of pions on the energy of the primary particle. This result was obtained on examination of extensive experimental data, beginning with accelerator energies and ending with the highest energies encountered in cosmic rays.

Table 45 and Fig. 54 show the experimental results. The straight line in Fig. 54 represents the dependence of $p_\perp$ on E_0 obtained on the basis of hydrodynamic theory.

In the region of low energies of the primary particles from 3.5 to 10 GeV, the average transverse momentum increases sharply (approximately threefold). In the next interval of energy (from 10 to 10^6 GeV), an extent of five orders of magnitude, the average value of transverse momentum increases by only a factor of 2. /210

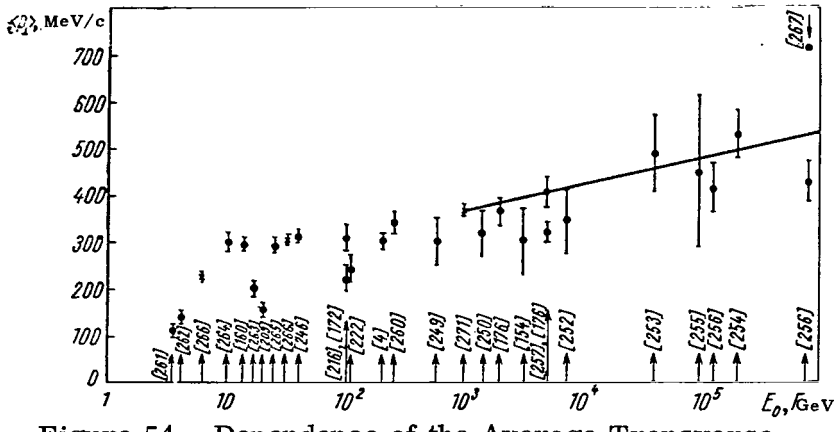

Figure 54. Dependence of the Average Transverse Momenta of Secondary Pions on the Energy of the Primary Particle:

$\bar{*}$—Results of the Averaging of the Transverse Momenta of Reliably Identified Pions from a Large Number of Experiments with Nearby Values of the Energies of the Primary Particles. The Straight Line is the Result of the Calculation Based on the Hydrodynamic Theory.

3.2. The average value of transverse momentum for particles of different kind

The dependence of $p_\perp$ on the nature of the secondary particles is well established in the region of accelerator energies.

Tables 46 and 47 give the results of measurement of $<p_\perp>$ for particles of different mass. A large amount of statistical material shows that as the mass of the secondary particle increases, so does its average transverse momentum.

In cosmic rays similar data have been obtained with a lower degree of reliability. In [172], at primary particle energies of about 100 GeV, it was found with the aid of a Wilson chamber in a magnetic field that the transverse momenta for pions (307 ± 26) MeV/c and for kaons (310 ± 44) MeV/c are practically identical. Kim [154], working with photoemulsions and at energies /211
$\sim 10^3$ GeV, found that $\langle p_\perp \rangle_\pi = (300 \pm 7)$ MeV/c, $\langle p_\perp \rangle_K = (330 \pm 10)$ MeV/c, and $\langle p_\perp \rangle_p = (350 \pm 11)$ MeV/c. The average values of the transverse momenta differ, but within the limits of the statistical accuracy of the measurements. In this work one hyperon with transverse momentum $p_\perp = 1300$ MeV/c was registered.

In [149, 161], Australian and Bristol groups of physicists, using photoemulsions, determined the transverse momenta of secondary neutral particles. In these cases the energy of the secondaries was estimated by the Castangnoli method from the emission angles of third-generation particles. The average values of the transverse momenta for the neutral particles turned out to be very high and different (1400 ± 200) and 2065 ± 900) MeV/c. In part, the anomalously high values could have been obtained as a consequence of the use of the Castagnoli method for determining the energy (see Chapter 2).

It should be mentioned that the hydrodynamic theory of Landau predicts a considerable increase in transverse momentum with the mass of the particles. Table 48 gives the average values of the transverse momenta of secondary particles of various kinds calculated on the basis of hydrodynamic theory and taken from work on cosmic rays [149, 154, 161].

TABLE 48. AVERAGE VALUES $\langle p_\perp \rangle$, MeV/c, FOR $E_0 \geq 1000$ GeV

π	K	p	n	Reference
370 ± 50	—	1465 ± 320	2065 ± 900	[149]
300 ± 70	330 ± 100	350 ± 110	—	[154]
—	—	—	1400 ± 200	[161]
360	—	900	—	Calulation [283]

The statistical accuracy and possible statistical errors of measurement do not as yet permit making definite conclusions about the transverse momenta of heavy secondary particles at super-high energies.

3.3. Anomalous values of the transverse momenta of secondary particles

Lal et al. [22] observed events with anomalously low values of transverse momentum in a total absorption spectrometer. The primary particles in these cases were pions, identified with the aid of a gaseous Cherenkov counter. The average energy of thepions was 30 GeV. The interactions were registered in a multi-plate Wilson chamber. The transverse momenta of photons were measured by the electromagnetic cascades in lead plates. A group of events with

low multiplicity of charged particles could be isolated, in which $\langle p_\perp \rangle_\gamma = (79 \pm 9)$ MeV/c, which corresponds to $\langle p_\perp \rangle_{\pi^0} \approx 160$ MeV/c.

The authors supposed that in these cases there was a peripheral collision of a pion with a target nucleon.

Anomalously high values of transverse momentum of photons are observed in cosmic ray experiments with photoemulsion piles and chambers [253, 254].

Kazuno [253] investigated a nuclear interaction arising from a primary particle with energy $\sim 10^5$ GeV in collision with the nucleus of an air atom and containing 65 charged particles and 34 electromagnetic cascades. The distribution of the transverse momenta of secondary π^0-mesons was observed extending to values of ~ 2 GeV/c. A photon with $p_\perp = (2.9 \pm {}^{2.9}_{1.5})$ GeV/c was registered.

The study of nuclear interactions of superhigh energy in an emulsion chamber has shown the possibility of the origination of heavy formations having excessively high transverse momenta. Nishimura [254] reports that such a super-heavy agglomerate, produced in a nuclear interaction with primary energy of 10^5 GeV, has a total transverse momentum relative to the primary surviving nucleon equal to ~ 4 GeV/c. Evidently, the origination of photons (or π^0-mesons) with anomalously high values of transverse momentum is connected with the formation in cosmic showers of particles with high mass that obtain a high transverse momentum when created.

3.4. Dependence of average transverse momenta of particles on their emission angle /213

The dependence of the transverse momenta on emission angle of secondary particles was investigated both in accelerators [130, 284-286] and in cosmic rays [148, 287-289].

A large amount of statistical material was used by Boos et al. [285] — 1536 pions formed in π-N interactions at an energy of 7.5 GeV. They decided that the observed weak dependence of $p_\perp$ on angle θ can be explained by the conservation law for momentum. There exists a certain limiting angle θ_1, depending on the energy of the primary particle, beginning with which the conditions imposed by the conservation laws will not come into play.

Thus, in the region of cosmic energies it may be assumed that $p_\perp$ should remain practically invariant with angle for $\theta > 30'$ on account of the limitations coming out of the momentum conservation law. Investigations of the function $p_\perp(\theta)$ at primary energies E_0 not in excess of 300 GeV are in agreement with the conclusion that the relation that exists is completely determined by the momentum conservation law [287].

In the region of super-high energies greater than 10^3 GeV, Fowler et al. [268] obtained data on the change of the transverse momenta of photons as a function of their emission angles and detected a tendency toward a decrease in

TABLE 49. DEPENDENCE OF θ_1 ON E_0

E_0, GeV	7.5	20	100	300	1000
θ_1	7°	2°30′	31′	10′	3′

$p_\perp$ in the region of the smallest angles ($\theta < 10^{-3}$ rad), which, evidently, is also connected with the conservation laws.

3.5. Conclusion

/214

The analysis we have made shows that the distributions of transverse momenta are due to the mechanism of production of particles in nuclear interactions. At the same time the average values of transverse momentum change slightly with change in energy and emission angle of the secondary particles and hence can be utilized for the determination of the energies of the secondary particles. The dependence of the average value of transverse momentum on the mass of the secondary particles is the strongest of all. This circumstance is of important in the region of very high energies, where the possibility of particle identification is limited and the proportion of heavy particles among the secondaries can be large. The considerable lack of coordination in the experimental results on transverse momenta in the region of high energy is probably a consequence of this dependence.

CHAPTER 8

COEFFICIENTS OF ELASTICITY

1. Definitions

In the investigation of the interactions of cosmic nuclear-active particles with nucleons all events in which electron-nuclear cascades arise are considered to be inelastic.

Thus, the characteristic feature of an inelastic interaction is the formation of new particles—pions, kaons, nucleon-antinucleon pairs, etc. From this point of view the splitting of an atomic nucleus is a quasi-elastic process, to use the terminology introduced for interaction cross sections (Chapter 4).

As a measure of the degree of inelasticity we have the coefficient of inelasticity K, which is defined as the fraction of the total energy of the colliding particles that is expended in the formation of newly created particles in a single interaction act:

$$K = \frac{\Sigma \varepsilon_i}{E_0}. \qquad (8.1)$$

Here ε_i are the energies of the secondary newly created particles in the L system, and E_0 is the total energy of the colliding particles. /215

In the case of a symmetrical collision K is invariant under Lorentz transformations (see Chapter 2):

$$K = K_C = K_M,$$

where K_C and K_M are the inelasticities in the C and mirror systems respectively. The inelasticity in the mirror system at high energies ($E_0 \gg mc^2$) is equal to the fraction of the energy of the target nucleon that is lost in the formation of new particles. Hence if the primary and target nucleons expend their energy unequally, $K_M \neq K$, and the collision will not be symmetrical. If there is such a pattern of interaction, nucleon-nucleon collisions are symmetric only on the average.

There are two approaches to determining K. The first depends on Eq. (8.1) and the second on a measurement of the recoil nucleon.

Let us consider the inelasticity in the mirror system and express it in terms of the parameters of particles in the L system:

$$K_M = \frac{\gamma_0 \Sigma (\varepsilon_i - p_i c \cos \theta_i)}{m_2 \gamma_0}, \tag{8.2}$$

where m_2 is the mass of the target, and γ_0 is the Lorentz factor of the transition from the L system to the mirror system. A very important peculiarity of (8.2) is its independence on the Lorentz factor γ_0 and consequently on the energy of the primary particle. For the nucleon-nucleon collision we have

$$<K> = <K_M>,$$

where K and K_M are the average inelasticities in the L and M systems. If the energy of the two colliding particles after interaction is known, the inelasticity can be determined as the difference between the initial and final energies. The situation is simplified by the fact that in the L system the energy of the recoil nucleon is small, whereas it is the energy of the primary nucleon that is small in the M system. Then

$$K' \approx \frac{E_0 - E_1}{E_0} = 1 - \beta_1, \tag{8.3}$$

where β_1 is the coefficient of inelasticity of the primary nucleon, i.e., the fraction of energy which it retains after collision. The quantity β_1 is sometimes called the conservation parameter. In the mirror system /216

$$K'_M = \frac{m_2 c^2 - E_2 + p_2 c \cos \theta_2}{m_2} = 1 - \beta_2 \tag{8.4}$$

(m_2 is the mass of the target, β_2 is the inelasticity of the target). Thus, K' characterizes the energy loss of the primary particle and K'_M, of the target particle.

In the case of the nucleon-nucleus collision Eq. (8.4) cannot be used, since it is difficult to identify the recoil nucleon. Equation (8.3) includes the energy of quasi-elastic processes, but Eqs. (8.1) and (8.2) do not. In the range of

cosmic energies the difference is not large, but at 10 GeV it can amount to 10%. For a more detailed description of the process, people use partial coefficients of inelasticity, which take into account the distribution of energy among the various secondary particles. We shall symbolize the partial coefficients by the letter α with different subscripts: α_0—the fraction of energy expended in the formation of photons (principally via the decay of a π^0-meson); $\alpha_\pm$—the fraction of the energy of charged pions; α_K—the fraction of energy of kaons; $\alpha_p \approx \beta_p$—the fraction of energy of protons; $\alpha_n \approx \beta_n$—the fraction of energy of neutrons; α_{si}—the fraction of energy taken by strongly ionizing particles. In the case of the statistical mechanism of creation of particles definite relations exist between the partial coefficients:

$$\langle \alpha_0 \rangle = \frac{1}{2} \langle \alpha_\pm \rangle; \tag{8.5}$$

$$\langle \alpha_{K^0} \rangle = \langle \alpha_{K^\pm} \rangle. \tag{8.6}$$

It should be emphasized that these relations are valid only on the average. In individual cases considerable fluctuations in the ratios $\alpha_0/\alpha_\pm$ and $\alpha_{K^0}/\alpha_{K^\pm}$ are possible.

Sometimes as a result of collision a nucleon is excited to the state of an isobar or hyperon. In the final state after the passage of sufficient time (which in the case of an isobar is close to nuclear) we have again to do with the nucleon and mesons. However, in order to emphasize the specifics of this process, the coefficient K is divided into two parts: $K = K_1 + K_2$ [142, 290, 291]. /217

The term K_1 describes that part of the energy that is transferred to secondary particles as the result of the process of multiple production of the statistical type. Since the specific mechanism of such processes is not clear, they are frequently labeled "ionization," understanding by this the collection of all processes of multiple generation of relatively low-energy particles.

The second part (K_2) is associated with the formation of mesons from the decay of isobars. These pions may have a very high energy, if the isobar is sufficiently heavy. Pions from the decay of hyperons of high energy appear far from the point of interaction and in practice are not included in the coefficient of inelasticity.

A somewhat different definition of the coefficient of inelasticity is introduced in the study of the interaction of pions with nucleons and nuclei. In this case the secondary particles are indistinguishable and we cannot say which of the secondary pions is the surviving primary. However, on the basis of the conclusions of Chapter 6 about the presence of an energetically isolated secondary pion in the π-N collision, we define the coefficient of inelasticity for pions as the fraction of the primary energy taken by all secondary pions except the one of highest energy.

The majority of theoretical models of interaction do not give precise predictions relative to the magnitude of K.

In peripheral models, the inelasticity depends on which Feynman diagram is presumed to describe the process. In certain cases it is small, in others it increases with energy.

In the isobaric model K depends on what the mass of the created isobar is supposed to be. Heavy isobars with mass M can indeed explain high inelasticities. The isobar 3/2, 3/2 (M = 1236 MeV) decays to give a pion that bears away on the average about 20% of the energy of the isobar.

In the hydrodynamic theory of multiple production, the collision process is completely inelastic. However, in a number of cases regeneration of a nucleon of high energy is possible, and from the point of view of determining K from the formulas (8.1)-(8.4) there is some elasticity. The average inelasticity is then equal to 0.87 [19].

Sometimes it is assumed that the interaction process goes according to the Landau theory; however nucleons expend only a portion of their energy in the creation of the excited system [291]. Such assumptions were made under the pressure of experiment and there is no theory involved in them. /218

2. Measurement of Inelasticity

The experimental determination of inelasticity is based on Eqs. (8.1)-(8.4). Equations (8.1) and (8.2) indicate that in each individual case it is necessary to measure the energy of all particles, both charged and neutral, but this cannot be done yet.

Use of Eq. (8.4) simplifies the problem. In this case it is necessary to find the recoil nucleon. It rather frequently has moderate energy, which can be determined by scattering. This approach, which is good for nucleon-nucleon collisions, leads directly to the magnitude of the mirror inelasticity. In rare cases it is possible to estimate the energy of a nucleon emitted in the forward direction at a small angle and to obtain the laboratory inelasticity K.

In all other cases one studies the partial coefficients α.

a. Measurement of the coefficient $\alpha_{\pm} + \alpha_{K^{\pm}}$ and α_0. —With a Wilson chamber in a magnetic field it is possible to measure particles with energy to 30-40 GeV. This means that for a primary energy of 100 GeV one can determine the momenta of all charged particles of the outer cone and a great number of those of the inner cone. At higher energies the number of unmeasurable particles increases. In a nucleon-nucleon collision the surviving primary nucleon will, as a rule, have a very high momentum. However, if the primary energy is known from ionization calorimeter data, for example, then the unmeasureability of the surviving nucleon cannot be an obstacle in the determination of α.

If the energies of all newly created particles can be measured, then it is possible to obtain both the laboratory and the mirror partial coefficients $\alpha_{\pm}+\alpha_{K^{\pm}}$.

In the mirror system /219

$$(\alpha_{\pm}+\alpha_{K\pm})_M=\frac{\sum_{i=1}^{n_c}(\varepsilon_i-p_ic\cos\theta_i)}{m_2c^2}=\alpha_M. \tag{8.7}$$

In the laboratory system

$$\alpha_{\pm}+\alpha_{K^{\pm}}=\frac{\sum_{i=1}^{n_c}\varepsilon_i}{E_0}. \tag{8.8}$$

If the shower has only one unmeasureable particle (besides the nucleon), it is already impossible to determine the inelasticity in the L system, since the unmeasured particle might make the principal contribution to $\Sigma\varepsilon_i$. This particle gives the smallest contribution to α_M, and errors in the determination of α_M can arise if the geometry of the Wilson chamber precludes the observation of particles at large angles.

Obviously, it is convenient to use the Wilson chamber also for the determination of $\alpha_{\pm c}+\alpha_{K^{\pm}c}$ (in the C system).

This quantity in the case of the N-N collision is

$$\alpha_{\pm c}+\alpha_{K^{\pm}c}=\frac{\sum_{i=1}^{n_c}(\varepsilon_i-p_i\,c_i\cos\theta_i)}{2m_pc^2}. \tag{8.9}$$

It should be noted that the inelasticity in the C system does not depend on the determination of the primary energy.

In all these cases it is assumed that there are only pions among the secondary particles. Actually, about 20% of these particles are kaons. Hence, a small indeterminacy arises in the determination of $\alpha_{\pm}$ associated with the fact that the momentum and angular distribution of kaons is different from those of pions.

In measurements in photoemulsions and in Wilson chambers without magnetic field the momenta of the secondary particles are unknown. Then one uses the

constancy of the average transverse momentum, its weak dependence on the particle emission angle and on energy.

Since only the sum of the energies of the secondary particles is of value for the determination of inelasticity, the conditions for the applicability of the method /220
are well fulfilled (see Chapter 6). In this case

$$\alpha_{\pm} + \alpha_{K^{\pm}} = \frac{c\sum_{i=1}^{n_c}(p_{\perp})_i \csc\theta_i}{E_0} = \frac{\langle p_{\perp}\rangle c\sum_{i=1}^{n_c}\csc\theta_i}{E_0}. \qquad (8.10)$$

The quantity $\langle p_{\perp}\rangle$ can be taken from Tables 45 and 46.

It is also possible to use the average energy in the C system $\langle\varepsilon_c\rangle$ for the determination of inelasticity (see Chapter 6). In this case

$$\alpha_{\pm c} + \alpha_{K^{\pm}c} = \frac{n_c\langle\varepsilon_c\rangle}{E_{0c}}.$$

Here E_{0C} is the total energy of the colliding particles in the C system, and n_c is the number of newly created charged particles. In calculating α it is again assumed that $\langle\varepsilon_c\rangle$ is the same for pions and kaons. On the average, it is possible to account for the difference by assuming that the fraction of kaons is 20% (see Chapter 5). This method depends strongly on errors in determining the energy of the primary particle. When the energy of the primary particle is known, one may use the data of Tables 39-42 for the determination of α.

The partial coefficient α_0 is determined from the known energy of the primary particle and the total energy of the photons arising in the interaction. The latter is measured from electromagnetic cascades (see Chapter 6, Section 1).

b. Distribution of total inelasticity. —The measurement of the distribution of total inelasticity in an accelerator is usually based on the study of the recoil nucleon. This opens up interesting possibilities.

In the case of the pion-nucleon collision, by transforming the momentum and angle of the observed recoil proton to the mirror system we find the parameters of the collision of the proton with a free π-meson corresponding to a primary energy of the proton:

$$\frac{m_p}{m_\pi}E_0 \sim 6E_0$$

(E_0 is the energy of the primary pion in the L system). If there exists a peripheral collision of the proton with an "almost real" pion in the pion cloud of the target nucleon, then at proton energies ~120 GeV the parameters of this interaction will be the same as for the pion-nucleon collision in the mirror system at 20 GeV. The distribution of total inelasticity for the nucleon in such a collision is obtained directly from the spectrum of recoil nucleons in the mirror system (Fig. 55). /221

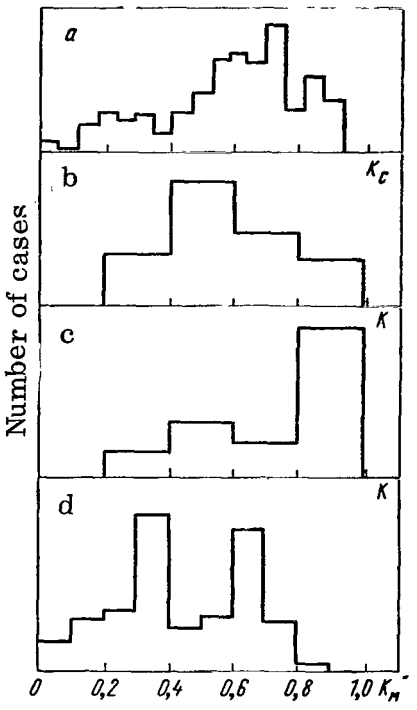

Figure 55. Distribution of Total Coefficients of Inelasticity:

a—In p-p Collision for 25 GeV [190]; b—In Collisions of Neutral Nuclear-Active Particles with Energy of the Order of 400 GeV with Carbon Nuclei; c—In Collisions of Neutral-Active Particles $E_0 \sim$ 400 GeV) with Iron Nuclei; d—In the Mirror Coordinate System for π-p Collisions [235].

The distribution of total inelasticity K_M, which has two maxima at $K_M = 0.3$ and $K_M = 0.7$, was obtained by this method [219, 235]. Hence, all events can be divided into two groups with $K_M < 0.5$ and $K_M > 0.5$. Cases of high multiplicity are found mainly in the second group, and for small multiplicity, values with $K_M > 0,5$ and $K_M < 0.5$ are encountered. A sharp asymmetry in pion emission is observed in the group with $K_M < 0,5$ In the C system, 3.8 times as many pions are emitted forwards as backwards. There is no asymmetry in the $K_M < 0.5$ group. The basic properties of these two types of event are given in Table 50.

The authors assume that events with $K_M > 0.5$ are well described by the statistical theory developed by Barashenkov [292]. Some of the cases with $K_M < 0.5$ can probably be explained by the creation of isobars.

In the proton-proton collision the spectrum of nucleons in the C system does not give the possibility of establishing the distribution of inelasticity. However, for one special case, when events involving the creation of hyperons are chosen, their energy spectrum in the C system permits finding the distribution of K_C, since in the majority of cases only one of the nucleons converts to a hyperon. /222

The energy distribution of hyperons in the C system for the p-p collision ($E_0 = 25$ GeV) was obtained by DeMarko Trabucco et al. [190]. The inelasticity is

$$K_c = 1 - E_{Yc}/E_c,$$

where E_{YC} is the hyperon energy.

This distribution is represented in Fig. 55a.

TABLE 50. CHARACTERISTICS OF EVENTS WITH DIFFERENT K_M

K_M	$\langle n_s \rangle$	a^*	Angular distribution	$\langle K_M \rangle$	Number of cases
<0,5	2.5±0.2	0.58	Sharp collimation forward	0.3	128
>0,5	3.5±0.3	0	Isotropic	0.68	86

*$a = \left| \frac{n_{sF} - n_{sB}}{n_{sF} + n_{sB}} \right|$ is the asymmetry parameter; n_{sF} and n_{sB} are the number of particles going forward and backward, respectively, in the C system.

In the cosmic energy region there is very little data on the distribution of total inelasticity.

At an energy of about 400 GeV the distribution of K was obtained with the aid of an ionization calorimeter in an analysis of the form of the nuclear-cascade curves (see Chapter 6—spectrum of secondary protons) [202]. The K distribution in the laboratory system is shown in Fig. 55 for the case of collision of primary nucleons with carbon and iron nuclei. In the latter case the distribution was obtained indirectly.

In the investigation of the collision of nuclear-active particles with iron nuclei nuclear cascades with a single maximum were observed in 15% of the cases (Fig. 42). The form of these cascades is evidence of the transfer of the main portion of the energy after interaction to π^0-mesons. Starting from isotopic invariance, it is necessary to assume that in another 30% of the cases /223
the principal part of the energy is carried by charged pions. Thus, in half of the events the collision is almost completely inelastic, i.e., central. If in the remaining noncentral collisions the K distribution is the same as in collisions with light nuclei, then we have the distribution shown in Fig. 55c.

With the assumptions we obtain the maximum possible estimate of the fraction of central collisions.

The minimum estimate may be found by assuming that the observed events with very large α_0 exhaust all the cases of central collisions. Then the total fraction of such events is 15%.

The method of analysis of the K distribution considered above gives extremely important results, since in the given case we see the means of determining the nature of the particle surviving after collision.

It is known that the hydrodynamic theory predicts the appearance of a secondary pion carrying the principal portion of the primary energy. Hence the experimental proof of the existence of such a pion in nucleon-nucleus collisions at high energies could serve as a weighty qualitative argument in favor of

hydrodynamic theory. If hydrodynamic properties appear only in the collision of nucleons with nuclei [200], the analysis of the nature of the emitted particle of high energy by the photoemulsion technique does not give the result, since the recoil nucleon, in the ordinary sense of this term, is absent, and the mirror system is not defined in the case of a collision with a nucleus. In photoemulsion work the particle of high energy emitted at a small angle is taken to be a nucleon.

Identification of the recoil nucleon is carried out for cases with $N_h \leqslant 2$, i.e., mainly for nucleon-nucleon collisions or collisions with the periphery of a nucleus.

We already mentioned in Chapter 6 the work of Kim [154], in which the recoil proton was identified with energies of the primary nucleon in the thousands of GeV. As follows from Eq. (8.4), there is no necessity to know the exact value of the primary energy in order to determine K_M from the recoil nucleon.

Table 51 gives the results of the determination of K_M obtained in this work for 11 identified baryons. /224

TABLE 51. THE MAGNITUDE OF K_M FOR IDENTIFIED BARYONS

Nature of particle	p	p	p	p	p	p	p	p	p	p	γ	Average*
K_M	0.71	0.25	0.77	0.59	—0.09	0.76	0.22	0.76	0.20	0.71	0.28	0.52 ± 0.16

*Without the value - 0.09.

Brook et al. [96] determined the spectrum of nucleons in the L system by an indirect method. (see Chapter 6). The analytical approximation to the spectrum found by the authors makes it possible to obtain the distribution of $K = 1 - \beta_p$. We shall not stop to consider here the work of Daniel et al. [232] on the identification of the surviving baryon, since the energy of the baryon in this work was determined from the angular distribution of secondary interactions, and the most energetic particle was always assumed to be a baryon.

All of the results considered above show that the inelasticity both on light as well as on heavy nuclei is characterized by considerable fluctuations, and in the collision of nucleons with light nuclei K, in the majority of cases, is significantly less than 1. The size of the fluctuation, which is characterized by the rms deviation, equals $\langle K^2 \rangle^{1/2} \sim K$. Still greater fluctuations of the total inelasticity were observed in work completed under the leadership of Zhdanov [293]. Collisions of protons of energy 25 GeV with the periphery of nuclei in the emulsion were studied, since stars were chosen with $N_h \leqslant 2$ and $N_g \leqslant 1$. A magnetic field

made it possible to measure the momenta of all charged particles. From the momentum balance the energy borne by π^0-mesons could also be established. In all cases when as a result of collision the primary proton did not experience charge transfer, the distribution of total inelasticity had two maxima (at $K<0.1$ and $K\sim0.75$). /225

c. Possible sources of the strong fluctuation of the total inelasticity.—The fluctuations of K obviously coincide with the fluctuations of the energy of the surviving particle. Often, large fluctuations in K are associated with the existence of two types of interaction, peripheral and central [219, 235, 292]. In peripheral collisions there occurs an exchange of one or several mesons. In such collisions the nucleon can sometimes retain almost all the primary energy. If several virtual mesons participate in the interaction, the loss of energy by the nucleon generally increases. Cases when there is a multipion interaction or exhange of heavy mesons are almost indistinguishable from central collisions.

The hydrodynamic theory with a travelling wave explains rather well the existence of a particle isolated in energy [294]. The nature of this particle may vary, and the average energy reaches one-half the initial value. When the most energetic particle is a nucleon, K will be distributed about its average value $\langle K\rangle = 1-\langle\beta\rangle$. According to estimates [294], the fraction of such cases amounts to 10%. It should also be kept in mind that the nucleon emitted as the highest energy particle from the hydrodynamic system will have a higher energy than a pion situated under the same conditions [150].

Thus, hydrodynamics predicts a K distribution of the following type: 80% events have K close to unity, and in the remaining 20% of the cases K is distributed about the average value $\langle K\rangle \leqslant 0.5$ with rms deviation

$$\sqrt{\langle \Delta K^2\rangle} \sim \langle K\rangle.$$

Comparing this conclusion with the distribution of K for light nuclei (Fig. 55), we see that only a small number of events is included in the interval 0.8–1.0, and consequently hydrodynamic processes give a small contribution.

In the collision of nucleons with heavy nuclei the situation may be different.

Gerasimova et al. [295] obtained the energy distribution of the fastest particle (in the framework of the hydrodynamic model): /226

$$\frac{dN}{dE} = \sum_{n=0}^{\infty} \frac{(-1)^n}{n+1} K_2[(n+1)\alpha] \times$$
$$\times \sum_{n=0}^{\infty} \frac{(-1)^n}{\gamma m_\pi} \exp\left[-\frac{(n+1)}{2\gamma}\cdot\frac{E}{m_\pi}\alpha\right]\left(\frac{E}{2\gamma m_\pi}+\frac{\alpha}{n+1}\right),$$

where $\alpha = \frac{T_k}{m_\pi}$ (T_k is the critical temperature, a parameter of the theory), K_2 is a

modified Bessel function of the second kind, and γ is the Lorentz factor of the particle in the L system.

When $T_k \sim m_\pi c^2$ the experimental distribution of the energy of the fastest particle agrees with that calculated from the formula above.

3. Average Values of the Inelasticity

3.1. Collisions of nucleons with nucleons and nuclei

The average values of the inelasticity in the p-N collision can be obtained starting from the quantities $\langle n_c \rangle$ and $\langle \varepsilon_c \rangle$ (see Figs. 27 and 48). In the region of energies to 50 GeV the average multiplicity increases almost proportionally to γ_c. Consequently, the average inelasticity in the C system

$$\langle K_c \rangle = \frac{3}{2} \langle n_{c^\pm} \rangle \frac{\langle \varepsilon_c \rangle}{2(\gamma_c - 1) mc^2} \tag{8.11}$$

will depend weakly on energy, since $\langle \varepsilon_c \rangle$ grows very weakly in this region. As the energy increases above 100 GeV, $\langle \varepsilon_c \rangle$ also increases, but simultaneously the increase of $\langle n_c \rangle$ slows down, and as a result $\langle K \rangle$ does not change (Table 52).

TABLE 52. DEPENDENCE OF $\langle K \rangle$ ON ENERGY E_0 /227

E_0, GeV	5	17	31	100	1000	10 000
n_c	1.5	2.75	3.8	6.4	10	16
$\langle \varepsilon_c \rangle$	0.35	0.45	0.50	0.60	1.3	2,8
$\langle K_c \rangle$	0.56	0.5	0.5	0.5	0.5	0.5
$\langle \csc\theta \rangle$				10.9*		
$\langle K \rangle$				0.49*		

*These data pertain to $E_0 = 28$ GeV [296], with $\langle p_{\perp\pi} \rangle = 0.28$ GeV/c; in [296] the value $\langle p_\perp \rangle = 0.38$ GeV/c was used and $\langle K \rangle$ was obtained equal to 0.66.

The average value of K can also be obtained from $\langle p_\perp \rangle$ using the formula

$$\langle K \rangle = \frac{3}{2} \langle p_\perp \rangle \langle n_c \rangle \frac{\langle \csc \theta_l \rangle}{E_0}, \tag{8.12}$$

or

$$\langle K\rangle = \frac{3}{2}\langle p_\perp\rangle\langle n_c\rangle \frac{\langle \csc\theta_{ic}\rangle}{2(\gamma_c - 1)mc^2}. \qquad (8.13)$$

The results for accelerator energies are given in the same Table 52.

In order for the quantity $\langle K\rangle$, obtained from these formulas to remain constant for $E_0 > 100$ GeV, it is necessary that $\langle \csc\theta_{ic}\rangle$ increase with energy as $\gamma_c^{1/2}$ or somewhat faster.

3.2. Results of direct measurements of average inelasticity

Table 53 gives the results of measurements of $\langle K\rangle$ for the collision of nucleons of various energies with light nuclei and with nucleons. In constructing this table, we used only those data in which the energy of the primary particle was determined by reliable methods.

The table illustrates the constancy of the inelasticity within the accuracy limits of 10-15% up to energies of several thousand GeV.

TABLE 53. MEASUREMENTS OF $\langle K\rangle$ IN THE INTERACTION OF NUCLEONS WITH LIGHT NUCLEI AND NUCLEONS

/228

E_0, GeV	Type of collision	$\langle K\rangle$ or $\langle K_c\rangle$, $\langle K_M\rangle$	Remarks	Reference
3	p-p	0.55	—	[298]
6.2	p-p	0.49 ± 0.05	—	[299]
9	p-N	0.28 ± 0.05	Formula (8.11)	[300]
9	p-N	$0.33 \div 0.44$	Photoemulsion	[133]
24	p-N	0.47 ± 0.05	" "	[293]
25	p-p	0.45 ± 0.03	Photoemulsion	[190]
25	p-C	0.43 ± 0.07	$\langle K_c\rangle$, formula (8.4)	[301]
27	p-p	0.38 ± 0.04	$3\langle\alpha_0\rangle$	[230]
27	p-n	0.41 ± 0.05	Formula (8.11)	[230]
27	p-p	0.60 ± 0.2	" "	[27]
28	p-N	0.49	—	[296]
40—250	p-C	0.23 ± 0.04	Formula (8.12)	[302]
70—700	(π, p)-C	0.48 ± 0.06	Calorimeter $3\langle\alpha_0\rangle$	[303]
>100	$(\bar{\pi}, p)$-C	(~ 0.6)	Calorimeter $3\langle\alpha_0\rangle$	[297]
200	(π, N)-LiH	≥ 0.33	Calorimeter $3\langle\alpha_0\rangle$	[297]
250	N-э.м	0.49 ± 0.1	Calorimeter	[24]
400	N-C	0.55 ± 0.05	Relative scattering $N_h < 5$	[304]
~1000	N-N	0.5	Calorimeter $3\langle\alpha_0\rangle$	[305]
30 000	N-N	0.43	$N_h \leq 2$; $\langle K_M\rangle$ (recoil nucleon)	[20]
			Fragmentation, Castagnoli method. Allowance made for the difference in the spectra of π- and K0-mesons $\langle K\rangle \approx 0.46$	

In addition to the results presented in the table, there are data on inelasticities obtained in the fragmentation of primary nuclei [25, 38, 93], where the inelasticity was estimated from formula (8.3). In these papers the primary energy is known (see Chapter 2); however, the energy of the secondary surviving baryon is estimated by the Castagnoli method, and the most energetic particle is assumed to be a nucleon. It is difficult to estimate the error introduced by such an assumption, but it is obviously not large, since the results agree with the data in Table 52 ($<K>\sim 0{,}5$).

The value $<\alpha_0>\simeq 0{,}3$ was found in [297] without accounting for nuclear splittings in the measured ionization of the electron -photon cascade as well as the interactions of primary pions. To obtain the true magnitude of $<K>$ the same corrections as in [304] were introduced.

The inelasticities in the collision of nucleons with heavy nuclei has not been studied as well. If in the nucleon-nucleus collision the quantity $<\varepsilon_c>$ is the same as in nucleon-nucleon collisions, and $<n_c>$ increases in proportion to $A^{0.15\pm0.05}$, then in the first approximation the average inelasticity increases as $A^{0.15\pm0.05}$. In fact, $<\varepsilon_c>$ decreases with increasing A and $<K>$ varies more slowly. /229

The dependence of $<K>$ on A was determined by Hoffmann et al. [306] at accelerator energies.

Results obtained from (8.12) for $N_h = 0.1$ and $N_h = 7$ show a difference in inelasticity of at most 10% (at 23 GeV) [296].

According to Lal et al. [302], there is almost no difference in the quantities $<\alpha_0>$ for collisions of nucleons with carbon and copper nuclei. Azimov et al. [303] found $<\alpha_0>$ for carbon to be 1.35 times less than for copper, which agrees with the conclusions of Erofeyeva et al. [304], although the absolute values of $<K>$ in these papers are the same.

Lohrman et al. [24] did not observe any difference in $<K>$ for collisions with $N_h<5$ and $N_h\geqslant 5$. Thus, in the high-energy region the data on the dependence of $<K>$ on A are contradictory.

At accelerator energies a significant portion of the primary particle energy is expended in the excitation and splitting of the nucleus. Secondary pions passing through the nucleus give up part of their enegry to nucleons, and so the increase of $<K>$ due to an increase in the number of interactions of the nucleon in the nucleus can to a certain extent be compensated by the energy lost by the pions. The next table gives the energy balance in the collision of a nucleon with heavy emulsion nuclei. In [158], from which Table 54 was taken, cases with $N_h\geqslant 8$ ($E_0=25$ GeV) were selected for analysis.

It follows from this table that slow particles take about 10% of the energy of the primary particle, and high-energy pions take 42 ± 4%. The total inelasticity, including all the energy lost by the nucleon, is 0.52, i.e., no different from that observed for nucleon-nucleon collisions.

At an energy of 9 GeV in proton-nuclues collisions in emulsion, about 4 GeV is given to mesons (44% of the primary energy), i.e., as much as at 24 GeV.

TABLE 54. ENERGY BALANCE IN COLLISION OF A NUCLEON WITH HEAVY EMULSION NUCLEI

Particles	Energy, GeV	Fraction of energy
Very slow ($\beta_i<0.34$)	0.6 ± 0.2	0.026 ± 0.009
Slow ($0.34\leqslant\beta_i\leqslant0.7$)	1.8 ± 0.2	0.079 ± 0.009
Pions ($\beta_i>0.7$)	9.7 ± 1.1	0.42 ± 0.04
High-energy protons	5.5 ± 0.6	0.238 ± 0.025
High-energy neutrons	5.5 ± 1.3	0.238 ± 0.050

The high numerical value of $<K>$ in the collision of nucleons with iron nuclei in [202] is based on the supposition that the fraction of central collisions is ~0.5. The minimum estimate within 15% was $<K>\simeq0.57$. However, the average value $<\alpha_0>$ in this work was obtained equal to 0.26. Hence, if in fact $<K>\simeq0.57$, then for no portion of the events is the relation $3<\alpha_0>=<K>$ fulfilled. /230

On the other hand, low values of $<K>$ in photoemulsions at cosmic energies are obtained under the assumption that the particle of highest energy is always a nucleon. The analysis of the surviving particle carried out by Daniel et al. [93] for nucleon-nucleus collisions showed that the fraction of charged particles among the conserved ones amounts to 74%. At accelerator energies the charge transfer coefficient η is close to 0.5 (see Chapter 12), and the excess of charged particles in Daniel's experiments could indicate an admixture of pions. However, the statistical confidence of this result is low.

The collision of primary nuclei with photoemulsion nuclei was studied by Lohrman et al. [24] Abraham et al. [38], Rybicki [307], and Loktionov et al. [308].

In [24] the average value $<K>$ was found equal to 0.22 ± 0.05, which is approximately one-half that for the nucleon-nucleon collision. This result agrees well with the conclusions of Chapter 6, where it was shown that on the average about half the nucleons of a nucleus interact in a collision of nuclei. Abraham et al. [38] and Rybicki [307] determined $<K>$. using similar methods. The energy of the primary particle is measured by some reliable means according to relative scattering or by the method of Castagnoli for nuclear disruption. The energy of the secondary nucleon of high energy is estimated by the Castagnoli method, the application of which to the present case, when the secondary particles have a broad energy distribution, is not so valid. In agreement with the preceding results $\frac{<K>}{\Delta A}\sim0.5$, where ΔA is the number of nucleons of the nucleus that have interacted. /231

The very weak dependence of $<K>$ on A can be explained on the basis of a hypothesis put forward by Zatsepin [311]. According to it, the nucleon loses its meson "coat" at the moment of collision and upon further motion through the nucleus interacts with nucleons with a cross section of the order of the dimensions of the nuclear kernel ($R\sim\hbar/m_pc$). The meson cloud is restored in a time sufficiently long for the nucleon to leave the nucleus.

3.3. Use of the Castagnoli method

Use of the Castagnoli method for energy determination leads to an apparent decrease in inelasticity with energy. Direct measurements of inelasticity has shown that its magnitude remains constant over a wide energy interval. However there is a large number of papers in which a fall of $<K>$ with energy is observed [6, 162, 216, 220, 309, 310]. They all used the Castagnoli method. Under these conditions the fall of inelasticity in the laboratory coordinate system as a function of measured energy is not unexpected, and the reason for it is explained in Chapter 1 (see Section 1.12).

However, in many investigations inelasticity is determined in the C system, and it does not depend on the magnitude of the measured primary energy. For the nucleon-nucleon collision

$$K_c = \frac{\Sigma (\varepsilon_i - p_i c \cos \theta_i)}{2 m_p c^2} \qquad (8.14)$$

and at first sight it seems that there should be no distortion of the values of K_c.

In experiment, the appearance of a dependence of $<K_c>$ on energy is brought about for different reasons. In the majority of papers formula (8.14) is not used for the determination of K_c, but others, based on model representations. For example, formula (6.16) is used and it is assumed that $<\varepsilon_c>$ is independent of energy. Thus errors are introduced on account of the assumption of the invariance of $<\varepsilon_c>$ and distortions in the measured energy, since in this case γ_c enters explicity into the formula for K_c. /232

To explain the drop in K_c, it was proposed [198] that the velocity of the center of emission increases with increasing γ_c and that $<\varepsilon_c>$ is a constant not in the C system, but in the emission-center system. Then $<\varepsilon_c> = \bar{\gamma} <\bar{\varepsilon}>$, where $<\bar{\varepsilon}>$ is the average energy of pions in the emission-center system, and $\bar{\gamma}$ is its Lorentz factor relative to the C system. If it is assumed that $\bar{\gamma} \sim \gamma_s^{1/2}$, then it follows from (6.15a) that K_c will be approximately constant. On the basis of a similar model Imaeda [6] determined K_c with allowance for the Lorentz factor γ, measured in the experiment from the angular distribution:

$$K_c = 1.5 n_s \frac{<\bar{\varepsilon}> \bar{\gamma}}{m_p \gamma_s}; \qquad (8.14a)$$

$$\bar{\gamma} = \frac{1 + \gamma_1/\gamma_2}{2\sqrt{\gamma_1/\gamma_2}}, \qquad (8.15)$$

where γ_1 and γ_2 are the Lorentz factors of the two centers of pion emission in the L system.

As a result of Imaeda's work, one concludes that K_c, as calculated from (8.14a), decreases with increasing energy γ_s. The Lorentz factor $\bar{\gamma}$ increases with an increase in the measured energy E_s, but at the same time, the smaller n_s, the greater $\bar{\gamma}$, and therefore there is a compensation of the factors n_s and $\bar{\gamma}$ in (8.14a), and $<K_c>$ does not grow with increasing $\bar{\gamma}$.

The drop of $<K_c>$ with energy in this work, as well as in others where the energy of the primary was determined by the Castagnoli method, is easily explained by the statistical character of the connection between γ_c and γ_s and the registration threshold, which for the events selected by Imaeda was about 50 to 100 GeV. If one uses Eq. (1.12), which establishes the relation between the average measured and true inelasticities, then it is easy to calculate the energy dependence of $<K>$, given the value of the selection threshold ε_0 ($\varepsilon_0 = 50$–100 GeV), the index of the spectrum of generated particles $\gamma - 1 = 2$, and the dispersion of the distribution γ_s about γ_c. /233

The results of such a calculation are shown in Fig. 2, together with the experimental data, whereby we find explanation not only for the fall of $<K>$ with energy as measured by the Castagnoli method, but also for the unreasonably large values $K > 1$ obtained in experiments close to the threshold.

It is more difficult to establish the reasons for the decrease of $<K>$ with energy in the experiments of Fretter and Hansen [312], since they used (8.14), which is free from the errors of the Castagnoli method. We can say the following. In measurements with a Wilson chamber in a magnetic field cases are usually observed in which one or several particles are unmeasurable, $p_i > 40$ GeV. These particles do not give a significant contribution to the magnitude of K_c. However, if events with unmeasurable particles are excluded from consideration, $<K_c>$ is underestimated, since this effect is strongest of all at the highest energies, where the quantity of unmeasured particles is particularly large.

The correlation between the magnitude of K_c in individual cases and the difference between γ_s and γ_c can lead to the same effect. If the difference in γ_s and γ_c is greater for small K_c, then events with small K_c will be important in the region of high γ_s and there will be an apparent decrease in $<K_c>$ with energy.

Thus, the analysis of these papers shows that the change in inelasticity with energy obtained in them is explainable on the basis of their methodology.

In the H-quantum model developed by Hasegawa et al. [313], it is assumed that the mass of the generated particle agglomerates $M \sim 2m_p$ is a constant and that their energies are quantized in the C system. The inelasticity decreases with energy in this model:

$$K_c = \frac{\Sigma \overline{\gamma} 2m_p}{2m_p(\gamma_c - 1)} = \frac{\Sigma \overline{\gamma}}{\gamma_c - 1}.$$

The summation is carried out over all H-quanta. Since $\overline{\gamma}$=const, we have /234

$$K_c \sim \frac{\nu}{\gamma_c},$$

where ν is the number of H-quanta, which is determined from the features of the angular distribution (see Chapter 9). In Hasegawa's model the inelasticity for each number ν decreases with energy; however, the magnitude of ν increases with energy.

3.4. Inelasticity of the pion-nucleus collision

In the study of pion-nucleus or pion-nucleon collisions the inelasticity of the interaction is different in the L and M systems. As was shown in a number of experiments that have already been mentioned, the nucleon in the π-N collision moves backwards in the C system, and the pion forwards. In the M system the collimation of nucleons is naturally enhanced. Experiments by Grote et al. [235] at 7.5 GeV showed that $\langle K_M \rangle = \frac{E'_{pM} - E''_{pM}}{E'_{pM}} = 0.5$, where E'_{pm} and E''_{pM} are the energies of the proton before and after collision in the mirror coordinate system. By studying π-N collisions at 4.5 GeV, Malhotra [314] arrived at a similar conclusion regarding the inelasticity of the nucleon. Thus, the nucleon in the C system after collision continues its motion in the initial direction, retaining about one half its energy. Similar investigations have not been carried out in cosmic rays.

Malhotra [314] studied the question of the conservation of the pion in the π^-N collision at 4.5 GeV and found that in events with small multiplicity the primary pion, as a rule, is conserved and bears a significant portion of the primary energy. This same conclusion was obtained from a consideration of the spectra of secondary pions in pion-nucleon collisions (Chapter 6, Section 2.5). Conservation of pions after collision was observed also by Walker [315], Friedländer et al. [191] and Goldsack et al. [237] in the interval of primary energies of the pions from 5 to 16 GeV. Similar experiments were also set up for the study of the sharply collimated forward π^0-mesons arising, evidently, as a result of the inelastic charge exchange of the surviving pion, $\pi^- \to \pi^0 +$ other pions. Kelson and Yekutieli [316] found that at an energy of the primary π^--mesons $E_0 = 4.2$ GeV about 10% of the photons occur on account of the emission of a sharply collimated π^0-meson. Similar data were obtained by Friedländer [191], who found sharply collimated forward π^0-mesons ($\theta < 5°$ at 7.5 GeV of π^-) that were created by primary pions and not by protons, which also speaks for the charge exchange mechanism in the formation of π^0-mesons. These phenomena /235

occur principally when the multiplicity of secondary particles is low. The presence of this mechanism should lead to sharp fluctuations in the partial coefficient of inelasticity in pion-nucleon collisions.

According to data of Brook et al. [96], obtained from a comparison of the free path lengths of absorption and interaction of pions in the atmosphere, the pion retains about 40% of its energy after collision. If the pion is sometimes emitted in the form of a π^0-meson as the result of charge exchange, then the energy retained by the energetically isolated pion is still greater.

Malhotra [314] obtained the distribution of the number of pions bearing away a fraction of the primary energy in excess of $u = E_\pi/E_0$ in the π^--p collision at 4.5 GeV. The results are presented in Table 55 (n_π is the number of pions per interaction which have a fraction of the energy greater than u).

TABLE 55. AVERAGE NUMBER OF SECONDARY PIONS TAKING DIFFERENT FRACTIONS OF THE PRIMARY PARTICLE ENERGY

u	0.30	0.40	0.50	0.60	0.80
n_π	0.8 ± 0.05	0.5 ± 0.03	0.3 ± 0.02	0.2 ± 0.02	0.02

The average multiplicity of charged pions in this experiment $\langle n_{c\pm}\rangle = 1.94\pm 0.12$, including $n_c = 0$.

In cases with high multiplicity no energetically isolated pion is observed.

Hoffmann et al. [148] studied the interaction of π^--mesons with $E_0 = 14$ GeV /236 with heavy nuclei of the emulsion (selection $N_h \geqslant 8$). The momenta were measured with the aid of a magnetic field. The fraction of energy borne off by all negatively charged secondary pions was 0.29 ± 0.02. About 12% of the energy is expended in the formation of slow particles, mainly products of nuclear fragmentation, and relativistic nucleons take at most only 2% of the energy in the L system. In this case, as also in pion-nucleon collisions, pions are observed which take more than 30% of the initial energy. Such pions are encountered in 20% of all interactions. In 5% of the events there are particles with $u > 0.6$.

Thus, in the collision of a pion with a nucleus, the energy of the primary particle is divided up more strongly than in the π-N collision.

4. Partial Coefficients of Inelasticity

4.1. The coefficient $\alpha_{\pm}$

We shall discuss some of the results concerning the fraction of energy carried away by different sorts of secondary particles. We shall examine only papers with "reliable" measurements of energy.

A measurement of $\alpha_{\pm}$ at energies in the hundreds of GeV was made by Guseva et al. [143] and Lohrman et al. [24] (Fig. 56). At $E_0 \approx 3000$ GeV the fraction of energy expended in the formation of secondary charged particles was studied by Koshiba et al. [20]. The distribution of $\alpha_{\pm}$ has a maximum at $\alpha_{\pm} \sim 0.15$–0.20 in the case of nucleon-nucleon collisions and is strongly smeared out in nucleon-nucleus collisions.

4.2. The coefficient α_0

The distribution of α_0 has qualitatively the same character. Figure 57 shows the distribution α_0 in carbon, according to data of Azimov et al. [303]. It was obtained with the aid of a calorimeter with Cherenkov counters as detectors. The distribution of α_0 in the interaction of nuclear-active particles on mountains with nuclei of carbon, iron, and lead is given in Fig. 58, according to data of [304], in which it was possible to distinguish charged from neutral primary particles. Assuming that protons and neutrons interact identically, it was possible statistically to isolate cases of the interaction of pions with energies in the hundreds of GeV and obtain the distribution of α_0 in interactions of pions with nuclei. The average value of α_0 was found to equal $\langle\alpha_0\rangle = 0.15$–$0.20$ in the interaction of nucleons with nuclei of carbon and $\langle\alpha_0\rangle = 0.26 \pm 0.03$ for the interaction in iron. These magnitudes agree with the results of measurements of $\langle K\rangle$. /237 /238

In the distribution of α_0 for pions, attention is drawn to the group of events with very high values of $\alpha_0 > 0.6$.

4.3. The existence of events with a high transmission of energy to γ-photons

These phenomena were first observed in cosmic rays by means of the ionization calorimeter [317]. It turned out that in 10% of the collisions of nuclear-active particles with energy ~ 600 GeV with iron nuclei, $\alpha_0 > 0.6$. Subsequently, the question of the existence of events with $\alpha_0 > 0.6$ was very widely discussed. A significant amount of material containing arguments supporting the existence of such acts was obtained in the papers of Grigorov et al. [52, 206] using the method of controlled emulsions. /239

They studied the pulses in the upper rows of ionization chambers (I and II, Fig. 15c), which correspond to an energy evolution, exceeding 140, 350 and 500

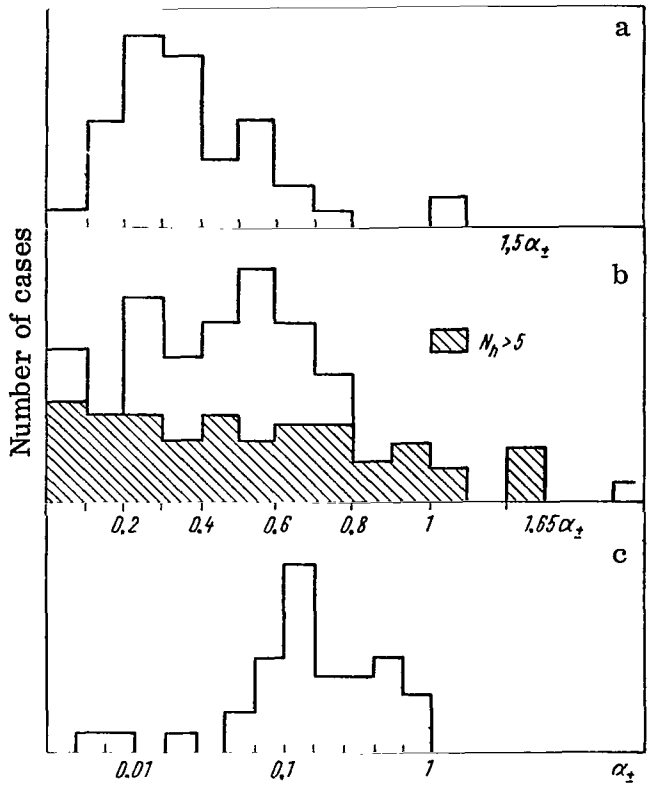

Figure 56. Distribution of Partial Coefficients of Inelasticity $\alpha_{\pm}$:

a—$E_0 \simeq 200$ GeV [260]; b—$E_0 \simeq 250$ GeV [24]; c—$E_0 \approx$ 3000 GeV [20].

GeV in different series of experiments. The showers were produced in a carbon target of thickness 60 g/cm^2. With the aid of a detector of the energy of the secondary particles, which consisted of a thick graphite filter (210 g/cm^2), it was possible to estimate the energy of the surviving nuclear-active particles. In the experiment it was found that in the majority of cases the evolution of energy in the graphite target was insignificant, and consequently the coefficient α_0 for the first act has a high magnitude ($\alpha_0 > 0.6$). The fraction of such events (after allowing for the probability of their specific selection) is as high as 10%. In a number of cases it was possible to find the showers in the photoemulsions corresponding to the registered pulses. Some of the properties of these showers are shown in Table 39. In this table events 1-9 have $\alpha_0 > 0.6$. /240

The total fraction of events with $\alpha_0 > 0.6$ (10%) obtained by Erofeyeva et al. [304] agrees with the results of the preceding paper.

However, in certain other papers interactions with $\alpha_0 > 0.6$. were not observed. This pertains principally to two papers [302, 303]. In the second of these a maximum value of $\alpha_0 \sim 0.55$ ($E_0 > 150$ GeV) was found using an ionization calorimeter

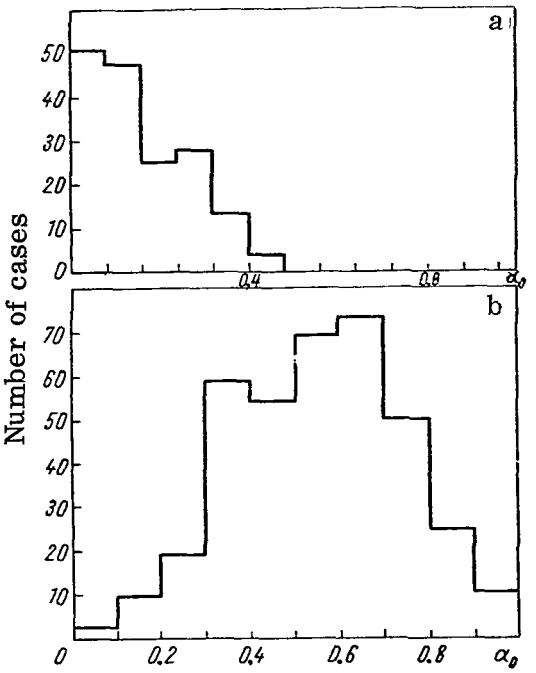

Figure 57. Distribution of Partial Coefficient of Inelasticity α_0:

a—For the Interaction of Nuclear-Active Particles with Carbon Nuclei [303]; b—In Experiments with "Pulse" Set-Ups [205].

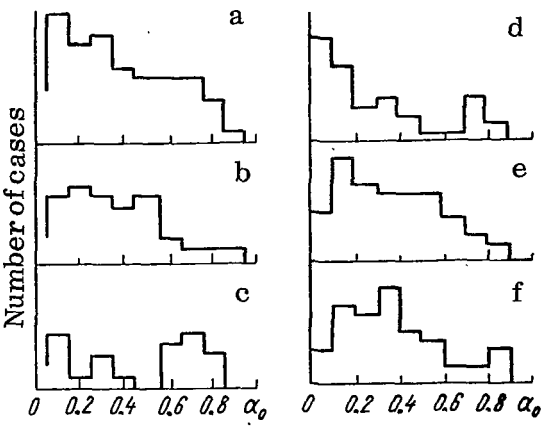

Figure 58. Distribution of Partial Coefficients of Inelasticity α_0 [304]:

a—For Interactions of Charged Primaries; b—Neutral Primaries; c—Difference of the Distributions a and b; d—for the Interactions of Nuclear-Active Particles with Carbon Nuclei; e—the Same with Iron Nuclei; f—the Same with Lead Nuclei.

with Cerenkov counters. In the first [302], the interactions were studied in a total absorption spectrometer (TAS, Chapter 3), and again events with high α_0 were not observed. The values of α_0 obtained were less than in other papers:

$$\langle \alpha_0 \rangle = (9.2 \pm 1.2)\% \text{ for carbon;}$$
$$\langle \alpha_0 \rangle = (8.1 \pm 1.4)\% \text{ for copper.}$$

The lack of events with $\alpha_0 > 0.6$ in these papers may be due to certain methodological reasons. For example, in the registration of nuclear interactions in a TAS it is required that the avalanche penetrate to depths corresponding to five interaction path lengths [41]. Events with $\alpha_0 > 0.6$ have very short cascades and will be lost in a system adjusted in this way. The electron-nuclear cascades will be even shorter in a set-up using Cherenkov counters, in which transition effects are important (see Chapter 6, Section 1). It is also possible that in the selection of separate nuclear-active particles, pions, which are mainly responsible for the events with $\alpha_0 > 0.6$, are excluded to a significant extent, if they enter more frequently than nucleons in the composition of air showers.

According to [304], pions give events with large and small α_0 with equal frequency. So great a fluctuation could be due to the mechanism already mentioned above, i.e., charge exchange in the inelastic collision of pions with nuclei.

5. The Relation Between the Coefficients α_0 and $\alpha_\pm$

In 1952, Watson [318] showed from considerations of isotropic invariance that in the multiple production of mesons by a nucleon on a nucleus having an equal number of neutrons and protons, the distribution of energy among the various isotopic components of the mesons should, on the average, be uniform. Hence the often used relations $K=3\alpha_0$; $K=1.5\alpha_\pm$ or $K=1.65\ \alpha_\pm$ (with allowance for kaons) are incorrect and pertain only to average values $\langle K\rangle$ and $\langle\alpha\rangle$. However, there are a number of reasons which might make these expression incorrect even on the average. In this, it needs to be remembered that in experiment one measures the energy of photons, and not of π^0-mesons, and the pionic origin of photons is a hypothesis requiring verification. The possibility of the violation of (8.5) was pointed out by Feinberg in [200, 319].

In these papers the fraction of energy which can be given to photons by means of their direct production by fluctuations of electrical charge in hydrodynamic system was estimated. Later, quantitative estimates of the effect was made by Vernov and Sisakyan [320]. It was ascertained that the fraction of energy carried by photons for the indicated reason depends on the equation of state describing the excited system, and at high energies $\sim 10^{14}$ eV can reach several tenths. This effect is particularly strongly manifested if the system is described by an equation of state of the Heisenberg type ($c^2=0$), since in this case the system exists for a relatively long time.

Thus, this source of photons at high energies is comparable with ionization.

The existence of resonances, e.g. η_0-mesons, with preferential decay into π^0-mesons or photons also can change the relation (8.5) [202].

Daibog [321] made an estimate of the relation of the energy transferred to photons to the energy of charged particles with the assumption of SU(3) symmetry.

In the limiting case of high energies, the following inequality was obtained, which is valid on the average with allowance for the η_0-meson:

$$0.76 < \frac{\alpha_0}{\alpha_\pm} < 1.02.$$

Now, other resonances with decay into photons are known, and the inequality can be revised in favor of α_0. Finally, in the case of the interaction of primary pions with nuclei, the pion is frequently conserved. There is a definite probability for its inelastic charge exchange: /242

$$\pi^- + N \to \pi^0 + N + \text{low-energy particles}.$$

If the probability of double charge exchange

$$\pi^- + N \to \pi^+ + N + \text{low-energy particles}$$

is significantly less, then only two channels will compete:

$$\pi^- \to \pi^- + n\pi;$$
$$\pi^- \to \pi^0 + n\pi.$$

Certain indications in this respect are given by Bellini et al. [322], who studied the asymmetry of the dispersal of secondary pions with different signs of the charges in collision of π^--mesons with nuclei in a propane bubble chamber. The asymmetry parameter $a = \frac{n_{sF} - n_{sB}}{n_{sF} + n_{sB}}$, which indicates the excess of particles emitted in the C system in the forward or backward hemisphere was found to be twice as great for π^--mesons and π^0-mesons than for π^+(+0.57 ± 0.12 for π^- and π^0 and +0.28 ± 0.1 for π^+). Thus, π^-- and π^0-mesons are strongly collimated forward and consequently have a higher energy than π^+-mesons in the L system.

Consequently, there is some possibility of violating the relation (8.5), and its experimental testing can expose new properties of the interactions [323, 202].

In the region of accelerator energies the relation of the energies of the neutral and charged pions for nucleon-nucleon collisions depends on the type of reaction studied. Galstyan et al. [293] studied proton-nucleon interactions in emulsion at an energy of 25 GeV. It was found that in those conditions when the proton remains a proton after collision, i.e., does not undergo charge exchange, the relation is $\langle \alpha_0/\alpha_\pm \rangle \sim 1$ for nonperipheral collisions. For peripheral collisions, in which the square of the four-dimensional transferred momentum is small, if only for one nucleon, a significant excess of neutral mesons is observed. In 1/3 of all cases (out of 21), $\langle \alpha_0 \rangle = 0.65$ and $\langle \alpha_\pm \rangle = 0.05$ (in 5 cases there were generally no charged mesons). In 14 cases, $\langle \alpha_0 \rangle = 0.15$ and $\langle \alpha_\pm \rangle = 0.50$. Isobars were identified in this group of events. /243

The average value $\left\langle \frac{\alpha_0}{\alpha_\pm} \right\rangle$ for all peripheral interactions with a surviving proton, as also for the nonperipheral ones, is close to unity. However, in the case of the charge exchange $p \to n$, positive charged particles should predominate among the created particles, and the total relation $\left\langle \frac{\alpha_0}{\alpha_\pm} \right\rangle$ can be close to one-half.

In the region of cosmic energies the relation between α_0 and $\alpha_\pm$ was investigated by Koshiba et al. [20]. The total energy of the charged particles $E_{\pi^\pm}$ was determined from their angular distribution with the assumption of $\langle p_\perp \rangle$, invariance, and the energy of the π^0-mesons E_{π^0} was determined from the electromagnetic cascades. As a result, the correlation between $E_{\pi^\pm}$ and E_{π^0} could be

determined and their average ratio found. The situation, however, is complicated by the presence of a threshold for the registration of electromagnetic cascades, which was close to 400 GeV. In order to avoid this difficulty, the authors introduced a threshold for $E_{\pi\pm}$ also, assuming the existence of the relation $\langle E_{\pi\pm}\rangle = \mu\langle E_{\pi^0}\rangle$. By constructing the distribution of the ratio $E_{\pi\pm}/E_{\pi^0}$ for different coefficients μ, they found that value for which the distribution of the ratio was symmetrical about μ.

In these experiments they obtained μ to be approximately 2, i.e., the relation (8.5) is fulfilled at energies $\sim 10^3$ GeV.

The authors applied the same method to the determination of the ratio $\langle\alpha_0/\alpha_\pm\rangle$ for the collision of primary nulcei with $Z\geqslant 2$ in emulsion and observed a magnitude of the ratio considerably less than one-half. However, the statistical accuracy of this result is poor.

A measurement of $\langle\alpha_0/\alpha_\pm\rangle$ was also carried out in [202] with an ionization calorimeter at 200 GeV, and a value close to unity was found. However, it was found later that this result pertains, apparently, only to cases of the interaction of primary pions [304]. /244

Thus, we can suppose that there are two groups of events with different α_0 (Fig. 58c) appearing as a consequence of the charge exchange of the most energetic surviving pion, and then the magnitude of $\alpha_0/\alpha_\pm$ is determined by the probability of this charge exchange. The ratio of the number of cases in the groups is of the order of unity. This may indicate the appearance of charged and neutral pions with equal frequency among the most energetic particles (see Section 5.1). The statistical accuracy of the result is still not large (about 10 pions in each group).

A marked excess of photons was also observed in work of Femino et al. [324], who investigated the collision of negative pions in an emulsion at 4.5 GeV.

With respect to nucleon-nucleon collisions, apparently no deviations from (8.5) are observed up to 3000 GeV.

Further investigations are necessary for final clarification of this matter.

6. Conclusion

The total coefficient of inelasticity $\langle K\rangle$ shows a remarkable invariance over three orders of energy change. The quantity $\langle K\rangle$ is related to many other characteristics of the interaction, such as the average energy of the secondary particles in the C system, the multiplicity, the angular distribution, and the average transverse momentum. All these parameters, with the exception of $\langle p_\perp\rangle$, vary strongly with energy (e.g., $\langle\varepsilon_c\rangle$ changes by a factor of ten in the interval of energies from 20 to 10^4 GeV), but their combination leads to an astonishing compensation of all changes in $\langle K\rangle$ and hence to its invariance. This strongly suggests that the inelasticity $\langle K\rangle$ is one of those fundamental parameters of the elementary act that determine the behavior of all the rest.

CHAPTER 9

ANGULAR DISTRIBUTION OF SECONDARY PARTICLES

1. Introduction

The angular distribution of the secondary particles arising in the process of multiple production is profoundly connected with the mechanism of interaction of the colliding particles. /245

Until recent times the investigation of the angular distribution of the secondary charged particles was the only method of estimating the energy of the primary particles generating showers in photoemulsion.

The study of the distribution of particles with respect to angle can be conducted in any of the five usually employed coordinate systems (see Chapter 2). However, the most graphic results are obtained in the system of the coordinates of the center of mass of the colliding particles, where the conservation laws have the limiting simple form, or in the symmetric system, which in some cases coincides with the center-of-mass system.

The symmetric system is used in experiments with the photoemulsion method because of the difficulties associated with the transformation to the C system. The indeterminacy in the measurement of the energy of the primary particle and the natures of the colliding particles do not allow one in these cases to determine the Lorentz factor of the center-of-mass system relative to the laboratory system.

The same reasons lead to the necessity of examining the angular distribution of secondary particles using information about the angles in the laboratory coordinate system, but in doing this to choose an appropriate coordinate representation. Such a coordinate representation which reflects the features of the dispersal of the particles in the center-of-mass system is the distribution of particle tracks according to the scale $x=\lg\operatorname{tg}\theta$. This is the so-called x-representation, which in individual events characterizes the angular distribution of charged particles in any system of taking readings.

2. Some Features of the X-Representation /246

2.1. The differential x-representation

The differential x-representation is frequently given in the form of vertical lines that mark the angles of emission of the charged particles on the x scale. This manner of representation is used in the study of the fine structure of the angular distributions in individual events.

By summation over some interval one can obtain the differential form of the x-representation g (x) dx, which is approximated by an appropriate analytical function. If particles in the C system are dispersed isotropically, the differential distribution over angle in the x-representation is close to a Gaussian with half-width $\sigma_{is} = 0.39$. If the dispersal of secondary particles after collision in the C system is anisotropic, the angular distribution in the x-representation in certain cases can again be approximated by a Gaussian, but with a halfwidth greater than that for isotropic dispersal. A more complex case is also possible, in which the angular distribution in the x-representation has to be approximated by the superposition of two or more Gaussian distributions. This case requires special interpretation and will be considered separately (see Sec. 4).

Thus, in the study of the angular distribution an analysis of the form of the distribution in the x-representation is essential. In this analysis, a controlling characteristic of the angular distribution is the dispersion $\sigma^2 = \langle (x - \langle x \rangle)^2 \rangle$. In more general form:

$$\sigma^2 = \int (x - \langle x \rangle)^2 g(x)\, dx = \int x^2 g(x)\, dx - [\int x\, g(x)\, dx]^2.$$

The dispersion of the angular distribution is related to the index m or n for the approximation of the angular distribution by a cosine or sine function. A graph of the dependence of σ on m and n is shown in Fig. 9 (Chapter 2). In this case the dispersion plays a greater role, since it is approximately invariant under Lorentz transformations.

However, these properties of the x-representation can be used only in the examination of individual events. And, if it is required to carry out an average /247 over many individual interactions, it is necessary to know the Lorentz factor of the coordinate system in which we desire to determine the angular distribution, and the scale $x = \log \tan \theta$ must be replaced by $X = \log \gamma_c \tan \theta$ (or $X = \log \gamma_s \tan \theta$), which corresponds to normalization of the available events to a single value of the primary energy (or to a single center of symmetry). Then the angular distribution of the secondary particles for a given group of events will be described by the function g(X)dX, to which all that has been said about g(x)dx also applies.

Figure 59 gives examples of the function g(x) [329].

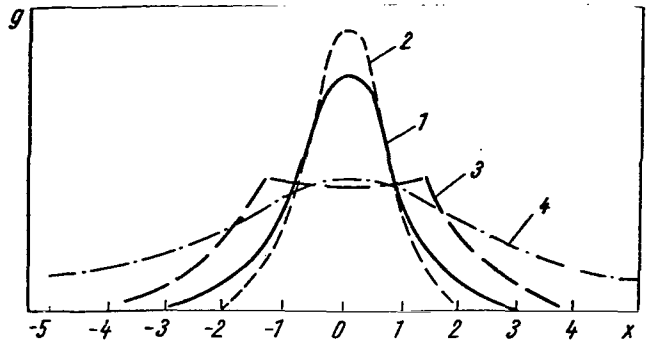

Figure 59. Differential Angular Distributions g(x):

1—for an Isotropic Angular Distribution; 2—According to the Heisenberg Theory [128]; 3—According to the Fermi Theory [126] with $\varrho_0 = 0.959$; 4—According to the Landau Theory [18], $E_0 = 10^5$ GeV.

2.2. Integral form of the x-representation

The usual integral form of the x-representation $F(>x) = \int_x^\infty g(x)\,dx$ is frequently replaced by an integral representation which is called the F-representation [13] (see Chapter 2, Section 2). In constructing the F-representation, the quantity F/(1-F) is plotted as the ordinate and x (or X) as the abscissa, where F is the fraction of particles emitted at angles less than θ, and 1-F is the fraction emitted at angles greater than θ.

The integral function of the angular distribution in the laboratory coordinate system that corresponds unambiguously to a function in the C system (or S system) can be obtained by using the formula for transformation of angles (2.4). If the angular distribution of particles in the C system is isotropic, i.e., /248

$$f(\theta_c)\,d\theta_c = \frac{1}{2}\sin\theta_c\,d\theta_c,$$

then

$$F(\theta_c) = \int_0^{\theta_c} f(\theta_c)\,d\theta_c = \sin^2\frac{\theta_c}{2}$$

or

$$\frac{F}{1-F} = \tan^2\frac{\theta_c}{2}. \qquad (9.1)$$

Let us determine the RHS of Eq. (9.1), using Eq. (2.4):

$$\tan^2\frac{\theta_c}{2}=\gamma_c^2\tan^2\theta\left\{1+\frac{1}{\dfrac{\beta_c/\beta_{ic}-1}{2\cos^2\dfrac{\theta_c}{2}}}\right\}^{-2} \tag{9.2}$$

In the special case $\beta_{ic}=\beta_c$, we obtain Eq. (2.54).

Thus, for an isotropic angular distribution in the C system the F-representation on a log-log plot will have the form of a straight line with a slope of 2. The line will pass through the origin if one is considering the dependence of F/(1-F) on X and will be shifted from the origin by the amount $\log\gamma_c$, if the argument is x.

If $\beta_{ic}\neq\beta_c$, then for an isotropic dispersal of secondary particles in the C system, the F-representation is different from a straight line (Fig. 60a).

If the angular distribution of particles in the C system is anisotropic but symmetrical relative to a plane perpendicular to the direction of motion of the primary particle, then in the F-representation the function will also differ from a straight line with $\tan\varphi=2$. For example, the angular distribution obtained in the Heisenberg theory [128] is given in the F-representation by a straight line with $\tan\varphi=1$ (φ is the angle between the line and the axis of abscissas). The Fermi distribution [126] is a line with $\tan\varphi\sim1.3$ (for an average collision parameter). The angular distribution calculated on the basis of the Landau theory [18] is a line having a slope in its central portion that is nearly 1.

All these distributions are shown in Fig. 60 [325]. In this same figure we show the F-representation obtained from the phenomenological picture of the collision, which consists of the following. We assume that in the system of the center of mass of the colliding particles two agglomerates of excited material b_1 and b_2 are formed and move away from each other along the direction of motion of the primary particle. The Lorentz factors of these agglomerates relative to the C system equal γ. Each agglomerate eventually disintegrates into individual particles that are emitted isotropically in the rest system of the agglomerate. The distribution of these particles with respect to angle in the F-representation is depicted by the curve drawn in Fig. 60f.

This phenomenological treatment of collision, which arises as a result of the analysis of the angular distributions in showers registered in photoemulsion, was first given by Zatsepin in 1950. The mathematical description of this process, called the two-fireball model, was given independently by some Japanese physicists [326, 327], as well as by Cocconi [325] and a Polish-Czechoslovakian group [328].

If the angular distribution of secondary particles in the C system has a cosine form and can be represented in the form

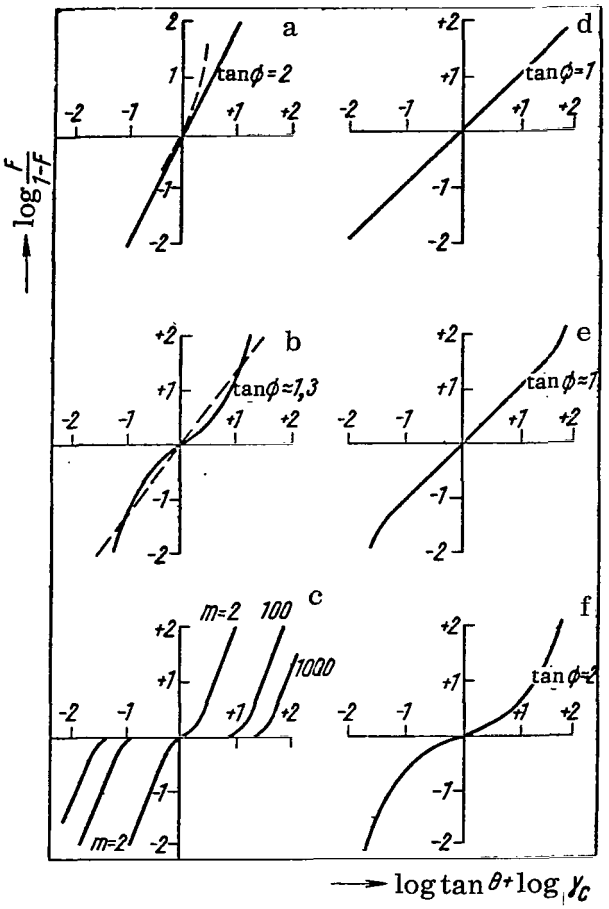

Figure 60. Integral Form of Angular Distribution:

a—for an Isotropic Distribution (Solid Line $\beta_i = \beta_c$. Dashed $\beta_i = 0.92 \cdot \beta_c$); b—from the Heisenberg Theory; c—from the Fermi Theory with Average Collision Parameter $v = 0.959$ (Solid Line), Dashed Line for a Central Collision; d—According to the Landau Theory for $E_0 = 10^5$ GeV; e—for the Approximation of the Angular Distribution in the C System in the Form $\cos^m \theta_c \, d\Omega_c$; f—for the Two-Fireball Model, $\overline{\gamma} = 100$.

$$f(\theta_c)\, d\Omega_c = A \cos^m \theta_c \sin \theta_c \, d\theta_c,$$

then in going over to the F-representation we obtain a picture resembling the preceding one. The only difference is that in the region of angles in the C system

close to $\pi/2$, there are no secondary particles, and as the degree of anisotropy m increases this region becomes larger according to the law (see Fig. 60e)

$$\Delta X \sim \tan^{-1}(m+1). \qquad (9.3)$$

In analyzing experimental data it is of interest to find out how the angular distribution behaves as the mass of the colliding particles changes. Bozoki et al. [329] have shown that the angular distribution calculated on the Landau theory for collisions of a nucleon with energy 10^3 GeV with different target particles becomes more and more isotropic as the mass of the target particle increases. /251

3. Experimental Data on the Angular Distribution of Secondary Particles

3.1. Introduction

The presently available cosmic ray experiments on the angular distribution of shower particles can be divided into two groups.

The first group of investigations [328, 330-343], carried out with photoemulsion techniques, does not delay, as a rule, accurate data on the energy of the primary particle. Moreover, the angular distribution of the secondary charged particles is usually employed for its determination. The Castagnoli method used in these cases gives the Lorentz factor γ_s of the symmetric system. In this connection, the majority of the data on the angular distribution of secondary particles obtained by photoemulsion techniques pertains to the laboratory and symmetric coordinate systems. The exceptions are [24, 38], which investigate the characteristics of the interaction of nucleons formed in the fragmentation of primary nuclei (see Chapter 2).

In the second group [22, 34, 136], an ionization calorimeter or a TAS was used to determine the primary particle energy, and a Wilson chamber was used for the measurement of the angular distribution of secondary particles. In these papers the energy of the primary particle is measured independently of the angular distribution of the secondaries. Then, with certain assumptions about the nature of the colliding particles, it is possible to find the Lorentz factor of the center-of-mass system and obtain a picture of the collision in this most informative coordinate system.

3.2. Analysis of experimental results in the x-representation /253

First we shall consider the result of cosmic ray investigations using photoemulsions exposed at high altitudes ($\sim$30 km). In this, we can figure that the showers registered in the photoemulsions are produced by primary cosmic particles: protons and heavy nuclei. Table 56 gives information about these investigations. This consists mainly of papers in which the most voluminous statistical material is collected. Data on the approximate energy rante of these events is also provided.

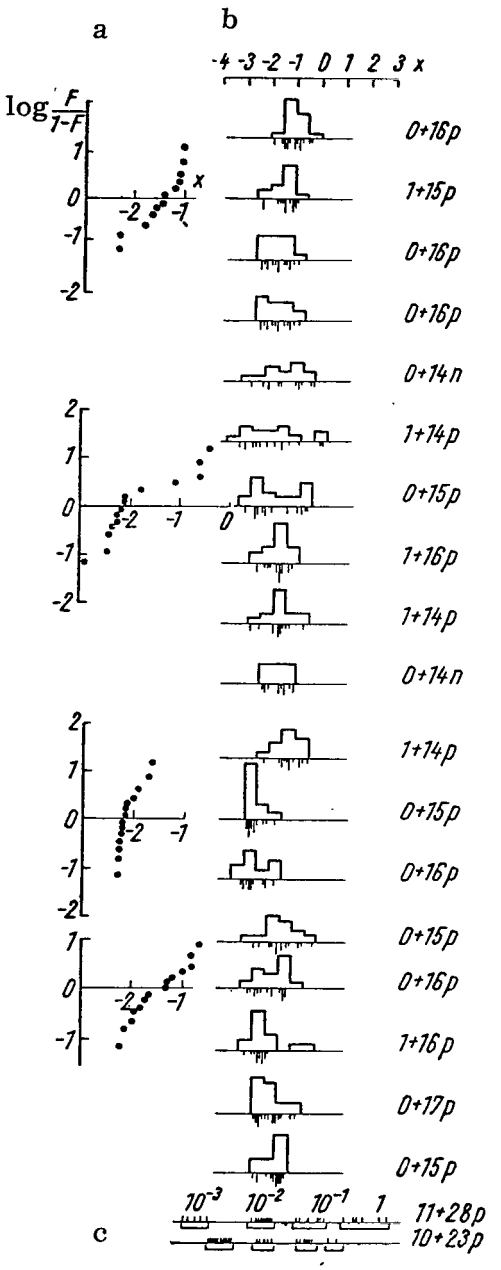

Figure 61. Angular Distributions of Secondary Particles Along the X-Coordinate for Individual Events:

a—Integral Distributions for Events Taken from the JCEF Collection [146]; Events Selected with $N_h=0,1$ and $14<n_s<17$. Formed in Photoemulsion by Primary Singly-Charged or Neutral Particles; b—Differential Distributions g(x); c—Events Used for the Proof of Existence of H-quanta.

The analysis of the form of the angular distributions in the x-representation is most advantageous for individual events. In doing this, an accurate value of the energy of the primary particle may not be known.

In Fig. 61 are shown typical angular distributions of particles for individual events. The distribution in x ($x_i=\log\tan\theta_i$), the differential distribution in x, $g(x)dx$ and the integral F-representation are shown for each shower. The events correspond to a narrow energy interval and have approximately the same multiplicity n_s. The number of gray and black tracks $N_h = 0$ or 1. In the selection of events no limitations of any kind were applied to the form of the angular distribution of the secondary particles.

In analyzing the form of the differential distributions g(x)dx, it is seen that distributions having a single maximum predominate.

Polish physicists [344] who had analyzed their own and foreign results concluded that angular distributions with a complex structure appear in approximately 20% of the events with primary particle energy greater than 1000 GeV. The complex structure of the angular distributions will be analyzed when we consider the angular distributions in the symmetric system.

The principal quantitative characteristic of the angular distribution is its dispersion $\sigma^2 = \langle(x-\langle x\rangle)^2\rangle$. Let us examine how the dispersion varies with changes in the interaction parameters, such as the primary particle energy, multiplicity n_s of the shower particles, number of gray and black tracks N_h, and the angular distribution.

TABLE 56. NUMBER OF CASES WITH DIFFERENT N_h AND APPROXIMATE ENERGY RANGE OF PRIMARY PARTICLES

Author	Number of cases with different N_h	Primary energy, Castagnoli, GeV	Remarks
Bozoki et al. [330]	$N_h \leqslant 5$—151 $N_h > 5$—74	10—200	Survey of many papers up to 1958
Ciok et al. [328]	$N_h < 5$ $n_s \geqslant 6$ } —119	$10-10^4$	—
Bartke et al. [331, 333]	$N_h \leqslant 5$—71 $N_h > 8$—61	$10-2\cdot10^4$	—
Giyerula et al. [332]	$N_h \leqslant 5$—45 $N_h > 5$—20	$>10^3$	Survey
Giyerula et al. [334]	$N_h \leqslant 5$—35 $N_h > 5$—23	$>10^3$	—
Barkow et al. [124]	$N_h \leqslant 5$—38 $N_h > 5$—19	$\sim 3.5\cdot10^3$	—
Lohrmann et al. [24]	$N_h \leqslant 5$—21 $N_h > 5$—23	~250	Energy of the primary particles by multiple scattering of nucleons from disintegrating nuclei
JCEF [340-342]	$N_h = 0,1$—68 $N_h \geqslant 2$—47	$\gtrsim 10^3$	—
Takibayev et al. [137] 335, 337]	$N_h < 2$—100 $N_h \geqslant 8$—157	10^2-10^5	Survey
Mishakova [338]	$N_h \leqslant 5$—13 $N_h > 5$—26	$10-10^4$	—
Tomashevskiy [339]	$N_h < 5$—105 $N_h > 8$—57	$>10^3$	Showers from α-particles
Imaeda [6]	$N_h < 5$ $N_h > 5$ } 227	>50	Survey of many papers
Zhdanov [343]	$N_h \leqslant 5$—53 $N_h > 5$—11	$(3-4)\cdot10^3$	—
Abraham et al. [38]	$N_h < 5$—32 $N_h \geqslant 5$—20	$\sim 10^3$	Showers from nucleons in nuclear fragmentation

a. Dependence of σ on γ_s and E_s. —Figure 62 shows the correlation field of the values of σ and γ_s (or E_s).* It is seen that events are encountered having

*Note that $\log\gamma_s = -\langle x_i \rangle = -\langle \log\tan\theta_i \rangle$. See Chapter 2 to find how accurately the energy of the primary particle E_s can be determined by using the value of γ_s.

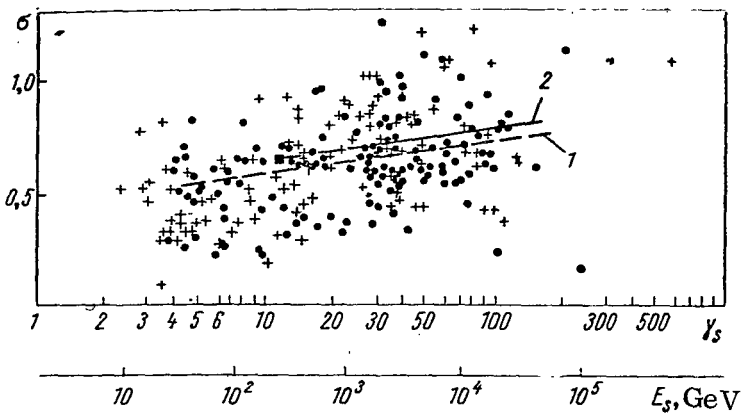

Figure 62. Dependence of the Dispersion of the Angular Distribution σ on γ_s (or E_s):

1—Averaged; 2—Normalized • — $N_h \leq 5$; + — $N_h > 5$); □ — Normalized Point.

values of the dispersion belonging both to the isotropic and the anistropic types of angular distribution at any energy of the primary particle.

An average over different energy intervals, separately for events considered to be quasi-nucleon-nucleon ($N_h \leqslant 5$) and nucleon-nucleus ($N_h > 5$) shows that there is a tendency for the degree of anistropy to increase with increasing energy of the primary particle. The dashed line in the figure runs through the obtained dependence of $<\sigma>$ on γ_s. It should be kept in mind that the absolute values of $<\sigma>$ will be somewhat higher if the errors inherent in the Castagnoli method are allowed for. However, the form of the dependence of $<\sigma>$ on γ_s at a sufficient distance from the threshold values remains unchanged. This effect was considered /256 in Chapter 2. The solid line in Fig. 62 represents the same dependence, but with allowance for threshold effects and normalized at the values $E_0 = 250$ GeV and $<\sigma> = 0.67$, taken from [24]. The energy of primary particles was measured by the multiple Coulomb scattering of the protons produced in the disintegration of the primary nuclei.

The obtained dependence of $<\sigma>$ on γ_s can be described by the function $<\sigma> = 0.15 \log \gamma_s + 0.40$.

b. Dependence of σ on n_s. —It is difficult to investigate this dependence on account of the superposition of effects associated with the growth of multiplicity with increasing energy and with the correlation between σ and γ_s. In order to decrease the influence of the latter dependence, we chose showers in a relatively narrow interval of γ_s ($23 < \gamma_s < 50$) and determined σ for events with multiplicity n_s equal to 4—8, 9—12, 13—16, 17—20, and $\geqslant 21$ for $N_h \leqslant 5$. We could not establish any dependence of σ on n_s at all.

*We used showers from JCEF collection [342] with $N_h \leqslant 5$.

Zhdanov [343] considered the change of σ with n_s in another range of n_s: $10<n_s\leqslant 19$; $20\leqslant n_s<40$ and $n_s\geqslant 40$. for showers with $N_h\leqslant 5$ and γ_s in the interval from 35 to 100, and noted a tendency for the degrees of anisotropy to decrease with increasing multiplicity.

If we select showers with low multiplicity $n_s<6$ and $N_h\leqslant 5$, we obtain for them, on the average, a somewhat higher dispersion. This result was obtained by Giyerula et al. [334, 345], who investigated showers formed with an energy of the order of 250 GeV from the disintegration of primary nuclei.

Showers from the JCEF collection, formed by nucleons of cosmic rays interacting with photoemulsion nuclei, were analyzed in [346, 347]. The Lorentz factor of the symmetric system in these interactions was relatively small (7-22). An increase in the dispersion with increasing n_s is observed, which is treated by the authors as the result of successive collisions of the nucleon with nucleons in the nucleus.

That this result contradicts the conclusions of the Landau theory is not surprising in this case, since one hardly expects the hydrodynamic ideas to apply /257 at these energies.

c. Increase of N_h.—In this case an increase in the dispersion is observed. This can be concluded both from a comparison of the function $\sigma(\gamma_s)$ for showers with $N_h\leqslant 5$ and $N_h>8$ [332, 333], and also from a study of the interactions specifically arising from the collision with heavy nuclei of a photoemulsion ($N_h>8$, $n_s>40$), $\gamma_s>23$ [348]. The dispersion of the angular distribution increases with an increase in the number of gray and black tracks.

This fact is in contradiction with the Landau theory, which predicts an increase in the degree of isotropy of the angular distribution with the mass of the target nucleus.

Along with this, the character of the function $\sigma(N_h)$ observed in experiment can be explained qualitatively, if one assumes the existence of an intranuclear cascade process.

d. Change of the form of the angular distribution with increasing dispersion.—Analysis of the form of the angular distribution for individual events divided into the two groups $\sigma<0.6$ and $\sigma>0.6$, shows that in the first group there are showers which have the normal Gaussian angular distribution in x-coordinates. Among the showers of the second group the deviation from the Gaussian form is more marked. A detailed analysis of the form of angular distributions is given in Section 5.

The conclusions of this section are valid in any coordinate system as long as angular distributions of charged particles for individual events in the x-representation are investigated. In subsequent sections we shall consider the specific peculiarities of angular distributions which arise in one or another of the coordinate systems.

4. Angular Distribution of Charged Particles in the Laboratory System of Coordinates

To a large extent, the properties of the angular distribution of charged particles in the laboratory coordinate system are determined by the kinematics of the collision. Thus, with increasing energy of the primary particle, the function $f(\theta)d\Omega$ becomes steeper, even if the dispersal of secondary particles in the C system is isotropic. The existence of anistropy in the C system is manifested /258
in the appearance of two cones of particles—a narrow one formed by particles going forwards in the C system, and a broad (diffuse) cone consisting of particles going backwards in the C system.

A consideration of the kinematics of the collision of particles leads to the conclusion that in the laboratory system all particles generated will be emitted between 0 and 90°, if their velocity in the C system does not exceed the velocity of the system itself. If the velocity of the particle β_c is greater than the velocity of the C system β_C and the particle flies backwards in the C system, then this particle will be emitted in the laboratory system at angles greater than 90° to the direction of motion of the primary particle.

Gerasimova [349] considered the emission of particles into the back hemisphere in the L system on the basis of the hydronamic picture of the collision. It was shown that the traveling shock wave evoked in the collision of a nucleon with a nucleus (or a nucleus with a nucleus) leads to the ejection of fast particles in the backward direction. Hence the study of relativistic particles flying in the backward hemisphere in the L system can serve as one more test of the validity of the hydrodynamic process in the collision of high energy particles.

A similar picture will be observed in the case when an excited nucleon (isobar) is formed during collision. In this case, because of the isotropy of the angular distribution of pions in the decay of isobars, emission of fast particles in the backward direction in the L system is also possible [350]. If the pions from isobar decay have on the average a greater magnitude of transverse momentum than pions originating as the result of the hydrodynamic process, then the emission angles of the backward pions in these two cases will be different.

In the majority of investigations of the angular distribution of secondaries, particles emitted backwards are usually not considered. Lohrmann [28] pointed to the existence of such particles. Out of 1571 secondaries, 26 particles were observed at emission angles $>90°$ in the L system.

Imaeda et al. [350] observed 5 showers out of 47 in which there were particles flying backwards. All these particles were identified as pions. The characteristics of these showers are indicated in Table 57.

The authors assume that these pions originate from isobars. The mass of /259
the isobars in this case must exceed 1500 MeV.

TABLE 57. CHARACTERISTICS OF SHOWERS WITH PARTICLES EMITTED BACKWARDS IN THE L SYSTEM

Shower type	γ_s	θ_i	T, MeV	MeV/c	θ_{is}	E_s, GeV
(0+1+12) p	8.9	117.4	87	159	3.29	2.74
(0+1+22) p	7.1	104.5	40.5	111	4.30	1.48
(1+0+12) n	17.4	130.0	81	130	1.98	4.69
(1+1+21) p	20.4	94.4	90	180	2.00	4.40
(0+1+17) p	52.2	132.0	65	112	0.40	15.8

Note: T is the kinetic energy of particles emitted backwards in the L system; E_s, θ_{is} are the total energy and emission angle of these particles in the S system (in the symmetric system).

5. Angular Distribution of Charged Particles in the Symmetric System (S System)

5.1. The S system and the x-representation

Study of individual events in the x-representation shows that the form of the distributions is symmetric in the majority of the cases. From this it follows that it is possible to find a coordinate system in which the dispersal of secondary charged particles will be symmetric relative to a plane perpendicular to the direction of motion of the primary particle.

The Lorentz factor of the symmetric system can be calculated either from the definition of the symmetric system ($\sum_{n_s} P_{is}=0$), or as the center of gravity of the x-distribution [16]:

$$\log \gamma_s = -\langle x_i \rangle = -\langle \log \tan \theta_i \rangle.$$

The first way is applicable if the nature of all the secondary charged particles is known and their momenta have been measured.

In the second way, the Lorentz factor of the symmetric system agrees with the Lorentz factor of the center-of-mass system provided the following conditions /260 are fulfilled: 1) all secondary particles are pions; 2) the velocities of secondary particles in the C system (β_{ic}) equal the velocity of the C-system (β_c); the secondary particles are emitted symmetrically relative to a plane perpendicular to the direction of motion of the primary particle.

In spite of the fact that it cannot always be proved that these conditions are fulfilled, in the majority of work with photoemulsions up until very recently, the Lorentz factor of the symmetric system has been identified with the Lorentz

factor of the C system. This leads to a distort on of some of the interaction characteristics. In order to avoid these distortions, we shall rigorously distinguish between the symmetric system and the center-of-mass system.

Inasmuch as the symmetric system is defined, as a rule, with the angular distribution of secondary charged particles as a starting point, the study of angular distributions in the S system does not add any new information, compared to the x-representation, that can help is elucidating the collision mechanism.

However, certain of the characteristics of the angular distribution examined in the x-representation acquire a new meaning when applied to the symmetric system.

Thus, the dispersion of the angular distribution, which in the x-representation characterizes the width of the distribution, can be considered in the symmetric system to be a measure of the anisotropy of the angular distribution of charged particles. This quantity is connected with the anisotropy index m (or n) in the approximation of the angular distribution in the form $\cos^m\theta_s$ (or $\sin^n\theta_s$) and depends on the velocity of the secondary particles in the symmetric system (see Fig. 9).

5.2. Form of the angular distribution

The study of the form of the angular distribution in the symmetric coordinate system receives very much attention in investigations using photoemulsion techniques. · Here, besides an examination of the individual angular distributions, an averaging process is carried out, amounting to the total distribution in the normalized coordinates $X=\log\gamma_s\tan\theta$.

Lindern [351], in a study of 22 showers registered in nuclear emulsion from /261
single charged or neutral primaries having an energy >20 GeV and number of gray and black tracks $N_h\leqslant 3$ was the first to construct the total differential angular distribution in X-coordinates and showed that the distribution is well approximated by a Gaussian curve with dispersion $<\sigma>=0.44\pm^{0.2}_{0.3}$.

Similar results are also obtained in other work done in approximately the same energy interval (up to ~500 GeV) [137, 215, 222, 338, 340]. The formula for the angular distribution in this energy region does not disclose any deviations from a distribution with a single maximum.* Thus, Ciok et al. [340] investigated showers in a wide energy interval of measured energies from 10^{10} to 10^{13} eV. If this result is confirmed in the energy region 10^{10}-10^{12} eV, then in going over to higher energies of the primary ($>10^{12}$ eV, measured by the Castagnoli method) a change in the form of the differential angular distributions was noticed. This is

*Takibayev [352] reports that even at $E_0\sim 25$ GeV, if one selects cases with $\sigma>0.6$ and parameter $D>0$ (see p. 210), the total angular distribution of these showers in the x-representation is obtained with two maxima.

manifested by the absence of tracks in the immediate vicinity of the angle $\pi/2$ in the symmetric system. In the differential distribution g(X)dX this fact is manifested as a deviation from the Gaussian curve.

This same group of authors subsequently [332, 334, 341, 344] undertook to analyze a wider selection of statistical material with the aim of showing that the experimental angular distribution of charged particles at primary particle energies $>10^3$ GeV differs from the Gaussian normal law.

To get a qualitative measure of this deviation, the total normalized angular distribution was constructed using the complete collection of streaks in normalized coordinates $\frac{x_i - \langle x_i \rangle}{\sigma} = \frac{X_i}{\sigma}$. The operation of dividing X_i by the halfwidth of the indivudual angular distribution σ eliminates the influence of the dependence of σ on γ_s on the total angular distribution and brings all distributions to a standard form with $\sigma = 1$. Intervals of X/σ were chosen such that for the normal law of distribution a constant number of tracks was contained in each interval. Then the distribution of the number of events over the coordinates X_i/σ for the Gaussian law should be represented by a straight line parallel to the axis of abscissas. Any deviation from the straight line (i.e., from the Gaussian law) can be easily detected. Figure 63 gives the total normalized angular distributions in these coordinates, constructed for events with $n_s \geqslant 6$, arising from single charged and neutral primary particles with energy $>10^3$ GeV, measured by the Castagnoli method. Data from papers by Giyerula et al. [332, 334] and the results of Coghen et al. [341] are considered. As a rule, the showers were sought among electromagnetic cascades. /262 /263

The distributions were given for the complete statistics and for various combinations of showers grouped according to the magnitude of the dispersion σ^2 and the number of gray and black tracks N_h.

A χ^2 analysis showed that the total distributions differed from the normal law by 2 to 3 standard deviations. The distribution for events with $\sigma > 0.6$ deviates from the Gaussian law, whereas the distribution for cases with $\sigma < 0.6$ can be described by a normal law (Fig. 63, a and b).

The possibility that all the observed distributions could be obtained fortuitously, as a result of statistical fluctuations in a single angular distribution, was checked. To do this, events were constructed by means of a random selection of the variables X by the Monte Carlo method, from the total angular distribution compiled for all showers in coordinates $X = x - \langle x \rangle$ (Fig. 64, b (1, 2)). As a result, showers were obtained that has the same distribution of n_s as in the experimental cases. These Monte Carlo showers were treated in the same way as the experimental ones. In Fig. 63c, the dashed line represents the distribution of these showers with respect to the variables X/σ. The difference between the experimental and synthetic distributions is of course reduced, but, as the χ^2 test shows, it amounts to about two standard deviations. The discrepancy between the Monte Carlo and experimental distributions convienced the authors that the angular distribution observed in individual cases is not simply a result of statistical fluctuations about the total angular distribution. /264

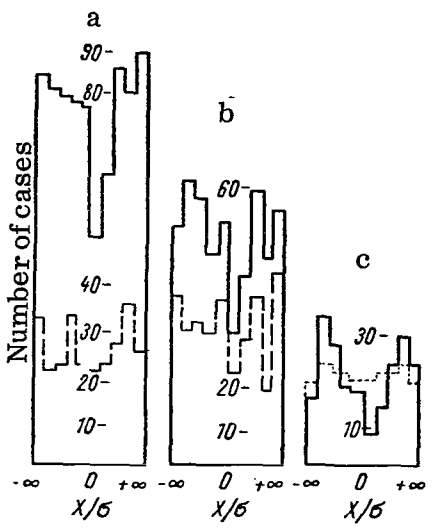

Figure 63. Total Normalized Angular Distribution in Coordinates X/σ. Constructed for Events with $N_h \leqslant 5$:

a—for Complete Statistics (Solid Histogram) and for Events with $\sigma<0.6$ (Dashed Histogram); b—for Events with $\sigma>0.6$: $n_s<20$ (Solid Histogram); the Same, for Events with $n_s<20$ (Dashed); c—for Monte Carlo Showers with $\sigma>0.6$ and $n_s>20$ (Dashed); Continuous Histogram for Observed Events with $\sigma>0.6$ and $n_s<20$.

The following quantity serves as another measure of the deviation of the experimental distribution from the normal law:

$$D = \frac{N_e - N_i}{N_e + N_i} = \frac{N_e - N_i}{n_s}$$

where N_i is the number of tracks in the internal interval $-0.67\sigma<X<+0.67\sigma$; N_e is the number in the external regions $X>0,67\sigma$ and $X<-0.67\sigma$ ($N_e=n_s-N_i$).

This quantity can be calculated for each individual event. For the normal distribution $N_e = N_i$ and $D = 0$. A non-zero value for D means that the distribution is not normal.

In [332, 334] values of D were calculated for showers with $N_h \leqslant 5$. $n_s<20$ and $n_s>20$, as well as for showers with $N_h>5$. The distribution of D as a function of the multiplicity of the event and its dispersion is shown in Fig. 65, a and c. For comparison, the quantity D as a function of σ for the Monte Carlo showers is presented in Fig. 65b.

Note that the distribution of experimental /265
showers with respect to D is assymetric in the number of positive and negative magnitudes of D, whereas the synthetic showers are distributed symmetrically. This asymmetry is due mainly to cases with $N_h>8$, for which practically all values of D are greater than zero.

Attention is directed to the fact that the magnitude of D increases with decreasing multiplicity n_s. The average value of D for case with $N_h \leqslant 5$, $n_s>20$ is +0.03, and for cases with $N_h \leqslant 5$, $n_s \leqslant 20$ it is +0.15.

On the basis of these data it may be concluded that a deviation of the angular distribution from normal is observed most frequently for showers arising from the collisions of primary particles with heavy nuclei (high N_h). Showers with $N_h<5$ and high multiplicity $n_s>20$ are well accommodated within the framework of the normal law. Among events with $N_h \leqslant 5$ and $n_s<20$ about 20% of the showers /266
cannot be described by the Gaussian distribution.

The total angular distribution in the differential form g(X)dX is a curve with a single maximum, but its shape does not correspond to a normal distribution with that value of dispersion obtained from experiment.

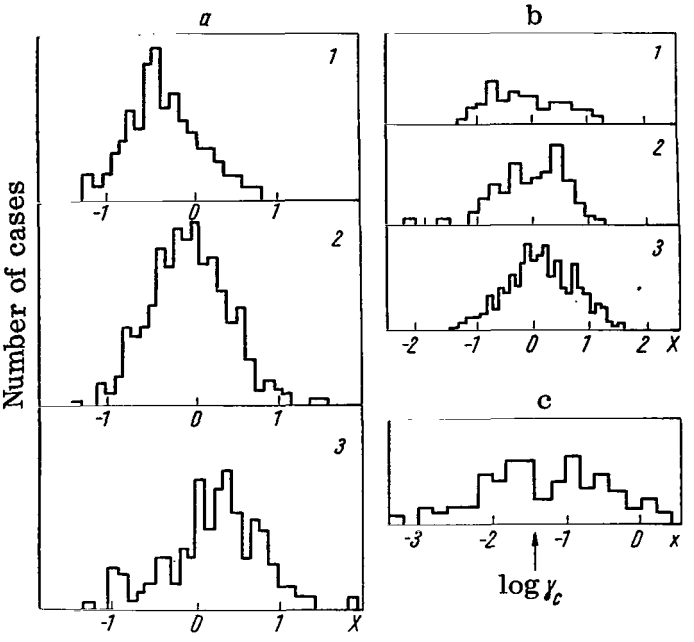

Figure 64. Total Angular Distributions in Coordinates $X=\log\gamma_c\tan\theta_i$ and x for Various Intervals of E_0 (or γ_c):

a—$E_0\approx30$ GeV, 1)—$1{,}4<\gamma_s/\gamma_c<2{,}8$; 2)—$0{,}7<\gamma_s/\gamma_c<1{,}4$, 3) $\gamma_s/\gamma_c<0.7$ [22]; b—from [24], $E_0\sim250$ GeV 1—$N_h\leqslant5$, $n_s<10$, 2—$N_h\leqslant5$, $n_s>10$, 3—$N_h>5$; c—Distribution over the X-Coordinate for Events with $E_0>1000$ GeV [25].

An investigation of the shape of the angular distribution in showers with very low multiplicity $n_s<6$, disclosed a definite deviation from the Gaussian curve and two distinct maxima in the angular distribution [334, 345].

However, in cases with higher multiplicity, the number of events with an angular distribution having two maxima is small. Such distributions appear at values of the dispersion $\sigma\geqslant0{,}9$. In these events the maxima are resolved, and the angular distribution of the secondary particles comprising each maximum can be analyzed.

This was done by Giyerula et al. [334]. From 54 showers, 8 events with $N_h\leqslant5$, $\sigma>0{,}9$ and $D>0$ were selected. The total number of tracks in these cases was 140. The total angular distribution in the F-representation for particles comprising each of the maxima appeared isotropic at first sight.* A similar

*Raczka [353] has shown that in certain cases a known anisotropic distribution has a similar form.

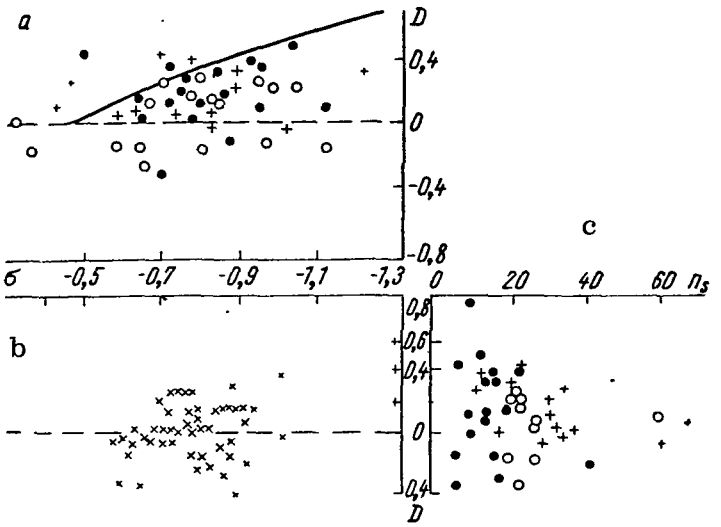

Figure 65. Dependence of the Distribution of D on the Multiplicity n_s of an Event and Its Dispersion σ. The Solid Lines Indicates the Dependence Expected on the Basis of the Two-Fireball Model of the Interaction. The X's Indicate the Values of D Calculated for Monte Carlo Showers:

● — $N_h \leqslant 5$, $n_s < 20$; ○ — $N_h \leqslant 5$, $n_s > 20$; + — $N_h > 8$.

analysis was made by Sanko [354]. He investigated showers with a two-maximum angular distribution. The separate maxima in the total angular distribution, taken in differential form g(X)dX, are well described by Gaussian curves, corresponding to an isotropic dispersal of particles with a power-law energy spectrum.

It is of interest to investigate the shape of the angular distribution for events among which one might expect the highest percentage of nucleon-nucleon interactions. This is an event with $N_h = 0$ or 1. From 119 showers contained in [332, 334, 24] were selected which satisfy this requirement and have $\sigma > 0.6$. The total normalized angular distribution for this group of cases differs from Gaussian /267 by more than two standard deviations.

Another group of events with $N_h > 8$ and $n_s > 40$, can undoubtedly be interpreted as a result of a collision of a primary particle with a heavy photoemulsion nucleus. Giyerula et al. [348] analyze the shape of the angular distribution for 14 such showers, formed singly by charged or neutral particles with a Castagnoli energy greater than 10^3 GeV. The distribution is three standard deviations away from a Gaussian. The sharp noncorrespondence of the angular distribution with the normal law shows up in the fact that for the majority of the events $D > 0$ (in eleven cases $D > 0$, in three $D < 0$). The wider the angular distribution, the more it differs from the normal law.

Of the 14 showers, six have an angular distribution with a clear two-maximum character. In these cases one can investigate separately the characteristics of both maxima, assuming that in the dispersal of particles in the symmetric system one of them is formed by particles of the narrow cone and the other by particles of the wide cone.

The characteristics of these events are given in Table 58.

TABLE 58. CHARACTERISTICS OF SHOWERS HAVING AN ANGULAR DISTRIBUTION WITH TWO MAXIMA

Shower type	ν_s	σ	n_1	n_2	σ_1	σ_2
14+52 n	28	0.81	16	36	0.29	0.52
35+59 p	23	0.91	33	26	0.29	0.52
16+57 p	29	0.96	18	39	0.24	0.54
20+56 p	28	1.03	24	30	0.32	0.56
17+41 p	58	1.09	17	24	0.32	0.58
23+47 p	83	1.25	24	23	0.40	0.62
Average values			22	28	0.34	0.53

Note: Here n_1, n_2 and σ^2_1, σ^2_2 are the multiplicities and dispersions for the narrow and wide cones, respectively.

Attention is directed to the slight asymmetry in the angular distributions /268
and multiplicities for particles of the narrow and wide cones $\sigma_1<\sigma_2$ and $n_1<n_2$. In addition, one sees an increase in σ^2 with an increase in the number of gray and black tracks N_h. These features may be a consequence of secondary interactions within the target nucleus.

By a comparison of the shape of the angular distributions obtained for different groups of events, one can establish a firm deviation of the angular distribution from the normal law for all groups. The exceptions are events with $N_h \leqslant 5$ and $n_s>20$, which agree well with the Gaussian distribution. Whereas showers with $N_h \leqslant 5$ and $n_s<20$ have the same character of angular distribution as events with $N_h>8$, the difference between them is manifested only in higher values of the dispersion for the latter group of events, which originate in interactions with heavy nuclei.

5.3. Dependence of the form of the angular distribution on the nature of the primary particles

The form of the angular distribution in showers formed by secondary charged particles (mostly pions), does not differ in any way from that observed in showers produced by primary nucleons. For the 29 showers from charged secondaries

and 10 from neutrals studied by Jain [355], the angular distribution of the generated particles in the symmetric system has an anisotropic character. The dispersion of the angular distribution increases with increasing γ_s. Showers with $\sigma \geqslant 0.4$ give an angular distribution in the X-representation differing in shape from the normal distribution. In an analysis of showers arising from primary α-particles [339], deviations of the angular distributions of secondary particles from the normal distribution law were observed, and events having two maxima in the angular distribution were found. It should be noted that in the collision of an α-particle with a nucleus, two of the four nucleons contained within the α-particle interact, on the average simultaneously.

5.4. Interpretation of results from the study of angular distributions in the symmetric coordinate system /269

These are the principal features of the angular distributions of secondary particles in the symmetric system of the collision at energies of the primaries greater than 10^3 GeV:

1. There is a large scatter of the anisotropy parameters σ for closely similar values of the Lorentz factor of the symmetric system γ_s.

2. The differential form of the angular distribution g(X)dX deviates from the Gaussian formal distribution for anisotropy parameters $\sigma > 0.6$.

3. Sometimes the deviation from the Gaussian law is observed in the appearance of structure in the angular distribution of secondary particles with two maxima. The maxima are most clearly resolved in distributions constructed for events with low multiplicity ($n_s \leqslant 6$, $N_h \leqslant 5$) and for cases of collision with heavy nuclei ($n_s > 40$, $N_h > 8$).

4. The greater the anisotropy parameter σ, the more distinct is the structure of angular distributions with two maxima.

5. If it is possible to separate the maxima of the function g(X), then the distribution of particles in the coordinate system fixed to the center of gravity of an individual maximum is nearly isotropic.

These properties of the angular distributions and the identification of the symmetric system with the center-of-mass system of the colliding particles led to the phenomenological picture of the collision known as the fireball model [325, 327, 328]. At first, the fireball model arose as a working hypothesis to explain the two maxima in the differential angular distribution of the secondary particles. In this two-fireball model it is assumed that during the collision of nucleons two agglomerates of excited material are formed (two fireballs) which more in opposite directions in the C system with equal velocities. Each of agglomerates decomposes isotropically into pions in its own rest system. The nucleons which have collided do not enter into the excited agglomerates and move independently of them.

Let us consider what new characteristics of the interaction appear as a result of the introduction of the two-fireball mode. One of these is the Lorentz factor of the fireball relative to the C system of the colliding particles $\bar{\gamma}$. If β_1 and β_2 are the velocities and γ_1 and γ_2 are the corresponding Lorentz factors of the fireballs in the laboratory coordinate system, then /270

$$\bar{\gamma} = \frac{\gamma_1 + \gamma_2}{2\sqrt{\gamma_1\gamma_2}}, \qquad (9.4)$$

where $\log\gamma_1 = \langle x_i\rangle_1, \log\gamma_2 = \langle x_i\rangle_2$. The greater the magnitude of γ, the more strongly does the fireball diverge before its own decay into pions and the more distinct does the structure in the differential angular distribution of secondary particles with two maxima appear. According to the two-fireball model, there ought to be an increase in the Lorentz factor of the fireball $\bar{\gamma}$ with increasing collision energy.

In one of the first papers [6] on the investigation of $\bar{\gamma}$ factors for showers with different γ_s, it was found that when $\gamma_s<10$ $\bar{\gamma}<2.2$, whereas for $\gamma_s>40$ $\bar{\gamma}$ varies from 1 to 9, and when $\gamma_s>100$, there are values of $\bar{\gamma}=10$. The statistical reliability of this result was not high. It was also noted that $\bar{\gamma}$ falls with increasing multiplicity [6, 356]. However, in an examination of showers having $N_h = 0$ or 1 from the JCEF collection [342], no such dependence of $\bar{\gamma}$ on γ_s was observed.

The motion of the fireballs in the C system should lead to the appearance of azimuthal anisotropy in the angular distribution of the secondary particles. This effect was studied in a number of papers [354, 357-360].

An analysis was made of the anisotropy for showers with $\sigma>0.6$ [354]. The result is shown in Fig. 66. The χ^2 test shows that the azimuthal distribution differs from isotropic, but as the mass of the target nucleus increases, the degree of anisotropy falls. The target diagram in the plane perpendicular to the direction of motion of the primary particle has an elliptical shape for these showers, which is evidence for the transfer of angular momentum to the secondary particles.

In work by Mishakova and Nikol'skiy [358], azimuthal anisotropy of the angular distribution was found for showers formed by pions. /271

The essential parameter of the fireball model is the mass of the fireball. Most advocates of this model are inclined to believe that the mass of the fireball remains constant. At the same time, estimates made in different papers indicate differences and vary from 2 to 10 GeV.

An alternative explanation of the observed features of the angular distribution can be proposed, based on an entirely different picture of the collision. It consists of the following. If a single excited system is formed in the collision, to which a large angular momentum is transferred, than when it decays into pions the angular distribution of the secondaries will have an anisotropy of the form $\cos^m\theta_c$. The more angular momentum the system acquires, the greater is m. In

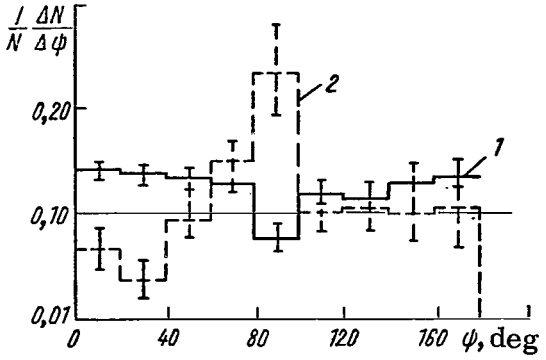

Figure 66. Azimuthal Angular Distribution in the Laboratory System:

1—for Showers with $N_h > 2$; 2—for Showers with $N_h < 2$. The Horizontal Straight Line is for an Isotropic Angular Distribution.

going over to the x-representation, the distribution $f(\theta_c)\, d\Omega_c = A \cos^m \theta_c\, d \cos \theta_c$ in the system will appear as a distribution with two maxima. In doing this, it is possible to introduce a quantity analogous to the $\bar{\gamma}$ factor of the fireball which will characterize in a given case the spacing between the two maxima in the g(x) distribution. Its value can be found from Eq. (9.4), in which /272

$$\log \gamma_1 = \log \gamma_s + \frac{1}{2} \log (m+1);$$
$$\log \gamma_2 = \log \gamma_s - \frac{1}{2} \log (m+1). \qquad (9.5)$$

A detailed treatment of the collision process based on field ideas was undertaken in a theoretical paper by Raczka [353]. By examining a collision with transfer of large amounts of angular momentum, they found that the angular distribution of secondary particles in the x-representation has a two-maximum structure, and the distribution of particles within the limits of each maximum in the F-representation is grouped about straight lines with a slope of 2. The separation between the maxima increases with increasing energy. Thus, these two ways of describing the collision process are experimentally equivalent, and the fireball model has no advantages over the model of a motionless agglomerate with high angular momentum.

5.5. Multi-fireball model (H-quanta)

By analyzing the angular distribution of secondary particles with respect to the scale $x = \log \tan \frac{\theta}{2}$ and observing the existence of irregularities in the x-representation, Hasegawa [313, 361] introduced a hypothesis about the existence of fundamental solitary formations, which he called H-quanta, making up the fine

structure of the angular distribution in the x-representation. He isolated along the x scale groups of particles with close values of $\log\tan\theta_i$ and more or less distinctly separated from other similar groups (each such group forms an H-quantum). From the point of view of this hypothesis, multiple production of secondary particles goes via the generation of H-quanta. Only an even number of H-quanta symmetrically emitted in the C system of the collision can arise. Each H-quantum subsequently decays independently into pions. The critical energy at which emission of H-quanta begins is estimated to be equal to 50 GeV.

In Fig. 61c are shown typical examples of the decomposition of angular distributions into H-quanta. Angular distributions of secondary particles were constructed in the rest system of each quantum. The Lorentz factor of the rest system was determined from the relation $\log\gamma_H = \frac{-1}{n_H}\Sigma\log\tan\theta_i$. These distributions in the F-representation have a dipolar character of the type $\sin^2\theta_c\, d(\cos\theta_c)$. /273

The mass of an H-quantum is determined from the distribution over the number of particles in each of the identified H-quanta and the distribution of the transverse momenta of the secondary particles. The average number of charged particles making up an H-quantum is 4.1 ± 1.2 for 377 identified H-quanta. If the average value of the transverse momentum is taken to be $\langle p_\perp \rangle \sim 0.4$ GeV/c and neutral pions are allowed for, then the mass of the H-quantum will be of the order $2\ Mc^2$ (M is the nucleon mass).

In view of the fact that H-quanta are emitted symmetrically in the C system of the colliding nucleons, it follows that $\gamma_H = m_i\gamma_c$ for the H-quanta flying forwards, and $\gamma_H = \frac{1}{m_i}\gamma_c$ for the H-quanta flying backwards. From this, $m_i = \gamma_{Hi}/\gamma_c$. Then for the Lorentz factor of the i-th H-quantum in the C system, we find

$$\bar{\gamma}_{Hi} = \frac{1}{2}\left(m_i + \frac{1}{m_i}\right),$$

where m_i is some number.

The distribution of m_i has distinct maxima. This gave the author of the hypothesis the idea that the Lorentz factor of the H-quantum in the C system is quantized, and the quantized values for $\bar{\gamma}_{H_i}$ are 1.4, 7.1, 41, 240 etc. The existence of high levels ($\bar{\gamma}_{H_i} = 41$) is not well borne out in available experimental data. Hasegawa believes that the generation of H-quanta in the collision of high-energy particles can explain many experimental peculiarities of the interactions over the whole energy range.

The weakest point of the theory is where it begins—the reliability of the division into isolated particle groups with the aid of the x-representation and the proof of the fact that the particles in these groups are genetically related. A criticism of this hypothesis from these points of view was made in [362].

It should be mentioned that the idea of the generation of particles as a result of the isotropic decay of many centers arising in the interaction was expressed also in the works of Zatsepin [311].

6. System of the Center of Mass of the Colliding Particles

6.1. Introduction

The angular distribution in the system of the center of mass of the colliding particles (C system) is of the most interest for the elucidation of the mechanism of multiple particle production. It is precisely in this coordinate system that we can speak of isotropic or anisotropic dispersal of the created particles and find the degree of anisotropy, as well as discover whether the dispersal of the secondary particles is symmetric or the angular distribution has an asymmetric character.

To define the C system it is necessary to know the nature of the colliding particles and the energy of the incoming particle. The Lorentz factor of the C system can be determined by using (2.36), which is a consequence of the laws for the conservation of energy and momentum. For very high energies of the primary particles satisfying the condition $\gamma_0 \gg M_1, M_2$, we obtain

$$\gamma_c = \sqrt{\frac{E_0}{2M_2}}.$$

From this it is seen that at high energies the mass of the in-flying particle does not affect the kinematics of the collision, whereas the mass of the target nucleus plays a decisive role. Information about the nature of the target particle is frequently uncertain, both in accelerator and cosmic ray experiments. This is particularly true of work with photoemulsions. The use of apparatus which utilizes a Wilson chamber to register secondary interactions has certain advantages. In this case, one places a filter-generator made of a homogeneous material above the chamber; collisions with the nuclei of this filter generate showers. However, this method has its own difficulties associated with the occurrence of successive collisions either in the nucleus itself (if it is a heavy one) or due to secondary interactions within the filter. These effects cannot always be detected in an experiment, but they lead to a distortion of the angular distribution of the secondary particles. /275

Methods of the determination of energy in cosmic ray experiments were detailed in Chapters 2 and 3. In examining the angular distribution of secondary particles in the C system we shall make use of the results of only those works in which reliable methods for measuring energy were employed (see Chapter 3, Section 6).

6.2. Asymmetric dispersal of particles in the C system

The study of the angular distribution of secondary particles in the C system gives new information about the character of the collision processes of high-energy particles. By definition, the C system is itself a symmetric system. The emergence of any asymmetry in an experiment is due first of all to the limitations of our knowledge about the parameters of the colliding particles and the newly created ones. Hence, an examination of collision processes in the C system gives the possibility of discovering new properties of the interaction.

For the investigation of collision symmetry we may introduce the following parameters:

1. The asymmetry in the number of charged particles flying forwards and backwards along the direction of motion of the primary particle can be defined as the quantity

$$a = \frac{n_{sf} - n_{sb}}{n_{sf} + n_{sb}}$$

(n_{sf} and n_{sb} are the numbers of particles scattered forward and backward, respectively). For a collision that is symmetric in the C system, a = 0. This asymmetry criterion can be applied with confidence only for cases with high multiplicity.

2. The ratio of the coefficients of inelasticity K and K_M in the laboratory and mirror systems. By definition, $K = \frac{\Sigma\varepsilon_i}{E_0}$, where E_0 and ε_i are the energies of the primary and created particles in the laboratory coordinate system. Analogously, $K_M = \frac{\Sigma\varepsilon_{iM}}{E_{0M}}$, where E_{0M} and ε_{iM} are the same quantities, but in the mirror system. This ratio can be defined in terms of quantities measured in the laboratory system:

$$\frac{K}{K_M} = \frac{\Sigma\varepsilon_i m_2 c^2}{E_0 \Sigma (\varepsilon_i - p_i c \cos\theta_i)}, \qquad (9.6)$$

where m_2 is the mass of the target particle (the summation must be carried out over all created particles). For a symmetrical shower $K/K_M = 1$. If $K/K_M > 1$ or $K/K_M < 1$, the showers are considered to be asymmetrical forward or backwards, respectively.

3. The most natural measure of asymmetry of the angular distribution, particularly when it is studied in the x-representation, is the comparision of the values of the Lorentz factors of the C system and the symmetric system. The Lorentz factor of the particles in x-coordinates: $\log \gamma_s = -\langle x \rangle$. Thus, if the Lorentz factor of the C system is known, then the difference $\log \gamma_s - \log \gamma_c = \log \gamma_s/\gamma_c$ characterizes the deviation of the angular distribution in the C system from a symmetrical distribution. If $\log \frac{\gamma_s}{\gamma_c} = 0$, then $\frac{\gamma_s}{\gamma_c} = 1$ and we have a symmetrical emission of particles in the C system. For values of the ratio $\frac{\gamma_s}{\gamma_c} > 1$ or $\gamma_s/\gamma_c < 1$, emission of particles is observed predominately forwards or backwards.

For the determination of the Lorentz factor of the S system it is desirable to take into account the momentum distribution of the secondary particles. Then one of the trivial sources of asymmetry, momentum fluctuations of the secondary particles, will not affect the magnitude of the ratio γ_s/γ_c.

If the momenta of the secondary particles are not measured, then by using the prescription proposed by Shen and Kaplon [10] (see Chapter 2, Section 4), one can take the velocities of the particles into account. In this case, the supposition of the equality of the velocities of the secondary particles in the symmetric system ($\beta_{is} = \beta_s$) is replaced by another condition, according to which $\beta_s = \langle \rho \rangle \beta_{is}$, $\langle \rho \rangle \neq 1$. In addition, it is assumed that the average transverse momentum of the secondary particles is a constant. The ratio γ_s'/γ_c determined after this will reflect an asymmetry associated with less trivial sources. /277

One of such sources can be an incorrectly chosen mass of the target particle for the determination of γ_c. For example, if the Lorentz factor γ_c is based on the presumption of a collision of a primary particle of known energy E_0 with a nucleon, i.e., $\gamma_c = E_0/2M_p$, then the ratio

$$\frac{\gamma_s'}{\gamma_c} = \sqrt{\frac{M_p}{M_2}}$$

will depend on the mass of the target particle M_2.

6.3. Study of asymmetrical dispersal of particles with the aid of the parameter a

Asymmetrical emission of charged particles in the C system was first observed in work [12, 136, 260, 363] done on Pamir (3860 m above sea level) using a Wilson chamber in a magnetic field and an ionization calorimeter. The authors assumed that the primary particles in these experiments were nucleons. Lithium hydride (LiH) served as the target. The average energy of the primary particles was 250 GeV.

The parameter a was selected as the measure of asymmetry. The experimentally observed distribution of showers with respect to this parameter was compared with the distribution calculated under the assumption that the flight of

particles in the forward and backward hemispheres was equally probable and statistically independent. The calculations were carried out with and without allowance for the laws of conservation of energy, momentum, and charges of the particles [364] (Table 59).

Based on the data of Table 59, it was concluded in [364] than an explanation of the nonsymmetrical showers solely by statistical fluctuations in the emission of charged and neutral particles should be rejected. A significant assumption in the calculations was the use of results of the statistical theory of particle production for the determination of the probability of observation of a shower with a given number of secondary particles.

TABLE 59. DISTRIBUTION OF SHOWERS WITH RESPECT TO THE ASYMMETRY PARAMETER

/278

a	Calculation for N-N collisions		Experiment
	Considering the law of conservation	Without considering the law of conservation	
0÷0.25	64	54	37
0.25÷0.50	27	30	26
0.50÷0.75	8	13	26
0.75÷1.00	1	3	11

As is known, the statistical theory predicts a quasiuniform distribution of energy among the secondary particles. At the same time, in an experiment, as a rule, one observes a particle that bears away a large fraction of the primary energy (see Chapter 8).

Hence, it is necessary to check whether or not the observed asymmetry of the angular distribution is a consequence of the energetic isolation of a few particles. This was indeed done in [365]. It was presumed that on the average the interaction act is standard, but an individual cases significant fluctuations are possible. The following simplifying assumptions were introduced for quantitative estimates:

a) it was assumed that the energy distribution of secondary particles moving in the C system in the direction of motion does not depend on the energy distribution of particles moving backwards. The only connection there is the conservation law for momentum $\sum_i P_{iB}=\sum_i P_{iH}$, P_{iB}; and P_{iH} are the momenta of particles scattering forward and backward, respectively;

b) the following definitions were used for the fraction of energy transferred to all secondary particles, with the exception of the fastest particle: $\varkappa_B=\frac{2\Sigma\varepsilon_{ic}^B}{E_{0c}}$ for particles moving forwards; $\varkappa_H=\frac{2\Sigma\varepsilon_{ic}^H}{E_{0c}}$; for particles moving backwards;

c) it was further assumed that the distribution of these quantities $f(x) = 1$ and $\langle x_B \rangle = \langle x_H \rangle = 0.5$, and all secondary particles, except the fastest, have identical energy;

d) the number of secondary particles flying in the C system forward and backward was found under the assumption that they were all charged. According to the Fermi-Landau model, the multiplicity will equal $n_{sf} = A\left(\frac{E_{0c}}{2}\right)^{1/2} x_f^{1/2}$, $n_{sb} = A\left(\frac{E_{0c}}{2}\right)^{1/2} x_b^{1/2}$.

Under these conditions the probability $W_1(n_{sf})$ that n_{sf} particles are emitted forwards $W_1(n_{sf}) = \frac{An_{sf}}{A^2 E_{0c}}$, and backwards $W_2(n_{sb}) = \frac{An_{sb}}{A^2 E_{0c}}$. If on the average the numbers of particles flying forward and backward are equal $\langle n_{sf} \rangle = \langle n_{sb} \rangle = \frac{\Sigma_i}{n} = \frac{n+1}{2}$, where n is the maximum possible number of particles for a given energy, then $A^2 = \frac{2n(n+1)}{E_{0c}}$, $n_{sf} = \frac{2n+1}{E_{0c}}$. In this case the average value of the asymmetry coefficient

$$|a| = \left| \frac{n_{sf} - n_{sb}}{n_{sf} + n_{sb}} \right|$$

will be

$$\langle a \rangle = 2 \sum_{n_{sf}} \sum_{n_{sb}} a W_1 W_2 = 2 \left(\frac{4}{A^2 E_{0c}} \right)^2 \times$$
$$\times \sum_{n_{sf}=1}^{n} n_{sf} \sum n_{sb} \frac{n_{sf} - n_{sb}}{n_{sf} + n_{sb}},$$

if $n_{sf} \gg 1$ then $\langle a \rangle = 2\left(0.1 + \frac{2}{3n_{sB}}\right)$. Assuming $n_{sf} = 5$, we obtain $\langle a \rangle = 0.4$. This agrees with experiment (see [364]).

Thus, the asymmetry of the angular distribution observed in the C system may be a simple consequence of the nonuniform distribution of particles with respect to energy.

This conclusion is confirmed by the existence of a correlation between the ratios of the coefficients of inelasticity (K/K_M) and the parameter a, found in [12]. The means of determining K and K_M in [12] are such that one can put an

equal sign between K and $\varkappa_f$ and between K_M and $\varkappa_b$. At the same time, for the observation of collision asymmetry not associated with the isolation of particles with respect to energy, it is necessary to use the values of inelasticity calculated from Eq. (9.6).

6.4. Distribution with respect to γ_s/γ_c

We now turn to an analysis of the asymmetry of the angular distribution of particles in the C system, based on an investigation of distributions with respect to the quantity $\log \frac{\gamma_s}{\gamma_c}$.

This was considered both in experiments in accelerators [230, 366-373, 121] and in cosmic ray experiments [20, 22, 24, 34, 38, 122, 341, 374]. In cosmic ray work, a necessary condition for carrying out this analysis is the determination of the energy of the interacting particles not from the angular distribution, but calorimetrically or from the fragmentation of heavy nuclei.

Accelerator experiments give the distribution over $\log \gamma_s$ for showers formed by nucleons or pions of controlled energy. Since photoemulsions are used to register the interactions, the mass of the target particle is unknown in these experiments.

To determine γ_s the Lorentz factor of the symmetric symmetric system, one applies either the Castagnoli or Shen and Kaplon method, or one used information about the momenta of the secondary particles, and the velocity of the symmetry system relative to the L system is found from the definition of the symmetric system:

$$\beta_s = \frac{\Sigma p_i c \cos \theta_i}{\Sigma \varepsilon_i}.$$

If the angular distribution of secondary charged particles in individual cases is symmetric in the C system of the colliding particles, then we should obtain a symmetric distribution of $\log \gamma_s$ around the known (usually to within 10%) value of $\log \gamma_c$.

Deviation of $\log \gamma_s$ from the average value is due to a number of reasons:

1. First of all, there are natural fluctuations in the angular distribution of the secondary particles. If this distribution in x-representation is described by a Gaussian law with standard deviation σ, then the distribution of $\log \gamma_s$ will also be of the Gaussian type with halfwidth $\sigma/\sqrt{n_s}$ [16]. /281

2. A broadening of the distribution of $\log \gamma_s$ can occur because of errors associated with the measurement of the emission angles of the secondary particles.

3. The halfwidth of the distribution can increase on account of a difference between the velocities of motion of the secondary particles β_{is} and the velocity of the S system β_s.

4. The broadening may be due to the Fermi motion of nucleons in the nucleus.

5. The presence of any kind of asymmetry in the angular distribution of the secondary particles also leads to a broadening of the distribution over $\log \gamma_s$.

In experiments with cosmic particles, we considered, in place of the distribution over $\log \gamma_s$, the distribution over $\log \frac{\gamma_s}{\gamma_c}$,* thus reducing showers arising from particles of different energies to a single value of primary energy. The accuracy of the determination of primary particle by reliable methods is completely satisfactory ($\sim 20\%$); hence the principal error in the determination of γ_c may be associated with the assumption about the nature of the colliding particles. Usually it is assumed that a nucleon-nucleon collision has taken place. If in reality any other kind of particle collided, this will lead to a significant broadening of the distribution under consideration.

Distributions of $\log \gamma_s$ or $\log \frac{\gamma_s}{\gamma_c}$ are of interest from the viewpoint of explaining the nontrivial reasons for them. In this connection, we shall treat the sources numbered 1 through 4 above as trivial and examine in more detail the possible reasons for asymmetry in the angular distribution of secondary particles (see Chapter 5).

The principal causes for asymmetric showers could be: /282

1. In an experiment only charged particles are registered, as a rule. If the neutral particles are not taken into account, this may lead to a symmetrical shower looking like an asymmetrical one. This apparent asymmetry is a consequence of the noncoincidence of the angular distributions of charged and neutral particles in individual cases.

2. The creation of a small number of energetically isolated particles may also be a source of asymmetrical showers. If such an energetically isolated particle is emitted in the C system of the collision in one direction, then the remaining particles will move in the opposite direction in order to compensate the momentum borne by the particle.

3. It is usually assumed that the collision is nucleon-nucleon (if the nature of the primary particle is unknown). But if in reality particles of different mass

*Sometimes instead of the ratio of the Lorentz factors γ_s/γ_c we use the ratio of energies E_s/E_0, where E_s is the energy of the primary particle found by the Castagnoli method, or $E_s = 1.5 \cdot \Sigma \varepsilon_{is}$, where ε_{is} is the energy of a secondary particle in the S system, E_0 is determined by one of the reliable methods.

collide, an asymmetry arises in the C system, which was defined under the condition of equality of the masses of the colliding particles.

4. Motion of the symmetric system relative to the C system with velocity β_{sc} (if such exists) leads to the appearance of additional velocity on the particle in the C system and, depending on which direction the symmetric system moves, will evoke either asymmetry forwards ($\beta_{sc}>0$) or asymmetry backwards ($\beta_{sc}<0$).

To establish the existence of such motion is not a simple task. Hence it is different to distinguish this source of asymmetry from the preceding one associated with the different nature of the colliding particles.

Obviously, as the primary particle energy increases, the velocity β_{sc} of the symmetric system relative to the C system must increase. At the same time, the asymmetry associated with the mass of the target particle should not depend on the energy of the primary particle. The presence or absence of such a dependence should be of assistance in distinguishing these two sources of asymmetry.

The investigations of Castagnoli et al. [372a, 372] were done in an accelerator at an energy of primary protons of 27 GeV. A photoemulsion was used to register proton-nucleon inelastic interactions, as well as collisions with light ($N_h=2.\ 3.\ 4$) and heavy ($N_h>8$) nuclei. Cases with $n_s\geqslant 4$ were selected. The distribution for light nuclei was symmetrical relative to the value $<\log \gamma_s>=0.59\pm 0.02$, which corresponds to assuming collision with a target of nucleonic mass. In the distribution for heavy nuclei there is no similar symmetry, and the average value $<\log \gamma_s>=0.38\pm>=0.38\pm 0.02$, pertains to collision with three nucleons in nucleus, on the average.

Thus, the distribution of the values of $\log \gamma_s$ is sensitive to the mass of the target particle. This conclusion is confirmed also by the results of Lohrmann et al. [24] and of Yerofeyeva et al. [34].

In [34] an ionization calorimeter was used to measure the energy of the primary particles. The emission angles of the charged particles were determined in a Wilson chamber. In addition, it was possible to measure the energy given up to neutral pions and to determine the charge on the primary particle (Fig. 15a).

The distribution over $\log \frac{\gamma_s'}{\gamma_c}$ for interactions with nuclei in graphite is illus- /284

trated in Fig. 67. Recall that γ_s' differs from γ_s in that the average velocity of the secondary particles in the symmetric system is taken into account in the first case.

Attention is called to the existence of two maxima in the distribution over $\log \frac{\gamma_s'}{\gamma_c}$ for interactions in graphite. The right-hand maximum corresponds to showers that are asymmetrical forwards. The central maximum consists of symmetricalshowers, and finally on the left are several events that are asymmetrical in the backward direction. The scale on the abscissa was chosen under the assumption of a nucleon-nucleon collision.

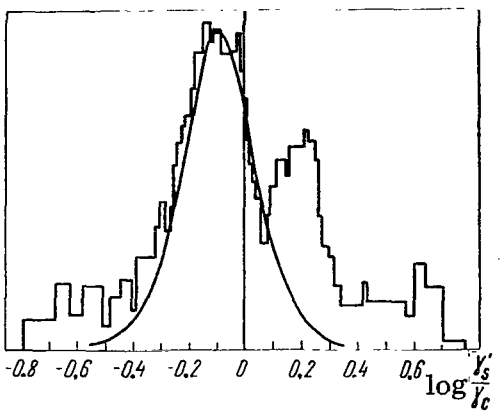

Figure 67. Distributions Over $\log \gamma'_s/\gamma_c$ for Interactions of Nuclear-Active Particles in Graphite. The Smooth Curve is a Gaussian Distribution with Halfwidth $\Delta \log \gamma'_s/\gamma_c = 0.16$.

An estimate of the width of the distribution of $\log \frac{\gamma'_s}{\gamma_c}$ for symmetrical events with account taken of possible errors in the measurement of the emission angles of the secondary particles and of fluctuations in the angular distributions gives the value $\Delta \log \frac{\gamma'_s}{\gamma_c} = 0.16$. This value was used in constructing the Gaussian distribution shown in the figure.

All the interactions were divided into groups according the asymmetry type, and their parameters are presented in Table 60.

The following pecularities are of interest:

1) the number of showers that are asymmetric forward is greater than the number asymmetric backward; 2) showers that are asymmetric forward are produced predominately by charged particles; 3) the multiplicity of showers that are asymmetric forward is less than the multiplicity of the showers of the other group.

The group of showers that are asymmetric backwards in collision with light nuclei in graphite deserves particular attention (see Fig. 67). If one considers them as the result of a collision of a particle with the nucleus of an atom, then he would have to assume that about six nucleons of the target nucleus participate simultaneously in the collision. At the same time, in these showers are notices an anomalously high value for the fraction of energy transferred to γ-quanta (α_0). Thus, it may be assumed that here we have to do with a new form of asymmetry (where the number of particles flying forward and backward is the same, but all the neutrals go forward and the charged particles go backward).

Corroboration of this interpretation can be found in a study of the angular distribution of this group of events. Figure 68 shows the total angular distribution in the x-representation. This has the form of a typical two-maximum distribution; however, all the charged particles in these showers are emitted backwards. In the forward direction we have π^0-mesons, since $\alpha_0 \approx 0.7$.

The peculiarities touched upon in the discussion of Table 60 permit the conclusion that it is most likely that symmetrical showers are produced by cosmic particles (nucleons and pions) on individual nucleons of the light nucleus, whereas the showers that are asymmetrical forwards are produced more often by /287
pions in collision with a target of smaller mass than the nucleon. This could be pions or kaons of the meson cloud surrounding the nucleon [375]. The angular distribution of shower particles for these interactions, constructed in the C

TABLE 60. PARAMETERS OF SHOWERS PRODUCED BY NUCLEAR-ACTIVE PARTICLES IN COLLISION WITH NUCLEI IN GRAPHITE

Asymmetry type*	No. of cases	$\langle E_0 \rangle$, GeV	$\langle n_s \rangle$	Nature of primary particles: charged	neutral	undetermined	$\langle \alpha_0 \rangle$
Backward $\left(\log\frac{\gamma_s'}{\gamma_c} < -0.3\right)$	4	290±90	12±3.5	2	1	1	0.66±0.06
Symmetrical $\left(-0.3 < \log\frac{\gamma_s'}{\gamma_c} < 0.1\right)$	20	200±10	14.3±0.5	7	7	6	0.41±0.01
Forward $\left(\log\frac{\gamma_s'}{\gamma_c} > 0.1\right)$	10	160±20	6.6±1.0	7	1	2	0.59±0.08

*The choice of bounds for the symmetrical events was made with allowance for the fact that collision with a light nucleus was observed.

system of the π-π (or N-π) collision has a symmetrical form. It may be assumed that these events are the result of peripheral collisions. Such as interpretation agrees with the conclusions of work done at lower energies to 30 GeV, both in cosmic rays [22, 122] and in accelerators, [367, 369-372, 372a] where the primary particles were pions.

In Fig. 69 are given the results of Gainotti et al. [371], who studied the collision of negative pions with energy 16.2 GeV with nucleons in photoemulsion. There were registered 147 cases with $N_h=0$ or 1 and $n_s \geqslant 2$. In the distribution of showers over $\log \gamma_s'$ two maxima are distinctly seen, one of which (left) corresponds to central π-N, and the other, to peripheral π-π collisions. The showers arising in these two types of collision differ in multiplicity. For the π-N collision $\langle n_s \rangle = 5$, and for the π-π interaction $\langle n_s \rangle = 3$. The Gaussian and $\sigma/\sqrt{\langle n_s \rangle}$, where $\sigma = \sigma_{iso} = 0.39$, and $\langle n_s \rangle$ was chosen to correspond with the values reliazable in the experiment. Out of the 147 cases, 50 ± 10 could be attributed to π-π collisions.

In acclerator experiments on the interaction of π^--mesons with nucleons ($N_h = 0.1$) [368, 369], it was shown that the angular distribution of showers

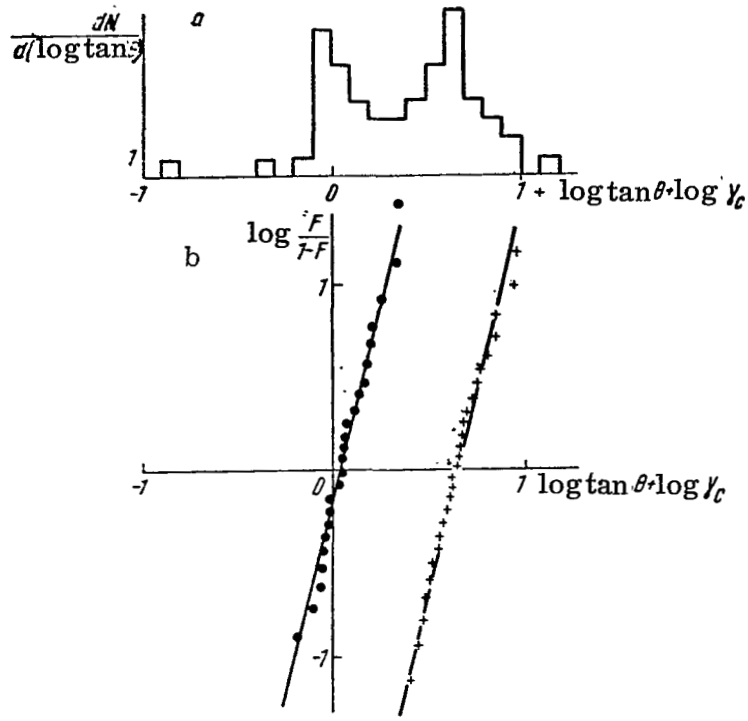

Figure 68. Total Angular Distribution of Secondary Particles for Showers Asymmetric Backwards:

a—Differential Distribution; b—F-Representation Separately for Particles Forming Each Maximum.

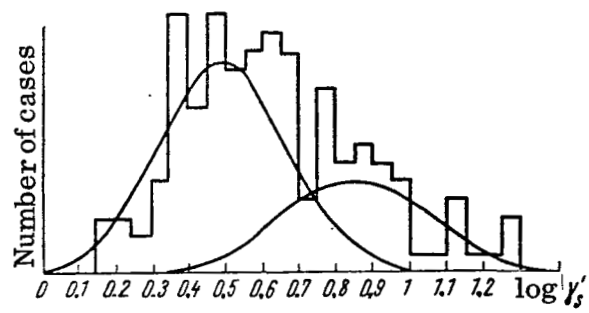

Figure 69. Distribution of Showers Formed by Negative Pions with Energy 16.2 GeV in Photoemulsion ($N_h = 0.1$ and $n_s \geqslant 2$) Over $\log \gamma'_s$ [371]—Histogram.

having a multiplicity $n_s \geqslant 4$ is significantly different from that for showers with $n_s < 4$. If in the first case it has a symmetrical form in the C system of the π-N collision, then for the second case the angular distribution becomes symmetrical only in the C system of the π-π collision (Fig. 70). Similar results were obtained at pion energies of 7 GeV [367].

To sum up, it can be stated that in the energy region 30-100 GeV peripheral collisions can occur in about 10% of the cases of the interaction of nucleons with nucleons, whereas in the interaction of pions with nucleons peripheral collisions occur much more frequently (in 30% of the cases). At higher energies (to 10^3 GeV) we have information only on the interactions of nucleons arising in the decay of heavy primary nuclei [20, 24]. The results of these papers do not contradict the conclusions we have made. In 44 showers from the work of Koshiba et al. [20] five were recorded that have an asymmetric forward angular distribution of secondary particles. /288

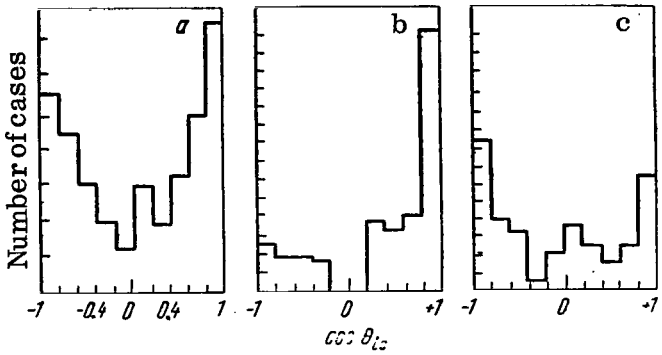

Figure 70. Angular Distribution of Secondary Particles Formed by π-Mesons with Energy 16 GeV in the C System [369]:

a—π-N Collision for Events with $N_h = 0, 1$ and $n_s > 4$; b—π-N Collision for Events with $N_h = 0, 1$ and $n_s < 4$; c—π-π Collision for Events with $N_h = 0, 1$ and $n_s < 4$.

6.5. Another interpretation of the distribution of γ_s/γ_c

In examining the distributions of $\log\frac{\gamma_s}{\gamma_c}$, obtained in different experiments, we discussed only one of the possible interpretations of the distribution and connected the observed asymmetry with the existence of different types of collision—central and peripheral.

However this treatment, based only on the form of the distribution of $\log\frac{\gamma_s}{\gamma_c}$, is not unique. Another interpretation of the observed peculiarities is possible.

Let us assume that in the C system an agglomerate of excited material is formed in the collision of two particles—a fireball, which moves relative to the C system with some velocity $\beta_p \neq 0$. Then the angular distribution of the secondary particles in the C system will have an asymmetrical character, even if the dispersal of particles in the system of rest of the fireball occurs symmetrically or isotropically. And, when $\beta_F > 0$ (motion of the fireball coincides in direction with that of the C system) showers arise that are asymmetric forward, whereas if $\beta_F < 0$ they are asymmetric backward. /289

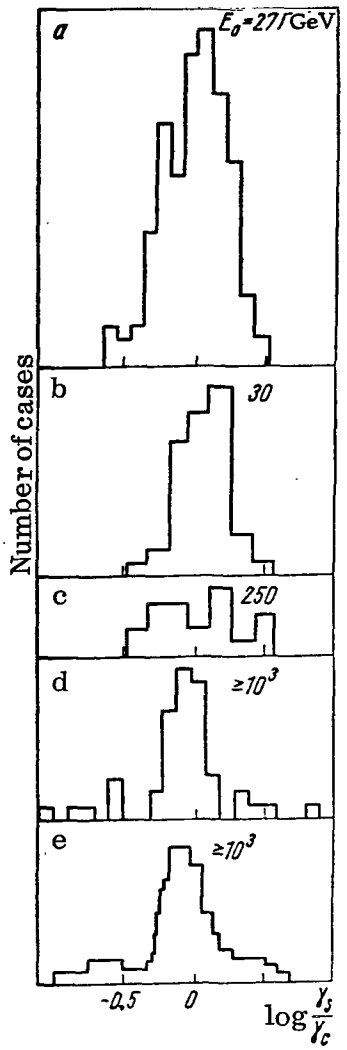

Figure 71. Distributions Over $\log\gamma_s/\gamma_c$ for Interactions with Nuclei at Various Energies of the Primary Particle.

An answer to the question of whether an aggregate of excited material is formed in the collision which moves relative to the C system or there are collisions with targets of different mass, can be obtained by checking the energy dependence of the asymmetry effect.

If when the energy is varied the separation between the maxima in the $\log\frac{\gamma_s'}{\gamma_c}$ distribution, which correspond to different target masses changes, or if the distribution becomes broader, then it is most likely that this is a consequence of the formation of an agglomerate of excited material moving with respect to the C system. But if the position of the maxima remains the same as the energy is increased, this will be an argument in favor of the existence of different types of collision. /290

Figure 71 gives the distributions of $\log\frac{\gamma_s}{\gamma_c}$ for interaction of nucleons with nuclei at three values of primary energy (~30 GeV, [22, 230, 372], 260 GeV, [24] and 1000 GeV [20, 25, 38].

This data is more in accord with an independence of the form of the distribution on the primary particle energy. Thus, for the present we have to give preference to the presumption that different target masses exist.

6.6. Evaluation of the role of the fireball mechanism

In evaluating the role of the fireball mechanism it is necessary to take into account methodological effects which lead to an overestimation of the number of phenomena that can be interpreted as fireballs.

The characteristic sign of fireball creation is considered to be the two-maximum (bimodal) angular distribution. Usually, two-maximum events are found among events with $\sigma>0.6$ and $D>0$; the estimated fraction of such cases is 30-40%. Since the primary energy is determined by the Castagnoli method, the fraction is too high.

We can use Eq. (1.1) to find out how high it is. From this formula it is easy to decide that the measured number of particles with energy E is overestimated $\exp\left[\frac{(\gamma-1)^2 d^2}{2}\right]$ times compared with the true value, because of the

overestimation of energy. The quantity d is, in first approximation, proportional to the half width σ and consequently for events with $\sigma > 0.6$ it will be twice as large as for events with $\sigma < 0.6$. Thus, the true fraction of interactions with $\sigma > 0.6$ may turn out to be many times smaller.

It should be mentioned that angular distributions with two maxima are encountered not only at high energies, but also at 100 GeV and even at 20 GeV (Chapter 9, Section 5).

In addition to this effect, overestimation of the number of two-maximum cases can occur on account of successive collisions of the nucleon with nucleons of the nucleus. It is important that of these successive collisions one should be symmetrical and the other asymmetrical. /291

An extremely serious hypothesis in the analysis of the entire problem is the proposition that charged and neutral pions are distributed identically with respect to angle. A difference in the distributions of π^0- and $\pi^{\pm}$-mesons in individual cases can cause apparent gaps in the distribution of the charged particles with respect to angle.

An artificial overestimation of the number of two-maxima events can arise for reasons associated with the normalization of the angular distributions with respect to energy. Usually, the Lorentz factor of the symmetric system is known but that of the C system is not. Consequently, in combining different angular distributions normalized to xi, one carries out a reduction of all showers to a common center of symmetry, and not to a common primary energy. This operation can lead to a significant distortion of the total angular distribution. Many kinds of distortion are possible: narrowing or broadening of the total distribution, as well as the appearance of two maxima in those cases when they really shouldn't be there.

7. Mass of the Target Particle

The question of the mass of the target particle (or the mass of the target) arises in connection with the concept of the existence of structure in the nucleon.

The possibility of determining the target mass and the "effective" target mass was first pointed out in papers by Birger and Smorodin [376, 377]. On the basis of the conservation laws for energy and momentum in the form proposed by Vernov, they obtained

$$E_0 + p_0 c + m_t c^2 = \sum_{i=1}^{N} (E_i - p_i c \cos \theta_i),$$

whence

$$m_t c^2 = \sum_{i=1}^{N} (E_i - p_i c \cos \theta_i) - (E_0 - p_0 c) \qquad (9.6a)$$

the subscript 0 pertains to the primary particle, i to particle after collision, /292
m_t is the mass of the target particle. In this definition the concept of target mass is kinematical and is independent of the interaction model.

If the incident particle has sufficiently high energy such that $E_0 - pc \ll 1$, we then obtain

$$m_t c^2 = \sum_{i=1}^{N} (E_i - p_i c \cos\theta_i) = \sum_{i=1}^{\prime} (E_i - p_i c \cos\theta_i) + \\ + (E_r - p_r c \cos\theta_r),$$

where r labels the recoil nucleon, and Σ' means summation over all secondary particles except the recoil nucleon. Since the incident particle, as a rule, retains the principal portion of its energy, the contribution to Σ', due to the incident particle is negligibly small.

Often it happens that it is difficult to isolate the recoil nucleon in experimental work; then the concept of effective target mass is introduced,

$$M_t c^2 = 1.5 \sum_{i=1}^{n_s} (E_i - p_i c \cos\theta_i), \qquad (9.7)$$

in the definition of which the recoil nucleon is disregarded; neutral pions are taken care of by the factor 1.5.

Usually, experiments determine the effective target mass M_t. It is difficult to interpret the value found in a physical sense, since the coefficient 1.5 can be used only on the average, and in individual cases this way of accounting for neutral pions brings in an incalculable error. Since the recoil nucleon is neglected, the effective target mass can be regarded only as the lower limit to the target mass, particularly if the recoil nucleon is of low energy.

Koba and Krzywicki [378] introduced the concept of an effective target mass m_t^* based on the division of the created particles into groups genetically related to the colliding particles:

$$m_t^* c = \sum_{i \in I} (p_{0i} - p_i \cos\theta_i).$$

The summation in this case is only over particles genetically related to the primary (over particles of the narrow cone in the L system), the recoil particle, together with the particles of the wide cone, is excluded from consideration. /293

Thus, this target mass is connected with the square of the transferred four-dimensional momentum Δ^2 (see Chapter 10).

The mass of the target particle can also be determined by using the considerations set forth in the preceding sections. This means of determining the target mass from an investigation of the form of the distributions of $\log \gamma'_s$ or $\log \frac{\gamma'_s}{\gamma_c}$ was suggested by Friedländer [121] and applied in [34, 230, 371, 372]. It seems to us to be the most promising.

CHAPTER 10

FOUR-DIMENSIONAL TRANSFERRED MOMENTUM

1. Definition of Four-Dimensional Transferred Momentum

/293

An effective analysis of the elementary process of collision can be carried out through the use of quantities that are invariant under Lorentz transformations, since they can be obtained from measurements made in the laboratory coordinate system. Such a quantity which characterizes the very dynamics of the process is the square of the four-dimensional momentum that is transferred from one object to another during the interaction. In order to calculate this quantity it is necessary to accept a specific model for the interaction. This circumstance significantly reduces the value of this characteristic in the study of inelastic processes.

The interaction momentum Δ was introduced for analysis of inelastic processes by Niu [327] for the two-fireball model and was thereafter employed also in the multi-fireball model of Hasegawa [361].

Let us see how the interaction momentum is defined in specific models.

Let two particles A and B collide, each of which is characterized by its own four-dimensional momentum $\mathscr{P}_A(P_A, E_A)$ and $\mathscr{P}_B(P_B, E_B)$, where P and E are the three-dimensional momentum and energy of the particle. In the collision N new particles are created, so that this inelastic process can be written in the form $A + B = A' + B' + N$. The Feynman diagrams for such a process are sketched in Fig. 72, a - c. If there is any criterion by which the newly created particles can be divided into two or more genetically related groups, then the process will be represented by diagrams Fig. 72, d and e. Figure 72a represnts a central collision. This can be a process of the hydrodynamic type. Figures 72b, c are typical peripheral processes with the exchange of one meson. Figure 72d is a peripheral interaction with the formation of two fireballs. Figure 72e is the completely peripheral model considered by Amati et al., [129] and Fig. 72f is the formation of a fireball and isobars.

The four-dimensional momentum of the meson exchanged in the interaction can be different in these processes. To define it the newly created particles are divided into two groups arbitrarily and it is assumed that one of these groups is

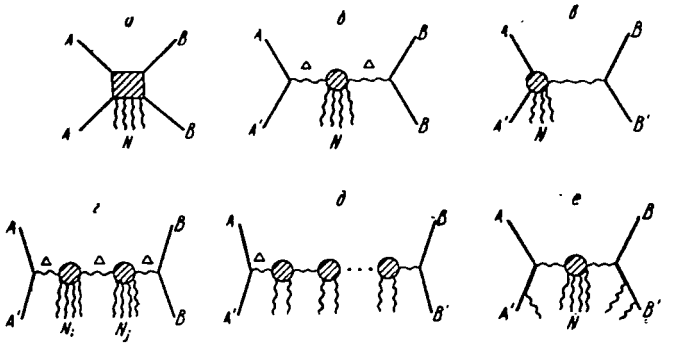

/294

Figure 72. Feynman Diagrams of Possible Processes.

genetically related to particle A and the other to particle B. If we write $A+B=A'+\sum_{i\in A} N_i+B'+\sum_{j\in B} N_j$, the four-dimensional momentum transferred from one group of particles to the other will be defined in the following way:

$$\Delta_A=\mathcal{P}_A-\mathcal{P}_{A'}-\sum_{i\in A}\mathcal{P}_i,\quad \sum_{i\in A}\mathcal{P}_i=\mathcal{P}_a;$$
$$\Delta_B=\mathcal{P}_B-\mathcal{P}_{B'}-\sum_{j\in B}\mathcal{P}_j,\quad \sum_{j\in B}\mathcal{P}_j=\mathcal{P}_b, \tag{10.1}$$

where $\mathcal{P}_i$ and $\mathcal{P}_j$ are the four-dimensional momenta of the created particles ($\mathcal{P}_i$ (P_i, ε_i)). The square of the transferred four-dimensional momentum, if the collision takes place symmetrically in the C system is *

/295

$$\Delta_A\cdot\Delta_A=\Delta_B\cdot\Delta_B=-\Delta^2=2(E_B-M_B)(E_{B'}-M_B)+$$
$$+\mathfrak{M}_b^2-2P_{B'}P_b,\qquad \mathfrak{M}_b^2=\mathcal{P}_b\cdot\mathcal{P}_b. \tag{10.2}$$

In this form the quantity Δ^2 can be evaluated in terms of the experimentally observed parameters, in the laboratory system, that characterize the recoil particle B [379].

Other methods of evaluating Δ^2 are given in the papers of Feinberg and Chernavskiy [19]. If S_a and S_b are the squares of the total energy of the particles of groups a and b in their own center-of-mass systems and S is the square of the total energy of the initial particles in the C system, then when $S_{a,\,b} \ll S$

*Here, as in the other equations of this chapter, the velocity of light c = 1.

$$\Delta^2 \simeq \frac{(S_a - M^2)(S_b - M^2)}{S} + \frac{(S_a + S_b) S_a S_b}{S^2} + \frac{S(1 - \cos\theta_c)}{2}, \tag{10.3}$$

where θ_c is the emission angle of one of the groups of particles in the C system. For given S_a, S_b, and θ_c we obtain

$$\Delta_\perp^2 \simeq \frac{S}{2}(1 - \cos\theta_c) \sim \frac{S\theta_c^2}{4}; \tag{10.4}$$

$$\Delta_\parallel^2 \simeq \frac{(S_a - M^2)(S_b - M^2)}{S} + \frac{(S_a - S_b) S_a S_b}{S^2}. \tag{10.5}$$

However, to use these formulas to calculate $\Delta^2 = \Delta_\perp^2 + \Delta_\parallel^2$ is not possible because of the extreme requirements placed on the accuracy of measurement of the quantities that go into them (particularly measurement of the small angle θ_c).

If one of the particle groups consists only of one nucleon with mass M (Fig. 72, a, b),

$$\Delta_{\text{мин}}^2 = \frac{S_b M^2}{S^2}, \quad S_a = M^2, \tag{10.6}$$

in this case Δ^2 can be connected with the inelasticity K and still another means of determining Δ^2 obtained: /29

$$\Delta^2 = M^2 \frac{K^2}{1 - K}. \tag{10.7}$$

If there are several particles in each of the rays and $S_a \gg M^2$, $S_b \gg M^2$,

$$\Delta^2 = \frac{(S_a - M^2)(S_b - M^2)}{S} \approx \frac{S_a S_b}{S},$$
$$S_a = -(\sum_{i \in A} \mathscr{P}_i)^2; \quad S_b = -(\sum_{i \in B} \mathscr{P}_j)^2, \tag{10.8}$$

where $S \sim E_c^2$, E_c being the total energy of the colliding particles in the C system; it equals the mass of the compound particle formed in the collision.

The square of the four-dimensional transferred momentum can be found from the effective target mass, defined in [378] for a symmetric collision:

$$\Delta^2 = 4m_t^{*2}\gamma_c^2. \qquad (10.9)$$

Still another means of determining Δ^2, used by Fujioka et al. [380], is related to directly measurable quantities -- the emission angles of the secondary particles. This method is also based on an arbitrary division of the secondary particles into two groups. One of the groups is united with the incident particle and the other with the particle at rest in the L system. The four-dimensional momentum transferred from one group of particles to the other is considered. This approach arose in analysis of the experimental data based on the two-fireball model of interaction

$$\Delta^2 = \Delta_{\parallel}^2 + \Delta_{\perp}^2, \qquad (10.10)$$

where $\Delta_{\parallel}^2 = (\Delta p_{\parallel})^2 - (\Delta E)^2$ is the square of the longitudinal component and $\Delta_{\perp}$ is the transverse component of the four-dimensional momentum.

It is obvious that $\Delta_{\parallel}^2 \leq \Delta^2$, since

$$\Delta^2 = (\Delta p_{\parallel})^2 + (\Delta p_{\perp})^2 - (\Delta E)^2.$$

Instead of Δ, the quantity Δ^2 is defined: /297

$$\Delta_{\parallel}^2 = -\left\{\sum_{i\in A}(p_{i\parallel} - \varepsilon_i) + (p_{A'\parallel} - E_{A'}) - (p_{A\parallel} - E_A)\right\} \times \left\{\sum_{j\in B}(p_{j\parallel} + \varepsilon_j) + (p_{B'\parallel} + E_{B'}) - (p_{B\parallel} + E_B)\right. \qquad (10.11)$$

Using these definitions, we obtain

$$\Delta_{\parallel}^2 = \left\{\sum_{i\in A} p_{\perp i}\operatorname{ctg}\theta_i\left[\sqrt{1+\tan^2\theta_i\left(1+\frac{\mu^2}{p_{\perp i}^2}\right)} - 1\right] + \frac{p_{\perp A}^2 + M^2K}{2E_A(1-K)}\right\}\left\{\sum_{j\in B} p_{\perp j}\operatorname{ctg}\theta_j\left[\sqrt{1+\tan^2\theta_j\left(1+\frac{\mu^2}{p_{\perp j}^2}\right)} + 1\right] + 2\left(\sqrt{E_B^2 - p_{\perp B}^2 - M^2} + E_B - M\right)\right\}, \qquad (10.12)^*$$

where

$$E_B = \frac{M(1-K_M)}{2}\left[1 + \frac{p_{\perp B}^2 + M^2}{M^2(1-K_M)^2}\right];$$

K and K_M are the inelasticities in the laboratory and mirror coordinate systems. This formula is valid for any arbitrary division of the secondary particles into groups. All quantities entering in the expression are defined in the laboratory coordinate system.

* This expression for $\Delta_{\parallel}^2$ was obtained in [381].

Equation (10.12) is considerably simplfied if each of the groups consists of not less than two particles and the emission angles of all particles are small ($\mathrm{tg}\theta_{i,j} \ll 1$); then

$$\Delta_{\parallel}^2 \approx \sum_{i \in A} p_{\perp i} \tan\theta_i \left(1 + \frac{\mu^2}{p_{\perp i}^2}\right) \sum_{j \in B} p_{\perp j} \operatorname{ctg}\theta_j. \qquad (10.13)$$

If it is assumed that $\langle p_{\perp} \rangle \sim \mu$, we obtain

$$\Delta_{\parallel}^2 = \langle p_{\perp} \rangle^2 \left(\sum_{i \in A} \tan\theta_i\right)\left(\sum_{j \in B} \operatorname{ctg}\theta_j\right). \qquad (10.14)$$

Since the summation in Eq. (10.14) is in practice carried over only charged secondary particles, a factor of 1.5 is introduced to account for π^0-mesons. This can lead to considerable distortion if the angular distribution of charged and neutral particles is not the same. The quantity $\Delta_{\parallel}^2$ gives the lower limit of Δ^2. The contribution of the transverse component $\Delta_{\perp}^2$ can be very great. According to an estimate given in [379], $\Delta_{\perp}^2 \approx n_i n_j p_{\perp}^2$, where n_i and n_j are the numbers of secondary particles in the corresponding groups. Equation (10.14) depends on the way in which the secondary particles are divided into groups. /29

The distribution of Δ^2 repeats the distribution with respect to the x-coordinate. Akimov and Dremin [381] showed that there is a relation between the distribution of particles in x ($x = \log\tan\theta$) and the distribution in Δ^2 obtained for the same shower for a division of secondary particles into groups ordered along the x scale. It was established that if there is a gap in the density of particles for the x-representation, then the same gap is seen in the distribution over Δ^2 for the corresponding values of the angles. It is natural that the same information is obtained from the distribution of Δ^2 with respect to x as from the x-representation. In addition, one can obtain the minimum values $\Delta_{\min}^2$ for a given shower, and these can be used later to construct $\Delta_{\min}^2$ distributions for many showers.

2. Analysis of Δ^2 Distributions

Distributions of Δ^2 for different ways of division were studied in [380] and [382]. The dependence of Δ^2 on x was obtained by Fujioka et al. [380] for a division of secondary particles into groups ordered along x. The maxima of the Δ^2 distributions agree with the maxima of the particle density along x. In order to investigate the behavior of the minimum possible values of Δ^2, $\Delta_{\min}^2$ was chosen for each shower and the distribution $f(\Delta_{\min})$ was constructed for many showers from the JCEF collection [146] ($E_0 \sim 1000$ GeV). The result is shown in Fig. 73 (histogram). For comparison the corresponding distribution derived from the completely peripheral model developed by Amati et al. [129] is given there also (Fig. 73, curve 1). The discrepancy between the experimental and calculated

distributions is clear. The average values of the minimal transferred momenta in the experiment are $\Delta \simeq 1$ GeV/c.

Erofeyeva et al. [382] determined the four-dimensional momentum transferred in interactions of particles with energy $\gtrsim$ 100 GeV with carbon nuclei from the group of particles comprising the narrow cone to the group in the wide cone. Such a division was possible because the energy of the primary particle was known (ionization calorimeter). Curve 3 of Fig. 73 represents the distribution over the longitudinal component of the transferred four-dimensional momentum for the interactions in graphite. Attention is called to the group of events with small values of the transferred four-dimensional momentum. In approximately 80% of the cases, charged particles produce events with $\Delta_{\parallel} < 0.3$ GeV/c. In addition, among these events are those for which $\Delta_{\parallel} = 0$. They arise when charged particles are absent in one of the cones. In some cases this may mean that instead of charged particles, neutral π^0-mesons, concentrated in one of the cones, are formed. Then the value obtained is fictitious. /299

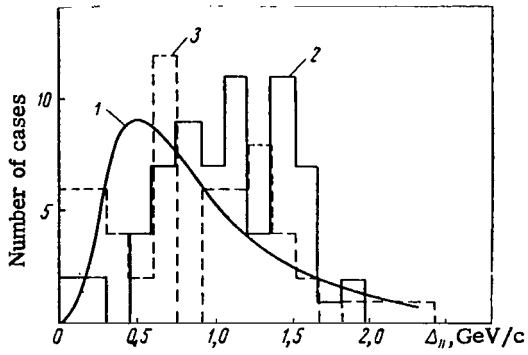

Figure 73. Distribution of $\Delta_{\parallel}$ (or Δ_{min}): 1 — Calculation on the Completely Peripheral Model of Amati [129]; 2 — Experimental Distribution [146]; 3 — Experimental Distribution [382].

However, there are events in which not only charged particles but also neutral particles are emitted only forward in the C system of the colliding nucleons. These cases we explained earlier as collisions with small target masses (see Chap. 9). For them, $\Delta = 0$ means that there has been no excitation of the target nucleon, i.e., the diagram of Fig. 72c evidently applies. The average values of the longitudinal components of the transferred four-dimensional momenta are given in Table 61. /300

TABLE 61. VALUES OF $\langle\Delta_{\parallel}\rangle$ FOR INTERACTIONS IN C AND LiH.

C[382]	LiH [136]
0.82 + 0.04 GeV/c	0.71 + 0.06 GeV/c

To distinguish central and peripheral collisions and to ascertain the specific diatrams which describe the interaction, Dremin proposed the use of the set of values of Δ^2 calculated for different divisions into groups. In doing this, information about the mass of the target particle is received.

In [383] this method is applied for the analysis of showers registered in a photoemulsion exposed in an accelerator to a beam of protons with energy 24 GeV. The momenta of the secondary particles were measured in a magnetic field of up to 180 kG.

Figure 74 shows the behavior of the Δ^2 distribution for various types of processes, experimental results for which are given in Table 62. Positive identification of the secondary nucleons and information about the momenta and nature of all secondary particles are required for the analysis.

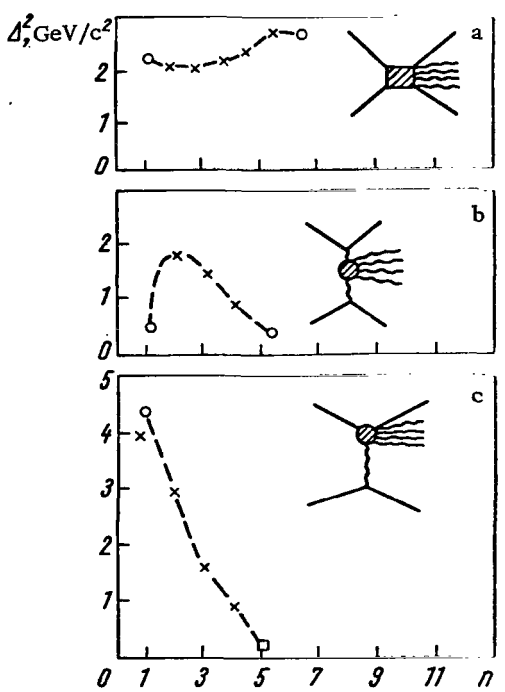

Figure 74. Distribution of Δ^2 for Processes of Different Type:

a — Collision of the Central Type; b and c — Peripheral Distributions (b — with Formation of One Fireball).

TABLE 62. FREQUENCY OF APPEARANCE OF DIFFERENT TYPES OF DIAGRAMS.

/301

Position in Fig. 74	Number of cases	Interpretation
a	7	Central interactions
b	1	Fireball with $M_F \sim 3$ GeV/c^2
	25	Peripheral interactions with unsymmetrical excitation of nucleons
c	15	Peripheral interactions with weak excitation of one of the nucleons

CHAPTER 11

A SUMMARY

One of the important problems which has been debated in recent years is the explanation of the mechanism of particle collision at high energies. Many different models have been proposed, some of which have been extremely attractive in construction but not in degree of validity. This is partly due to the fact that the experimental situation in the investigation of the basic parameters of the process of interaction at high energies either admits of various interpretations (because complete information about the interaction is lacking) or the data are not sufficiently reliable.

The complexity and variety of the phenomena occurring at superhigh energies do not permit working with solely the average parameters and require an individual approach to the processes being studied. /302

Unfortunately, there is no theory of strong interactions, only a series of theoretical models, which may conveniently be divided into models describing central collisions (with the participation of many particles as propagators of the interaction) and peripheral collisions, which occur as the result of the exchange of one meson. Central collisions are described on the basis of statistical or hydrodynamical ideas, whereas the picture of peripheral collisions contains much arbitrariness and is based on specific models of the interaction drawn by means of Feynman diagrams. The confrontation of experimental and theoretical results is carried out almost blindly, since it is very difficult, and sometimes even impossible, to subdivide the investigated events beforehand into central and peripheral classifications.

In this chapter we shall sum up the analysis of the experiments considered earlier.

1. The principal parameter of the process, the effective cross section of the nucleon-nucleon interaction at cosmic energies is in no case ever smaller than at energies ~ 30 GeV

$$\sigma_{NN} = 46 \pm \frac{?}{6} \text{ for } E_0 \sim 10^3 \text{ GeV}$$

The cross section of the interaction of a nucleon with a carbon nucleus remains constant up to energies of 10^3 GeV, with a probability of 90% (twice the standard deviation). For the cross section of the interaction of a nucleon with a lead nucleus, there may be an increase of up to 15% (twice standard deviation) when the energy changes from 10 to 10^4 GeV.

Since the predictions based on various theoretical treatments give a change of the effective cross section within limits of 10 - 15%, the available experimental results do not permit any definite conclusions in favor of any model in particular.

2. The experimental dependence of n_s on E_0 is given by Eq. (5.4). However, it is not yet possible to categorically deny a dependence of the type $E_0^{1/4}$, and so this criterion cannot be used to distinguish between the hydrodynamic and peripheral models. /303

We are not yet able also to solve the question of whether there are successive collisions with nucleons in the nucleus, or whether the nucleon interactions at once with the whole system, merely by analyzing the connection between n_s and A, since in both cases the functions are very much alike.

More definite information can be obtained in the study of the fluctuations of n_s at a fixed energy. At high energies, experiment gives greater fluctuations in n_s than are predicted by hydrodynamic theory (see Chap. 5, Sec. 6.3).

It should be mentioned that in the collision of nuclei the distribution over multiplicity corresponds to the independent collision of the nucleons that enter into the nucleus.

3. The relation between the various sorts of created particles is predicted by the statistical and hydrodynamic theories. In experiment a better agreement is obtained with hydrodynamic theory, both in the region of high and at low energies of the primary particles. The average momenta of heavy particles is found to be greater than those of light particles, which also agrees with hydrodynamics.

4. At moderate energies (< 200 GeV), a comparison has been made of the energy spectra of secondary particles with statistical theory. Satisfactory agreement was obtained.

At high energies pions appear with energy proportional to the energy of the primary particle. Their existence is explained by the creation of isobars. It is extremely important that the primary particle in the nucleon-nucleon (pion-nucleon) collision retains its nature and a significant part of its energy (Chap. 6, Sec. 2). Until not this phenomenon has not been successfully explained from the viewpoint of hydrodynamic theory.

There are indications that in the collision of nucleons with heavy nuclei the primary particle is not always conserved, and a pion takes on the role of the most energetic particle.

5. According to the Landau theory, the inelasticity should be close to unity. The peripheral theories, on the other hand, give small inelasticities.

From the distributions of inelasticity for nucleon-nucleon collisions it follows that there exist in nature interactions with large and small inelasticities (see Chap. 8).

In pion-nucleon collisions the ratio of central to peripheral collisions is unknown. Feinberg [384], on the basis of data obtained mainly from an analysis /304
of angular and transverse momentum distributions, decided that the probability of existence of central and peripheral collisions was the same.

There is another path to the elucidation of the role of peripheral collisions. In nucleon-nucleon interactions the predominance of nucleons among the most energetic secondary particles (nucleon conservation) is evidence in favor of the peripheral character of the collision. In pion-nucleon collisions it is impossible to separate central from peripheral collisions by means of this criterion, since the appearance of an energetically isolated pion is possible as the result of its conservation in a peripheral collision or of its regeneration in the shock wave. Since in the latter case the process is statistical, all three kinds of pions ($\pi^{\pm}$, π^{0}) should arise with equal frequency, whereas in the peripheral collision the appearance of pions of other signs is determined by the charge exchange probability. It is assumed that charge exchange occurs with a unit change of charge (see Chap. 8). This leads to deviations from the relation implied by the isotopic invariance in π - N collisions.

6. The distribution of transverse momenta for pions in the region of very high energies, as well as the dependence of $<p>$ on E_0 and the mass of the secondary particles, agrees well with hydrodynamic theory.

In peripheral collisions the average value of the transverse momenta should not be large, which does not contradict experiment. However, the peripheral theories could also explain high transverse momenta if one considers the exchange of heavier particles than pions.

So far, by comparing the central and peripheral collision theories, we have not gain any insight into the mechanism of the peripheral interaction, where- /305
as by central we have usually understood the hydrodynamic picture for the interaction.

The analysis of angular distributions permits specific assumptions about the model for peripheral collisions. In this, one most frequently considers the fireball model, the isobaric model, or assumes that the peculiarities of the angular distribution are determined by the structure of the nucleon.

The isobaric model arises in connection with the presence in the energy spectrum of the secondary particles, of pions having an energy proportional to the primary energy. At accelerator energies proof has been obtained of the existence of isobars. At cosmic energies there is no such proof as yet. There are only certain indications that a similar process exists (see Chap. 13).

To explain the anomalies in the angular distribution of secondary particles, the fireball model for the interaction mechanism was proposed, but it is not the only one that explains the anomalies seen. A competing explanation is the assumption that the collision produces a motionless agglomerate of excited material having a large angular momentum (see Chap. 9, Sec. 4). The decay of this agglomerate leads to a cosine form for the distribution law for secondary particles in the C system. As was shown by Ezave et al. [385], the magnitude of the angular momentum of the system of mesons is given by the relation

$$J_m = \frac{\sqrt{3}}{4} m \sqrt{n_s}\, \hbar,$$

where m is the degree of the angular distribution.

The arguments considered thus far do not give conclusive evidence in favor of the predominance of the fireball mechanism at high energies (see Chap. 9, Sec. 6.6).

Sometimes it is assumed that the existence of asymmetric showers may serve as proof of the emergence of one fireball. However, as was shown in Chap. 9, Sec. 6, this interpretation likewise is not unique.

In a number of papers, the existence of structure in the nucleon is given as an explanation for the very same experimental facts. Analysis of the experiments shows that the observed asymmetrical showers are symmetrized in the system with target mass $\sim m_\pi$. This value for the target mass for the asymmetric cases is obtained both at accelerator energies (see, e.g., Gainotti et al [371] and at cosmic energies [34]. If the asymmetry is a consequence of the emergence of a fireball moving with Lorentz factor $\bar{\gamma}$ relative to the C system, then this Lorentz factor will be different at accelerator and cosmic energies. Proof of a change in $\bar{\gamma}$ with increasing energy could be an argument for the fireball model. However, results with reliable measurement of energy of the primaries, evidently, indicate no significant dependence of $\bar{\gamma}$ on energy (see Chap. 9, Sec. 6). /306

Highly asymmetric showers with low multiplicity are rarely encountered.

Zatsepin and Nikishov [386] showed that such showers can be interpreted as the result of photonuclear creation. Still lower multiplicity ($n_s \approx 3$) and asymmetric dispersal can be observed in the coherent creation of pions.

It is obvious that not one of these theoretical models by itself can explain the collection of experimental facts. Hence attempts have been made to unite them. In [387] and [388] the possibilities for the generation of resonances as a result of a hydrodynamic process are considered. Feinberg and Chernavskiy [389] propose a hydrodynamic peripheral model in which both central and peripheral processes are simultaneously present.

It is extremely important that in the investigation of the interactions of pions and nucleons it has been found very recently that there are differences in a whole series of parameters. These include: interaction cross section,

multiplicity, inelasticity, spectrum of secondary particles, angular distribution, and transverse momentum distribution (see the appropriate sections).

This difference appears both in the region of accelerator energies, as well as at energies of the order of 10^3GeV.

PART III

CHAPTER 12

ENERGY SPECTRUM AND COMPOSITION OF THE PRIMARY COSMIC RADIATION

1. Direct Measurements

1.1. Methods Applicable at Moderate Energies /307

The form of the energy spectrum and the absolute intensity of the primary radiation are of the first importance in understanding the processes of development of the components of the cosmic radiation in the atmosphere, as well as in studying the origin of cosmic rays.

However, the question of the spectrum and absolute intensity still continues to be discussed, and different sources yield contradictory results.

There are several ways to establish the form of the spectrum and determine the intensity of the primary radiation. In the region of moderate energies (to $\sim$ 15 GeV), investigation of the latitude effect at the limits of the atmosphere gives the possibility of solving this problem, since the magnetic field of the Earth intercepts those particles having a momentum less than a certain critical value p_c, depending on latitude. The intensity of radiation with momentum greater than p_c does not change thereby. The critical values p_c for different geographical coordinates were calculated not long ago by Quenby and Wenk [390]. Since the geographic and geomagnetic coordinates do not coincide, the critical values p_c, or to be more exact, the magnetic rigidity $\xi = Arc/Ze$, depend not only on the geographic latitude, but also on longitude. (A and Z are the mass and charge numbers of the nucleus, and p is the momentum of each of the nucleons entering into the nuclear composition.) The magnitude of the magnetic rigidity for vertically incident particles is presented in Table 63 (for more detailed data, see [390] and [391].

TABLE 63. DEPENDENCE OF MAGNETIC RIGIDITY ON GEOGRAPHIC LATITUDE AND LONGITUDE (IN GeV).

Geographic latitude		East longitude								
		0°	20°	40°	60°	80°	100°	120°	140°	160°
South	70°	0.274	0.376	0.453	0.505	0.54	0.55	0.56	0.57	0.512
	60°	1.12	1.28	1.42	1.54	1.70	1.82	1.87	1.90	1.76
	50°	3.06	3.60	3.81	3.77	3.84	3.98	4.15	4.26	4.37
	40°	6.7	7.20	7.60	7.80	8.2	9.4	9.6	9.0	8.5
	30°	11.2	11.6	12.6	13.5	14.3	14.5	14.5	13.9	13.1
	20°	14.4	14.9	15.5	16.1	16.5	16.8	16.4	16.0	14.8
	10°	15.1	15.6	16.4	17.0	17.6	17.7	17.1	16.5	16.0
	0°	14.4	14.9	15.7	16.3	16.8	17.2	17.0	16.5	16.2
North	10°	12.5	12.4	13.4	14.4	14.9	15.0	15.1	15.2	15.2
	20°	10.5	10.2	10.7	10.5	10.8	10.9	10.5	11.1	12.1
	30°	8.9	7.9	6.8	5.9	5.1	4.62	4.70	5.2	6.2
	40°	6.3	4.59	3.77	3.18	2.48	2.03	1.98	2.28	3.01
	50°	3.76	2.65	1.81	1.34	0.90	0.63	0.55	0.63	1.02
	60°	1.90	1.24	0.77	0.512	0.281	0.136	0.096	0.096	0.194
	70°	0.82	0.512	0.294	0.136	0.055	0.0136	0.0033	0.0024	0.6256

TABLE 63 (Continued)

Geographic latitude		West longitude								
		20°	40°	60°	80°	100°	120°	140°	160°	180°
South	70°	0.151	0.061	0.0177	0.082	0.152	0.056	0.161	0.288	0.421
	60°	0.72	0.365	0.181	0.125	0.174	0.381	0.75	1.20	1.55
	50°	2.24	1.28	0.73	0.63	0.85	1.44	2.23	3.22	4.09
	40°	4.94	3.01	2.06	1.97	2.52	3.83	4.99	6.2	7.7
	30°	8.8	5.8	4.48	4.45	5.6	7.3	8.9	10.4	12.3
	20°	12.8	10.1	8.5	8.3	9.8	12.0	13.2	13.7	14.2
	10°	14.6	13.6	12.4	11.8	13.3	14.5	14.7	15.0	15.4
	0°	12.2	14.1	13.6	13.5	14.6	15.1	15.4	15.6	15.9
North	10°	13.1	13.4	13.6	14.0	14.6	14.8	14.8	15.2	15.3
	20°	11.4	12.2	12.8	13.6	14.0	14.0	13.8	13.3	12.6
	30°	9.9	11.1	11.6	12.6	13.1	12.6	11.7	9.5	7.7
	40°	8.0	9.3	10.2	10.4	9.7	8.3	6.7	5.2	4.03
	50°	5.1	6.7	7.3	6.8	5.6	4.50	3.39	2.29	1.45
	60°	2.81	3.85	4.15	3.89	3.05	2.19	1.42	0.82	0.458
	70°	1.24	1.61	1.69	1.57	1.27	0.85	0.512	0.269	0.109

Thus the Earth's magnetic field permits the analysis of cosmic particles /310
arriving along the vertical with momenta less than 17 GeV/c for singly charged particles.

In this work we shall not consider the region of very small primary energies ($E_{kin} < 1 - 3$ GeV). In this region the cosmic radiation is subject to temporal changes and is treated in special monographs and surveys [392, 393]. The energy region above several GeV is relatively stable in time.

Measurement of the energy spectrum and absolute intensity at such energies has been made by many authors (see e.g., [394]). The principal instruments are usually Cerenkov or Geiger counters. Above these instruments there is always a certain amount of material (container lining, body of satellite, residual atmosphere, if the measurement is carried out at balloon heights). The final value of the intensity of the primary radiation is obtained by extrapolating the data obtained to the limits of the atmosphere ($x = 0$). One has to take into account also the albedo, i.e., particles scattered in the atmosphere or in the material surrounding the measuring apparatus which imitate the primary particles. In the older literature the intensity was very greatly overestimated because of failure to allow for albedo [394]. The more recent data may be considered to be sufficiently reliable.

In the higher energy region the only direct method was for a long time the observation of nuclear interactions in photoemulsions raised by balloons to a height of about 40 km (several grams of residual atmosphere). The energy of the particles was estimated by the Castagnoli method or by the energy of secondary electron-photon cascades. As we have already mentioned many times, the first method leads to a strong distortion of the spectrum and intensity (see Fig. 8, in which the spectra of the same events measured by these two methods are compared). The second method does not distort the form of the energy spec- /311
trum much, if the magnitudes of α_0 and λ do not vary with energy. The absolute intensity in this case depends on assumptions about the transfer from the total energy of photons to the energy of the primary particles and on the selection criteria (threshold of registration, see Chap. 1). Haber-Shain, using the Castagnoli method, obtained the index of the primary spectrum $\gamma - 1 = 1.3$ at energies $\sim 10^{11}$ eV, which is markedly less than other methods give in this energy region. Lal [396] measured the primary intensity from electron-photon cascades. His value is too high on account of the use of too high a coefficient of transfer from the energy of the photon shower to the energy of the generating particle.

1.2. Ionization Calorimeter Method

The method of the ionization calorimeter for investigations of primary radiation is extremely promising [397], and its application was made possible by the creation of heavy satellites in the Soviet Union. The use of an ionization calorimeter in a satellite permits the investigation of the energy spectrum in the energy interval from 10^{11} to 10^{14} eV with a single apparatus. In the lower energy region measurements with the calorimeter are less reliable, since the error in determining energy increases.

According to preliminary results with the "Proton" satellite, the index of the energy spectrum of all primary particles $\gamma - 1 = 1.73^{+0.1}_{-0.08}$ in the interval from 40 to 2 x 10^5 GeV.

In this work an apparatus of the calorimetric type with scintillators as ionization detectors was used. The thickness of material in the apparatus was 2.5 nuclear path lengths of iron.

As is shown in Chap. 3, in an apparatus with an absorber of this thickness the fraction of evolved energy depends on the energy generating the interaction of the particle. One finds from Table 8 (Chap. 3) that a calorimeter with absorber thickness of about 2.5 λ can increase the index of the energy spectrum of protons in the energy interval 10^{11} - 10^{12} eV by about 0.2.

The spectra of nuclei can be measured more reliably, since for them the effective calorimeter thickness (expressed in interaction path lengths) is greater than for protons. The contribution of heavy nuclei to the number of registered particles of the global flux is equal to the contribution of protons at energies of 10 - 100 GeV. Consequently, the spectrum of all particles is less distorted than the proton spectrum. In addition, there is a compensating factor — the decrease in the role of nuclear fragmentations with increasing energy. All of this means, evidently, that the spectrum of all particles measured in the "Proton" satellites is not distorted too strongly. /312

Because of the small thickness of the absorber in the calorimeter, it is impossible to determine the absolute intensity of particles with a given energy. However, if one uses the data of geomagnetic measurements at an energy of about 20 GeV, then it is possible to reduce the spectrum at high energies by extrapolating it with a slope $\gamma - 1 = 1.7$ from the point with energy 20 GeV. An increase of absorber thickness would make it possible to obtain more accurate values of the exponent of the energy spectrum and of the absolute intensity.

1.3. Measurement of the Energy Spectrum in the High Energy Region

In the region of energies above 10^{14} eV measurements of the spectrum of primary particles are based on the observation of broad atmospheric showers. By summing the energy of the electron-photon component, the nuclear component, as well as of muons and neutrinos, one can determine the total energy of the shower and, consequently, the energy of the primary particle. Thus, this method is in essence calorimetric.

The difficulty, however, is that observation of the shower is made at only one level, and the number of detectors is limited. Hence each shower is treated with respect to some averaged parameters. An analysis of the errors arising in the determination of the number of particles in the shower was made by Clark [398] and by Soloveva [399] and showed that these errors do not exceed 20 - 40%.

The transition from the number of particles N_e at the level of observation to the primary energy of particles E_0 that evoke the shower is made on the basis

of specific models for the development of a wide shower. It has been found that the final result (i.e., the relation between E_0 and N_e) depends little on the choice of model [2, 400, 401].

In work done under the leadership of Zatsepin [2, 402] it was shown that /313
fluctuations in the number of interactions of nuclear-active particles in the atmosphere and slight fluctuations in the elementary act (more specifically, fluctuations in the fraction of energy transferred to photons from case to case) are of extreme importance. As a result of these fluctuations the measured number of particles at the level of observation increases by about a factor of 2.

The energy spectrum of primary particles from data on broad showers was traced out to energies of 10^{20} eV [403]. The spectrum of all particles is registered in this way, although a more detailed analysis of the properties of broad showers can assist in the determination of the fraction of nuclei in the primary radiation. In [404 - 406] an increase was observed in the number of multi-branched showers in the region of 10^{15} eV, which can be interpreted as the result of the enrichment of the primary radiation by nuclei.

According to data from the "Proton" satellites, the spectrum of the cosmic radiation is enriched by nuclei beginning already at 2×10^3 GeV, and the spectrum of protons becomes very steep ($\gamma - 1 \sim 2.6$).

A decrease in the fraction of protons in the primary radiation with increasing energy can cause the spectrum of protons in the bottom of the atmosphere, proceeding without the accompaniment of air showers, to be markedly steeper than the spectrum of all nucleons. This, in particular, can explain the experiments of Grigorov and Zatsepin [69, 70] in which the steep spectrum of protons was interpreted as the result of a reduction of the interaction path of nucleons with energy (see Chap. 4).

A study of the spectrum of broad atmospheric showers with respect to the number of particles at sea level shows that when $N_e \gtrsim 10^6$ an increase in the exponent of the shower spectrum is observed [398, 407]. The effect can be explained by a change of the primary spectrum in the region $\gtrsim 10^{15}$ eV. At very high energies $\sim 10^{17}$ eV, the spectrum looks as if it again becomes flatter ($\gamma - 1 \sim 1.7$) [408]. This second change is confirmed by the observation of the spectrum of muons in showers [409]. Thus, primary spectrum cannot be represented by a power law with a constant exponent γ (Fig. 75).

Measurements show that, in the region of energies sensitive to a magnetic /314
field, the value of $\gamma - 1$ varies from 1 to 1.5 at energies of 1 — 20 GeV. Then the exponent of the spectrum becomes relatively stable, and in the interval 10^2 — 10^5 GeV it equals $\gamma - 1 = 1.7$, although a smooth change to 1.9 cannot be excluded. At energies of the order 10^{16} — 10^{17} eV, the spectrum determined from data on broad showers has an exponent 2.3 ± 0.2 [403].

The change of the exponent of the spectrum with energy must lead to certain peculiarities in the deepest parts of the atmosphere. Thus, if the spectrum of the primaries experiences a sharp change in any region, then the secondary com- /315
ponents of the radiation must feel it at significantly lower energies, particularly at the bottom of the atmosphere.

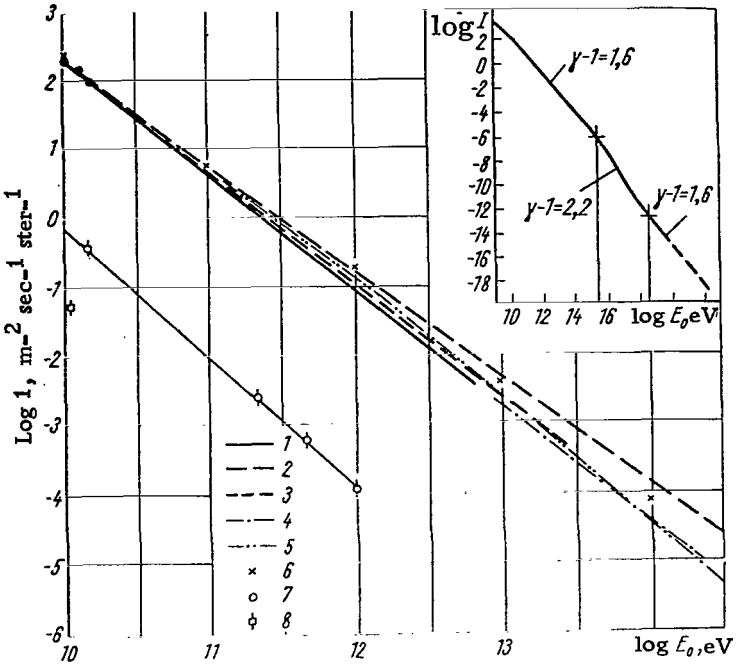

Figure 75. Integral Energy Spectrum of the Primary Cosmic Radiation:

1 — $\gamma - 1 = 1.7$; 2 — [410]; 3 — [411]; 4 — [2]; 5 — [412]; 6 — [96]; 7 — [413] and [414]; 8 — [415]; Black Points, Geomagnetic Measurements. Upper Right — Approximation of the Primary Spectrum from [416]. (7 and 8 — Measurements on Mountains).

2. CHEMICAL COMPOSITION OF THE PRIMARY COSMIC RADIATION

2.1. Introduction

The composition of the nuclear component of the primary cosmic radiation observed at the limits of the Earth's atmosphere depends on the cosmic abundances of the elements, the acceleration mechanism, and the diffusion of cosmic rays from the sources of their creation to the point of observation.

Experiments on the determination of the composition of cosmic rays observed on the Earth and its comparison with the cosmic abundances of the elements (according to the well known listing of Suess and Urey) have shown that the processes of diffusion and acceleration play an important role. In particular, before they strike the Earth, the cosmic particles pass through 2 — 3 g/cm^2 of the material in interstellar space. Fragmentation of heavier primary nuclei explains the considerable content of Li, Be, and B nuclei in the composition of the primary cosmic radiation. Another feature of the mass spectrum is the

enrichment of the cosmic radiation by heavy nuclei. Iron nuclei are encountered 15 — 20 times more frequently than expected from the abundance of this element, /316 and nuclei heavier than iron are 100 times more frequent. The latter are observed a million times less frequently than protons.

These features are of surpassing importance for the solution of the problem of the origin of cosmic rays, and special monographs have been devoted to them. The presence of nuclei in the cosmic radiation is of practical interest, since it gives the possibility of investigating collisions of the nucleus-nucleus type at high energies. In addition, the composition of the cosmic radiation determines certain of the characteristics of the secondary components in the atmosphere. For these purposes, it is necessary to know the chemical composition of the cosmic rays, the energy spectra of the different nuclear components, the absorption paths, and the interactions and fragmentation parameters of nuclei.

Up to the present time the majority of the results of the study of the chemical composition has been obtained in the region of energies that can be analyzed with the aid of the Earth's magnetic field. The energies of particles of different mass but the same rigidity are different. The difference is determined by the ratio A/Z, which for protons is equal to 1 and for light and average nuclei about 2, and by the dependence of energy on mass for the same momenta. In the region of very high energies ($E \gg mc^2$) the latter ceases to play a role and the energy per nucleon for the same rigidity is half as great for nuclei as for protons.

2.2. Chemical Composition at Different Energies

The chemical composition is constant over a wide energy interval. Many investigators have come to this conclusion [35, 392, 417]. Table 64 gives the results of the measurement of the exponent of the energy spectrum in the interval of energy from 1.5 to 20 GeV/nucleon for nuclei from geomagnetic measurements, as well as the results obtained in the region of high energies by the method of relative scattering during fragmentation.

It should be kept in mind that the exponent of the energy spectrum of nuclei and protons in the low-energy region depends on the solar activity [392]. Hence, the difference in the exponents in different papers is partially explained by this. A comparison of the data presented in Table 64 shows that no significant difference exists in the energy spectra of different nuclei up to energies in the hundreds of GeV. The energy spectrum of protons at energies 4 — 20 GeV has an exponent close to $\gamma - 1 \sim 1.5$, which also differs little from the exponent of the spectrum of nuclei.

Badhwara et al. [145] and Durgaprasad [427] examined the ratio of intensities of different nuclei at 1.5 and 7.5 GeV/nucleon. Their analysis also showed the absence of any strong changes in composition in the interval from 1.5 to 7.5 GeV/nucleon.

The results are given in Table 65.

TABLE 64. EXPONENT OF THE INTEGRAL ENERGY SPECTRUM OF NUCLEI.

a) Helium Nuclei

Energy Interval, GeV	$\gamma - 1$	Reference
1.5—7.0	1.45 ± 0.04	[418]
1.5—7.5	1.31 ± 0.15	[418]
2—7.5	1.41 ± 0.12	[392]
6—20	1.84 ± 0.22	[419]
1.5—800	1.49 ± 0.22	[420]
15—1500	1.58 ± 0.20	[421]
2—1000	1.65	[419]

b) Nuclei of Groups M and H[a]

Energy Interval, GeV	$\gamma - 1$		Reference
	M	H	
1.64—7.5	1.59 ± 0.09 [b]	—	[422]
1.64—7.5	1.77 ± 0.11	1.65 ± 0.17	[398]
0.2—8.0	1.65 ± 0.30	1.78 ± 0.35	[423]
1.6—10	$1.54 \pm {}^{0.16}_{0.13}$	—	[424]
4—16		1.82 ± 0.19	[425]
4—26		1.26 ± 0.30	[417]
1.5—7.0	1.51 ± 0.10	1.59 ± 0.15	[426]
7—100	1.57 ± 0.20	1.62 ± 0.20	[421]

[a] M and H are groups of medium and heavy nuclei, respectively.
[b] M + H.

TABLE 65. INTENSITY RATIOS OF DIFFERENT NUCLEI AT THE LIMITS OF THE ATMOSPHERE.

Ratio[a]	7.5 GeV [427]	1.5 GeV [145]
H/M	0.48 ± 0.07	0.42 ± 0.07
H_2/H_3	0.18 ± 0.06	0.12 ± 0.08
H_1/H_2+H_3	0.31 ± 0.09	0.34 ± 0.13

[a] $H_1 - Z > 20$; $H_2 - Z = 16 - 19$; $H_3 - Z = 10 - 15$.

Information on the chemical composition of nuclei in the region Z > 30 are contradictory. /318

In [428], which presents data obtained from satellites, the fraction of nuclei with Z > 30 — 40 with respect to nuclei with Z ≥ 15 was found equal to 3×10^{14}.

The average values of the ratios of the intensity of nuclei with Z ≥ 30, Z ≥ 40, and Z ≥ 48 to the intensity of nuclei with Z ≥ 21 obtained from measurements by the "Proton-1" and "Proton-2" satellites are [429]:

$$\frac{I(Z \geqslant 30)}{I(Z \geqslant 21)} = (3.8 \pm 0.4) \cdot 10^{-2};$$
$$\frac{I(Z \geqslant 40)}{I(Z \geqslant 21)} = (1.5 \pm 0.1) \cdot 10^{-2};$$
$$\frac{I(Z \geqslant 48)}{I(Z \geqslant 21)} = (3.6 \pm 0.6) \cdot 10^{-3}.$$

In this same paper the intensity ratio

$$\frac{I(Z \geqslant 21)}{I(Z \geqslant 2)} = (4.8 \pm 0.26) \cdot 10^{-3}$$

is given, which gives the possibility of evaluating the absolute fluxes of different nuclei according to the results of Tables 65 and 66.

TABLE 66. INTENSITIES OF NUCLEI AT THE LIMITS OF THE ATMOSPHERE, $m^{-2}sec^{-1}ster^{-1}$ [392].

Cutoff energy for nuclei, GeV/nucleon	Z ≥ 2	Z ≥ 5	Z ≥ 12 - 14
1.2	120.6±8.7	9.8±0.7	1.3±0.2
2.2	121.3±8.7	8.5±0.6	0.7±0.2
3.9	80.0±7.3	5.7±0.5	0.40±0.15
5.6	38.0±5.3	3.2±0.2	—
6.7	29.3±4.7	2.0±0.3	0.15±0.06
7.4	26.0±4.7	2.3±0.3	—

2.3. Absolute Intensities of Nuclei and Nucleons at the Limits of the Atmosphere

Table 66 gives the results of the measurement of the intensity of different nuclei obtained at the time of the flight of the third Soviet capsule-satellite [392].

Anand et al. [419] summarized the results of the measurement of the absolute intensity of α - particles over a wide energy interval [418-421][430-432]. /319

If one averages the results obtained at the same energy, the following data are obtained (Table 67):

TABLE 67. ABSOLUTE INTENSITY OF HELIUM NUCLEI AT THE LIMITS OF THE ATMOSPHERE.

Cutoff energy for nuclei, GeV/nucleon	$I_0(>E_0)$ $m^{-2}sec^{-1}ster^{-1}$	Depth g/cm^2
6.4	26.6 ± 2.2	10.2
7.2	22.7 ± 1.4	10—18
8.2	15.7 ± 1.2	6—11
8.6	16.5 ± 1.1	7—16
10.7	10.5 ± 1.2	10.2
15.5	4.7 ± 0.9	10.2
800.0	$1.7\cdot10^{-2}$	9.3
1500	$3.6\cdot10^{-3}$	10.0

Most of the results presented in Table 67 were obtained with the aid of photoemulsions. The measurements were carried out under a considerable layer of the atmosphere and require extrapolation to the limits of the atmosphere. This extrapolation is carried out either from measurements at several heights or from calculations with allowance for the interaction paths of the nuclei and their fragmentation parameters. For these purposes, the absorption paths in air may be used. The absorption path lengths are considerably reduced as the nuclear charge increases. Thus, according to data of Webber and Ormes [433], the absorption path length of α-particles in air is 52 g/cm^2. For other nuclei it is $L_M = (35.1 \pm 10.7)$ g/cm^2 [145], $L_M = (32 \pm 1.2)$ g/cm^2 [417], $L_M = (26.6 \pm 8.9)$ g/cm^2 [145], $L = 24.5 \pm 2.5$ g/cm^2, $L_{\alpha+M} = 33 \pm 1.7$ g/cm^2 [417].

The same problem arises in the measurement of the intensity of primary protons. To calculate the intensity at the limits of the atmosphere it is impossible to use the absorption paths of protons measured at the bottom of the atmosphere, since the loss of protons on account of interactions close to the limits of the atmosphere is replenished because of nuclear fragmentation. Calculations of the absorption curve of protons with allowance for this effect were made by Waddington [426]. According to recent measurements, the intensity of primary protons near the equator ($p_c > 16$ GeV/c) is [434-436] /320

$$I_p = (100 \pm 7)\ m^{-2}\cdot sec^{-1}\cdot ster^{-1}.$$

This value can serve as a basis for the construction of the spectrum in the region of higher energy.

The data of [434] and [435] also agree with respect to the intensity of protons at momenta of about 4 GeV/c:

$$I_p = (550 \pm 40)\,\text{м}^{-2} \cdot \text{сек}^{-1} \cdot \text{стер}^{-1}.$$

These two values determine the exponent of the proton spectrum in the interval 4 — 16 GeV. It turns out to be $\gamma - 1 = 1.42 \pm 0.11$ in [434] and 1.50 ± 0.10 in McDonald's paper [437].

3. MEASUREMENTS OF THE INTENSITY OF THE COSMIC RADIATION AT THE BOTTOM OF THE ATMOSPHERE

3.1. Absorption Path Length L

The character of the primary spectrum extended to the region of very high energies makes it possible to introduce a parameter characterizing the passage of radiation through the atmosphere, called the absorption path length. This is defined as the path (in g/cm^2) in which radiation with a given energy is reduced e times.

If the energy spectrum has a constant exponent γ, then in the determination of L one can equally well use the differential or the integral intensity at different altitudes. But if γ changes with energy, then the L obtained by these two methods may be different. In the majority of cases the absorption path is determined from the integral intensity. The absorption path is closely related to three parameters: the interaction path λ, the exponent of the energy spectrum of the particles γ, and the distribution of the fraction of energy retained by a nucleon after interaction β:

$$L = \frac{\lambda}{1 - \langle \beta^{\gamma-1} \rangle}\,^{*}. \qquad (12.1)^{*}$$

Particles with energy E observed at the bottom of the atmosphere originate from primary nucleons and nuclei with ten times greater energy. Hence, if the exponent of the primary spectrum changes significantly when the energy is increased ten times, then L at the bottom of the atmosphere will differ from L in the upper layers. If all the variables that enter in L remain constant with energy, then the spectra of nucleons in the atmosphere should exactly repeat the primary spectrum, and the primary intensity is related to the intensity at the level of observation x by the formula

/321

$$I(x) = I(0)\,e^{-x/L}. \qquad (12.2)$$

*This formula was first obtained by Zatsepin [197].

If the primary spectrum experiences a change of exponent at some energy $E_k(0)$, the absorption path will be different in different energy regions.

The energy at which a change in the form of the spectrum occurs at the bottom of the atmosphere is significantly less than the primary energy. If it is assumed that when $E_0 < E_k$ the spectrum has exponent γ_1, and when $E_0 > E_k$ the exponent is γ_2, then the energy at which the spectrum undergoes a change will be reduced with depth according to the law [438]

$$E_k(x) = E_k(0) \exp\left\{-\frac{\beta^{\gamma_1-1} - \beta^{\gamma_2-1}}{\gamma_2 - \gamma_1} \cdot \frac{x}{\lambda}\right\}. \qquad (12.3)$$

If $\gamma_1 = 1.6$ and $\gamma_2 = 2.1$, then for $\beta \sim 0.5$, E_k changes by a factor of 10 at mountain heights. If the change in the primary spectrum sets in at 3×10^{14} eV (as assumed in [438]), the change in the exponent of the nucleon spectrum will be observed at 3×10^{13} eV, i.e., in a region which is practically unexplored at the present time. In the region of energies greater than $E_k(0)$ absorption of nucleons occurs with a path length

$$L_2 = \frac{\lambda}{1 - \beta^{\gamma_2-1}}.$$

If the exponent of the primary spectrum is known, the absorption path length can be determined from the energy distribution of protons arising in nuclear collisions from Eq. (12.1) or from the distribution of the total coefficients of inelasticity

$$\langle \beta^{\gamma-1} \rangle = \langle (1-K)^{\gamma-1} \rangle. \qquad (12.4)$$

Using the spectra presented in Chap. 6, we find $\langle \beta^{\gamma-1} \rangle = 0.27 \pm 0.04$ and $L \sim 115^{+9}_{-4}$ g/cm^2. The exponent of the primary spectrum is not very different from $\gamma - 1 = 2$. Hence /322

$$\langle \beta^{\gamma-1} \rangle \approx \langle \beta^2 \rangle = \langle (1-K)^2 \rangle$$

and

$$\frac{\lambda}{L} = 2\langle K \rangle - \langle K^2 \rangle. \qquad (12.5)$$

The magnitude of $\langle K^2 \rangle = 0.34 \pm 0.03$, and $\langle K \rangle = 0.55$. Consequently, $\lambda/L = 0.76 \pm 0.03$ and $L = 112 \pm 4$ g/cm^2.

3.2. Measurements of Absolute Intensity at the Bottom of the Atmosphere

Let us first consider the absorption path lengths of nucleons in the energy region where the measurements are made by magnetic methods. For this we compare the results of intensity measurements at the limits of the atmosphere

[426, 436, 437, 439] (magnetic field of the Earth) and at the bottom [413, 415] using magnetic spectrometers. We need to allow for the fact that only protons were measured in these investigations. In order to obtain the total number of nucleons, we shall assume that at depths of 700 and 1000 g/cm^2 the ratio of protons and neutrons is equal respectively to 1.15 and 1.0. In addition, it should be remembered that nucleons observed in the atmosphere occur not only from primary protons, but also from nuclei. Due to the fragmentation of primary nuclei the absorption of nucleons in the highest layers of the atmosphere is not exponential.

Estimates show that the absorption will be almost exponential beginning with 40 g/cm^2, where the intensity of nucleons with energy greater than a given amount differs little from the primary. Results of the calculation of L in the 10 GeV region are presented in Table 68.

TABLE 68. ABSORPTION PATH LENGTH IN AIR AT 20 GeV.

Depth, g/cm^2	Absolute intensity, $m^{-2}sec^{-1}ster^{-1}$	L, g/cm^2	Reference
40	200	122 ± 3	[434]
700	0.93	125 ± 2	[414]
1000	0.092	129 ± 7^{10}	[96]

Thus, the absorption of nucleons does in fact appear to be exponential with L = 125 ± 2 g/cm^2. /323

Most of the investigations of nuclear interactions at the bottom of the atmosphere are accomplished with "pulse" instruments or emulsion chambers. In all cases the determination of absolute intensity requires a conversion from the measured energy to the primary particle energy, based on certain assumptions.

Ionization calorimeters can give more definite data. The value of the absolute intensity of nucleons was obtained in [414] at an energy E_0 = 450 GeV and depth 700 g/cm^2, I(E ≥ 450 GeV, 700 g/cm^2 = (5.9 ± 0.8) x $10^{-8}cm^{-2}sec^{-1}ster^{-1}$. In the energy calculation no account was taken of the counting error in nuclear splitting and the energy output of the calorimeter (see Chap. 3). With these corrections, I(E > 450 GeV, x = 700 g/cm^2) = (8 ± 1) x $10^{-8}cm^{-2}sec^{-1}ster^{-1}$. These results were obtained at the same altitude as those of Kocharyan et al [413] and agree with them in absolute magnitude.

A value for the absolute intensity that is twice as large was obtained in [440] using a TAS. This value may be too high, since the individual detectors were too large and did not allow exclusion of cases of simultaneous incidence of several particles. The value obtained for the absolute flux of nucleons should be considered

is an upper limit. Comparison of the intensity on mountains with the primary intensity measured by the "Proton" satellites (with correction) gives the following values of the absorption path length at an energy of 450 GeV:

$$L = 110 \pm 3 \text{ g/cm}^2$$

$$L \leqslant 120 \pm 5 \text{ g/cm}^2 \text{ [440]}.$$

Thus, the absorption path length decreases somewhat with energy, which can be explained by a change in the primary spectrum between 10^{10} and 10^{12} GeV from 1.5 to 1.7. There are no direct measurements of absolute intensity in the energy region above 10^3 GeV.

3.3. Measurement of Nuclear-Active Particles with "Pulse" Instruments /324

A typical apparatus for measuring pulses is shown in Fig. 15 f. The graphite filter placed in the upper part of the apparatus serves as a target in which nuclear interactions take place. The photons produced in the target undergo cascade multiplication in the lead layers above the ionization chambers. The thickness of lead is such that the number of electrons in the maximum of the cascade shower is measured in the ionization chambers.

As is known, at the cascade maximum the number of electrons N_{max} is simply related to the energy of the photon evoking the shower. For lead this relation can be expressed by the formula

$$E_{e\text{-}ph} \approx 10^8 N_{max} \text{ eV}$$

Registration of an ionization pulse occurs when the amount of ionization exceeds a specific threshold ε. In this case the number of pulses $N_T(>\varepsilon)$ registered by the apparatus is

$$N_T(>\varepsilon) = N_0(>\varepsilon)\left\{\left(1 - e^{-\frac{x_C}{\lambda_C}}\right)\int_0^1 \alpha_C^{\gamma-1} f(\alpha_C)\, d\alpha_C + \right.$$
$$\left. + e^{-\frac{x_C}{\lambda_C}}\left(1 - e^{-\frac{x_{Pb}}{\lambda_{Pb}}}\right) W_{Pb}\int_0^1 \alpha_{Pb}^{\gamma-1} f(\alpha_{Pb})\, d\alpha_{Pb}\right\} =$$
$$= N_0(>\varepsilon)\left\{\left(1 - e^{-\frac{x_C}{\lambda_C}}\right)\langle\alpha_C^{\gamma-1}\rangle + e^{-\frac{x_C}{\lambda_C}} \times \right.$$
$$\left. \times \left(1 - e^{-\frac{x_{Pb}}{\lambda_{Pb}}}\right) W_{Pb}\langle\alpha_{Pb}^{\gamma-1}\rangle\right\}, \qquad (12.6)$$

where $N_0(>\varepsilon)$ is the number of nuclear-active particles with energy greater than ε; x/λ is the thickness of the filter in nuclear path lengths (C and Pb); $f(\alpha)$ is the distribution of the fraction of energy transferred to π^0-mesons in

the collision of nuclear-active particles with the nucleus; γ is the exponent of the energy spectrum at the level of observation; W_{Pb} is a coefficient that takes into account that the cascades arising in the depths of the lead filter are registered with less effectiveness, since the cascade is unable to reach a maximum. /32

Usually, the thickness of the lead filters is not large, and therefore the contribution of the second term is small in comparison with the first. The magnitude of $< \alpha^{\gamma-1} >$ can be directly obtained from the distributions of α for collision of nuclear-active particles with various nuclei (see Chap. 8). According to [304], $< \alpha^2_C >_p = 0.02$ for protons and $< \alpha^2_C >_\pi = 0.22$ for pions interacting in carbon.

When $x_C/\lambda_C << 1$ only one interaction can occur in the graphite filter and $f(\alpha)$ will pertain to the distribution of inelasticity α_0 in an act. Often it happens that the thickness x_C is comparable with λ_C [412, 440a]; then it is necessary to take into account repeated interactions, which can markedly increase $< \alpha_C^{\gamma-1} >$.

If the composition of the generating particles is complex, i.e., there are pions along with the nucleons, for example, Eq. (12.6) becomes more complicated, since terms that take into account the contribution of pions in making pulses appear in it:

$$N_\tau(>\varepsilon) \sim N_p(>\varepsilon)\left(1 - e^{-\frac{x_C}{\lambda_C}}\right) < \alpha_C^{\gamma-1} >_p + \\ + N_\pi(>\varepsilon)\left(1 - e^{-\frac{x_C}{\lambda_C}}\right) < \alpha_C^{\gamma-1} >_\pi. \qquad (12.7)$$

Since $< \alpha_C^{\gamma-1} >_\pi$ and $< \alpha_C^{\gamma-1} >_p$ are different, the ratio

$$\frac{N_\tau(>\varepsilon)}{N_0(>\varepsilon)} = \frac{N_\tau}{N_p + N_\pi} \qquad (12.8)$$

varies as a function of the fraction of pions in the generating component.

Hence without special analysis and calculation of all the enumerated factors it is not possible to determine the absolute intensity and absorption path of nucleons from pulse measurements.

As an example, we consider [412, 440a, b] where similar instruments were used at depths of about 200, 300 g/cm^2 [412] and 700 g/cm^2 [440a]. The number of pulses decreased 48 times between 197 g/cm^2 and 700 g/cm^2, from which it follows that the absorption path length of the particles creating the showers is /32

$$L = 129 \pm \frac{6}{4} \text{ g/cm}^2 \text{ for } E = 4 \cdot 10^{11} \text{ eV}$$

Using the results of measurement of pulses at a depth of 1000 g/cm^2 [440a], we obtain a still larger value for the absorption path lengths [412] (see Table 68).

This length is considerably greater than that obtained earlier for nucleons, (110 ± 3) g/cm^2, for the same energy region. The difference is even sharper if we compare the effective fraction of energy transferred to the photons in the measurements in the two cited references.

According to [412], in measurements at a height of 200 g/cm^2 the energy of the primary particle was $E_0 = (4.4 \pm 0.6)E_T$, whereas at 700 g/cm^2 [440b], the ratio is $E_0/E_T \sim 2.0$ (E_T is the energy of the pulse).

This difference is not hard to understand if it is realized that the pions are present in the nuclear component at the two altitudes in different amounts. Calculations based on various models show that the fraction of pions strongly decreases in the transition to low depths. The choice of any particular model for the development of a nuclear cascade in the atmosphere changes this conclusion only quantitatively. Calculations show that the fraction of pions between 200 and 800 g/cm^2 increases 3 to 4 times [411, 412, 440a, b]. Considering that at a depth of 700 g/cm^2 the fraction of pions amounts to about 30% (at 500 GeV), we obtain $N_\pi/N_p \lesssim 10\%$ for a height of 200 g/cm^2. The number of pulse at the two heights equals (N_p is the number of nucleons, N_π the number of pions)

$$\begin{aligned} N_T(200) &= N_p(200)\, W \langle \alpha^{\gamma-1} \rangle_p + N_\pi(200)\, W \langle \alpha^{\gamma-1} \rangle_\pi; \\ N_T(700) &= N_p(700)\, W \langle \alpha^{\gamma-1} \rangle_p + N_\pi(700)\, W \langle \alpha^{\gamma-1} \rangle_\pi. \end{aligned} \qquad (12.9)$$

The ratio of the number of pulses at the two heights equals

$$\frac{N_T(200)}{N_T(700)} = e^{\frac{500}{L_p} \frac{\langle \alpha^{\gamma-1} \rangle_p + 0{,}1 \langle \alpha^{\gamma-1} \rangle_\pi}{\langle \alpha^{\gamma-1} \rangle_p + 0{,}3 \langle \alpha^{\gamma-1} \rangle_\pi}}. \qquad (12.10)$$

(taking $L_p = 110$ g/cm^2 for the absorption path length of nucleons). The values of $\langle \alpha^{\gamma-1} \rangle$ for protons and pions were given earlier. However, in the present case further secondary interactions in the graphite filter should be taken into account. Then

$$\langle \alpha^{\gamma-1} \rangle_\pi^{\text{meas.}} = \frac{1}{2} \langle \alpha^{\gamma-1} \rangle_{\pi 2} + \frac{1}{2} \cdot \frac{1}{2} \langle \alpha^{\gamma-1} \rangle_{\pi 2} = \qquad /327$$

$$= \frac{3}{4} \langle \alpha^{\gamma-1} \rangle_{\pi 2} \sim 0{,}4;$$

$$\langle \alpha^{\gamma-1} \rangle_p^{\text{meas.}} = \langle \alpha^{\gamma-1} \rangle_p e^{-\frac{x_C}{2\lambda_C}} + \left\langle \left(\alpha + \frac{1}{2}\alpha\right)^{\gamma-1} \right\rangle_p \times$$
$$\times \left(1 - e^{-\frac{x_C}{2\lambda_C}}\right) \approx 1.4 \langle \alpha^{\gamma-1} \rangle_p \approx 0.04.$$

For the calculation we take $\gamma - 1 = 2$; however, the ratio obtained does not change much if one takes $\gamma - 1 = 1.8$ or 1.9. Substituting these values into (12.9), we find

$$\frac{N_\tau(200)}{N_\tau(700)} = 94 \frac{0.08}{0.16} = 47,$$

which is practically the same as the experimental value. At a depth of 1000 g/cm^2 the fraction of pions increases slightly compared to the fraction at 700 g/cm^2 (10 - 20%). Substituting $(N_\pi/N_p)_{1000} = 0.30$ into (12.9), we find

$$\frac{N_\tau(700)}{N_\tau(1000)} = 13.5,$$

which equals the experimental ratio measured in [440c].

Thus the absorption path length of nucleons with energy ~500 GeV equals ~ 110 g/cm^2 on the basis of data from pulse instruments also. The results of the measurement of the height dependence of the number of nuclear interactions in emulsion [440d] are in agreement with these conclusions, although the absolute values of the intensity obtained from the photoemulsion data are more complicated (Fig. 76). If one starts from the measured absorption path length of the component generating the pulses, and from the absorption path of nucleons L_p = 110 g/cm^2, then one can estimate the absorption path of pions in the interval of depths 200 - 700 g/cm^2 at an energy of 500 GeV:

$$L_\pi \sim 140 \text{ g/cm}^2$$

Measurements of the absolute intensity of pions on mountains and at sea level also give the possibility of evaluating the absorption path of pions. If we start with the data of Kocharyan et al. [413] at the 700 g/cm^2 level and the measurements of Brook et al. [96] at sea level, we can find the following value for the absorption path length of pions for $2 \cdot 10^9 < E_0 < 3 \cdot 10^{10}$ eV: $L_\pi = \left(155 \pm \frac{35}{20}\right)$ g/cm^2. /328

Figure 77 shows the dependence of L_π on energy obtained by Brook et al. [96] by comparing the calculated intensity of pions at sea level with the experimental value. The calculation was based on the spectrum of pion generation, which was found from the muon spectrum at sea level:

$$F(E_\pi)\, dE_\pi = N_\mu \left(\frac{E_\pi}{r}\right)\left(1 + \frac{E_\pi}{rB}\right) D(E_\pi) \frac{1}{r}\, dE_\pi, \qquad (12.11)$$

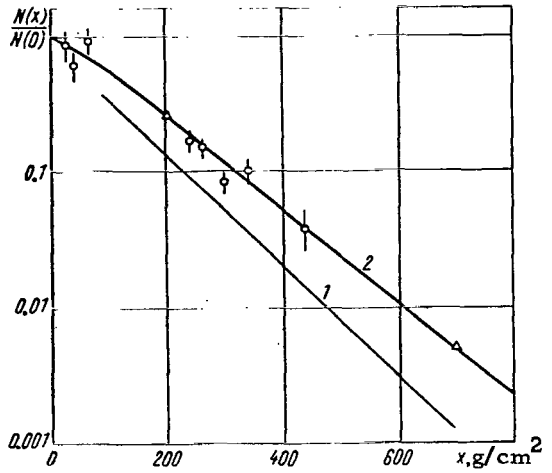

Figure 76. Dependence of the Number of Nuclear Interactions on Atmospheric Depth:

1 - - for Nucleons; 2 - for Nuclear-Active Particles; ○ — Photoemulsion, △— "Pulses".

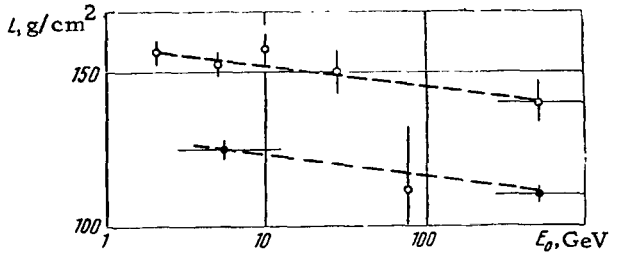

Figure 77. Dependence of Absorption Lengths on Energy:

○ — for Pions.

where N_μ is the muon spectrum; $B=90$ GeV; $r=1{,}32=\frac{m_\pi}{m_\mu}$; $D(E_\pi)$ takes into account $(\mu-e)$ - decay and ionization losses. This formula was obtained in [441]. Then

$$\pi(E, x)\,dx = F(E)\,dE\cdot e^{-\frac{x}{L_\pi}}\frac{x}{L_p}\times \qquad /329$$

$$\times\left\{\frac{1}{1+\frac{B}{E}}-\frac{\frac{x}{L'}}{2+\frac{B}{E}}+\frac{1}{2!}\cdot\frac{\left(\frac{x}{L'}\right)^2}{3+\frac{B}{E}}+\ldots,\right\} \qquad (12.12)$$

$$\frac{1}{L'}=\frac{1}{L_p}+\frac{1}{L_\pi}.$$

In order that this coincide with experiment, it is necessary to take the values of L_π given in Fig. 77. The point at $E \sim 10^{11}$ eV is located considerably below the others. However, this point is based on a result obtained with higher statistical error. The arguments considered above are evidence that the absorption path length of pions is markedly larger than for nucleons in the energy region 10^{11} - 10^{12} eV.

The difference between the absorption and interaction paths of pions is thought to be due to the existence of a mechanism leading to the regeneration of pions [442]. It can be assumed that in each interaction one of the pions retains about 45% of the initial energy. Considering that in 1/3 of 1/2 of the cases the pion may be neutral, we must conclude that on the average the energy conserved in the pion (charged or neutral) is greater than this.

3.4. High-Energy Photons in the Atmosphere

/330

The energy spectrum and absolute number of photons arising in 1 g of air was studied in [443, 444 - 447]. Measurements of photon (or electron) cascades are carried out with photoemulsions, pulse instruments, or calorimeters. Duthie et al. [444] obtained the spectrum close to the limits of the atmosphere in the interval of energies from 500 to 1500 GeV. The index of the integral spectrum $\gamma - 1 = 2.0 \pm 0.5$, and the absolute number of photons

$$\Gamma\ (0;\ 470\ \text{GeV} = (1.6 \pm 0.2) \cdot 10^{-8} / \ (\text{g} \cdot \text{sec} \cdot \text{ster})$$

Abraham et al. [445] found that at a depth of 9 g/cm^2 in the atmosphere and 5 g/cm^2 of a dense substance the photon flux $\Gamma_s(\varepsilon)$ equals

$$\Gamma_s(\varepsilon > 1000\ \text{GeV} = (10.5 \pm 3.5) \cdot 10^{-8} / (\text{cm}^2 \cdot \text{sec} \cdot \text{ster})$$

whereas Kidd [446] gives

$$\Gamma_s(\varepsilon > 1000\ \text{GeV} = (5.5 \pm 3.0) \cdot 10^{-8} / \ (\text{cm}^2 \cdot \text{sec} \cdot \text{ster})$$

The total result from these two papers

$$\Gamma_s(>\varepsilon) = 8 \cdot 10^{-8} \left(\frac{\varepsilon}{1000}\right)^{-1.9 \pm \substack{0.3 \\ 0.2}} / \ (\text{cm}^2 \cdot \text{sec} \cdot \text{ster})$$

This result may be expressed in the same units as in [444]

$$\Gamma(>\varepsilon) = 2.3 \cdot 10^{-8} \left(\frac{\varepsilon}{470}\right)^{-1.9 + \substack{0.3 \\ 0.2}} / (\text{g} \cdot \text{sec} \cdot \text{ster})$$

This is 1.5 times greater than in [444].

Measurements by Malhotra et al [140] at a depth of about 20 g/cm^2 lead to the following value for the intensity of photons from air:

$$\Gamma(>\varepsilon) = 1.2 \cdot 10^{-8} \left(\frac{E}{450}\right)^{-1.72}.$$

In the work of Baradzei et al. [443, 447] the number of generated photons was measured at a depth of about 200 g/cm^2

$$\Gamma(>\varepsilon) = (3.8 \pm 0.4) \cdot 10^{-9} \left(\frac{470}{\varepsilon}\right)^{1.76 \pm 0.22} / \text{g} \cdot \text{sec} \cdot \text{ster}$$

Consequently, within the limits of experimental error, the spectra in the depth interval 0 - 200 g/cm^2 remain the same, at least to energies ~2 - 3 x 10^{12} eV. In the case of registration of photons the requirement for the identity of apparatus is less rigid, since the efficiency of registration of photons is close to unity. However, even in this case, there is a significant difference between emulsions, where it is possible to register individual photons, and pulse instruments, in which groups of particles are often registered, particularly at high energies and in the bottom of the atmosphere. /331

Since photons are extremely effectively generated by π-mesons, the absorption path of the component producing photons in air should be greater than the absorption path length of nucleons.

Baradzei et al. [443] determined the number of photons from air at depths of 200 and 1000 g/cm^2 (see Table 69).

TABLE 69. ABSORPTION PATH LENGTH OF PARTICLES PRODUCING PHOTONS.

Energy, eV	$5 \cdot 10^{11}$	10^{12}	10^{13}	$5 \cdot 10^{13}$
L (nuclear interactions in filter, g/cm^2)	149 ± 10	146 ± 10	132 ± 10	120 ± 15
L (photons), g/cm^2	—	148 ± 10	135 ± 10	120

In these experiments the measured quantity is the photon flux, and the generation spectrum (i.e., the number of photons of different energies created per gram of substance) is determined by calculating the effective thickness of the layer in which the registered photons (or electrons) arise.

In the case of registration of individual photons, the thickness of the effective layer T_γ is independent of energy, but varies with depth. The effective thickness is particularly simply determined near the limits of the atmosphere, $x \ll t$, where x is the depth of atmosphere in g/cm^2 and t is the length of the avalanche unit (t = 37 g/cm^2 in air). In this case the effective layer equals x. Table 70 gives the dependence of T on x, as calculated in [412].

TABLE 70. DEPENDENCE OF T ON x.

x g/cm^2	7	200	310	740	▼1000
T_γ	0.20	1.88	1.98	2.0	2.0

If the photon is converted into an electron-positron pair, then immediately several particles are incident on the apparatus and the total energy of the particles is measured. Depending on the size of the detector and on the energy of the photons, the thickness of the layer T_e from which the particles are collected will vary. The thickness T_e is a strong function of the energy. Hence an inaccuracy in determining $T_e(E)$ can distort the form of the photon spectrum, and in a different way at each height. /3 /3

Hence, it is now difficult to be certain that a physical meaning can be attached to any variance of the photon production spectra at different depths.

Table 71 gives measured values of the exponents of the photon spectra at several depths. At a certain energy of the photons, close to 1000 GeV, the photon spectrum becomes, apparently, more steep. This increase in exponent has been reported in a number of papers and is illustrated in Table 71. The first indication of the existence of a "break" in the photon spectrum was obtained in work by Fudzimoto et al. [448], who observed that at a height of 730 g/cm^2 there occurred a change in the exponent from $\gamma - 1 = 1.8 \pm 0.2$ to 2.8 ± 0.2 in the vicinity of 10^{12} eV.

Later data of the Japanese-Brazilian emulsion group indicates that at energies greater than 10^{12} eV the exponent equals 2.3 ± 0.15 and 2.2 ± 0.15 at depths of 730 and 550 g/cm^2, respectively. At lower energies the photon spectrum gradually becomes flatter. In work by Akashi et al. [453] measurements were taken, just as in the preceding work, with an emulsion chamber set up on Mt. Norikura in Japan (730 g/cm^2). In this work, the existence of a break in the photon spectrum at an energy of about 10^3 GeV was again confirmed. At a depth of 220 g/cm^2 a change in the exponent of the photon spectrum from $\gamma - 1 = 2.3 \pm \pm 0.2$ to 2.8 ± 0.2 was noted with the aid of the photoemulsion technique [444]. This change occurs at 1.5×10^3 GeV. Near the limits of the atmosphere no change was found in the spectrum up to energy $(1.5 - 2) \times 10^3$ GeV [444, 446] and Malhotra et al. [140] found a change in the photon spectrum at 3×10^3 GeV.

Thus, with the aid of photoemulsions, which give the possibility of studying the spectrum of individual photons, a change is observed in the exponent of the spectrum in the region of photon energies $(1 - 3) \times 10^3$ GeV. Of course, it should be mentioned that the statistical reliability of this result is still insufficient. Obviously, if the energy at which a change in exponent is observed is not the same

TABLE 71. EXPONENT OF THE PHOTON SPECTRUM /332

Depth in atmosphere g/cm²	Place of method of measurement	Exponent of the photon spectrum		Exponent of the spectrum of the total photon energy ΣE_γ		Reference
		$E_\gamma < 10^{13}$ eV	$E_\gamma > 10^{13}$ eV	$\Sigma E_\gamma < 10^{13}$ eV	$\Sigma E_\gamma > 10^{13}$ eV	
9	Emulsion pile	$1.9 \pm {}^{0.3}_{0.2}$	—	—	—	[446]
20	Emulsion chamber	1.72	3.0 ± 0.8	1.44 ± 0.05	1.44	[140]
22	Emulsion chamber	1.75 ± 0.20	—	2.04 ± 0.22	2.0	[139]
30	Emulsion chamber	2.0 ± 0.2	—	—	—	[449]
197	Airplane, ionization chamber	1.76 ± 0.11	—	1.6 ± 0.1	—	[412]
220	Airplane, emulsion pile	2.3 ± 0.2	2.8 ± 0.3	2.0 ± 0.1	2.0	[444] [440r]
310	Airplane, ionization chamber	1.83 ± 0.13	—	1.53 ± 0.12	—	[412]
550	Mt. Chakaltaya, emulsion chamber	—	2.2 ± 0.15	2.0 ± 0.5	—	[84]
700	Tien Shan, calorimeter	2.1 ± 0.1	—	—	—	[450]
730	Mt. Norikura, emulsion chamber	1.8 ± 0.2 2.0 ± 0.2	2.8 ± 0.2 2.3 ± 0.2	2.21 ± 0.3	—	[448] [203, 451]
730	Mt. Norikura, ionization chamber	1.82	—	—	—	[452]
1000	Ionization chamber	1.86	—	—	—	[452]
1000	Ionization chamber	2.0 ± 0.2	—	1.96 ± 0.03	—	[412]

at different depths, the absorption path of the number of photons will strongly depend on energy [454]. /334

Measurements of the photon spectrum with an ionization chamber do not show a change in the spectra up to energies 10^{13} eV [412]. Observation of "young" atmospheric showers, which are showers produced from photons in air not far from the apparatus, also gives a spectrum with constant slope $\gamma - 1 = 1.69 \pm 0.08$ to energies $\geq 10^{13}$ eV (on mountains) [455]. The spectra of electron-photon cascades which are engendered in the apparatus in nuclear interactions, as already mentioned, have an almost constant slope.

The difference between experiments involving the observation of individual photons with photoemulsions and of photon showers with pulse instruments is that in the latter case groups of photons can be registered, i.e., the total energy transferred in the act to all photons. Just as in the case when cascades are

produced in the apparatus, a "break" in the spectrum may turn up at energies that are several times or even an order of magnitude greater, if the total energy of the photons per act is several times greater than the energy of the individual photons [448].

Other explanations of the difference in the spectrum of local cascades or pulses compared with the spectrum of individual photons are based on the assumption that there is a change in the characteristics of the elementary act at energies $\sim 10^{14}$ eV.

Nikolskiy and Smorodin [456], as well as Fudzimoto [448], assumed that the inelasticity α_0 is independent of energy, but that the partition of energy is increased in its distribution among the secondary π^0-mesons. There may be, for example, a rapid rise in the multiplicity of neutral mesons.

On the other hand, Duthie et al. [457] hypothesize that the decrease in α_0 with energy should lead to the same change in the spectrum of local (i.e., emerging in the apparatus) cascades as for photons, when the total energy transferred to photons in an act is measured, and that it is not observed in the experiment.

If there is a change in the elementary act the break in the photon spectrum should be observed at all heights at the same energy. * Data has already been presented that indicates an apparent shift of the spectral break toward higher /335
energies at great heights. There is not enough information at present to establish accurately the region of the break as a function of height. If the shift of the /336
break with height is confirmed by further experiments, the interesting possibility of explaining the breaks in the photon spectrum by the change in slope of the primary spectrum in the vicinity of 3×10^{14} eV will be opened up [438, 454].

Pal and Tandon [454] calculated the photon spectra in the atmosphere at various depths on the basis of the isobar model developed earlier by Pal and Peters [411]. The result agrees well with the experimental photon spectra at different heights and with the muon spectrum at sea level, if it is assumed that the break in the primary spectrum occurs near 3×10^{14} eV (Fig. 78). ** During the interaction, a significant fraction of the primary particle energy is retained by nucleons. Therefore the nucleon spectrum will change at higher energies than the photon spectrum.

---

*Hayakawa and Ogita [458] proposed a mechanism which may explain a shift of the break in the energy spectrum with depth. They assumed that at an energy $\sim 10^{14}$ eV the spectrum of generation of secondary nuclear-active particles softens. Such a softening must be felt by photons in the depths of the atmosphere.

** Pal and Tandon considered the primary spectrum to consist of two components, one of which sustains a break, and the other, of lower intensity (consisting of nucleons), extends out to the highest energies.

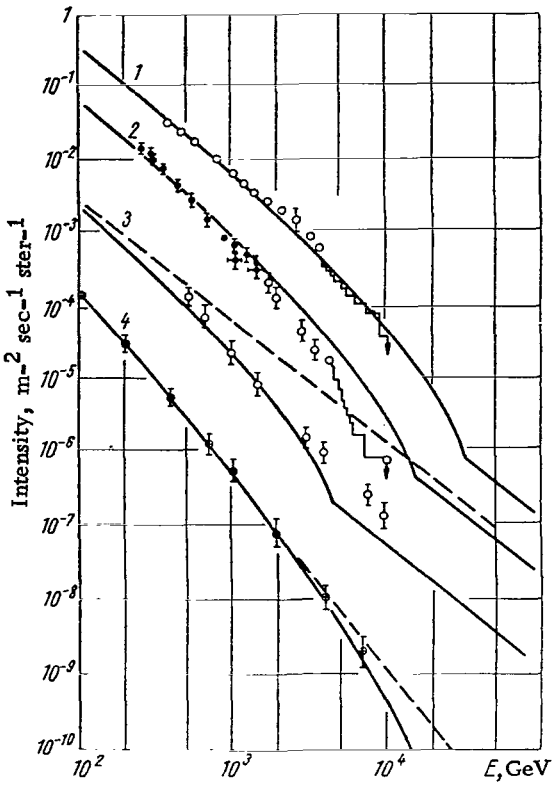

Figure 78. Energy Spectra of Photons at Different Depths in the Atmosphere [454]:

1 - Depth 20 g/cm^2 [140]; 2 - 220 g/cm^2 [444]; 3 - 550 g/cm^2 [84]; 4 - Spectrum of Muons at Sea Level; ⊕ - Intensity of Muons Underground; Solid Lines - Calculation on the Isobar Model [454]. Dashed Lines - Calculation without Accounting for a Change in the Primary Spectrum.

Estimates show that if $<\beta^{\gamma-1}> \approx 0.25$, the change in the nucleon spectrum on mountains will occur at an energy approximately 10 times less than in the primary radiation. Hence if the assumption of Pal and Tandon about the change in the primary spectrum in the region of 10^{14} eV is correct, the change in the nucleon spectrum on mountains should be expected at energies $\sim 10^{13}$ eV. There are too few data on the nucleon spectrum in this region to check this possibility.

The spectrum of solitary photons in the atmosphere should experience a break at considerably lower energies than the nucleon spectrum.

In [438] the location of the break point in the photon spectrum was obtained under the same conditions that apply to Eq. (12.3):

$$E_{k\gamma}(x) = 0.40 \langle u \rangle E_k(x),$$

where $E_k(x)$ is the break point in the nucleon spectrum at depth x. The quantity $\langle u \rangle$, the average fraction of photon energy, amounts to several percent.

As already mentioned, the nucleon spectrum in the atmosphere has a slope /337
$\gamma - 1 \sim 1.9 - 2.0$ compared with $\gamma - 1 = 1.7$ for the primary spectrum.

It is possible to explain a small change in the spectrum by assuming a change in any of the variables entering into Eq. (12.1). Since there is no large amount of data about the elementary act at energies greater than 10^{13} eV, one can take a change in λ, as is done by Grigorev et al. [68], or a change in β (i.e., in inelasticity). However, a further possibility is a change in the slope of the primary spectrum from 1.7 to 1.9 in the region $\geq 10^{13}$ eV. If the primary spectrum changes strongly in the region $\geq 10^{14}$ eV, it is obvious that this change cannot occur suddenly at a definite energy, but must develop at lower energies.

In conclusion we remark that there is a difference in the position of the break in the primary spectrum found by the method of broad showers ($\geq 10^{15}$eV) and from the change of slope in the photon spectrum ($\sim 10^{14}$ eV) (see Chap. 13).

However, it should be remembered that this latter estimate is obtained on the basis of specific assumptions about the mechanism of the elementary act (isobar model). Other models may give different estimates for the critical energy.

3.5. Differences between the Spectra of Photons and the Spectra of ΣE_γ

In Table 71 are shown the results of the measurement of the exponent of the spectra of photons and the spectra of the total energy transferred to photons per act. One sees a small, but systematic, difference in the spectra, which is usually explained by an increase in the effective multiplicity of photons N_γ. If it is assumed that $N_\gamma = bE_0^m$, where E_0 is the energy of the primary particle, then, letting γ_1 and γ_2 be the exponents of the spectra of photons and nuclear-active particles, we find [459]

$$m = \frac{\gamma_1 - \gamma_2}{\gamma_1 - 1}.$$

Substituting values of γ_1 and γ_2 from [140], we find

$$m = 0.23 \pm 0.17.$$

The same value of m is obtained from measurements at heights to 10 km [459]. /338
Thus, the multiplicity increases in the region of energies $\sim 10^3 - 10^4$ GeV. However, it should be kept in mind that this pertains not to the total, but to the effective multiplicity, i.e., on the average to the more energetic photons.

4. RATIO OF NEUTRAL AND CHARGED PARTICLES PRODUCING SHOWERS.

4.1. Experimental Determination of the Ratio of Charged and Neutral Particles

The study of the ratio of charged and neutral particles creating nuclear interactions of high energy has been conducted in various energy intervals with the aid of electronic instruments and photoemulsions. In the outer reaches of the atmosphere the ratio of neutral to charged particles N/C is determined as the fraction of neutrons which have arisen as a result of the fragmentation of primary nuclei or charge exchange of protons during nuclear interactions.

At depths greater than 40 g/cm^2, where primary nuclei are able in large part to interact and dissociate into their composite particles, N/C is defined as the ratio of neutrons and protons

$$\frac{N}{C} = \frac{n}{p}.$$

Most of the neutrons come from nuclear fragmentation, since protons are still unable to interact.

As one gets deeper into the atmosphere, the fraction of neutral particles due to proton conversion (probability η_{pn}) increases. Simultaneously, pions and possibly kaons will show up in the charged component. Thus, at great depths

$$\frac{N}{C} = \frac{n}{p+\pi+K}.$$

Therefore, the study of the ratio N/C gives information about the composition of the nuclear component of the cosmic radiation.

If the interaction cross section and the probability η_{pn} are independent of /339
energy, the quantity N/C should not depend on energy at great depths. However, at those depths where pions are present, an energy dependence of N/C should be observed up to energies of 1 to 5 x 10^{11} eV, since the ratio is affected by pion decay at the lower energies.

Table 72 gives the results of the measurement of the ratio N/C at different heights. The method of determination depends on finding the presence of charge on the particles that have evoked a nuclear interaction.

TABLE 72. RATIO OF THE NUMBER OF CHARGED AND NEUTRAL NUCLEAR-ACTIVE PARTICLES.

Depth g/cm^2	Energy, GeV	N/C	Reference
5—50	10^3	0.083 ± 0.03	[146]
610	200—2000	0.74 ± 0.08	[460]
670	10	0.77 ± 0.035	[461]
670	3	0.70 ± 0.14	[462]
700	—	0.70 ± 0.20	[463]
700	200—1000	0.57 ± 0.10	[464]
710	80	0.77 ± 0.12	[465]
710	200—2000	0.65 ± 0.007	[460]
780	200—2000	0.56 ± 0.11	[460]
800	20—150	0.69 ± 0.13	[466]
800	60	0.40 ± 0.12	[467]
800	20—40	0.66 ± 0.11	[467]
1000	27	0.64 ± 0.08	[96]

The considerable scatter in the data is due principally to different methods of event selection. The presence of an air accompaniment of the registered particles is of considerable significance. For example, in [467] cases in which air showers were incident on the apparatus were excluded. In [410], high-density showers were excluded. In some of the papers, all events were recorded. If it is admitted that pions have a different air accompaniment from nucleons, the ratio N/C can be distorted if cases with showers are excluded.

4.2. Ratio of Protons and Neutrons at Different Depths and the Charge Exchange Coefficient η /3

a. Relation between the ratio n/p and η. Because of the difficulties in determining the nature of particles at high energies there is a dearth of experimental data on the ratio of protons and neutrons at great depths in the atmosphere.

An exception is [467], where protons and pions could be distinguished by means of a gaseous Cerenkov counter in the energy interval 20 - 40 GeV. In this interval the ratio $n/p = 0.98 \pm 0.18$. The ratio n/p depends on the probability of the inelastic conversion of a proton into a neutron η_{pn}. It is usually assumed that the reverse reaction $n \to p$ has the same probability

$$\eta_{pn} = \eta_{np} = \eta.$$

If after collision a nucleon retains a fraction of energy β, the ratio of the number of neutrons and protons can be described by the following expression:

$$\frac{n}{p} = \frac{1 + \rho_0 + (\rho_0 - 1)\, e^{-2x/\lambda \langle \eta \beta^{\gamma-1} \rangle}}{1 + \rho_0 - (\rho_0 - 1)\, e^{-2x/\lambda \langle \eta \beta^{\gamma-1} \rangle}}, \qquad (12.13)$$

where ρ_0 is equal to the ratio n/p in the primary radiation 0.15. The magnitude of ρ_0 can be determined from the composition of the primary radiation, which is known with sufficient accuracy to energies of 10^3 GeV and $\rho_0 = 6.7$.

b. Charge exchange coefficient. The balance of the energy of the secondary components in the interaction of protons with heavy emulsion nuclei has been studied [158] (see Table 54). It was found that at a proton energy of 24 GeV the average fraction of the energy borne off by protons and neutrons was the same. Consequently, $\eta \sim 0.5$. At the same primary energy, interactions of protons with light nuclei ($N_h \leq 3$) were studied in [293], where conservation of the proton was found in 60% of the cases, i.e., $\eta = 0.4 \pm 0.06$.

Table 73 gives the results of the determination of η in proton-nucleon collisions at 23 GeV [468]. The quantity η was analyzed as a function of the total number of particles in stars (n).

TABLE 73. CHARGE EXCHANGE COEFFICIENT η AT 23 GeV [468]. /341

$n<4$	$n\geqslant 5$	$n\leqslant 8$		Average
		pp (even n)	pn (odd n)	
0.36 ± 0.05	0.42 ± 0.06	0.33 ± 0.06	0.43 ± 0.06	0.39 ± 0.04

In the vicinity of 100 GeV, η was determined by comparing the ratio n/p calculated from Eq. (12.13) and the measured value $n/p = 0.98 \pm 0.18$ at 20 - 40 GeV; however, the authors assume that the observed nucleons originate from particles with an energy of $\sim$ 100 GeV. By varying the parameters in the formula ($L = 120$ g/cm^2, $\lambda = 72 - 90$ g/cm^2), the authors concluded that the minimum value of η is 0.2. The most probable value is $\eta = 0.3^{+0.2}_{-0.1}$. This depends on what the ratio of λ to L is presumed to be.

In [232] the surviving nucleon was analyzed at energies of 10^{12} eV. In doing this, the interaction length is used to calculate the number of secondary interactions of nucleons which should be observed for a given experimental geometry. The value of λ was taken to be 36 cm. The expected number was found to be 20.

Then, the 20 interactions having the greatest energy were selected from among the secondary interactions found in the experiment (the energy was measured by the Castagnoli method). It was assumed that these interactions were produced by a surviving nucleon. In a similar manner, six tertiary baryons

were found. Of the 20 first-generation particles, 5 were neutral and 14 were charged. From this the authors obtained the probability

$$\eta = \frac{5}{19} = 0.26 \pm 0.12.$$

However, in this paper it had been previously assumed that an energetically isolated nucleon always exists. As was shown in Chap. 8, if pions are present among the most energetic particles in heavy nuclei, the charge exchange coefficient η is underestimated. /342

On the basis of the data in Chap. 8, we can correct this value. Considering that about 2/3 of all interactions in emulsions occur at heavy nuclei and the probability of emission of a pion in this case reaches 0.5, we obtain

$$[\eta \approx 0.4 \pm 0.15.$$

In a study of the interaction of π^--mesons with nucleons at $E_0 = 4.4$ GeV/c, Malhotra found $\eta = 0.45 \pm 0.07$. In p-N collisions at 6.2 GeV, the value is 0.51 ± 0.05 [469].

Thus, most of the data gives $\eta = 0.4 - 0.5$.

c. Ratio n/p. Since there is so little experimental data on the ratio of protons and neutrons in the atmosphere, we have to find it from (12.13) by assuming some values for η, $\langle \beta^{\gamma-1} \rangle$, and λ. Table 74 gives the results of such a calculation.

TABLE 74. THE RATIO n/p AT VARIOUS DEPTHS IN THE ATMOSPHERE, AS CALCULATED FROM EQ. 12.13.

η	$\langle \beta^{\gamma-1} \rangle$	x/λ										
		1	2	3	4	5	6	7	8	9	10	11
0.5	0.3	0.29	0.41	0.50	0.62	0.71	0.77	0.83	0.87	0.91	0.92	0.95
	0.25	0.27	0.39	0.48	0.57	0.65	0.71	0.77	0.83	0.85	0.88	0.91
0.3	0.37	0.25	0.36	0.45	0.54	0.61	0.67	0.73	0.77	0.82	0.85	0.88
		for $\lambda = 85 g/cm^2$ x equals										
		85	170	255	340	425	510	695	680	765	850	935

4.3. The Ratio of Pions and Nucleons.

Table 75 gives the results of the measurement of the ratio π/p at different heights in the atmosphere and at different energies.

TABLE 75. RATIO OF THE INTENSITIES OF PIONS AND PROTONS. /343

Height g/cm^2	Energy GeV	$\frac{\pi}{p}$	Method of measurement	Reference
1000	2 5 10 27 80	0.17 ± 0.05 0.30 ± 0.05 0.60 ± 0.10 0.50 ± 0.10 0.39 ± 0.17	Magnetic spectrometer —	[96]
800	20—40	0.48 ± 0.11	Gaseous Cerenkov counter	[467]
700	200—1000	0.50 ± 0.08	Ratio $\frac{N}{C}\left(\frac{n}{p}=0.85\right)$	[410]
700	1.8—22	0.06 ± 0.02	Magnetic spectrometer	[470]
700	1÷2	0.05	Magnetic spectrometer	[471]

Thus, the fraction of pions in the flux of the nuclear component increases with energy. It reaches 25 - 30% at $E_0 \gtrsim 10^{11}$ GeV.

5. THE MUON COMPONENT OF COSMIC RAYS

5.1. Energy Losses by Muons

Muons are formed in cosmic rays as the result of the decay of π - or K-mesons in the upper atmosphere. Because of a weak interaction with material and a relatively long lifetime, the muon flux reaches sea level with practically no attenuation of its intensity and energy.

The amount of energy lost by muons in a material is determined principally by electromagnetic interactions and is contributed to by ionization and excitation of atoms in the material, pair formation, and retardation radiation. To these we should also add losses from nuclear interactions. Up to the present time, these have been determined the least accurately. The average value of the energy lost by muons in air is taken to be $<\varepsilon> = 2.2$ MeV $(g/cm^2)^{-1}$. A muon having an energy E_μ at sea level will be formed at depth x_0 from the decay of π - or K-mesons with energy /344

$$E_{\pi,K} = \frac{1}{r}\left[E_\mu + \varepsilon(x_0 - x)\right],$$

where

$$r = \frac{m_\mu}{m_{\pi,K}}.$$

The flux of muons with energy in the interval from E_μ to $E_\mu + dE_\mu$ arising from the decay of π- or K-mesons at a depth x in the atmosphere was calculated by Zatsepin and Kuzmin [472]. Solving the kinetic equation for the passage of muons in the atmosphere, they found

$$N^{\mu}_{\pi,K}(E_\mu, x, \theta) = AB_{\pi,K} \exp\left\{-\frac{m_\mu cL(\theta)}{\tau_0 E_\mu} + b\lambda x\right\} \times \\ \times E_\mu^{-\gamma} \sum_{i=1}^{\infty} \frac{d^{i-1}}{1 + i\frac{k_{\pi,K}}{E_{\pi,K}(\theta)} E_\mu}, \qquad (12.14)$$

where

$$B_{\pi,K} = \frac{1 - \left(\frac{m_\mu}{m_{\pi,K}}\right)^{2\gamma}}{\gamma\left(1 + \frac{m_\mu^2}{m_{\pi,K}}\right)};$$

$$k_{\pi,K} = \frac{\gamma + 1}{\gamma} \cdot \frac{1 - \left(\frac{m_\mu}{m_{\pi,K}}\right)^{2\gamma}}{1 + \left(\frac{m_\mu}{m_{\pi,K}}\right)^{2(\gamma+1)}};$$

m_μ and τ_0 are the mass and lifetime of the muon; $m_{\pi,K}$ is the mass of the pion or kaon giving birth to the muons; λ is the mean free path for the interaction of nuclear-active particles; b is a coefficient taking into account the losses of muons in pair formation and radiative retardation; $L(\theta)$ is the geometric path traversed by the muon from its point of origin to the point of observation; $E_{\pi,K}(\theta)$ is the critical energy at which the probability of decay for the π- or K-meson becomes equal to the probability of a nuclear collision; $d = 1 - L^{-1}$, where L is the mean free patch for absorption of nuclear-active particles; $\gamma - 1$ is the exponent of the integral energy spectrum of the particles producing muons; x is the path length; (θ) is the zenith angle for muons in the atmosphere; A is a normalizing factor. /34

Values of $k_{K,\pi}$, $B_{\pi,K}$, and $E_{\pi,K}(\theta)$ are given in Table 76 for various values of γ and θ.

TABLE 76. VALUES OF THE CONSTANTS NECESSARY FOR CALCULATING THE MUON FLUX.

a

$\gamma-1$	k_π	k_K	B_π	B_K
1.5	1.22	1.40	0.706	0.419
2.0	1.21	1.33	0.635	0.350
2.5	1.20	1.28	0.575	0.300

b

$\cos\theta$	0	0.05	0.1	0.2	0.3	0.4	0.6	1.0
$E_\pi(\theta)$, TeV	1.14	1.025	0.846	0.540	0.381	0.287	0.193	0.116
$E_K(\theta)$, TeV	8.41	7.58	6.25	3.99	2.82	2.12	1.43	0.858

The energy spectrum of muons depends on their generation mechanism. Osborne and Wolfendale [165, 473] calculated the spectrum under the assumption that muons are generated from the decay of π- and K-particles. The results were compared with measurements made with a magnetic spectrometer [473]. Accounting only for pions, the measured spectrum deviates from the calculated one by 11% at ~ 300 GeV and by 25% at ~4000 GeV. For K-mesons, the differences are much greater. These data give the fraction of K-mesons with respect to π-mesons to be between 10 and 40%.

By making use of the differential spectrum of muons in the atmosphere and the path-to-energy ratio, it is possible to calculate the angular distribution of muons at different depths in the ground under the assumption that they arise from the decay of π- or K-mesons [474]. A comparison of the results of the calculation with the experimental angular distribution should also throw light on the mechanism of muon production and give the magnitude of the ratio between the numbers of π- and K-mesons. /346

The obtained dependence of the exponent of the angular distribution (approximated by a cosine function) on depth in the ground agrees with the assumption that the fraction of K-mesons with respect to π- mesons is about 20 %.

The ratio of K-mesons to π-mesons was investigated by Asatiani et al. [475] from the polarization of cosmic muons. The experimental data on the fraction of K-mesons at different energies of cosmic particles are given in Table 35, from which it is seen that muons come from K-mesons in 10 - 40% of the cases. /347

The magnitude of the ratio μ^+/μ^- for a vertical flux of muons at different energies is of interest for the analysis of the passage of cosmic radiation through the atmosphere. These data are presented in Fig. 79. At energies < 50 GeV, the ratio $\mu^+/\mu^- \sim 1.25$ and increases somewhat with increasing energy.

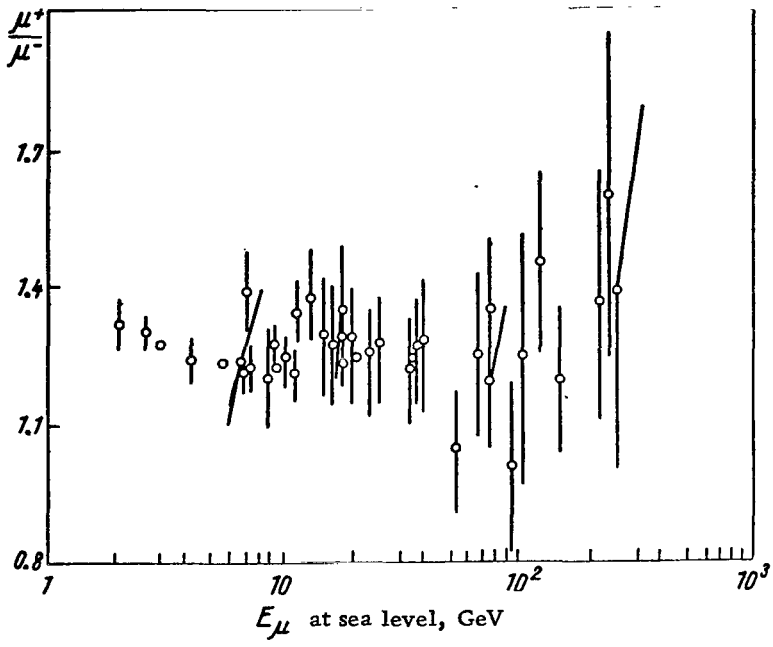

Figure 79. The Ratio μ^+/μ^- for a Vertical Muon Flux at Different Energies [411].

5.2. Energy Spectrum of Muons

The most reliable information on the energy spectra of muons was obtained with a magnetic spectrometer in [476-478]. Figure 80 shows the muon spectrum from [479].

To obtain data on the spectrum of muons in the region of energies greater than 10^3 GeV, use is made, usually, of indirect methods based on the measurement of the absorption curve of muons in the ground or of the spectra of pulses from muons. Both methods require accurate information about the effective cross sections of the elementary interaction processes of muons (electromagnetic and nuclear). Usually the average energy loss of the muons is represented in the form

$$-\left\langle \frac{dE_\mu}{dx} \right\rangle = a(E_\mu) + b(E_\mu) E_\mu, \qquad (12.15)$$

$$a(E_\mu) = 1{,}888 + 0{,}0768 \ln \frac{E'_\mu}{m_\mu} \frac{\text{MeV}}{\text{g/cm}^2}$$

where $E'_\mu = E^2_\mu (E_\mu + m^2_\mu/2m_e)^{-1}$ is the maximum energy transferred to an electron in a μ-e collision. The term $a(E_\mu)$ accounts for losses due to ionization and excitation of atoms in the medium. Retardation radiation ($b_R(E_\mu)$), pair

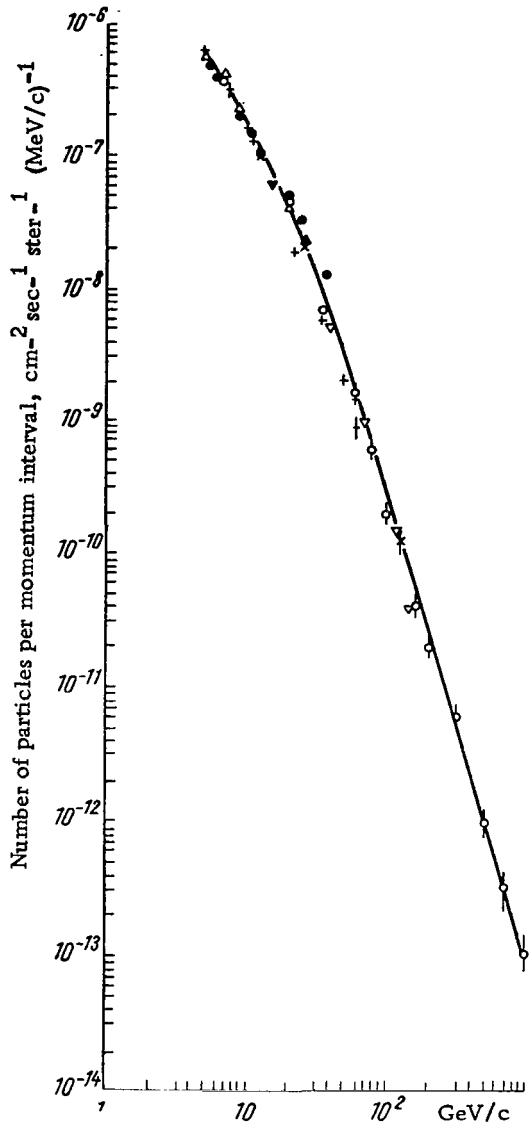

Figure 80. Differential Energy Spectrum of Muons.

formation ($b_P(E_\mu)$), and nuclear losses ($b_N(E_\mu)$) are combined in the second term:

$$b(E_\mu) = b_R(E_\mu) + b_P(E_\mu) + b_N(E_\mu). \qquad (12.16)$$

Much attention has been given to the calculation of these coefficients [441, 480-485]. Kobayakawa [486] used the latest information on the various constants entering in these expressions and also made a detailed analysis of the data on the

nuclear energy losses. He obtained the following relations for a standard earth having Z = 11, A = 22, Z/A = 0.50, and $Z^2/A = 5.5$: /349

$$b_R(E_\mu) = \begin{cases} 1.795 \cdot 10^{-7}\left(\ln\frac{E_\mu}{m_\mu} - 0.257\right) g^{-1}\,cm^2 \text{ for } E_\mu < \\ < 2.46 \text{ TeV} \\ 1.759 \cdot 10^{-6}\, g^{-1}\cdot cm^2 \text{ for } E_\mu \geqslant 2.46 \text{ TeV} \end{cases} \quad (12.17)$$

$$b_P(E_\mu) = \begin{cases} 4.154 \cdot 10^{-7}\left(\ln\frac{E_\mu}{m_\mu} - 2.787\right) \times \\ \times\, g^{-1}\cdot cm^2 \text{ for } E_\mu < 25.5 \text{ GeV} \\ 2.066 \cdot 10^{-6}\left(\frac{\ln\frac{E_\mu}{m_\mu} - 2.787}{\ln\frac{E_\mu}{m_\mu} - 0.485}\right) \\ \text{for } E_\mu \geqslant 25.5 \text{ GeV} \end{cases} \quad (12.18)$$

The values of the coefficient $b_N(E_\mu)$ calculated for various muon energies are given in Table 77. Figure 81 shows the dependence of the average muon energy loss $\langle dE/dx \rangle$ on muon energy E_μ (for earth with $\langle Z \rangle = 13$).

TABLE 77. VALUES OF THE COEFFICIENT b_N FOR VARIOUS MUON ENERGIES.

E_μ, TeV	b_N	E_μ, TeV	b_N	E_μ, TeV	b_N	E_μ, TeV	b_N
0.01	0.257	0.20	0.280	1.5	0.294	15	0.309
0.02	0.263	0.30	0.283	2.0	0.295	20	0.311
0.03	0.267	0.40	0.285	3	0.298	30	0.314
0.05	0.270	0.5	0.286	4	0.300	40	0.316
0.07	0.273	0.7	0.288	5	0.302	50	0.317
0.10	0.275	1.0	0.291	7	0.304	70	0.319
0.15	0.278	—	—	10	0.306	—	—

There are two kinds of loss in the ground: continuous losses, occurring in small batches, and fluctuating losses, in which large amounts of energy can be transferred from the muon to an electron. Because of this the relations obtained for the energy losses are valid only on the average, and in the transition from the absorption curve to the energy spectrum (using the path-energy relation), it is necessary to take fluctuations into account. The problem of fluctuations of the energy losses has been treated in many papers [487-489, 482, 486]. The accurate solution of this problem requires examination of the kinetic equations for the /350

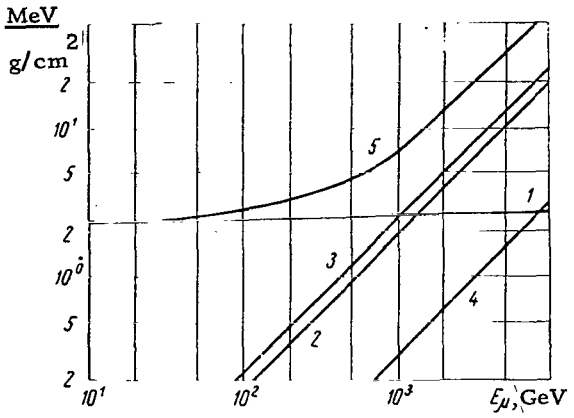

Figure 81. Energy Losses of Muons as a Function of Energy:

1 — Ionization and Excitation of Atoms; 2 — Retardation Radiation; 3 — Pair Formation; 4 — Photo-nuclear Losses; 5 — Total Losses.

passage of muons in the ground. However, the fluctuations can be taken into account by introducing a correction factor χ that depends on the observation depth and on the exponent of the energy spectrum of muons at sea level.

If the differential energy spectrum of muons at sea level is

$$N^{\mu}(E, 0) = N^{\mu}(0) E^{-(\varkappa+1)}, \qquad (12.19)$$

and the intensity of muons at depth x below sea level is $I_0(x)$ (assuming that the energy losses do not fluctuate), then the intensity of muons with allowance for the fluctuations will be $I(x) = I_0(x)\chi^{-1}$. Values of the correction factor are given in Table 78. /351

In determining the integral energy spectrum of muons from their intensity underground, it is necessary to know the direction of arrival of the muons or the function for their angular distribution at a given depth.

The integral energy spectrum of muons obtained from the study of the absorption curve for muons underground is given in Fig. 78. The greatest depth in the investigations was 6380 m (water equivalent). It was attained in the work of the Bombay group [485, 490].

The study of the spectra of pulses made by muons in dense substances and registered by ionization chambers or scintillators has been carried out in many papers [491-494].

TABLE 78. VALUES OF THE CORRECTION FACTOR χ AT DIFFERENT DEPTHS.

Depth, g/cm^2	χ			Reference
	x=2.5	x=3	x=3.5	
2	0.83	0.73	0.63	[484][a]
	0.88	0.80	0.71	[488]
	0.93	0.88	0.82	[489]
	0.93	0.88	0.83	[484][b]
	0.957	0.920	0.879	[486]
4	0.62	0.46	0.33	[484][a]
	0.74	0.60	0.47	[488]
	0.80	0.69	0.60	[489]
	0.87	0.78	0.69	[484][b]
	0.95	0.84	0.73	[485]
	0.867	0.780	0.692	[486]
6	0.43	0.27	0.16	[484][a]
	0.59	0.42	0.29	[488]
	0.07	0.51	0.41	[489]
	0.79	0.66	0.55	[484][b]
	0.86	0.68	0.55	[485]
	0.750	0.621	0.503	[486]
8	0.46	0.28	0.17	[488]
	0.55	0.37	0.27	[489]
	0.69	0.51	0.38	[485]
	0.624	0.471	0.343	[486]
10	0.33	0.17	0.09	[488]
	0.493	0.335	0.217	[486]
12	0.357	0.206	0.114	[486]

[a] Results obtained for Values of the Coefficients b in (12.15) and (12.16): $b_R = 1.05$, $b_N = 0.5$.

[b] $b_R = 1.8$, $b_N = 1.7$.

CHAPTER 13

THE NUCLEAR CASCADE PROCESS IN THE ATMOSPHERE

1. INTRODUCTION

The conservation of a primary primary particle of high energy after collision considered in Chap. 6 creates the possibility of originating a nuclear cascade process in a medium. This process consists of successive collisions of the conserved nucleon with nuclei, which leads to the development of a cascade of interactions of secondary charged pions and an electron-photon cascade. The hypothesis of the existence of a nuclear cascade process in the atmosphere was first expressed by Zatsepin [495]. Later a nuclear cascade process was observed also in dense media by means of a multiplate Wilson chamber and an ionization calorimeter (see examples of nuclear-cascade curves in Fig. 42). Knowing the characteristics of an elementary act, as well as the composition and energy spectrum of the primary cosmic radiation, it is possible to calculate the various parameters in the lower atmosphere by solving the equations describing the nuclear cascade process. Such calculations, made first by Rozental', were subsequently carried out by many others [496-500], and many models for the elementary act were employed. All were done with certain simplifications that permitted solution of the kinetic equations. The purpose of these calculations was to check the correctness of our ideas about the elementary act at high energies and the possibility of reconciling them with the integral parameters of the components of the cosmic radiation existing in the atmosphere. Thus, in this case the statistical approach to cosmic ray phenomena is employed, and individual interaction acts are not considered. At the present time, a considerable number of calculations of the nuclear cascade process in the atmosphere have been completed. /352 /353

We shall examine only some of these which have been accomplished in recent years and which have been called upon to explain phenomena in the region of energies 10^2 - 10^4 GeV. The fundamental properties of interactions in this energy region are the invariance of the inelastic interaction cross section, the difference between the interaction cross sections of pions and nucleons, the conservation of a pion or nucleon after collision, the invariance of the inelasticity, the gradual increase of multiplicity with energy, and a number of others.

The considerable uncertainty in the interpretation of processes occurring in the atmosphere and the freedom of maneuvering with various models are related to the uncertainty in the primary spectrum. In turn, the latter is due to the absence of methods for the measurement of the energy of primary particles in the energy interval 10^2 - 10^4 GeV which are suitable for use at the edge of the atmosphere. Recently, it has been proposed to measure the spectrum of the primary radiation with a calorimeter carried aboard a satellite [397]. However, this idea has not yet been realized. The measurements made in the "Proton" series of satellites have still not provided conclusive results, since the apparatus of the calorimetric type on these satellites contains too little material (less than 2.5 λ_p). Such an instrument is not suitable for measurements of absolute intensity; moreover, the dependence of the fraction of energy registered by it on the energy of the primary particle can lead to distortion of the spectrum.

The latest results obtained with the "Proton" satellites show that the proton spectrum apparently becomes steeper at an energy greater than 1000 GeV, whereas the spectrum of all primary particles changes more slowly up to energies that are 100 times greater.

Among the secondary particles, pions play the principal role. The contribution of kaons is much less. Therefore, in the solution of the equations for the nuclear cascade process one frequently considers only two types of secondary particles: nucleons and pions. In doing this it is assumed that pions do not generate nucleons of high energy.

2. THE EQUATIONS OF THE NUCLEAR CASCADE PROCESS /354

2.1. Formulation of the Problem

The development of a nuclear cascade process in the atmosphere is described by the following equations:

$$\frac{\partial N(x,E)}{\partial x} = -\frac{1}{\lambda_p} N(x,E) + \\ + \frac{1}{\lambda_p} \int_E^\infty N(x,E')\, n_p(E',E)\, dE'; \tag{13.1a}$$

$$\frac{\partial \pi(x,E)}{\partial x} = -\frac{\lambda_p}{\lambda_\pi} \pi(x,E) + \frac{1}{\lambda_p} \int_E^\infty N(x,E')\, n_1(E',E)\, dE' + \\ + \frac{1}{\lambda_\pi} \int_E^\infty \pi(x,E')\, n_2(E',E)\, dE' - \frac{C}{Ex} \pi(x,E). \tag{13.1b}$$

Here N(x, E) is the intensity of nucleons at depth x; π(x, E) is the same for pions; C = 1.8 x 10^{11} eV; λ_p and λ_π are the interaction lengths of nucleons and pions; $n_p(E', E)$ is the spectrum of secondary nucleons; $n_1(E', E)$ is the spectrum of generation of pions by nucleons; $n_2(E', E)$ is the spectrum of generation of pions by pions.

Thus, this system of equations functions and parameters of two types:

1. The parameters of an elementary act: $n_p(E', E)$, λ_p, λ_π, $n_1(E', E)dE$, $n_2(E', E)dE$.

2. Parameters of the radiation in the atmosphere N(x, E), π(x, E); to these we should add another series of quantities expressed in terms of those enumerated above and certain constants, viz.: M(x, E), the intensity of muons; Γ(x, E), the intensity of photons.

Thus, even in such a simplified treatment, where, for example, kaons are not taken into account, the number of quantities measurable at one level is less than the number of important parameters of the elementary act. These latter admit of a certain arbitrariness, particularly with respect to $n_p(E', E)dE$, $n_1(E', E)dE$ and $n_2(E', E)dE$..

2.2. Solution of the Equation Describing the Nucleon Component

/355

In Chap. 8 it was shown that the inelasticity is independent of the energy of the primary particle, i.e., the fraction of energy retained by a nucleon after interaction is constant. This is possible if the function $n_p(E', E)dE$ is homogeneous

$$n_p(E', E)\,dE = n_p\left(\frac{E}{E'}\right)\frac{dE}{E'};$$

$$\frac{E}{E'} = \beta. \tag{13.2}$$

Then, assuming an exponential primary spectrum, we have

$$N(x, E)\,dE = N(0, E)\,dE e^{-x/L_p}, \tag{13.3}$$

where N(O, E) is the spectrum of nucleons at the top of the atmosphere, and

$$L_p = \frac{\lambda_p}{1 - <\beta^{\gamma-1}>}. \tag{13.4}$$

Thus, in this case the spectrum at the bottom of the atmosphere is the same as the primary spectrum, and the intensity of nucleons diminishes according to an exponential law. If the primary spectrum is not purely exponential, e.g., γ increase with energy, then L_p will also vary with energy. This makes the spectrum

at the bottom of the atmosphere become steeper than the primary one in the same energy interval. In particular, if the primary spectrum undergoes a break at a certain energy E_c, then the break point will change with depth according to the law specified by Eq. (12.3). As a result of collision the nucleon may change its charge. Then the proton and nucleon fluxes at the bottom of the atmosphere may be represented in the following form [438]:

$$N_p(x, E) = N_p(0,E)\, e^{-x/L_p}\left\{\frac{1}{2}\left(1 + \delta_0 e^{(-2x/\lambda_p)\langle\beta^{-1}-1\rangle}\right)\right\}; \qquad (13.5)$$

$$N_n(x, E) = N_n(0, E)\, e^{-x/L_p}\left\{\frac{1}{2}\left(1 - \delta_0 e^{(-2x/\lambda_p)\langle\beta^{-1}-1\rangle}\right)\right\}. \qquad (13.6)$$

Here δ_0 is the excess of protons at the top of the atmosphere /356

$$\delta_0 = \frac{N_p(0, E) - N_n(0, E)}{N_p(0, E) + N_n(0, E)};$$

η is the charge exchange coefficient (see Chap. 12, Sec. 4). The ratio N_p/N_n is defined by Eq. (12.13). Since in the primary radiation nuclei are present, the intensity of nucleons near the top of the atmosphere will not vary exponentially, since nuclei, by disintegrating into nucleons during collision, will partially compensate their loss. With this taken into account, the equation describing the change in intensity of nucleons takes the form

$$dN(E, x)\, dE = -dx\, N(E, x)\, dE + \sum_i \int_E^\infty \frac{\lambda_p}{\lambda_i} dx B_i(E', x) \times$$

$$\times dE' W_i(E', E)\, dE + \int_E^\infty dx N(E', x)\, dE' n_p(E', E)\, dE. \qquad (13.7)$$

(13.7)

Here E' is the energy per nucleon; $B_i(E', x)dE'$ is the spectrum of nuclei at depth x;

$$B_i(E', x)\, dE' = B_i(E', 0)\, dE' e^{-x/L_i};$$

L_i is the absorption length of nuclei of the i-th kind, $W_i(E', E)$ is the probability of formation from a nucleus of the i-th kind of a nucleon with energy E. In the interaction of a primary nucleus of mass number A with nuclei in the atmosphere there is formed on the average about $A/2 \sim Z$ secondary nucleons (the remaining portion of the nucleus goes into fragments). It follows from the properties of the interaction of nuclei that about half of the secondary nucleons have the same energy per nucleon as in the primary nucleus, and the remainder are distributed over the same spectrum as in the nucleon-nucleus collision. Consequently,

$$W_i(E', E)\,dE = Z_i n_p(E', E)\,dE + \\ + Z_i \delta(E - E')\,dE. \tag{13.8}$$

Then

$$N(E, x) = N(E, 0)\,e^{-x/L_p} + \sum \frac{\lambda_p}{\lambda_i} \cdot Z_i B_i(E, 0) \times \\ \times (1 + <\beta^{\gamma-1}>) \frac{L_i L_p}{L_i - L_p} \left(e^{-\frac{x}{L_i}} - e^{-\frac{x}{L_p}}\right), \tag{13.9}$$

where L_i is expressed in lengths of the nuclear interaction of nucleons. Substituting into this formula the numerical values of $B_i(E, 0)/N(E, 0)$, L_i, L_p, λ_p, λ_i, $<\beta^{\gamma-1}>$ (see Chaps. 4 and 12), we find /357

$$N(E, x) \approx N(E, 0)\left\{1{,}4e^{-x/L_p} - 0.4e^{-x/L_\pi}\right\}.$$

Or

$$N(E, x) \approx N(E, 0)\left\{1{,}4e^{-x/110} - 0.4e^{-x/55}\right\}, \tag{13.10}$$

where x is in g/cm^2.

In obtaining the preceding relations, the fact that helium nuclei play the principal role has been taken into account.

2.3. Solution of the Equation for Pions

If the solution of the second equation of (13.1) is represented in the form of a series $\pi(x, E) = \Sigma\pi_i(x, E)$, then by requiring that all π_i vanish at x = 0 (the boundary condition π(O, E), we obtain a system of recurrence equations

$$\left.\begin{aligned} \frac{\partial \pi_i}{\partial x} + \left(\frac{\lambda_p}{\lambda_\pi} + \frac{C}{Ex}\right)\pi_1(x, E) &= \int_E^\infty N(x, E)\, n_1(E', E)\,dE'; \\ \frac{\partial \pi_i}{\partial x} + \left(\frac{\lambda_p}{\lambda_\pi} + \frac{C}{Ex}\right)\pi_i(x, E) &= \\ = \int_E^\infty \pi_{i-1}(x, E_0)\, n_2(E', E)\,dE'. & \end{aligned}\right\} \tag{13.11}$$

Here π_i(x, E) is the dependence on depth of the intensity of pions of the i-th generation. If the function n_1(E', E)dE is known, these equations can be solved, numerically at least. Thus, to make further progress it is necessary to choose a specific form of the differential spectrum of pions created in the collision of nucleons and pions with nuclei.

In its more general form, Eq. (13.11) can be solved if the spectra of generation of pions in an act is represented in the form of homogeneous functions

$$n_1(E', E)\,dE = n_1 f_1\left(\frac{E}{E_1}\right)\frac{dE}{E'} = n_1 f(u)\,du. \qquad (13.12)$$

It follows from the results of Chap. 6 that the spectrum of generation of pions varies as a function of the energy of the primary particle. However, because of the steep drop of the intensity of cosmic radiation with increasing energy, the highest energy pions play the principal role in the formation of the secondary components. There are a number of mechanisms which predict the emergence of pions with an energy proportional to the energy of the primary particle. Mathematically, this means that the function $n_1(E', E)$ can be expressed in the form (13.12). Among these mechanisms, the most frequently considered is the isobar model, which assumes that in each act of collision the surviving baryon is emitted in an excited state and thereafter decays into pions and nucleons. The first to point to the possibility of the existence of this model was Zatsepin [11]. The hyperon model of Peters [168] has similar properties. The difference between these models is mainly in the specific features of the existing hyperons and isobars. The isobar model was examined by Baradzey et al. [499].

/35

Hydrodynamic theory also predicts the existence of secondary particles with energy proportional to the primary energy and the homogeneity of the high-energy part of the pion energy spectrum. Thus, in all these cases a solution of Eq. (13.1) can be accomplished by identical methods regardless of model.

2.4. The Special Case of a Homogeneous Function $n_1(E', E)$

Assuming the function $n_1(E', E)$ to be homogeneous, we find

$$\int N(x, E')\,n_1\left(\frac{E}{E'}\right)\frac{dE}{E'}\,dE' = N(E, x)\,n_1 \langle u^{\gamma-1}\rangle\,dE. \qquad (13.13)$$

In this case the solution to (13.11) can be written

$$\pi_i(x, E) = \langle n_i u^{\gamma-1}\rangle x^{-C/E} e^{-\lambda_p x/\lambda_\pi} \times$$
$$\times \left[\int_0^x N(E, 0) e^{-\mu\xi} e^{\lambda_p \xi/\lambda_\pi}\,\xi^{C/E}\,d\xi\right];$$
$$\mu = 1/L.$$

This integral can be determined by numerical methods [500]. However, assuming that $L \sim \lambda_\pi$ and consequently $\lambda_p/\lambda_\pi \sim \mu$, we have, approximately, /359

$$e^{-\mu\xi} e^{\lambda_p \xi/\lambda_\pi} \sim 1.$$

Then

$$\pi_1(x, E) = N(x, E) < n_1 u^{\gamma-1} > \frac{x}{\frac{C}{E}+1} =$$

$$= N(0, E)\, e^{-x/L_p} < n_1 u^{\gamma-1} > \frac{x}{\frac{C}{E}+1}. \qquad (13.14)$$

Comparing this expression with Eq. (13.3) describing the nucleon component, we see that to obtain a new characteristic of cosmic radiation — the pion spectrum — we need a new parameter $<n_1 u^{\gamma-1}>$, determined from the spectrum of the generation of pions by nucleons. Equation (13.14) contains only the product of three fundamental parameters: the absolute intensity at the top of the atmosphere, an exponential factor which describes the absorption of nucleons, and the quantity $<n_1 u^{\gamma-1}>$. By choosing the three cofactors such that their product remains constant we can get identical solutions for completely different models. The least arbitrariness is permitted in L_p. All data sets L_p within the limits 110 - 120 g/cm^2. Hence, the principal uncertainty arises because of the absence of good data on N(O, E) and $<n_1 u^{\gamma-1}>$. Thus, for example, Grigorov [500] chose a very large value for $<n_1 u^{\gamma-1}> \approx 0.11 - 0.13$ and a very low intensity of the primary radiation.

Baradzey [499] found $<n_1 u^{\gamma-1}>$ to be about twice as small and the primary intensity was taken to be twice as large as in Grigorov's work [500]. Hence in both papers the product N(O, E) $<n_1 u^{\gamma-1}>$ turned out to be about the same, and this made it possible to describe satisfactorily the behavior of nucleons and pions in the atmosphere from two completely different conceptions about the elementary act of collision.

Grigorov [500] showed that the accepted value $<n_1 u^{\gamma-1}> = 0.11 - 0.12$ is /360
too large if all pions arise as a result of pionization. Using the pion spectrum obtained by Guseva et al. [143], one can determine the magnitude of $<n_1 u^{\gamma-1}>$ due to pionization: $<n_1 u^{\gamma-1}> = 0.027$. The isobar model, too, cannot provide the necessary value, if the isobar which arises is not too heavy. Thus, for example, the isobar (3/2, 3/2) with mass 1236 MeV adds only 0.032 to $<n_1 u^{\gamma-1}>$.

The same magnitude is obtained if a hyperon is formed each time instead of an isobar. Thus, both of these mechanisms of the interaction can explain only half of the required magnitude $<n_1 u^{\gamma-1}>$. Grigorov [500] concluded from this that the existence of a more effective process for the generation of pions is

necessary. As such a mechanism, he postulated a completely elastic interaction of a nucleon with a light nucleus with the formation of two fast excited clouds flying in opposite directions with very high Lorentz factors in the C system $\gamma \geq 2.5$. It is sufficient to allow the existence of 30 - 40% of such events in order to obtain a large value of $\langle n_1 u^{\gamma-1} \rangle$.

However, the data considered in the preceding chapters show that the primary intensity is evidently greater than that taken by Grigorov [500], and $\langle n_1 u^{\gamma-1} \rangle$ is considerably less. In particular, the value of 0.08 found in [499] is close to that given by direct measurement (see Chap. 6).

To explain such a value for $\langle n_1 u^{\gamma-1} \rangle$ it is completely sufficient to postulate the emergence of a light isobar and pionization. This example shows that the same experimental data on the integral characteristics of radiation in the atmosphere can be used in support of completely different mechanisms for the elementary act.

2.5. Photons and Muons in the Atmosphere

If all photons arise as the result of the decay of π^0-mesons, then the study of the spectrum and intensity of photons in the atmosphere does not give any new information whatever about the elementary act. The number of photons produced /361 by nucleons at a depth x with energy E, E + dE per gram of substance, is

$$\Gamma(E, x)\,dE = \frac{2dE}{\lambda_p}\int_0^1 \frac{dy}{y}\int_0^\infty \frac{1}{2} n_1\left(\frac{E}{y}, E'\right) N(x, E')\,dE' = \frac{N(x, E)\langle n_1 u^{\gamma-1}\rangle}{\gamma\lambda_p}\,dE. \tag{13.15}$$

Near the top of the atmosphere, primary nuclei contribute significantly to the formation of photons. Substituting the sum N(E, x) + B(E, x) into Eq. (13.15) and considering that for nuclei we should use $Z\langle n_1 u^{\gamma-1} \rangle$ instead of $\langle n_1 u^{\gamma-1} \rangle$, we obtain

$$\Gamma(E, x) \approx \frac{\langle n_1 u^{\gamma-1}\rangle}{\gamma\lambda_p} N(E, 0)\left\{1.4e^{-x/110} - 0.2e^{-x/55}\right\}.$$

Thus, a choice of N(O, E), L_p, and $\langle n_1 u^{\gamma-1} \rangle$ uniquely determine the intensity not only of charged pions, but also of photons. The intensity of muons is determined by the decay of π-mesons in the interval of depths from the top of the atmosphere to the level of observation of the muons x_0 is

$$\pi(x_0, E)\,dE = dE\int_0^{x_0}\pi(E, x)\frac{Cdx}{Ex} =$$

$$= \frac{N(E, 0)\,dE\,\langle n_1 u^{\gamma-1}\rangle}{E\left(\frac{C}{E}+1\right)} C\int_0^{x_0}\frac{e^{-x/L}\,dx}{x}. \qquad (13.16)$$

To go from this to the muon spectrum, we need to replace E by $1.3E\mu$, where $E\mu$ is the muon energy:

$$M(x, E_\mu)\,dE_\mu = \frac{N(E_\mu, 0)\,dE_\mu\,\langle n_1 u^{\gamma-1}\rangle}{E_\mu\left(\frac{C}{1.3E_\mu}+1\right)1.3^\gamma}\int_0^{x_0}\frac{e^{-x/L}dx}{x}. \qquad (13.17)$$

The contribution of primary nuclei to the formation of muons can be as high as 25%. Consequently, the muon spectrum is uniquely determined by the product of the same quantities as the spectra of photons and pions. Hence it makes no difference at all whether one determines this product from the spectrum of photons or muons or from the intensity of pions.

3. THE ROLE OF PIONS IN THE ATMOSPHERE /362

3.1. Calculation of Successive Generations of Pions in the Atmosphere

Up until now we have considered only nucleons and the first generation of pions. However, as a matter of fact, it is necessary to take into account the contribution of succeeding generations as well. For this, we solve equations (13.11), substituting into them $\pi_1(x, E)$ and a new function $n_2(E', E)dE$. Thus, to refine the calculation we must introduce a new parameter, which is chosen from experiment or from some theory of the interaction of pions with nuclei.

Different authors have approached this problem differently. For example, in the work of Grigorov that we have discussed [500], it was assumed that pions generate secondary particles only as a result of pionization. Then pions do not create secondary pions of high energy, and therefore the second and later generations of pions give practically no contribution to the integral characteristics of the cosmic radiation in the atmosphere. In this case, the entire pion component in the atmosphere proceeds directly from nucleons. Pal and Peters [438] carried out calculations on the basis of the isobar model and considered two limiting cases, when the pions are completely regenerated after collision (elastic interaction) or completely absorbed. The latter case, obviously, is close to that considered in [499] and [500].

The analysis of data on the interaction of pions with nuclei has led us to conclude that there is a significant probability for the regeneration of pions in an act (see Chaps. 6 and 8). The surviving pion carries a significant fraction of the primary energy. Data obtained in accelerators, as well as with ionization

calorimeters, at 400 GeV show that marked fluctuations in the transfer of energy to π^0-mesons apparently exist, which we attributed earlier to the peripheral character of the interaction of pions and with their charge conversion during interaction. In this case fluctuations arise on account of the formation of a small number of secondary pions of high energy.

Utilizing these ideas and considering that the principal role in the development of processes in the atmosphere is played by particles of the highest energy, we may assume that charged secondary pions arise whenever the primary pion is conserved, and neutral ones arise when the primary undergoes charge conversion: $\pi^{\pm} \to \pi^0$. Let the probability for this be q. We shall take the spectrum of secondary pions of high energy to be a δ-function, which makes it possible to obtain the analytic solution /363

$$n_2(E', E)\,dE = q\langle n_2\rangle\,\delta\left(E - \frac{\langle a\rangle E'}{\langle n_2\rangle}\right) \tag{13.18}$$

Here $\langle n_2\rangle$ is the average multiplicity of secondary pions of high energy; $\langle a\rangle$ is the average fraction of the energy carried by these pions. At accelerator energies, $\langle n_2\rangle \sim 1$. It will also be easy to consider $\langle n_2\rangle \neq 1$, in order to see how sensitive the results are to this parameter.

Then using (13.11), we obtain

$$\pi_2(x, E) = N(x, E)\,q\frac{\langle a\rangle^{\gamma-1}}{\langle n_2\rangle^{\gamma-2}}\cdot\frac{x}{L_p}\times \\ \times\frac{x}{\left(\frac{\langle a\rangle C}{\langle n_2\rangle E}+1\right)\left(\frac{C}{E}+2\right)}. \tag{13.19}$$

Similarly, we can find also the successive generations of pions, which are important at great depths. They need also to be taken into account in determining the spectrum of generation of photons

$$\Gamma(E, x)\,dE = \frac{N(E, 0)\,e^{-x/L_p}}{\gamma\lambda_p}\,dE\langle n_1 u^{\gamma-1}\rangle\left\{1 + \right. \\ \left. + \frac{\lambda_p}{\lambda_\pi}qx\left[\frac{\langle a\rangle^{\gamma-1}}{\langle n_2\rangle^{\gamma-2}} + q\frac{x}{2L_p}\cdot\frac{\langle a\rangle^{2\gamma-2}}{\langle n_2\rangle^{2\gamma-4}}\right]\right\} \tag{13.20}$$

or

$$\Gamma(E, x)\,dE = N(E, 0)\,e^{-x/L_p}\langle n_1 u^{\gamma-1}\rangle\,\varphi_\gamma(x, E). \tag{13.21}$$

The contribution of successive generations to the muon intensity is small. Substituting the numerical values

$$q\frac{\langle a\rangle^{\gamma-1}}{\langle n_2\rangle^{\gamma-2}}\cdot\frac{1}{L_p}=\mu_\pi,$$

we can determine the intensity of the various components of the cosmic radiation.

Some of the results of the calculations with $\langle n_2\rangle = 1$, $\langle a\rangle = 0.7$, and $q = 1/2$ are shown in Fig. 82 together with other data. /364

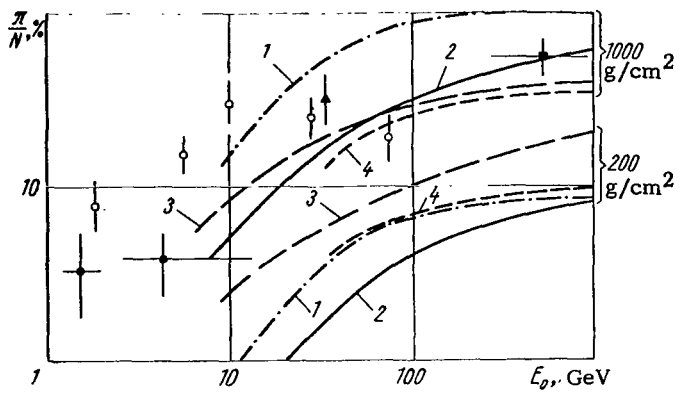

Figure 82. The Pion-Nucleon Ratio; Comparison of Calculations with Experiment:

1 — [411]; 2 — Calculation, see p. 294 ; 3 — [440b]; 4 — [412]; ⊙ — Experiment at Sea Level; ●, ▲, ■ — Measurements on Mountains, Reduced to Sea Level (see Table 75).

3.2. The Nuclear Component at Very High Energies

The various components of the cosmic radiation are described particularly simply in case pion decay can be neglected, i.e., when $E \gg C$ (≈ 180 GeV). Then the intensity of nuclear-active particles can be written in the following form:

$$N_{\mathrm{NA}}(E,x)\,dE = N(E,x)\,dE + \pi(E,x)\,dE =$$
$$= N(E,0)\,e^{-x/L_p}\left\{1+\langle n_1 u^{\gamma-1}\rangle x\sum_{n=0}^{\infty}\frac{(\mu_\pi x)^n}{(n+1)!}\right\}, \qquad (13.22)$$
$$\mu_\pi = 0.126 \quad \text{for } \langle n_2\rangle = 2;$$
$$\mu_\pi = 0.20 \quad \text{for } \langle n_2\rangle = 1.$$

Using this formula for calculation, and comparing the results for difference x with

$$N_{NA}(E, x) = N_{NA}(E, 0)\, e^{-x/L_N}, \qquad (13.23)$$

we can determine L_N, the absorption length of the nuclear component, for various depth intervals. The results are given in Table 79. /36

TABLE 79. ABSORPTION LENGTH OF NUCLEAR-ACTIVE PARTICLES.

Depth interval, g/cm^2	L_N, g/cm^2	
	$\langle n_z\rangle=2$	$\langle n_z\rangle=1$
0—200	120	119
0—700	119	122
0—1000	120	124
700—1000	121	132
200—1000	119	125
Absorption length of nucleons	110	110

The difference in the absorption of nucleons and nuclear-active particles is due to the effect of pions, which are absorbed considerably more slowly than nucleons.

Since to a marked extent photons are generated by pions in the bottom of the atmosphere, the absorption length L_γ calculated from the photon intensity should differ from the absorption length of the nuclear component

$$\Gamma(E, x)\, dE = \frac{N(E, x) \langle n_1 u^{\gamma-1}\rangle\, dE}{\gamma\lambda_p}\, e^{\mu_\pi x} = \frac{N(E, 0) \langle n_1 u^{\gamma-1}\rangle dE}{\gamma\lambda_p}\, e^{-(\beta-\mu_\pi)x} \qquad (13.24)$$

for $\langle n_2\rangle = 1$, $1/(\beta - \mu) = L_\gamma = 150$ g/cm^2, and for $\langle n_2\rangle = 2$, $L_\gamma = 130$ g/cm^2. The first of these results agrees better with the data of Smorodin et al. [501], who used pulse instruments to measure photon cascades and found

$$L_\gamma = (146 \pm 10) \quad \text{g/cm}^2$$

for the depth interval 200 - 1000 g/cm^2 at photon energies of about 10^3 GeV. The same value of L_γ is obtained in the interval 200 - 300 g/cm^2, within experimental error.

4. CALCULATION OF THE CHANGE OF SLOPE OF THE PRIMARY SPECTRUM

/366

Again we emphasize that recently there has appeared an indication of a two-fold change in slope of the energy spectrum of primary particles in the high energy region. Some data on the influence of this change on the various components of the cosmic radiation at the bottom of the atmosphere were already presented in Chap. 12.

Pal and Tandon [454] calculated the spectra of photons and muons at various depths in the atmosphere, assuming a change in the primary spectrum at a certain energy E_c, which entered into the calculation as a definite parameter. The calculation was based on the isobar model considered earlier by Pal and Peters. The primary spectrum was represented as the sum of spectra with different exponents, and two breaks in the spectrum were taken into account. The portion of the spectrum with a break at high energies was approximated by the expression

$$N(E, 0)\,dE = \frac{AdE}{E^{\gamma_0+1}} \sum_{j=1}^{11} c_j E^{\frac{j-6}{10}}, \tag{13.25}$$

and the portion with the break at low energies by

$$N(E, 0)\,dE = \frac{AdE}{E^{\gamma_0+1}} \left(1 - \sum_{j=1}^{11} c_j E^{\frac{j-6}{10}}\right). \tag{13.26}$$

With the proper choice of the coefficients c_j, it is possible to approximate any change in the primary spectrum by means of a smooth function.

In choosing the form of the primary spectrum the atuhors supposed that it consists of two components A and B, with the component B having the same slope as A (the authors took the value of the exponent of the differential spectrum for components A and B to be $\gamma_0 = 2.67$ and consisting only of protons. The component A consists of protons and nuclei and has an intensity 15 - 20 times that of B. The component A undergoes a break at a certain energy E_c.

The results of the calculation agree with experiment if it is assumed that $E_c \sim 2 \times 10^5$ GeV (see Fig. 78). According to data on broad atmospheric showers [403, 416], a change in the exponent of the primary spectrum takes place in the region of energies $E > 10^6$ GeV. However, if for any reason nuclei predominate in this energy region, then the break at $E > 10^6$ GeV corresponds to a break in the spectrum of energies per nucleon of the order of 3×10^5 GeV, which is close to the value E_c obtained above. McCusker et al. [138] actually observed a predominance of multistemmed broad atmospheric showers in this

/367

energy region, which is interpreted by them as the result of the enrichment of the primary radiation with nuclei. As we have already mentioned, the results of measurements with the "Proton" satellites seem to indicate an increase in the fraction of nuclei at energies as low as 10^3 GeV.

5. CONCLUSION

A consideration of the process of passage of cosmic radiation through the atmosphere shows that the intensity and spectra of the various components depend principally on the product of the intensity of the primary radiation and $< n_i u^{\gamma-1} >$. Refinement of the solutions of the kinetic equations leads to the appearance of new parameters. A proper choice of the quantities entering in the solution can produce agreement between calculation and experiment for various interpretations of the interaction mechanism. In order to be able to make a choice among these different models on the basis of the methods set forth in this chapter, it is necessary to refine substantially our knowledge about the spectrum and composition of the primary cosmic radiation in the high energy region and about the intensity of the various components at the bottom of the atmosphere.

APPENDIX

/368

1. Some Physical Constants

Velocity of light in vacuum	$c = 2.997925 \cdot 10^{8}$ m/sec
Electron charge	$e = 1.60210 \cdot 10^{-19}$ c
Planck's constant	$h = 6.6256 \cdot 10^{-34}$ J · sec
	$\hbar = \frac{h}{2\pi} = 1.05450 \cdot 10^{-34}$ J · sec
Boltzmann constant	$k = 1.38054 \cdot 10^{-23}$ J/deg
Avogadro's number	$N_A = 6.02252 \cdot 10^{26}$ (kg · mol)$^{-1}$
Classical radius of the electron	$r_e = \frac{l^2}{m_e c^2} = 2.8176 \cdot 10^{-15}$ m
Compton wavelength of the electron	$\lambda_e = \frac{h}{m_e c^2} = 2.4265 \cdot 10^{-12}$ m
Fine structure constant	$\alpha = \frac{e^2}{\hbar c} = 1/137,027$
Number of molecules per cm^3 at standard conditions	$L = 2.687 \cdot 10^{19}$ cm^{-3}.

2. Units of Measurement

1 eV = $1.60210 \cdot 10^{-7}$ J = $1.60210 \cdot 10^{-12}$ erg
1 MeV = 10^6 eV
1 GeV = 10^9 eV
1 TeV = 10^{12} eV

3. Particle Masses

Electron	$m_e = 0.511$ MeV = $9.109 \cdot 10^{-31}$ kg
Proton	$m_p = 1836\, m_e = 0.939$ GeV = $1.672 \cdot 10^{-27}$kg
Pions	$m_{\pi^\pm} = 273.2\, m_e = 139.63$ MeV
	$m_{\pi^0} = 264.2\, m_e = 135.0$ MeV

/369

Muons $m_{\mu} = 206.76\, m_e = 105.655$ MeV

Kaons $m_{K\pm} = 966.6\, m_e = 439.9$ MeV

4. Lifetimes

Pions $\tau_{\pi\pm} = 2.55 \cdot 10^{-8}$ sec

$\tau_{\pi^0} = 2.1 \cdot 10^{-16}$ sec

Muons $\tau_{\mu\pm} = 2.212 \cdot 10^{-6}$ sec

$\tau_{K\pm} = 1.22 \cdot 10^{-8}$ sec

Kaons $\tau_{K_1^0} = 1.00 \cdot 10^{-10}$ sec

$\tau_{K_2^0} = 6.1 \cdot 10^{-8}$ sec

5. Relation between Height above Sea Level, Pressure of the Air Column, and Density

Height above sea level, km	Pressure, g/cm^2	Air density, x 10^3 g/cm^3	Height above sea level, km	Pressure, g/cm^2	Air density, x 10^3 g/cm^3
0	1030	1.225	5.50	513	0.697
0.5	969	1.167	6.0	478	0.660
1.0	914	1.112	7.0	417	0.590
1.5	860	1.058	8.0	362	0.525
2.0	808	1.006	9.0	312	0.466
2.25	783	0.981	10	268	0.413
2.50	759	0.957	11	230	0.364
2.75	735	0.933	12	196	0.311
300	712	0.909	13	168	0.265
3.25	690	0.886	14	143	0.227
3.50	668	0.863	15	122	0.194
3.75	646	0.841	16	104	0.165
4.00	626	0.819	17	89	0.141
4.25	606	0.798	18	76	0.121
4.50	586	0.777	19	65	0.103
4.75	567	0.756	20	55.5	0.088
5.00	549	0.736			

6. Values of t-Units and Critical Energies ε for Various Elements and Complex Substances [503]: /370

a) Elements

Element	Z	A(rounded)	Density at standard conditions, g/cm³	t, g/cm²	ε, MeV	
					Without density effect	With density effect
H	1	1	$0.0899 \cdot 10^{-3}$	62.8	350	—
He	2	4	$0.1785 \cdot 10^{-3}$	93.1	250	—
Li	3	7	0.534	83.3	180	138
Be	4	9	1.84	66.0	141	110
B	5	11	2.33	53.6	115	91
C	6	12	2.22 (Graphite)	43.3	97	77
N	7	14	$1.25 \cdot 10^{-3}$	38.6	85	—
O	8	16	$1.429 \cdot 10^{-3}$	34.6	75	—
F	9	19	$1.69 \cdot 10^{-3}$	33.4	67.5	—
Na	11	23	0.97	28.2	55.5	46.5
Al	13	27	2.7	24.3	47	40
Si	14	28	2.35	22.2	44	37.5
Ar	18	40	$1.783 \cdot 10^{-3}$	19.7	34	—
Ca	20	40	1.54	16.3	30.4	26.7
Fe	26	56	7.6—7.88	13.9	23.3	20.7
Cu	29	63.5	8.89	13.0	20.9	18.8
Br	35	80	$1.139 \cdot 10^{-3}$	11.5	17.2	15.7
Ag	47	108	10.5	9.0	12.7	11.9
Xe	54	131	$5.85 \cdot 10^{-3}$	8.5	11.0	—
W	74	184	19.3	6.8	8.3	8.1
Pb	82	207	11.34	6.4	7.5	7.4

b) Complex Substances

Substance	Density, g/cm³	t, g/cm²	ε, MeV	
			Without density effect	With density effect
Air	$1.29 \cdot 10^{-3}$	37.1	81	—
Water	1.0	36.4	90	73
Lithium hydride (LiH)	0.6	80	207	157
Polystyrene (C_8H_8)	—	44.4	110	88
Clay ($Al_2SiO_3 \cdot 2SiO_2 \times 2H_2O$)	1.3—2.5	28.8	60,9	50.6
Quartz (SiO_2)	2.65	27.4	56.2	47.3
Limestone ($CaCO_3$)	2.93	24.2	51.2	43.4
Salt (NaCl)	2.16	22.2	42.1	35.2
Nuclear emulsion NIKFI-R	3.9	11.4	17.8	16.4

REFERENCES

1. Nikishov, A.I. and I.L. Rozental', Zh. Eksp. i Teoret. Fiz., Vol. 35, p. 165, 1958. /371
2. Zatsepin, G.T. and L.G. Dedenko, V kn. Trudy Mezhdunarodnoy Konferentsii po Kosmicheskim Lucham (In Book: Proceedings of the International Conference on Cosmic Rays), Vol. 2, AN SSSR, Moscow, 1960, p. 222.
3. Takibayev, Zh.S., Zh. Eksp. i Teoret. Fiz., Vol. 35, p. 279, 1958.
4. Montanet, L., et al., Nuovo Cimento, Vol. 17, p. 166, 1960.
5. Murzin, V.S., Yadernaya Fizika (Nuclear Physics), Vol. 1, p. 835, 1965.

5a. Murzin, V.S., Izvestiya AN SSSR, Ser. fiz., Vol. 29, p. 1644, 1965.

6. Imaeda, K., Nuovo Cimento, Vol. 26, p. 417, 1962.
7. Rozental', I.L. and V.V. Shestakov, Izvestiya AN SSSR, Ser. fiz., Vol. 29, p. 1751, 1965.
8. Lohrmann, E., Suppl. Nuovo Cimento, Vol. 1, p. 1227, 1963.
9. Farrow, E., et al., Nuovo Cimento, Vol. 28, p. 1238, 1963.
10. Shen, M.L. and M.F. Kaplon, Ann. of Phys., Vol. 32, p. 452, 1965.
11. Zatsepin, G.T., V kn. Trudy Mezhdunarodnoy Konferentsii po Kosmicheskim Lucham (In Book: Proceedings of the International Conference on Cosmic Rays), Vol. 1, AN SSSR, Moscow, 1960, p. 170.
12. Dobrotin, N.A. and S.A. Slavatinskiy, Proc. Int. Conf. on High Energy Phys., 1960, p. 819.
13. Duller, N.M. and W.D. Walker, Phys. Rev. Lett., Vol. 8, p. 166, 1958.

14a. Bradt, H., M. Kaplon and B. Peters, Helv. Phys. Acta, Vol. 23, p. 24, 1950.

14b. Dilworth, C., et al., Nuovo Cimento, Vol. 10, p. 1261, 1953.

15. Boos, E.G. and Zh.S. Takibayev, V kn. Trudy Mezhdunarodnoy Konferentsii po Kosmicheskim Lucham (In Book: Proceedings of the International Conference on Cosmic Rays), Vol. 1, AN SSSR, Moscow, 1960, p. 76.
16. Castagnoli, G., et al., Nuovo Cimento, Vol. 10, p. 1539, 1953.
17. Imaeda, K., Nuovo Cimento, Vol. 36, p. 1376, 1965.
18. Landau, L.D., Izvestiya AN SSSR, Ser. fiz., Vol. 17, p. 51, 1953.
19. Feynberg, Ye.L. and D.S. Chernavskiy, Uspekh. Fiz. Nauk, Vol. 82, p. 3, 1964.
20. Koshiba, M., et al., Suppl. Nuovo Cimento, Vol. 1, p. 1091, 1963.
21. Lim, Y.K., Nuovo Cimento, Vol. 28, p. 1228, 1963.
22. Lal, S., et al., Proc. Int. Conf. on Cosmic Rays, Jaipur, Vol. 5, p. 363, 1964.
23. Alekseyeva, K.I. and oth., Izvestiya AN SSSR, Ser. fiz., Vol. 28, p. 1794, 1964. /372
24. Lohrman, E., M. Teucher and M. Shein, Phys. Rev., Vol. 122, p. 672, 1961.
25. Abraham, F., et al., Proc. Int. Conf. on Cosmic Rays, London, Vol. 2, p. 844, 1965.
26. Settles, R.D. and R.W. Huggett, Phys. Rev., Vol. 133, p. 1305, 1964.
27. Barbaro-Galtiery, A., et al., Nuovo Cimento, Vol. 20, p. 487, 1961.
28. Jain, P., et al., Phys. Rev., Vol. 115, p. 643, 1959.

29. Aly, H., C. Fisher and A. Masin, Nuovo Cimento, Vol. 28, p. 1117, 1963.
30. Meyer, H., E. Lohrmann and M. Teucher, Nuovo Cimento, Vol. 28, p. 1399, 1963.
31. Kamal, A.A. and G.K. Rao, Phys. Lett., Vol. 3, p. 35, 1962.
32. Hayakawa, S., Int. Conf. High Energy Phys. CERN, 1962, p. 643.
33. Imaeda, K. and T.P. Shah, Nuovo Cimento, Vol. 41A, p. 405, 1966.
34. Yerofeyeva, I.N., L.G. Mishchenko, V.S. Murzin and L.I. Sarycheva, Izvestiya AN SSSR, Ser. fiz., Vol. 31, p. 1412, 1967.
35. Hildebrand, B., and R. Silberberg, Suppl. Nuovo Cimento, Vol. 1, p. 1118, 1963.
36. Kaplon, M., B. Peters, H. Reynolds and D. Ritson, Phys. Rev., Vol. 85, p. 295, 1952.
37. Lohrmann, E. and M. Teucher, Phys. Rev., Vol. 115, p. 636, 1959.
38. Abraham, F., J. Gierula, R. Levi Setti, et al., Preprint EFINS 65-44, 1965.
39. Wolter, W., Nukleonika, Vol. 9, p. 265, 1964.
40. Grigorov, N.L., V.S. Murzin and I.D. Rapoport, Zh. Eksp. i Teoret. Fiz., Vol. 34, p. 506, 1958.
41. Ramana Murthy, R., B. Sreekantan, A. Subramanian and S. Verma, Nuclear Inst. a Methods, Vol. 23, p. 245, 1963.
42. Grigorov, N.L., A.V. Podgurskaya, L.M. Poperekova and A.I. Savel'yeva, Zh. Eksp. i Teoret. Fiz., Vol. 35, p. 3, 1958.
43. Grigorov, N.L., V.S. Murzin and I.D. Rapoport, Zh. Eksp. i Teoret. Fiz., Vol. 36, p. 1069, 1959.
44. Yerofeyeva, I.N., L.G. Mishchenko and V.S. Murzin, Izvestiya AN SSSR, Ser. fiz., Vol. 30, p. 1628, 1966.
45. Powell, C.F., P. Fowler and D. Perkins, Study of Elementary Particles by the Photographic Method, Pergamon Press, N.Y., 1959.
46. Grigorov, N.L., G.A. Skuridin, I.A. Savenko and I.D. Rapoport, Kosmich. Issled., Vol. 11, p. 727, 1964; Murzin, V.A., Ionizatsionnyy Kalorimetr (The Ionization Calorimeter), FIAN, A-5, 1965.
47. Babayev, M.I., R.Z. Denikayev, Yu.A. Yemel'yanov and oth., Izvestiya AN SSSR, Ser. fiz., Vol. 29, p. 1719, 1965.
48. Dmitriyev, V.A., Zh. Eksp. i Teoret. Fiz., Vol. 35, p. 553, 1958.
49. Kellermann, E.W. and M.G. Silk, Proc. Int. Conf. on Cosmic Rays, London, Vol. 2, p. 883, 1965.
50. Azimov, S.A., A.M. Abdulayev, V.M. Myalkovskiy and oth., Izvestiya AN SSSR, Ser. fiz., Vol. 26, p. 613, 1962.
51. Dobrotin, N.A., Ye.V. Denisov, S.L. Dubrovina and oth., Proc. Int. Conf. on Cosmic Rays, London, Vol. 2, p. 817, 1965.
52. Grigorov, N.L., V. Ya. Shestoperov, S.I. Brikker and oth., Proceed. Int. Conf. on Cosmic Rays, London, Vol. 2, p. 851, 1965. /373
53. Tolkachev, B.V., Zh. Eksp. i Teoret. Fiz., Vol. 46, p. 43, 1964.
54. Grigorov, N.L., M.A. Kondrat'yeva, A.I. Savel'yeva and oth., V kn. Trudy Mezhdunarodnoy Konferentsii po Kosmicheskim Lucham (In Book: Proceedings of the International Conference on Cosmic Rays), Vol. 1, AN SSSR, Moscow, 1960, p. 122.
55. Baradzey, L.T., V.I. Rubtsov, Yu.A. Smorodin and oth., Izvestiya AN SSSR, Ser. fiz., Vol. 26, p. 575, 1962.
56. Denisov, Ye.V., V.I. Zatsepin, S.I. Nikol'skiy and oth., Zh. Eksp. i Teoret. Fiz., Vol. 40, p. 419, 1961.

57. Perkins, D.H., Progr. in Cosmic Ray and Elem. Part. Phys., Vol. 5, p. 257, 1960.
58. Belletini, G., et al., Nucl. Phys., Vol. 79, p. 609, 1966.
58a. Belletini, G., et al., Phys. Rev. Letters, Vol. 14, p. 164, 1965.
59. Rossi, B., High-Energy Particles, Prentice-Hall Publ., Englewood Cliffs, N.J., 1952.
60. Hofstadter, R., Ann. Rev. of Nucl. Sci., Vol. 7, p. 231, 1957.
61. Barashenkov, V.S., Secheniya Vzaimodeystviy Elementarnykh Chastits (Cross Sections of the Interactions of Elementary Particles), Nauka Press, Moscow, 1966.
62. Vasilova, R.N., N.L. Grigorov, G.P. Kakhidze and oth., Izvestiya AN SSSR, Ser. fiz., Vol. 30, p. 1610, 1966.
63. Bozoki, G., E. Fenivesh, G. Christov, et al., Proc. Int. Conf. on Cosmic Rays, London, Vol. 2, p. 870, 1965.
64. Daniel, R., N. Durgaprasad, P. Malhotra, et al., Suppl. Nuovo Cimento, Vol. 1, p. 1163, 1963.
65. Bartlett, M., Phil. Mag., Vol. 44, p. 249, 1953.
66. Grigorov, N.L., I.N. Yerofeyeva, L.G. Mishchenko and oth., Izvestiya AN SSSR, Ser. fiz., Vol. 28, p. 1798, 1964.
67. Askowith, J. and K. Sitte, Phys. Rev., Vol. 97, p. 159, 1955.
68. Grigorov, N.L., V.A. Sobinyakov, A.V. Podgurskaya and V.Ya. Shestoperov, Zh. Eksp. i Teoret. Fiz., Vol. 33, p. 1099, 1957.
69. Dovzhenko, O.I., G.T. Zatsepin, Ye.A. Murzina and oth., V kn. Trudy Mezhdunarodnoy Konferentsii po Kosmicheskim Lucham (In Book: Proceedings of the International Conference on Cosmic Rays), Vol. 2, AN SSSR, Moscow, 1960, p. 144.
70. Babayan, Kh.P., N.L. Grigorov, E.A. Mamidzhanyan and oth., Izvestiya AN SSSR, Ser. fiz., Vol. 29, p. 1652, 1965.
71. Ashmore, A., A. Diddens, G. Cocconi, et al., Phys. Rev. Lett., Vol. 5, p. 576, 1960.
72. Coor, T., D. Hill, W. Hornijak, et al., Phys. Rev., Vol. 98, p. 1369, 1955.
73. Bowen, T., M. Dicorato, W. Moore, et al., Nuovo Cimento, Vol. 9, p. 908, 1958.
74. Barrett, P., Phys, Rev., Vol. 114, p. 1374, 1959.
75. Singha, M. and N. Das, Phys. Rev., Vol. 105, p. 1587, 1957.
76. Atkinson, J., W. Hess, V. Perez-Mendez and R. Wallace, Phys. Rev. Lett., Vol. 2, p. 168, 1959.
77. Pantuyev, V.S. and M.N. Khachaturyan, Zh. Eksp. i Teoret. Fiz., Vol. 42, p. 909, 1962.
78. Berzhanov, R.V., Zh. Eksp. i Teoret. Fiz., Vol. 34, p. 725, 1958.
79. Peacock, R., B. Hahn, E. Hugentubler, et al., Nuovo Cimento, Vol. 22, p. 1290, 1961.
80. Williams, R., Phys. Vol. 98, p. 1193, 1955.
81. Bozoki, G., E. Fenevesh and L. Yanoshi, V kn. Trudy Mezhdunarodnoy Konferentsii po Kosmicheskim Lucham (In Book: Proceedings of the International Conference on Cosmic Rays), Vol. 1, AN SSSR, Moscow, 1960, p. 171. /374
82. Bolotov, V.N., M.I. Devishev, L.F. Klimanova and A.V. Shmeleva, Proc. Int. Conf. on Cosmic Rays, London, Vol. 2, p. 863, 1965.

83. Alekseyeva, K.I., N.L. Grigorova, I.N. Yerofeyeva and oth., Proc. Int. Conf. on Cosmic Rays, Jaipur, Vol. 5, p. 356, 1964.
84. Akashi, M., C.M. Lattes, L. Nishimura, et al., Proc. Int. Conf. on Cosmic Rays, London, Vol. 2, p. 878, 1965.
85. Duthie, J., Thesis, University of Bristol, 1961.
86. Rubtsov, V.I., Yu.A. Smorodin and B.V. Tolkachev, Zh. Eksp. i Teoret. Fiz., Vol. 44, p. 462, 1963.
87. Longo, M.I. and B. Moyer, Phys. Rev., Vol. 125, p. 701, 1962.
88. Vernov, S.N. and oth., V kn. XII Mezhdunarodnoy Konferentsii po Fizike Vysokikh Energiy (In Book: Twelfth International Conference on High Energy Physics), Vol. 1, Dubna, 1964. Atomizdat, Moscow, 1966, p. 167.
89. Gribov, V.N. and I. Ya. Pomeranchuk, Zh. Eksp. i Teoret. Fiz., Vol. 42, p. 1141, 1962; Vol. 43, p. 308, 1962.
90. Gell-Mann, M. and B. Udgaonkar, Phys. Rev. Lett., Vol. 8, p. 346, 1962.
91. Koshiba, M., Proc. Int. Conf. on Cosmic Rays, Jaipur, Vol. 5, p. 293, 1964.
92. Gould, C., A. Gray, C. McCusker, et al., Proc, Int. Conf. on Cosmic Rays, Jaipur, Vol. 5, p. 31, 1964.
93. Daniel, R.R., N. Durgaprasad, P. Malhotra and B. Vijaya-Takshmi, Proc. Int. Conf. on Cosmic Rays, Jaipur, Vol. 5, p. 17, 1964.
94. Birger, N.G., V.D. Mikhaylov, I.L. Rozental' and L.I. Sarycheva, Uspekh. Fiz. Nauk, Vol. 79, p. 523, 1963.
95. Cocconi, G., Int. Conf. on Theoret. Aspects of Very High-Energy Phenomena, Geneva, CERN 61-22, 1961, p. 128.
96. Brook, G., P. Haymann, Y. Kamiya and A. Wolfendale, Proc. Phys. Soc., Vol. 83, p. 853, 1964.
97. Lloret, A., A. Bezaguet, M. Bloch, et al., Nuovo Cimento, Vol. 31, p. 54, 1964.
98. Bradt, H.L. and B. Peters, Phys. Rev., Vol. 77, p. 54, 1950.
99. Kaplon, M., H. Noon and R. Racette, Phys. Rev., Vol. 96, p. 1408, 1954.
00. Radjapadhya, V.Y. and C. Waddington, Phil. Mag., Vol. 3, p. 19, 1958.
01. Fowler, P., T. Hiller and C. Waddington, Phil. Mag., Vol. 2, p. 293, 1957.
02. Cester, R., A. Debenedetti, C. Garelli, et al., Nuovo Cimento, Vol. 7, p. 371, 1958.
03. Aditya, P.H., Proc. Int. Conf. on Cosmic Rays, Jaipur, Vol. 5, p. 64, 1964.
04. Waddington, C., Phil. Mag., Vol. 45, p. 1312, 1956.
05. Appa Rao, M.V.K., R. Daniel, et al., Proc. Ind. Acad. Sci., Vol. A43, p. 181, 1956.
06. Stiller, B. and F. O'Dell, Bull. Amer. Phys. Soc., Vol. 1, p. 319, 1956.
07. Daniel, R., J. Davies, J. Milvey, et al., Phil. Mag., Vol. 43, p. 753, 1952.
08. Rama, B., Proc. Ind. Acad. Sci., Vol. 39, p. 162, 1954.
09. Badhwara, G., N. Durgaprasad and B. Vijayalakshmi, Proc. Int. Conf. on Cosmic Rays, Jaipur, Vol. 3, p. 8, 1964. /375
09a. Daniel, R. and N. Durgaprasad, Nuovo Cimento Suppl., Vol. 23, p. 82, 1962.
10. Zhdanov, G.B. and A.L. Lyubimov, Doklady AN SSSR, Vol. 55, p. 119, 1947. Veksler, V.I., L.V. Kurnosova and A.L. Lyubimov, Zh. Eksp. i Teoret. Fiz., Vol. 17, p. 1026, 1947. Birger, N.G., V.I. Veksler, N.A. Dobrotin, G.T. Zatsepin and oth., Zh. Eksp. i Teoret. Fiz., Vol. 19, p. 826, 1949.

111. Alekseyeva, K.I. and oth., Zh. Eksp. i Teoret. Fiz., Vol. 43, p. 783, 1962.
112. Lord, J.J., J. Feinberg and M. Shein, Phys. Rev., Vol. 80, p. 970, 1950.
113. Brown, W., U. Camerini, P. Fowler, et al., Phil. Mag., Vol. 40, p. 862, 1949.
114. Lock, W., Proc. Int. Conf. on Cosmic Rays, Jaipur, Vol. 5, p. 105, 1964.
115. Jain, P., H. Glake, J. Rinaldo and P. Bharadwaj, Nucl. Phys., Vol. 67, p. 641, 1965.
116. Waddington, C.J., Nuovo Cimento, Vol. 31, p. 748, 1964.
117. Gibson, T., Proc. Roy. Soc., Vol. A210, p. 540, 1952.
118. Kamerini, U., W. Lock and D. Perkins, Fizika Kosmicheskikh Luchey pod red. Vil'sona (Physics of Cosmic Rays — Wilson, ed.), Vol. 1, IL, Moscow, 1954, p. 7.
119. Harding, J.B., S. Lattimore and D. Perkins, Proc. Roy. Soc., Vol. A196, p. 325, 1949.
120. Menon, M.G. and O. Rochat, Phil. Mag., Vol. 42, p. 1233, 1951.
121. Friedlander, E., Nuovo Cimento, Vol. 14, p. 796, 1959.
122. Lal, S., R. Raghavan and T.N. Rangaswamy, Proc. Int. Conf. on Cosmic Rays, Jaipur, Vol. 5, p. 368, 1964.
123. Coghen, T., Z. Czachowska, J. Gierula, et al., Nukleonika, Vol. 9, p. 257, 1964.
124. Barkow, A., B. Chamani and D. Haskin, Phys. Rev., Vol. 122, p. 617, 1961.
125. Friedländer, E., Nuovo Cimento, Vol. 24, p. 342, 1962.
126. Fermi, E., Progr. Theor. Phys., Vol. 5, p. 570, 1950.
127. Belen'kiy, S.Z., V.M. Maksimenko, A.I. Nikishov and I.L. Rozental', Usp. Fiz. Nauk, Vol. 62, p. 1, 1957.
128. Heisenberg, W., Z. Phys., Vol. 129, p. 560, 1949; Vol. 133, p. 65, 1952.
129. Amati, D., Nuovo Cimento, Vol. 22, p. 569, 1961; Vol. 26, p. 896, 1962.
130. Malhotra, P., Nucl. Phys., Vol. 46, p. 559, 1963.
131. Piserchio, F. and R. Kalbach, Nuovo Cimento, Vol. 26, p. 717, 1962.
132. Winzeler, K., B. Klaiber and W. Koch, Nuovo Cimento, Vol. 17, p. 8, 1960.
133. Barashenkov, V.S., V.M. Belyakov, V.N. Glagolev and oth., Nucl. Phys., Vol. 14, p. 522, 1960.
134. Cvijanovich, G., B. Daiton, B. Egli, et al., Nuovo Cimento, Vol. 20, p. 1012, 1961.
135. Dodd, P., M. Jobos, J. Kinson, et al., Proc. Aix-en-Provence Conf., 1961.
136. Grigorov, N.L., V.V. Guseva, N.A. Dobrotin and oth., V kn. Trudy Mezhdunarodnoy Konferentsii po Kosmicheskim Lucham (In Book: Proceedings of the International Conference on Cosmic Rays), Vol. 1, AN SSSR, Moscow, 1960, p. 140.
137. San'ko, L.A., Zh.S. Takibayev and P.A. Usik, Proc. Int. Conf. on Cosmic Rays, Jaipur, Vol. 5, p. 58, 1964. /376
138. McCusker, C. and L.S. Peak, Nuovo Cimento, Vol. 31, p. 525, 1964.

139. Fowler, P., Proc. Int. Conf. on Cosmic Rays, Jaipur, Vol. 5, p. 182, 1964.
140. Malhotra, P., P. Shukla, S. Stephens, et al., Nuovo Cimento, Vol. 40, p. 365, 1965; Vol. 40, p. 385, 1965.
141. Barashenkov, V.S., V.M. Mal'tsev and I. Patera, Preprint OIYaI R-1577, Dubna, 1964.
142. Zatsepin, G.T., Izvestiya AN SSSR, Ser. fiz., Vol. 26, p. 674, 1962.
143. Guseva, V.V., N.A. Dobrotin and N.G. Zelevinskaya, Izvestiya AN SSSR, Ser. fiz., Vol. 26, p. 549, 1962.
143a. Friedländer, M., K. Neelkanatan, S. Tokunaga, et al., Phil. Mag., Vol. 8, p. 1691, 1963.
144. O'Dell, M., M. Shapiro and B. Stiller, Journ. Phys. Soc. Japan, Vol. 17, Suppl. A III, p. 23, 1962.
145. Badhwara, G., N. Durgaprasad and B. Vijayalakshmi, Proc. Indian Acad. Sci., Vol. 61, p. 374, 1965.
146. ICEF Collaboration, Nuovo Cimento, Suppl. 1, p. 1039, 1963.
147. Brisbout, F., C. Gould, G. McCusker, et al., Nucl. Phys., Vol. 26, p. 217, 1961.
148. Hoffman, L., N. Rao, M. Shaukat, et al., Nucl. Phys., Vol. 66, p. 657, 1965.
149. Brisbout, F., C. Gould, J. Lehane, et al., Nucl. Phys., Vol. 26, p. 634, 1961.
150. Mur, V.D. and I.L. Rozental', V sb. Fizika Elementarnykh Chastits (In Coll.: Physics of Elementary Particles), Atomizdat, Moscow, 1966, p. 3.
151. Fowler, P. and D. Perkins, Proc. Roy. Soc., Vol. A278, p. 400, 1964.
152. Artykov, I.Z., V.S. Barashenkov and S.M. Yeliseyev, Yadern. Fiz., Vol. 2, p. 156, 1966.
153. Nakagava, S., S. Tanaka and K. Ito, Preprints Int. Conf. on Cosmic Rays, Kyoto, part III, J III-6-20, 1961.
154. Kim, C. Phys. Rev., Vol. 136B, p. 515, 1964.
155. Bigi, A., S. Brandt and A. De Marco-Trabucco, Nuovo Cimento, Vol. 33, p. 1249, 1964.
156. Bartke, J., W. Cooper, B. Czapp, et al., Nuovo Cimento, Vol. 29, p. 8, 1963.
157. Slavatinskiy, S.A. and I.N. Fetisov, Izvestiya AN SSSR, Ser. fiz., Vol. 28, p. 1758, 1964.
158. Garbovska, K., T. Sanievska, Skrzypczak, et al., Nucl. Phys., Vol. 60, p. 654, 1964.
159. Kobzev, V.A., Yu.T. Lukin and Zh.S. Takibayev, Zh. Eksp. i Teoret. Fiz., Vol. 41, p. 742, 1961.
160. Csejthey-Barth, M., Nuovo Cimento, Vol. 32, p. 545, 1964.
161. Edwards, B., J. Losty, D. Perkins, et al., Phil. Mag., Vol. 3, p. 237, 1958.
162. Lal, C., Y. Pal and R. Raghavan, Nucl. Phys., Vol. 31, p. 415, 1962.
163. Agnew, L.E., et al., UCRL-87-85, 1959.
164. Cocconi, G., Proceed. of the High Energy Physics, Rochester, 1960, p. 801.
165. Osborn, I.L. and A.W. Wolfendale, Proc. Phys. Soc., Vol. 84, p. 901, 1964.
166. Bowen, T., I. Hardy, G.T. Reynolds, et al., Phys. Rev., Vol. 119, pp. 2030, 2041, 1961.

167. Apshev, S.Zh., A.M. Dadov, I.I. Sakvarelidze and R.A. Pakov, Izvestiya AN SSSR, Ser. fiz., Vol. 29, p. 1667, 1965. /377
168. Peter, B., Nuovo Cimento, Vol. 23, p. 28, 1962.
169. Kotov, Yu.D. and I.L. Rozental', Zh.Eksp. i Teoret. Fiz., Vol. 43, p. 1411, 1962.
170. Belen'kiy, S.Z., Doklady AN SSSR, Vol. 99, p. 523, 1954.
171. Glastyan, D.A., G.B. Zhdanov and M.I. Tret'yakova, Proc. Int. Conf. on Cosmic Rays, London, Vol. 2, p. 885, 1965.
172. Hansen, L. and W. Fretter, Phys. Rev., Vol. 118, p. 812, 1960.
173. Pinkau, K., Phil. Mag., Vol. 2, p. 1389, 1957.
174. Fowler, P., D. Perkins and K. Pinkau, V kn. Trudy Mezhdunarodnoy Konferentsii po Kosmicheskim Lucham (In Book: Proceedings of the International Conference on Cosmic Rays), Vol. 2, AN SSSR, Moscow, 1960, p. 320.
175. Buya, Z., B. Geller, Ye. Massal'skiy, and oth., Nukleonika, Vol. 9, p. 323, 1964.
176. Minakawa, O., Y. Nishimura, M. Tsuzuni, et al., Suppl. Nuovo Cimento, Vol. 11, p. 125, 1959.
177. Duthie, D., S.M. Fisher, P. Fowler and oth., V kn. Trudy Mezhdunarodnoy Konferentsii po Kosmicheskim Lucham (In Book: Proceedings of the Conference on Cosmic Rays), Vol. 1, IL, Moscow, 1960, p. 28.
178. Malhotra, P.K., P. Shuola, S.A. Stephens, et al., Nuovo Cimento, Vol. 40, p. 385, 1965.
179. Ivanenko, I.P. and B. Ye. Samosudov, Izvestiya AN SSSR, Ser. fiz., Vol. 30, p. 1651, 1966.
180. Koshiba, M. and M. Kaplon, Phys. Rev., Vol. 97, p. 193, 1955.
181. Borselino, A., Phys. Rev., Vol. 89m, p. 1023, 1953.
182. Friedländer, E.M., E. Combosi, M. Marcu and M. Spirchoz, Nucl. Phys., Vol. 32, p. 168, 1962.
183. Chudakov, A. Ye., Izvestiya AN SSSR, Ser. fiz., Vol. 19, p. 651, 1955.
184. Grigorov, N.L., A.V. Podgurskaya, V.A. Sobinyakov, and oth., Soveshchaniye po Metodike Tolstosloynykh Fotoemul'siy (Conference on Thick-Layer Photoemulsion Technique), Vol. 1, OIYaI, Dubna, 1958, p. 168.
185. Rapoport, I.D., Zh. Eksp. i Teoret. Fiz., Vol. 34, p. 998, 1958.
186. Metody Izmereniya Osnovnykh Fizicheskikh Velichin Yadernoy Fiziki (Methods for the Measurement of the Fundamental Physical Quantities of Nuclear Physics). K.L. Lyuk, Yuan and Wu Chien-Hsiung, Eds., Mir Press, 1964.
187. Kaplon, M. and D. Ritson, Phys. Rev., Vol. 88, p. 386, 1952.
188. Kaplon, M., B. Peters and D. Ritson, Phys. Rev., Vol. 85, p. 900, 1952.
189. Cocconi, G., et al., URL-Report UC-ID-1444, 1960.
190. De Marko Trabucco, A., L. Montanet and S. Nilsson, Nucl. Phys., Vol. 60, p. 209, 1964.
191. Friedlander, E.M., E. Gambosi, M. Marcu and M. Spirchez, Nucl. Phys., Vol. 40, p. 13, 1963.
192. Dekkers, D., J.A. Geibel, R. Mermod, et al., Phys. Rev., Vol. 137, 4B, p. 962, 1965.
193. Fidecaro, M., G. Finocchiaro, G. Gatti, et al., Nuovo Cimento, Vol. 24, p. 73, 1962.

194. Aly, H.H., M. Kaplon and M. Shen, Nuovo Cimento, Vol. 32, p. 905, 1964.
195. Aly, H.H., M. Kaplon and M. Shen, Proc. Int. Conf. on Cosmic Rays, Jaipur, Vol. 5, p. 85, 1964.
195a. Babu, P., R. Cowsic and P. Yash, Nuovo Cimento, Vol. 29, p. 785, 1963.
196. Watagin, G., Phys. Rev., Vol. 75, p. 693, 1949. /378
197. Zatsepin, G.T., Zh. Eksp. i Teoret. Fiz., Vol. 19, p. 1104, 1949.
198. Dobrotin, N.A., N.G. Zelevinskaya, K.A. Kotel'nikov and oth., Izvestiya AN SSSR, Ser. fiz., Vol. 29, p. 1627, 1965.
199. Belen'kiy, S.Z. and L.D. Landau, Usp. Fiz. Nauk, Vol. 56, p. 309, 1955.
200. Feynberg, Ye.L., Usp. Fiz. Nauk, Vol. 70, p. 335, 1960.
201. Babayan, Kh.P., N.L. Grigorov, M.M. Dubrovin and oth., V kn. Trudy Mezhdunarodnoy Konferentsii po Kosmicheskim Lucham (In Book: Proceedings of the International Conference on Cosmic Rays), Vol. 1, AN SSSR, Moscow, 1960, p. 76.
202. Murzin, V.S., Proc. Int. Conf. on Cosmic Rays, Jaipur, Vol. 5, p. 240, 1964.
203. Akashi, M., Z. Watanabe, A. Misani, et al., Suppl. Prog. Theor. Phys. Vol. 32, p. 1, 1964.
204. Heidbreder, E. and K. Pinkau, Proc. Int. Conf. on Cosmic Rays, Jaipur, Vol. 5, p. 227, 1964.
205. Babayan, Kh.P., N.L. Grigorov, Ch.A. Tret'yakova, and oth., Izvestiya AN SSSR, Ser. fiz., Vol. 29, p. 1648, 1965.
206, Babayan, Kh.P., N.L. Grigorov, S.I. Brikker, and oth., Nukleonika, Vol. 9, p. 291, 1964.
207. Akashi, M., S. Shimisu, Z. Watanabe, et al., J. Phys. Soc. Japan, Vol. 17, Suppl. A-111, p. 427, 1962.
208. Baldin, A.M., V.I. Gol'danskiy and I.L. Rozental', Kinematika Yadernykh Reaktsiy (Kinematics of Nuclear Reactions), Fizmatgiz, Moscow, 1959, Chap. 2.
209. Abraham, F. and R. Kalbach, Nuovo Cimento, Vol. 26, p. 718, 1962.
210. Piserchio, R. and R. Kalbach, Nuovo Cimento, Vol. 26, p. 729, 1962.
211. Hagedorn, R., Nuovo Cimento, Vol. 15, p. 434, 1960.
212. Behr, J. and R. Hagedorn, CERN 60-20.
213. Vinitskiy, A.Kh., I.G. Golyak, Zh.S. Takibayev and I. Ya. Chasnikov, V kn. Trudy Mezhdunarodnoy Konferentsii po Kosmicheskim Lucham (In Book: Proceedings of the International Conference on Cosmic Rays), Vol. 1, AN SSSR, Moscow, 1960, p. 61.
214. Milekhin, G.A., Zh. Eksper. i Teoret. Fiz., Vol. 35, p. 1185, 1956.
215. Matsumoto, S., J. Phys. Soc. Japan, Vol. 18, p. 1, 1963.
216. Fujioka, G.T., Phys. Soc. Japan, Vol. 16, p. 1107, 1961.
217. Grote, C., I. Klabuhn, U. Krecker, et al., Nucl. Phys., Vol. 34, p. 659, 1962.
218. Belyakov, V.A. and oth., Zh. Eksp. i Teoret. Fiz., Vol. 39, p. 937, 1960.
219. Vinitskiy, A.Kh., I.G. Golyak, N.P. Pavlova, and oth., V kn. Trudy Instituta Yadernoy Fiziki AN KazSSR (In Book: Proceedings of the Institute of Nuclear Physics, Academy of Science, Kazan SSR), Vol. 6, AN KazSSR, Alma-Ata, 1963, p. 144.
220. Glagolev, V.V. and K.D. Tolstov, Nucl. Phys., Vol. 68, p. 657, 1965.

221. Perkins, D., Proc. Int. Conf. on Theoretical Aspects at Very High Energy Phenomena CERN 61-22, 1961, p. 100.
222. Takachata, O., J. Phys. Soc. Japan, Vol. 18, p. 936, 1963.
223. Barashenkov, V.S., Izvestiya AN SSSR, Ser. fiz., Vol. 29, p. 1634, 1965.
224. Amaldi, E., G. Baroni, G. Belletini, et al., Nuovo Cimento, Vol. 14, p. 977, 1960.
225. Botvin, V.A., Zh.S. Takibayev and K.V. Shaparov, V kn. Trudy XII Mezhdunarodnoy Konferentsii po Fizike Vysshikh Energiy (In Book: Proceedings of the Twelfth International Conference on High Energy Physics), Dubna, 1964; Vol. 1, Atomizdat, Moscow, 1966, p. 156.
226. Rajapadhija, V.Y., Phil. Mag., Vol. 5, p. 537, 1960.
227. Kalbach, R., J. Lord and C. Tsao, Phys. Rev., Vol. 113, p. 330, 1959. /379
228. Daniel, R., N. Kameswara Rao, P.K. Malhotra, et al., Nuovo Cimento, Vol. 16, p. 1, 1960.
229, Vishki, T., I. Gramenitskiy, Z. Korbel, and oth., Zh. Eksp. i Teoret. Fiz., Vol. 41, p. 1069, 1961.
230. Pal, Y. and P. Rengarajan, J. Phys. Soc. Japan, Vol. 17, Suppl. A. III, p. 387, 1962.
231. Kanenko, S., O. Kusumoto, S. Matsumoto and M. Takahata, V kn. Trudy Mezhdunarodnoy Konferentsii po Kosmicheskim Lucham (In Book: Proceedings of the International Conference on Cosmic Rays), Vol. 1, AN SSSR, Moscow, 1960, p. 100.
232. Daniel, R.R., et al., Suppl. Nuovo Cimento, Vol. 1, p. 1169, 1963.
233. Femino, S., S. Jannelli and F. Mezzanares, Nuovo Cimento, Vol. 31, p. 272, 1964.
234. Grote, C., J. Klugow, U. Krecker and K. Zanius, Nucl. Phys., Vol. 34, p. 685, 1962.
235. Grote, C., J. Klabuhn, U. Krecker, et al., Nucl. Phys., Vol. 34, p. 676, 1962.
236. Bozoki, G., E. Fenjves, A. Frennel, et al., Nuovo Cimento, Vol. 24, p. 29, 1962.
237. Goldsack, S., L. Riddiford, B. Tallini, et al., Nuovo Cimento, Vol. 23, p. 941, 1962.
238. Huson, F.R. and W.B. Fretter, Nuovo Cimento, Vol. 33, p. 1, 1964.
239. Spergel, M.S., et al., Nuovo Cimento, Vol. 42, p. 251, 1964.
240. Milekhin, G.A. and I.L. Rozental', Zh. Eksp. i Teoret. Fiz., Vol. 33, p. 197, 1957.
241. Fukuda, H. and C. Yso, Preprint. The Relation between Elastic Diffraction Scattering and Dynamics of Multiple Meson Production in Very High Energy Regions, Tokyo Inst. Techn., 1965.
242. Barashenkov, V.S., V.M. Mal'tsev and I. Patera, Preprint OIYaI P-1577, Dubna, 1964.
243. Birger, N.G., and oth., Zh. Eksp. i Teoret. Fiz., Vol. 41, p. 1461, 1961.
244. Takobayev, Zh.S., E.G. Boos and N.P. Pavlova, V kn. Trudy Instituta Yadernoy Fiziki AN KazSSR (In Book: Proceedings of the Institute of Nuclear Physics, Academy of Science, Kazan SSR), Vol. 6, AN KazSSR, Alma-Ata, 1961, p. 90.
245. Tolstov, K.D., OIYaI P-1469, Dubna, 1963.
246. Awunor-Renner, E.R.T., L. Blaskovitch, B.R. French, et al., Nuovo Cimento, Vol. 17, p. 134, 1960.

247. Peters, B., Proc. Conf. High Energy Phys., CERN, p. 623, 1962.
248. Jain, P.L., Nuovo Cimento, Vol. 24, p. 698, 1962.
249. Schein, M., D.M. Haskins, E. Lohrmann, et al., Phys. Rev., Vol. 116, p. 1238, 1959.
250. Debenedetti, A., C.M. Garelli, L. Talone, et al., Nuovo Cimento, Vol. 4, p. 1142, 1956.
251. Ciok, P., M. Danycz, I. Gierula, et al., Nuovo Cimento, Vol. 6, p. 1409, 1957.
252. Nishikawa, K., J. Phys. Soc. Japan, Vol. 14, p. 879, 1959.
253. Kazuno, M., Nuovo Cimento, Vol. 24, p. 1014, 1962.
254. Nishimura, Y., Proceed. Int. Conf. on Cosmic Rays, London, Japanese and Brazilian Emulsion Groups, Vol. 2, p. 835, 1965.
255. Hasegawa, S., Nuovo Cimento, Vol. 14, p. 909, 1959.
256. Lattes, C.M.G., C.A. Orsini, Y.G. Pacca, et al., Nuovo Cimento, Vol. 33, p. 680, 1964.
257. Grigorov, N.L. and oth., Izvestiya AN SSSR, Ser. fiz., Vol. 30, p. 1621, 1966. /380
258. Gramenitskiy, I.M., G.B. Zhdanov, Ye.A. Zamchalova, and oth., Zh. Eksp. i Teoret. Fiz., Vol. 32, p. 936, 1957.
259. Boos, Z.G., A.Kh. Vinitskiy, Zh.S. Takibayev, and oth., Zh. Eksp. i Teoret. Fiz., Vol. 34, p. 622, 1958.
260. Guseva, V.V., N.A. Dobrotin, N.G. Zelevinskaya, and oth., J. Phys. Soc. Japan, Vol. 17, Suppl. A-III, p. 375, 1962.
261. Piserchio, R.Y. and R.M. Kalbach, Nuovo Cimento, Vol. 26, p. 729, 1962.
262. Blue, M.H., J. Lord, I.G. Parks, et al., Nuovo Cimento, Vol. 20, p. 274, 1961.
263. Jain, P.L., H.C. Glake, I.D. Rinaldo, et al., Nuovo Cimento, Vol. 32, p. 873, 1964.
264. Bigi, A., S. Brandt, A. DeMarco-Trabucco, et al., Nuovo Cimento, Vol. 33, p. 1265, 1964.
265. Lim, Y.K., Nuovo Cimento, Vol. 26, p. 1221, 1962.
266. Friedländer, E.M., Nuovo Cimento, Vol. 41, p. 418, 1966.
267. Malhotra, P.K., Proc, Int. Conf. Cosmic Rays, London, Vol. 2, p. 840, 1965.
268. Fowler, P.H. and D.H. Perkins, Proceed. Roy. Soc. A, pp. 278, 401, 1964.
269. Zhdanov, G.B., Zh. Eksp. i Teoret. Fiz., Vol. 34, p. 856, 1959.
270. Pinkau, K., Phil. Mag., Vol. 6, p. 657, 1961.
271. Imaeda, K. and Y. Avidan, Nuovo Cimento, Vol. 32, p. 1497, 1964.
272. Milekhin, G.A., Trudy Fizicheskogo Instituta im. P.N. Lebedeva AN SSSR (Proceedings of the P.N. Lebedev Physics Institute, Academy of Science, USSR), Vol. 16, p. 50, 1961.
273. Friedlander, E.M., Rev. Roumain Phys., Vol. 11, p. 99, 1966.
274. Willis, W.I., CERN 61-22, p. 153, 1963.
275. Morrison, D.R.O., CERN TC-63-1, 1963, p. 153.
276. Bellini, G., E. Fiorini, A. Herz, et al., Nuovo Cimento, Vol. 27, p. 816, 1963.
277. Bardalin, M., L. Michejda, S. Otwinowsky, et al., Nucl. Research Report 511/VI, Warsaw, 1964.

278. Hilder, G., Tsitiruyetsya. Sm. rabotu [266] (Cited, see Ref. [266]).
279. Goldsack, S.I., L. Riddiford, B. Tallini, et al., Nuovo Cimento, Vol. 23, p. 941, 1962.
280. Ferrero, M.J., C.M. Garelli, Marzarichiesa, et al., Nuovo Cimento, Vol. 27, p. 1066, 1963.
281. Bartke, J., R. Budde, W.A. Cooper, et al., Nuovo Cimento, Vol. 24, p. 876, 1962.
282. Ferbel, T. and H. Taft, Nuovo Cimento, Vol. 28, p. 1214, 1964.
283. Volzhenskaya, V.P. and L.I. Sarycheva, Izvestiya AN SSSR, Ser. fiz., Vol. 30, p. 1594, 1966.
284. Boos, E.G., Zh. Eksp. i Teoret. Fiz., Vol. 41, p. 747, 1961.
285. Boos, E.G., A.Kh. Vinitskiy and Zh.S. Takibayev, Yadernaya Fiz., Vol. 1, p. 148, 1965.
286. Malhotra, P.K., Nucl. Phys., Vol. 59, p. 551, 1964.
287. Pernegr, I., V. Simak and M. Votruba, Nuovo Cimento, Vol. 17, p. 129, 1960.
288. Boos, E.G., V.A. Botvin, N.P. Pavlova, and oth., Zh. Eksp. i Teoret. Fiz., Vol. 42, p. 3, 1962.
289. Babayan, Kh.P. and N.A. Marutyan, Zh.Eksp. i Teoret. Fiz., Vol. 44, p. 832, 1963.
290. Koba, Z., Progr. Theor. Phys., Vol. 17, p. 288, 1957. /381
291. Koba, Z. and Sh. Takagi, Uspekh. Fiz. Nauk, Vol. 70, p. 287, 1960.
292. Barashenkov, V.C., Preprint OIYaI, Dubna, No. 540, 1960.
293. Galstyan, D.A., G.B. Zhdanov and M.I. Tret'yakova, Zh. Eksp. i Teoret. Fiz., Vol. 51, p. 417, 1966.
294. Gerasimova, N.M. and D.S. Chernavskiy, Zh. Eksp. i Teoret. Fiz., Vol. 29, p. 372, 1955.
295. Gerasimova, N.M., Zh. Eksp. i Teoret. Fiz., Vol. 39, p. 1087, 1960.
296. Pinkau, K., Fortschr. Phys., Vol. 12, p. 141, 1964.
297. Azimov, S.A., Yu.V. Polyak and R.S. Abdullayev, Proc. Int. Conf. on Cosmic Rays, Jaipur, Vol. 5, p. 74, 1964.
298. Bigg, W. and D. King, Phys. Rev., Vol. 119, p. 1407, 1960.
299. Radjapadhya, R., Phil, Mag., Vol. 5, p. 537, 1960.
300. Bogachev, N.P., Ye.L. Grigorov and Yu.P. Merekov, Doklady AN SSSR, Vol. 148, p. 793, 1963.
301. Pal, Y. and T. Rangarajan, Proc. Phys. Soc. Japan, Vol. 17, Suppl. A-III, p. 387, 1962.
302. Lal, S., R. Raghavan and T.N. Rangaswami, Proc. Int. Conf. on Cosmic Rays, Jaipur, Vol. 5, p. 377, 1964.
303. Azimov, S.A., A.M. Abdullayev, B.V. Lugovskoy, and oth., Izvestiya AN SSSR, Ser. fiz., Vol. 28, p. 1773, 1964; Proc. Int. Conf. on Cosmic Rays, Jaipur, Vol. 5, p. 69, 1964.
304. Yerofeyeva, I.N., L.G. Mishchenko, V.S. Murzin, and oth., Proc. Int. Conf. on Cosmic Rays, London, Vol. 2, p. 833, 1965.
305. Huggett, P., K. Mori, C. Kim and R. Levi Setti, Proc. Int. Conf. on Cosmic Rays, Jaipur, Vol. 5, p. 3, 1964.
306. Hoffmann, et al., Sm. rabotu [114] (see Ref. [114]).
307. Rybicki, K., Nuovo Cimento, Vol. 28, p. 1437, 1963.
308. Loktionov, A.A. and Zh.S. Takibayev, Izvestiya AN SSSR, Ser. fiz., Vol. 26, p. 596, 1962.

309. Boos, E.G. and Zh.S. Takibayev, V kn. Trudy Mezhdunarodnoy Konferentsii po Kosmicheskim Lucham (In Book: Proceedings of the International Conference on Cosmic Rays), Vol. 1, AN SSSR, Moscow, 1960, p. 76.
310. Kita, I., Phys. Soc. Japan, Vol. 16, p. 1099, 1961.
311. Zatsepin, G.T., J. Phys. Soc. Japan, Vol. 17, Suppl. A-III, p. 495, 1962.
312. Fretter, V.B. and L.F. Khansen, V kn. Trudy Mezhdunarodnoy Konferentsii po Kosmicheskim Lucham (In Book: Proceedings of the International Conference on Cosmic Rays), Vol. 1, AN SSSR, Moscow, 1960, p. 134.
313. Hasegawa, S., Progr. Theor. Phys., Vol. 26, p. 150, 1961.
314. Malhotra, P., Proc. Ind. Acad. Sci., Vol. 62, p. 189, 1965.
315. Walker, W.D., Phys. Rev., Vol. 108, p. 872, 1957.
316. Kelson, I. and G. Yekutieli, Nuovo Cimento, Vol. 30, p. 734, 1963.
317. Grigorov, N.L., V.S. Murzin and I.D. Rapoport, Zh. Eksp. i Teoret. Fiz., Vol. 36, p. 1068, 1959.
318. Watson, K.N., Phys. Rev., Vol. 85, p. 852, 1952.
319. Feynberg, Ye.L., Usp. Fiz. Nauk, Vol. 70, p. 335, 1960.
320. Vernov, Yu.S. and I.N. Sisakyan, Izvestiya AN SSSR, Ser. fiz., Vol. 26, pp. 622, 642, 1962.
321. Daybog, Ye.I., Pis'ma v ZhETF (Letters to J. Exper. and Theor. Phys.), Vol. 3, p. 237, 1966.
322. Bellini, G., M. Dicorato, F. Duimio and E. Fiorini, Nuovo Cimento, Vol. 40, p. 948, 1965.
323. Subramanian, A. Proc. Int. Conf. on Cosmic Rays, Jaipur, Vol. 5, p. 166, 1964. /382
324. Femio, S., S. Jannelli and F. Mezzanares, Nuovo Cimento, Vol. 31, p. 272, 1964.
325. Cocconi, G., Phys. Rev., Vol. 111, p. 1699, 1958.
326. Takagi, S., Progr. Theor. Phys., Vol. 7, p. 123, 1952.
327. Niu, K., Nuovo Cimento, Vol. 10, p. 994, 1958.
328. Ciok, P., T. Coghen, I. Gierula, et al., Nuovo Cimento, Vol. 8, p. 166, 1958.
329. Bozoki, G., E. Fenyves and E. Gombosi, Nucl. Phys., Vol. 8, p. 199, 1958.
330. Bozoki, G. and E. Gombosi, Nucl. Phys., Vol. 9, p. 400, 1958.
331. Bartke, I., P. Ciok, I. Gierula, et al., Nuovo Cimento, Vol. 15, p. 18, 1960.
332. Gierula, I., M. Miesowicz and P. Zielinski, Nuovo Cimento, Vol. 18, p. 102, 1960.
333. Bartke, Ya.P., P. Chiok, Ya. Gerula, and oth., V kn. Trudy Mezhdunarodnoy Konferentsii po Kosmicheskim Lucham (In Book: Proceedings of the International Conference on Cosmic Rays), Vol. 1, AN SSSR, Moscow, 1960, p. 106.
334. Gierula, I., D.M. Haskin and E. Lohrmann, Phys. Rev., Vol. 122, p. 626, 1961.
335. Takibayev, Zh.S., Trudy Instituta Yadernoy Fiziki AN KazSSR (Proceedings of the Institute of Nuclear Physics, Academy of Science, Kazan SSR), Vol. 1, AN KazSSR, Alma-Ata, 1958.

336. Takibayev, Zh.S., L.A. San'ko and P.A. Usik, Izvestiya AN SSSR, Ser. fiz., Vol. 28, p. 1767, 1964.
337. San'ko, L.A., Dissertatsiya (Dissertation), Alma-Ata, 1964.
338. Mishakova, A.P., Dissertatsiya (Dissertation), Moscow, 1964.
339. Tomashewski, A., Nuovo Cimento, Vol. 33, p. 993, 1964.
340. Ciok, P., T. Coghen, I. Gierula, et al., Nuovo Cimento, Vol. 10, p. 741, 1958.
341. Coghen, T., Czachowska, I. Gierula, et al., Suppl. Nuovo Cimento, Vol. 1, p. 1157, 1963.
342. Imaeda, K. and M. Kazuno, Suppl. Nuovo Cimento, Vol. 1, p. 1197, 1963.
343. Zhdanov, G.B., Trudy Fizicheskogo Instituta im. P.N. Lebedeva AN SSSR (Proceedings of the P.N. Lebedev Physics Institute, Academy of Science, USSR), Vol. 26, p. 207, 1964.
344. Miesowicz, M., J. Phys. Soc. Japan, Vol. 17, Suppl. A-III, P-111, p. 458, 1962.
345. Gierula, J., Fortischritte der Physik, Vol. 11, p. 109, 1963.
346. Guseva, V.V., A.M. Lebedev and V.V. Sokolovskiy, Proc. Int. Conf. on Cosmic Rays, London, Vol. 2, p. 909, 1965.
347. Guseva, V.V., S.A. Dubrovina, A.M. Lebedev and oth., Izvestiya AN SSSR, Ser. fiz., Vol. 28, p. 1761, 1964.
348. Gierula, I., F. Holinski and M. Miesowicz, J. Phys. Soc. Japan, Vol. 17, Suppl. A-III, P-III, p. 405, 1962.
349. Gerasimov, N.M., Proc. Int. Conf. on Cosmic Rays, London, Vol. 2, p. 194, 1965.
350. Imaeda, K., M. Kazuno, L. Peak, et al., Nuovo Cimento, Vol. 43, p. 206, 1966.
351. Lindern, L.V., Nuovo Cimento, Vol. 49, p. 491, 1957.
352. Takibayev, Zh.S., Izvestiya AN SSSR, Ser. fiz., Vol. 31, p. 1407, 1967.
353. Raçzka, R. and A. Raçzka, V kn. Trudy XII Mezhdunarodnoy Konferentsii po Fizike Vysokikh Energiy (In Book: Proceedings of the Twelfth International Conference on High Energy Physics), Dubna, 1964; Atomizdat, Moscow, 1966, p. 312.
354. San'ko, L.A., Trudy Instituta Yadernoy Fiziki AN KazSSR (Proceedings of the Institute of Nuclear Physics, Academy of Science, Kazan SSR), Vol. 6, p. 64, 1963. /383
355. Jain, P.L., Nuovo Cimento, Vol. 24, p. 565, 1962.
356. Pernegr, Ya., Trudy Mezhdunarodnoy Konferentsii po Kosmicheskim Lucham (Proceedings of the International Conference on Cosmic Rays), Vol. 1, AN SSSR, Moscow, 1960, p. 114.
357. Pernegr, Ya., V. Petrzhilka and V. Shimak, V kn. Trudy Mezhdunarodnoy Konferentsii po Kosmicheskim Lucham (In Book: Proceedings of the International Conference on Cosmic Rays), Vol. 1, AN SSSR, Moscow, 1960, p. 119.
358. Mishakova, A.P. and B.A. Nikol'skiy, Yadern. Fiz., Vol. 8, p. 703, 1966.
359. Bogdanowicz, I., P. Ciok, Z. Galster, et al., Nucl. Phys., Vol. 40, p. 270, 1963.
360. Abudzhamilov, Sh. and S.A. Azimov, Zh. Eksp. i Teoret. Fiz., Vol. 45, p. 407, 1963.
361. Hasegawa, S., Progr. Theoret. Phys., Vol. 29, p. 130, 1963.
362. Chernov, G.M. and V.M. Chudakov, Zh. Eksp. i Teoret., Fiz., Vol. 47, p. 1273, 1964.

363. Dobrotin, N.A., N.G. Zelevinskaya, K.A. Kotel'nikov, and oth., Proceed. Int. Conf. on Cosmic Rays, Jaipur, Vol. 5, p. 79, 1963.
364. Zelevinskaya, N.G., V.M. Maksimenko, S.A. Slavatinskiy and V.V. Sokolovskiy, Izvestiya AN SSSR, Ser. fiz., Vol. 29, p. 1640, 1965.
365. Rozental', I.L. and L.I. Sarycheva, Izvestiya AN SSSR, Ser. fiz., Vol. 31, No. 10, 1967.
366. Friedländer, E.M., M. Maren and M. Spirchez, Nuovo Cimento, Vol. 18, p. 623, 1960.
367. Belyakov, V.A., Wang Shu-fen, V.V. Glagolev, and oth., Zh. Eksp. i Teoret. Fiz., Vol. 39, p. 937, 1960.
368. Ciurlo, I., V.V. Glagolev, V.A. Nitin, et al., Nuovo Cimento, Vol. 25, p. 1197, 1962.
369. Ciurlo, I., E. Picasso, G. Tomasini, et al., Nuovo Cimento, Vol. 27, p. 791, 1963.
370. Babu, P., R. Cowsic and Y. Pal, Nuovo Cimento, Vol. 29, p. 785, 1963.
371. Gainotti, A., C. Lamborizio and S. Mora, Nuovo Cimento, Vol. 29, p. 1209, 1963.
372. Barbaro-Galtieri, A., A. Manfredini, B. Qussiati, et al., Nuovo Cimento, Vol. 21, p. 469, 1961.
372a. Baudinet-Robinet, Y., M. Morand, Tsai-Chu, et al., Nucl. Phys., Vol. 32, p. 452, 1962.
373. Finney, P.I. and I.V. Major, Nuovo Cimento, Vol. 41A, p. 77, 1966.
374. Hilldebrand, B. and R. Silberberg, Proceed. Int. Conf. on Cosmic Rays, Jaipur, Vol. 5, p. 20, 1963.
375. Blokhintsev, D.I., Nuovo Cimento, Vol. 18, p. 193, 1960.
376. Birger, N.G. and Yu.A. Smorodin, Zh.Eksp. i Teoret. Fiz., Vol. 36, pp. 1159, 1355, 1959.
377. Birger, N.G., S.A. Slavatinskiy and Yu.A. Smorodin, V kn. Trudy Mezhdunarodnoy Konferentsii po Kosmicheskim Lucham (In Book: Proceedings of the International Conference on Cosmic Rays), Vol. 1, AN SSSR, Moscow, 1960, p. 154.
378. Koba, Z. and A. Krzywicki, Report No. 260/VII, 1964.
379. Khayakava, S., Uspekh. Fiz. Nauk, Vol. 89, p. 259, 1966.
380. Fujioka, G., Y. Maeda, O. Minakawa, et al., Suppl. Nuovo Cimento, Vol. 1, p. 1143, 1963.
381. Akimov, V.N. and I.M. Dremin, Preprint FIAN (Preprint Physics Institute, Academy of Science), Moscow, 1966.
382. Yerofeyeva, I.N., L.G. Mishchenko, V.A. Murzin, and oth., Proc. Int. Conf. on Cosmic Rays, London, Vol. 2, p. 831, 1965. /384
383. Dremin, I.M., G.B. Zhdanov, M.I. Tert'yakova and M.M. Chernavskiy, Pis'ma v ZhETF (Letters to J. Experimental and Theoretical Phys.), Vol. 4, p. 152, 1966.
384. Feynberg, Ye.L., V kn. Trudy XII Mezhdunarodnoy Konferentsii po Fizike Vysokikh Energiy (In Book: Proceedings of the Twelfth International Conference on High Energy Physics), Dubna, 1964, Vol. 1, Atomizdat, Moscow, 1966, p. 337.
385. Yezava, Kh., O. Kamei, K. Mori, and oth., V kn. Trudy Mezhdunarodnoy Konferentsii po Kosmicheskim Lucham (In Book: Proceedings of the International Conference on Cosmic Rays), Vol. 1, AN SSSR, Moscow, 1960, p. 276.

386. Zatsepin, G.T. and A.I. Nikishov, Izvestiya AN SSSR, Ser. fiz., Vol. 28, p. 1824, 1964.
387. Murzin, V.S., Izvestiya AN SSSR, Ser. fiz., Vol. 28, p. 1790, 1964.
388. Takibayev, Zh.S., P.A. Usik and L.A. San'ko, Doklady AN SSSR, Vol. 157, p. 328, 1964.
389. Feynberg, Ye.L. and D.S. Chernavskiy, Izvestiya AN SSSR, Ser. fiz., Vol. 31, No. 10, 1967.
390. Quenby, J.J. and G.J. Wenk, Phil. Mag., Vol. 7, p. 1457, 1962.
391. Dorman, L.I., Variatsii Kosmicheskikh Luchey (Variations of Cosmic Rays), AN SSSR, Moscow, 1963, p. 194.
392. Ginzburg, V.L., L.V. Kurnosova, L.A. Rasorenov and M.I. Fradkin, Uspekh. Fiz. Nauk, Vol. 32, p. 585, 1964.
393. Badhwar, G., N. Durgaprasad and B. Vijayalakshni, Proc. Ind. Acad. Sci., Vol. 62, p. 17, 1965.
394. Zinger, S., V kn. Fizika Elementarnykh Chastits Kosmicheskikh Luchey (In Book: Physics of Elementary Particles in Cosmic Rays), pod red. Vil'sona (Wilson -- ed.), IL, Moscow, 1960, p. 201.
395. Haber-Shain, U., Nuovo Cimento Suppl., Vol. 2, p. 336, 1955.
396. Lal, S., Proc. Ind. Acad. Sci., Vol. A38, p. 93, 1953.
397. Grigorov, N.L., I.D. Rapoport, I.A. Savenko, and oth., Izvestiya AN SSSR, Ser. fiz., Vol. 29, p. 1656, 1965.
398. Clark, G., Phys. Rev., Vol. 122, p. 639, 1961.
399. Solov'yeva, V.I., Dissertatsiya (Dissertation), Moscow, 1965.
400. Zatsepin, G.T., S.I. Nikol'skiy and G.B. Khristiansen, Proc. Int. Conf. on Cosmic Rays, Jaipur, Vol. 4, 1964.
401. Sarycheva, L.I., Dissertatsiya (Dissertation), Moscow, 1953.
402. Zatsepin, G.T. and L.I. Sarycheva, Doklady AN SSSR, Vol. 99, p. 951, 1954.
403. Rossi, B., V kn. Trudy Mezhdunarodnoy Konferentsii po Kosmicheskim Lucham (In Book: Proceedings of the International Conference on Cosmic Rays), Vol. 2, AN SSSR, Moscow, 1960, p. 17.
404. Goryunov, N.N., A.D. Yerlykin, G.T. Zatsepin and A.B. Kamnev, V kn. Trudy Mezhdunarodnoy Konferentsii po Kosmicheskim Lucham (In Book: Proceedings of the International Conference on Cosmic Rays), Vol. 2, AN SSSR, Moscow, 1960, p. 71.
405. Nikol'skiy, S.I. and Ye.I. Turkin, V kn. Trudy Mezhdunarodnoy Konferentsii po Kosmicheskim Lucham (In Book: Proceedings of the International Conference on Cosmic Rays), Vol. 2, AN SSSR, Moscow, 1960, p. 139.
406. Bray, A.D., D. Crawford and D. Jauncey, Nuovo Cimento, Vol. 32, p. 827, 1964.
407. Kulikov, G.V. and G.B. Khristiansen, Zh. Eksp. i Teoret. Fiz., Vol. 35, p. 635, 1959.
408. Linsley, J., Proc. Int. Conf. on Cosmic Rays, Jaipur, Vol. 4, p. 77, 1964.
409. Vernov, S.N., and oth., Izvestiya AN SSSR, Ser. fiz., Vol. 29, No. 10, 1966.
410. Yerofeyev, I.N., L.G. Mishchenko, V.S. Murzin and A.I. Sarycheva, Yadern. Fiz., Vol. 30, p. 1624, 1966. /38
411. Pal, Y. and B. Peters, Mat. Fys. Medd. Kgl. Danske Vid. Selskab, Vol. 33, No. 15, 1964.
412. Baradzey, L.T., V.I. Rubtsov, Yu.A. Smorodin, and oth., Trudy Fizicheskogo In-ta im. P.N. Lebedeva AN SSSR (Proceedings of the P.N. Lebedev Physics Institute, Academy of Sciences, USSR), Vol. 26, p. 224, 1964.

413. Kocharyan, N.M., G.S. Saakyan and Z.A. Kirakosyan, Zh. Eksp. i Teoret. Fiz., Vol. 35, p. 1335, 1958.
414. Grigorov, N.L., I.N. Yerofeyev, L.G. Mishchenko and oth., Izvestiya AN SSSR, Ser. fiz., Vol. 28, p. 1801, 1964.
415. Brook, G., M. Meyer and A. Wolfendale, Proc. Phys. Soc., Vol. 83, p. 871, 1964.
416. Greisen, K., Proceed. Int. Conf. on Cosmic Rays, London, Vol. 2, p. 609, 1965.
417. Miyagaki, M., J. Phys. Soc. Japan, Vol. 17, p. 1824, 1962.
418. Shukla, P., Proc. Int. Conf. on Cosmic Rays, London, Vol. 1, p. 360, 1965.
419. Anand, K.C., K. Daniel and S.O. Stephens, Proc. Int. Conf. on Cosmic Rays, London, Vol. 1, p. 362, 1965.
420. Fowler, P. and C. Waddington, Phil. Mag., Vol. 1, p. 637, 1956.
421. Jain, P., E. Lohrmann and M. Teucher, Phys. Rev., Vol. 115, p. 654, 1959.
422. Bodhwar, G.D., S. Biswas, R. Daniel and N. Durgaprasad, Proc. Int. Conf. on Cosmic Rays, Jaipur, Vol. 3, p. 38, 1964.
423. Biswas, S., Nuovo Cimento, Vol. 16, p. 644, 1960.
424. Shapiro, M., B. Stiller and F. O'Dell, Nuovo Cimento Suppl., Vol. 8, p. 519, 1958.
425. Danielson, R., Phys. Rev., Vol. 113, p. 1311, 1959.
426. Waddington, C.J., Phil. Mag., Vol. 5, p. 1105, 1960.
427. Durgaprasad, N., Ph.D. Thesis, TIER, Bombay, 1964.
428. Kurnosova, L.V., V.I. Logachev, L.N. Razorenov and M.I. Fradkin, Trudy FIAN (Proc. Phys. Inst., Acad. Sci.), Moscow, 1964; Vol. 26, Kosmicheskiye Luchi (Cosmic Rays), p. 3, Nauka Press.
429. Volodichev, N.N., N.L. Grigorov, V.Ye. Nesterov, and oth., Preprint, AN SSSR, Moscow, 1966.
430. Shapiro, M.M., B. Stiller and F. O'Dell, Nuovo Cimento Suppl., Vol. 8, p. 519, 1958.
431. Kajarekar, Thesis, Univ. of Bombay, 1965.
432. Webber, W.R., Nuovo Cimento Suppl., Vol. 8, p. 532, 1958.
433. Webber, W.R. and J. Ormes, Proc. Int. Conf. on Cosmic Rays, Jaipur, Vol. 3, p. 3, 1963.
434. Daniel, R.R. and N. Sreenivasan, Nuovo Cimento, Vol. 35, p. 391, 1965.
435. Waddington, C.J., J. Phys. Soc. Japan, Vol. 17, Suppl. A-III, Vol. 14, 1962.
436. Balasubramanian, V., S. Ganguli, G. Gorkhale, et al., Journ. Phys. Soc. Japan, Vol. 17, Suppl. A-III, p. 8, 1962.
437. McDonald, F., Phys. Rev., Vol. 109, p. 1367, 1958.
438. Hayakawa, S., I. Nishimura and Y. Yamamoto, Suppl. Progr. Theor. Phys., Vol. 32, p. 104, 1964.
439. Vernov, S.N., A.M. Kulikov and A.N. Charakhch'yan, Izvestiya AN SSSR, Ser. fiz., Vol. 17, p. 13, 1953.
440. Pal, Y., Proc. Conf. on the Interaction between Cosmic Rays and High Energy Phys., Cleveland, Ohio II-3, 1964. /386
440a. Babetski, Ya.S., Z.A. Burya, N.L. Grigorov, and oth., Zh. Eksp. i Teoret. Fiz., Vol. 40, p. 1551, 1961.
440b. Grigorov, N.L., Zh. Eksp. i Teoret. Fiz., Vol. 45, p. 1544, p. 1919, 1963.
440c. Babayan, Kh.P., Ya.S. Babetski, N.G. Boyadzhan, and oth., Izvestiya AN SSSR, Ser. fiz., Vol. 26, p. 559, 1962.

440d. Bowler, M., I. Duthie, P. Fowler, et al., Proc. Phys. Soc. Japan, Vol. 17, Suppl. A-III, p. 424, 1962.
441. Barret, P., L. Bollinger, G. Cocconi, et al., Rev. Mod. Phys., Vol. 24, p. 133, 1952.
442. Subramanian, S. and S. D. Verma, Nuovo Cimento, Vol. 13, p. 572, 1959.
443. Baradzey, L. T., V. I. Rubtsov, Yu. A. Smorodin, and oth., Proc. Phys. Soc. Japan, Vol. 17, Suppl. A-III, p. 433, 1962.
444. Duthie, J., P. Fowler and A. Kaddura, Nuovo Cimento, Vol. 24, p. 122, 1962.
445. Abraham, F., J. Kidd, M. Koshiba, et al., Nuovo Cimento, Vol. 28, p. 221, 1963; Vol. 29, p. 315, 1963.
446. Kidd, J., Nuovo Cimento, Vol. 27, p. 57, 1962.
447. Baradzey, L. T., V. I. Rubtsov, Yu. A. Smorodin, and oth., Nukleonika, Vol. 9, p. 277, 1964.
448. Fujimoto, I., S. Hayakawa, M. Kazuno, and oth., V kn. Trudy Mezhdunarodnoy Konferentsii po Kosmicheskim Lucham (In Book: Proceedings of the International Conference on Cosmic Rays), Vol. 1, AN SSSR, Moscow, 1960, p. 38.
449. Minakawa, O., Y. Nishimura, S. Hasegawa, et al., Nuovo Cimento, Suppl., Vol. 8, p. 761, 1958.
450. Babayev, M. K., R. Z. Denikayev, Yu. A. Yemel'yanov, and oth., Izvestiya AN SSSR, Ser. fiz., Vol. 29, p. 1719, 1965.
451. Lattes, C. M. G., T. Borello, M. Cruz, et al., Ninth Int. Conf. on Cosmic Rays, London--Abstracts He--p. 8, 1965.
452. Kameda, T. and T. Maeda, Journ. Phys. Soc. Japan, Vol. 15, pp. 1175, 1367, 1960.
453. Akashi, M., et al., J. Phys. Soc. Japan, Vol. 17, p. 427, 1961.
454. Pal, Y. and S. Tandon, Proc. Int. Conf. on Cosmic Rays, London, Vol. 2, p. 890, 1965.
455. Babayan, Kh. P., N. L. Grigorov, A. Mamidzhanyan, and oth., Nukleonika, Vol. 9, p. 299, 1964.
456. Nikol'skiy, S. I. and Yu. A. Smorodin, Zh. Eksp. i Teoret. Fiz., Vol. 39, p. 1156, 1960.
457. Duthie, J., S. Fisher, P. Fowler, and oth., V kn. Trudy Mezhdunarodnoy Konferentsii po Kosmicheskim Lucham (In Book: Proceedings of the International Conference on Cosmic Rays), Vol. 1, AN SSSR, Moscow, 1960, p. 28.
458. Hayakawa, S. and N. Ogita, V kn. Trudy Mezhdunarodnoy Konferentsii po Kosmicheskim Lucham (In Book: Proceedings of the International Conference on Cosmic Rays), Vol. 2, AN SSSR, Moscow, 1960, p. 242.
459. Bowler, M., P. Fowler and D. Perkins, Nuovo Cimento, Vol. 26, p. 1182, 1962.
460. Farrow, C., Phys. Rev., Vol. 107, p. 1687, 1957.
461. Brown, R., U. Camerini, P. Fowler, et al., Phil. Mag., Vol. 40, p. 862, 1949.
462. Cervasi, M., G. Fidecaro and L. Mezzetti, Nuovo Cimento, Vol. 1, p. 300, 1955.
463. Kasmitz, H. and K. Sitte, Phys. Rev., Vol. 94, p. 977, 1954. /387
464. Murzin, V. S., and oth., Yadern. Fiz., Vol. 5, p. 612, 1967.
465. Greisen, K. and W. Walker, Phys. Rev., Vol. 90, p. 915, 1953.
466. Lal, S., Y. Pal and R. Raghavan, Nucl. Phys., Vol. 31, p. 415, 1962.

467. Lal, S., R. Raghavan, T. Rangaswami, et al., Proc. Int. Conf. on Cosmic Rays, Jaipur, Vol. 5, p. 260, 1964.
468. Galstyan, D.A., G.B. Zhdanov and M.I. Tret'yakova, Izvestiya AN SSSR, Ser. fiz., Vol. 30, p. 1598, 1966.
469. Daniel, R., Rao Kamesawa, P. Malhotra and Y. Tsuzuki, Nuovo Cimento, Vol. 16, p. 1, 1960.
470. Khrimyan, A., V. Avakyan, N. Nalbandyan, and oth., Zh. Eksp. i Teoret. Fiz., Vol. 42, p. 664, 1962.
471. Khrimyan, A., V. Avakyan, M. Pleshko and G. Khrimyan, Izvestiya AN SSSR, Ser. fiz., Vol. 28, p. 180, 1964.
472. Zatsepin, G.T. and V.A. Kuz'min, Zh. Eksp. i Teoret. Fiz., Vol. 39, p. 1677, 1960.
473. Osborne, I.L., A.W. Wolfendale and N.S. Palmer, Proc. Phys. Soc., Vol. 84, p. 911, 1964.
474a. Wolfendale, A.W., Proc. Int. Conf. on Cosmic Rays, London, Vol. 2, p. 989, 1965.
474b. Il'ina, N.L. and L.I. Sarycheva, Yadern. Fiz., Vol. 4, No. 1, 1966.
475. Asatiani, T.L. and R.O. Sharokhatunyan, Izvestiya AN SSSR, Ser. fiz., Vol. 28, p. 1861, 1964.
476. Osborne, I.L., S.S. Said and A.W. Wolfendale, Proc. Phys. Soc., Vol. 86, p. 93, 1965.
477. Hayman, P.I. and A.W. Wolfendale, Proc. Phys. Soc., Vol. 80, p. 710, 1962.
478. Hayman, P.I. and A.W. Wolfendale, Proc. Phys. Soc., Vol. 80, p. 800, 1962.
479. Bull, R.M., W.F. Nash and B.C. Rastin, Nuovo Cimento, Vol. 40A, p. 365, 1965.
480. George, E., Fizika Kosmicheskikh Luchey (Physics of Cosmic Rays), pod red. Vil'son (Wilson, ed.), Vol. 1, IL, Moscow, 1954, p. 328.
481. Mando, M. and L. Ronchi, Nuovo Cimento, Vol. 9, p. 517, 1952.
482. Rozental', I.L. and V.N. Strel'tsov, Zh. Eksp. i Teoret. Fiz., Vol. 35, p. 1440, 1958.
483. Osaki, S., J. Phys. Soc. Japan, Vol. 17, Suppl. A-III, p. 330, 1962.
484. Hayman, P.L., N.S. Palmer and A.W. Wolfendale, Proc. Roy. Soc., Vol. 275A, p. 391, 1963.
485. Miyake, S., V.S. Narashimuham and P.V. Ramana-Murthy, Nuovo Cimento, Vol. 32, p. 1524, 1964.
486. Kobayakawa, K., Preprint University of Utah, Salt Lake City, 1966; Nuovo Cimento, Vol. 47B, p. 156, 1967.
487. Mando, M. and P.G. Sona, Nuovo Cimento, Vol. 10, p. 1275, 1953.
488. Zatsepin, G.T. and Ye.D., J. Phys. Soc. Japan, Vol. 17, Suppl. A-III, p. 356, 1962.
489. Nishimura, I., Proc. Int. Conf. on Cosmic Rays, Jaipur, Vol. 6, p. 224, 1964.
490. Miyake, S., V.S. Narashimham and P.V. Ramana-Murthy, Nuovo Cimento, Vol. 32, p. 1505, 1963.
491. Krasil'nikov, D.D., Izvestiya AN SSSR, Ser. fiz., Vol. 28, p. 1854, 1964.
492. Vernov, S.N., G.B. Khristiansen, Yu.A. Nechin, and oth., V kn. Voprosy Fiziki Elementarnykh Chastits (In Book: Problems in the Physics of Elementary Particles), AN ArmSSR, Yerevan, 1966, p. 591. /388

493. Borog, V. V., V. G. Kirillov-Ugryumov, A. A. Petrukhin, and oth., Izvestiya AN SSSR, Ser. fiz., Vol. 30, p. 1669, 1966.
494. Bezus, V. A., L. A. Gedevanishvili, R. Ye. Kazarov, and oth., Izvestiya AN SSSR, Ser. fiz., Vol. 30, p. 1662, 1966.
495. Zatsepin, G. T., Doklady AN SSSR, Vol. 67, p. 993, 1949.
496. Rozental', I. L., Doklady AN SSSR, Vol. 80, p. 731, 1951.
497. Messel', G., Fizika Kosmicheskikh Luchey (Physics of Cosmic Rays), Vol. 2, IL, Moscow, 1956, p. 69.
498. Grigorova, N. L., Uspekh. Fiz. Nauk, Vol. 58, p. 599, 1956.
499. Baradzey, L. T., V. I. Rubtsov, Yu. A. Smorodin, and oth., Trudy Fizicheskogo Instituta im. P. N. Lebedeva AN SSSR (Proceedings of the P. N. Lebedev Physics Institute, Acad. Sci. SSSR), Vol. 26, p. 224, 1964.
500. Grigorov, N. L., Zh. Eksp. i Teoret. Fiz., Vol. 45, p. 1544, 1963; Vol. 45, p. 1920, 1963.
501. Baradzey, L. T., V. I. Rubtsov and Yu. A. Smorodin, J. Phys. Soc. Japan, Vol. 17, Suppl. A-III, p. 433, 1962.
502. Andronikashvili, E. L., G. Ye. Chikovani, Z. Sh. Mandzhavidze, and oth., Proc. Int. Conf. on Cosmic Rays, Vol. 2, London, p. 916, 1965.
503. Dovzhenko, O. I. and A. A. Pomanskiy, Trudy FIAN (Proceedings of the Physics Institute, Acad. Sci.), Vol. 26, p. 166, 1964.

NASA-Langley, 1970 —— 30 F-594

NATIONAL AERONAUTICS AND SPACE ADMINISTRATION
WASHINGTON, D.C. 20546
OFFICIAL BUSINESS

FIRST CLASS MAIL

POSTAGE AND FEES I
NATIONAL AERONAUTI
SPACE ADMINISTRAT

020 001 55 51 30S 70151 00903
AIR FORCE WEAPONS LABORATORY /WLOL/
KIRTLAND AFB, NEW MEXICO 87117

ATT E. LOU BOWMAN, CHIEF, TECH. LIBRARY

POSTMASTER: If Undeliverable (Sectio
Postal Manual) Do Not

"The aeronautical and space activities of the United States shall be conducted so as to contribute . . . to the expansion of human knowledge of phenomena in the atmosphere and space. The Administration shall provide for the widest practicable and appropriate dissemination of information concerning its activities and the results thereof."

—NATIONAL AERONAUTICS AND SPACE ACT OF 1958

NASA SCIENTIFIC AND TECHNICAL PUBLICATIONS

TECHNICAL REPORTS: Scientific and technical information considered important, complete, and a lasting contribution to existing knowledge.

TECHNICAL NOTES: Information less broad in scope but nevertheless of importance as a contribution to existing knowledge.

TECHNICAL MEMORANDUMS: Information receiving limited distribution because of preliminary data, security classification, or other reasons.

CONTRACTOR REPORTS: Scientific and technical information generated under a NASA contract or grant and considered an important contribution to existing knowledge.

TECHNICAL TRANSLATIONS: Information published in a foreign language considered to merit NASA distribution in English.

SPECIAL PUBLICATIONS: Information derived from or of value to NASA activities. Publications include conference proceedings, monographs, data compilations, handbooks, sourcebooks, and special bibliographies.

TECHNOLOGY UTILIZATION PUBLICATIONS: Information on technology used by NASA that may be of particular interest in commercial and other non-aerospace applications. Publications include Tech Briefs, Technology Utilization Reports and Technology Surveys.

Details on the availability of these publications may be obtained from:

SCIENTIFIC AND TECHNICAL INFORMATION DIVISION

NATIONAL AERONAUTICS AND SPACE ADMINISTRATION

Washington, D.C. 20546